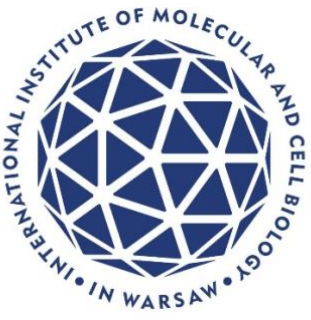

5′ terminal nucleotide modulates the immunogenicity of RNA

by

Jacek Nikodem Szymański

Doctoral dissertation
Laboratory of RNA-Protein Interactions – Dioscuri Centre
International Institute of Molecular and Cell Biology in Warsaw
Warsaw PhD School in Natural and BioMedical Sciences

Supervisor: Prof. Gracjan Michlewski

Auxiliary Supervisor: Dr Magdalena Wołczyk

Warsaw, September 2025

I wish to acknowledge people who have contributed to the development of this PhD thesis:

***Prof. Gracjan Michlewski**, my supervisor, for his invaluable guidance, encouragement throughout the entire research process, and for creating a supportive environment that helped me develop my scientific skills.*

***Dr Magdalena Wołczyk**, my auxiliary supervisor, for sharing her extensive knowledge, for her continuous support, constructive feedback, and all our insightful discussions.*

***Agnieszka Bolembach**, my friend in and outside the lab, for all the motivational support, her willingness to listen to my complaints and worries, and for her patience with my jokes at the bench.*

***My LOR coleagues**, for sharing great moments, creating memories, and building the best working atmosphere I've ever experienced.*

***My Princess Ciri**, for sharing her amazing energy and making me smile in the toughest moments.*

***My wife, Julia**, for believing in me even during my most hopeless moments, cheering me on from beginning to end, sharing in all the successes and losses, and being the best friend, I never even dreamed I could have.*

Abstract

The innate immune response is the first line of defence in mammalian cells against various pathogens, including RNA viruses. While activation of the innate immune system is crucial to produce antiviral agents such as interferons, overstimulation can lead to autoimmune disorders. One of the key regulators of innate immunity against RNA viruses is the cytoplasmic pattern recognition receptor - retinoic acid-inducible gene I (RIG-I). RIG-I detects double-stranded RNA (dsRNA) transcripts bearing a 5′-triphosphate (5′-ppp) or 5′-diphosphate (5′-pp) moiety, triggering a signaling cascade that includes phosphorylation of IRF3 and induction of type I interferon production.

In addition to viral and certain endogenous intracellular RNA polymerase III transcripts, RIG-I recognizes dsRNA byproducts generated during *in vitro* transcription reaction (IVT), a widely used method to manufacture mRNA therapeutics. Notably, IVT reaction using T7 RNA polymerase exclusively produces transcripts with either 5′-pppA or 5′-pppG as the initiator nucleotide; however, the immunogenic potential depending on the identity of the 5′-terminal nucleotide has not yet been investigated. In the first part of my PhD thesis, I demonstrate that RNA IVT products initiating with 5′-pppA show higher immunogenicity than those starting from 5′-pppG. This immunogenic potential of 5′-pppA initiating RNAs is driven by higher amount of dsRNA byproducts formation during IVT production.

Notably, naturally occurring RIG-I agonists also vary in their 5′-end nucleotide. While many viral RNA genomes begin with 5′-pppA, most polymerase III transcripts in higher eukaryotes initiate with 5′-pppG. The biological significance of this variation remains unexplored. My research shows that dsRNAs with a 5′-pppA end more robustly activate RIG-I/IFN pathway than 5′-pppG dsRNAs in concentrations mimicking early phases of viral infection. Furthermore, I provide potential explanation of this phenomenon showing GTP-binding proteins selectively interact with 5′-pppG dsRNAs, thereby inhibiting RIG-I.

In summary, this study examines both technical and biological aspects of how 5′-terminal nucleotides influence the immunogenic potential of RNA. Technically, it identifies features of IVT that promote immune activation. Biologically, it demonstrates that variation in the 5′-terminal structure of dsRNAs modulates innate immune recognition, establishing a direct link between RNA sequence and immune sensing. The characterisation of IVT mechanisms that trigger immunogenicity provides a foundation for optimising next-generation mRNA therapeutics. The observed reduction in immunogenicity of 5′-pppG dsRNAs further suggests a viral and pol III evasion strategy in which RNAs recruit GTP-binding proteins via 5′-pppG ends. Collectively, these findings reveal a previously underappreciated role for 5′-terminal nucleotides in modulating antiviral immune responses.

Streszczenie

Wrodzona odpowiedź immunologiczna stanowi pierwszą linię obrony w komórkach ssaków przed różnymi patogenami, w tym wirusami RNA. Choć jej aktywacja jest kluczowa dla wytwarzania czynników przeciwwirusowych, takich jak interferony, nadmierna stymulacja może prowadzić do chorób autoimmunologicznych. Jednym z głównych regulatorów odporności wrodzonej przeciwko wirusom RNA jest cytoplazmatyczny receptor – RIG-I (ang. *retinoic acid-inducible gene I*). RIG-I rozpoznaje dwuniciowe RNA (dsRNA) zawierające grupę 5′-trifosforanową (5′-ppp) lub 5′-difosforanową (5′-pp), co uruchamia kaskadę sygnałową obejmującą fosforylację IRF3 oraz produkcję interferonów typu I.

RIG-I wykrywa nie tylko wirusowe i niektóre endogenne transkrypty polimerazy RNA III, ale również dwuniciowe produkty uboczne powstające podczas reakcji transkrypcji *in vitro* (IVT), szeroko stosowanej metody wytwarzania terapeutycznych cząsteczek mRNA. Istotnie, IVT z użyciem polimerazy RNA T7 wytwarza wyłącznie transkrypty rozpoczynające się od nukleotydu 5′-pppA lub 5′-pppG. Jednak immunogenny potencjał zależny od nukleotydu na końcu 5′ nie został dotychczas zbadany. W pierwszej części mojej rozprawy doktorskiej wykazuję, że produkty IVT rozpoczynające się od 5′-pppA wykazują wyższą immunogenność niż te inicjowane przez 5′-pppG. Ten potencjał immunogenny RNA inicjowanych od 5′-pppA wynika z większej ilości produktów ubocznych dsRNA powstających podczas reakcji IVT.

Naturalnie występujące agonisty RIG-I również różnią się pod względem nukleotydu końcowego 5′. Wiele wirusowych genomów RNA zaczyna się od 5′-pppA, natomiast większość transkryptów polimerazy III u organizmów wyższych inicjuje od 5′-pppG. Biologiczne znaczenie tej różnicy pozostaje nieznane. Moje badania pokazują, że dsRNA z końcem 5′-pppA silniej aktywują szlak RIG-I/IFN niż dsRNA z końcem 5′-pppG, w stężeniach reprezentujących wczesne fazy infekcji wirusowej. Ponadto przedstawiam potencjalne wyjaśnienie tego zjawiska, wskazując, że białka wiążące GTP selektywnie oddziałują z dsRNA 5′-pppG, a tym samym hamują działanie RIG-I.

Reasumując, niniejsze badania pokazują techniczne i biologiczne aspekty wpływu nukleotydu końcowego 5′ na potencjał immunogenny RNA. Technicznie zidentyfikowano cechy transkrypcji IVT sprzyjające aktywacji układu odpornościowego, a biologicznie wykazano, że zmienność struktury końca 5′ dsRNA moduluje rozpoznawanie przez odporność wrodzoną, ustanawiając bezpośredni związek między sekwencją RNA a jej detekcją przez układ odpornościowy. Charakterystyka mechanizmów IVT wywołujących immunogenność stanowi podstawę do optymalizacji terapii mRNA nowej generacji. Zaobserwowane obniżenie immunogenności dsRNA 5′-pppG sugeruje strategię unikania odpowiedzi immunologicznej stosowaną przez wirusy i transkrypty polimerazy III poprzez rekrutację białek wiążących GTP do końców 5′-pppG. Wyniki te ujawniają dotąd niedocenianą rolę nukleotydów końcowych 5′ w modulowaniu przeciwwirusowych odpowiedzi immunologicznych.

Table of contents

1. Introduction

In recent years, RNA viruses have been among the most frequent causes of severe infectious diseases worldwide. According to the statistics provided by the World Health Organization, approximately 1 billion people are infected with seasonal influenza each year. Of these, around 250,000 to 600,000 cases result in respiratory-related deaths annually[1,2]. Moreover, the emergence of the novel SARS-CoV-2 virus in 2019 led to a global pandemic, resulting in global crisis and over 7 million deaths[1,3]. To mount an effective response against RNA viruses, a deep understanding of cellular antiviral strategies is crucial.

The first line of defence in human cells against viral infections is the innate immune system. This response is characterized by non-specific recognition of viral presence, independent of species or strain, which triggers the production of antiviral agents, such as cytokines, and initiates signals that activate the adaptive (species-specific) immune response[4]. The detection of RNA viruses by the innate immune system largely depends on RNA-protein interactions[5]. My PhD research was primarily focused on gaining a deeper understanding of these interactions and identifying novel features of RNAs involved in the innate immune detection.

1.1. RNA sensing – Pattern Recognition Receptors

The first step in the host response to viral infection is the detection of foreign molecules or structures known as pathogen-associated molecular patterns (PAMPs). Host proteins responsible for recognizing these PAMPs are called pattern recognition receptors (PRRs). Notably, PRRs are found not only in specialized immune cells such as macrophages, dendritic cells, and natural killer (NK) cells, but also in most human cell types, including epithelial cells, endothelial cells, and fibroblasts[4]. PRRs can detect PAMPs derived from various viral components, including capsid proteins, envelope lipids, and viral nucleic acids. In this work, I focus specifically on PRRs that sense the genetic material of RNA viruses. Several families of PRRs detect viral RNA in humans, including transmembrane Toll-like receptors (TLRs), as well as cytoplasmic sensors such as RIG-I-like receptors (RLRs), NOD-like receptors (NLRs), and a few others, which will be reviewed in this thesis. Figure 1 presents a schematic representation of the pathways activated by RNA PRRs.

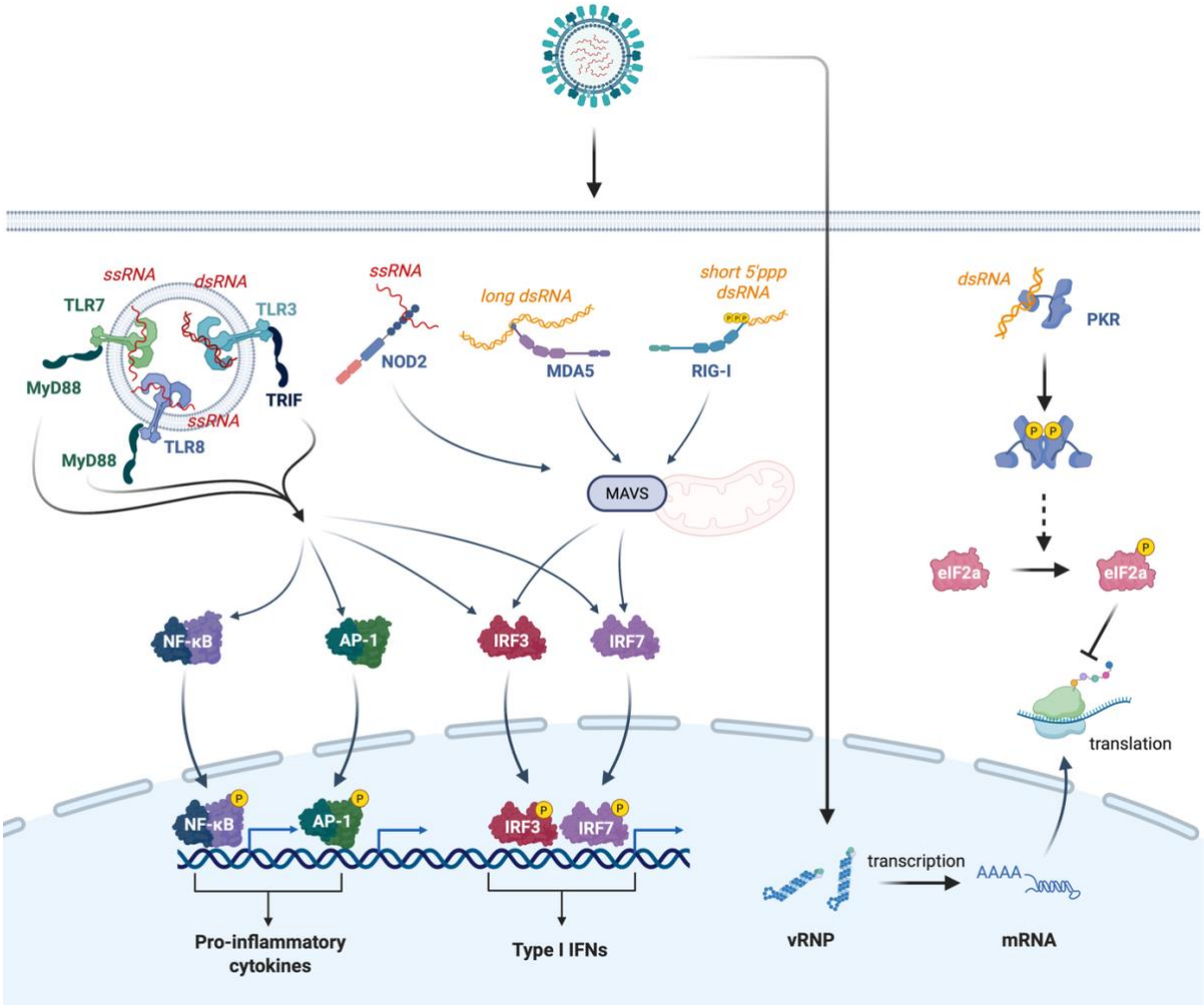

Figure 1. *Recognition of viral RNA by pattern recognition receptors (PRRs), including Toll-like receptors (TLRs), RIG-I-like receptors (RLRs), nucleotide-binding oligomerization domain-containing protein 2 (NOD2), and protein kinase R (PKR), which together constitute key components of the innate immune system responsible for detecting viral RNA in different cellular compartments and initiating antiviral signaling pathways.*

1.1.1. Toll-Like Receptors (TLRs)

Toll-like receptors (TLRs) are a family of transmembrane proteins and represent one of the most well-characterized groups of PRRs. TLRs detect pathogen-associated molecular patterns (PAMPs) either at the cell surface or within intracellular compartments such as endosomes and lysosomes[4]. The human genome encodes ten TLRs (TLR1–TLR10), each composed of an N-terminal ectodomain containing leucine-rich repeats (LRRs), a single transmembrane domain, and a cytosolic Toll/interleukin-1 receptor (TIR) domain responsible for signaling[6]. Upon ligand binding to the ectodomain, TLRs undergo dimerization, which brings the TIR domains into proximity, facilitating the recruitment of adaptor proteins and initiation of downstream signalling cascades[7].

Most TLRs expressed on the cell surface recognize microbial surface components, whereas endosomal TLRs—specifically TLR3, TLR7, and TLR8—are involved in the recognition of viral RNAs[8]. TLR3 recognises viral dsRNA, synthetic polyinosinic-polycytidylic acid (poly I : C), polyadenylic-polyuridylic acid (poly A : U) and viral ssRNA with stable stem loop structures[9–11]. In contrast, TLR7 and 8, which are very similar in characteristics, detects specifically viral ssRNA containing guanosine- and uridine-rich sequences[12,13].

Although, those three TLRs are using different adaptor proteins – TLR3 is recruiting TIR domain-containing adaptor protein inducing IFN-β (TRIF), whereas TLR7 and 8 induce signalling via a TIR-containing adaptor named myeloid differentiation primary response gene 88 (MyD88) – further downstream signalling is similar. TLRs are activating three main signalling pathways: mitogen-activated protein kinases (MAPKs), interferon regulatory factors 3 or 7 (IRF3/7) depending on TLR and nuclear factor kappa–light-chain-enhancer of activated B cells (NF-κB). All those pathways lead to the production of antiviral, proinflammatory agents – IRF3 and IRF7 promote production of a type I interferons (IFNs), MAPKs induce activator protein 1 (AP-1) and combined with NF-κB promote adaptive immune activation and production of inflammation cytokines, including IL-1β, IL-6, IL-18, and tumour necrosis factor (TNF)[14,15].

1.1.2. RIG-I-Like Receptors (RLRs)

The RIG-I-like receptors are proteins, which are present in most human cells, recognising viral RNA. They are predominantly cytosolic proteins[16–18], however some studies show their nuclear localisation[19]. Common feature for all RLRs is belonging to ATP dependent DExD/H family of helicases[15], possessing conserved D-E-x-D motif, where "x" can be any amino acid. It means they use the energy from ATP hydrolysis to unwind RNA structures or remodel RNA-protein complexes[20]. Second domain shared across all RLRs is carboxy-terminal domain (CTD), together with helicase domain involved in specific recognition of immunostimulatory viral RNA[21].

The most similar in structure and molecular functions are two members of RLRs – retinoic acid-inducible gene I (RIG-I) and melanoma differentiation-associated gene 5 (MDA5). Apart from RNA recognition domains – helicase and CTD, both PRRs possess two additional caspase activation and recruitment domains (CARDs), responsible for downstream pathway activation[22,23]. Although RIG-I and MDA5 similarities decide that both bind viral dsRNA, RNA molecular patterns crucial for its recognition are different. RIG-I specifically binds to short double-stranded panhandle structures bearing triphosphate moiety at 5′ terminal nucleotide[24–26] (more details in section 1.2.), whereas MDA5 recognises longer dsRNA molecules that typically exceed 500 nucleotide base pairs[27,28]. In essence, binding RNA to helicase domain together with ATP recruitment leads to conformational changes and release of CARDs for further signalling. Then RIG-I/MDA5 CARDs interact with similar CARDs found in

mitochondrial antiviral-signalling protein (MAVS), which acts as main adaptor protein for RLRs signalling. In next steps of signalling, MAVS recruits two kinases – TANK-binding kinase 1 (TBK1) and IκB kinase-ε (IKKε), activating interferon regulatory factors 3 and 7 via phosphorylation. Those, together with NF-κB, activate transcription of type I interferons encoding genes and other antiviral agents[29,30].

Third member of RLRs – laboratory of genetics and physiology 2 (LGP2) is much less characterised. In opposite to RIG-I and MDA5, LGP2 does not contain downstream pathway stimulatory CARDs, but still has ability to recognise viral RNA. Studies show that recognition and binding to RNA by LGP2 is independent of 5′-triphosphates[31]. Currently, its role is described as regulatory protein of other RLRs, and depending on various viral infections it can stimulate or inhibit RIG-I and MDA5 activation[15,32,33].

1.1.3. Nucleotide-binding oligomerization domain 2 (NOD2)

Nucleotide-binding oligomerization domain 2 (NOD2) is cytosolic protein belonging to broad family of proteins called (NOD)-like receptors (NLR), which regulates inflammatory and apoptotic responses. NLRs consist of 3 domains: C-terminal LRR domain is considered as sensor domain, central NACHT domain that is responsible for oligomerisation and activation of NLR protein and N-terminal effector-binding domain – CARD or alternatively a pyrin domain (PYD). Although, many NLRs are involved in PAMPs recognition of many microbial organisms, NOD2 is the only one to sense nucleic acids[34]. However, primarily NOD2 was found to be sensor of bacterial PAMPs including muramyl dipeptide – component of bacterial peptidoglycan[35], another study shown its ability to recognise viral ssRNA genomes[36]. Interestingly, downstream signalling of ssRNA-dependent activation of NOD2 is similar to RLRs activation pathway, ligand binding leads to exposition of CARD, which interacts with MAVS and facilitates further cascade of events leading to IRF3 activation and IFN type I production[36].

1.1.4. Protein Kinase R (PKR)

In contrast to other described innate immune sensors, protein kinase R (PKR) does not directly activate signalling pathways leading to the production of cytokines or other inflammation-inducing agents. PKR is a sensor protein, containing two double-stranded RNA-binding motifs (dsRBMs) at its N-terminus and a kinase domain at its C-terminus, which specifically recognizes double-stranded RNA (dsRNA) during viral infection. The binding of dsRNA – typically at least 30 base pairs in length – by two PKR molecules via their dsRBMs promotes dimerization, leading to autophosphorylation and activation of the kinase in the form of a homodimer[37–39].

Once activated, phosphorylated PKR can phosphorylate the eukaryotic initiation factor 2 alpha (eIF2α), which inhibits cap-dependent translation initiation and global protein synthesis. This ultimately suppresses both cellular proliferation and viral replication[38,40]. Similar to other

pattern recognition receptors (PRRs), PKR is an interferon-stimulated gene (ISG); thus, stimulation by type I interferons (produced in response to other PRRs) leads to its upregulation during viral infection[38].

To summarize, cells activate multiple signaling pathways to sense immunogenic RNA, all of which converge on the induction of interferons and the suppression of viral replication.

1.2. RIG-I agonists

As briefly mentioned, RIG-I uses its helicase and C-terminal domain (CTD) to selectively recognize viral RNAs that form double-stranded structures with a 5′-terminal triphosphate group (section 1.1.2.). Studies have shown that additional structural and chemical features of the RNA molecule must also be considered when evaluating RIG-I agonists.

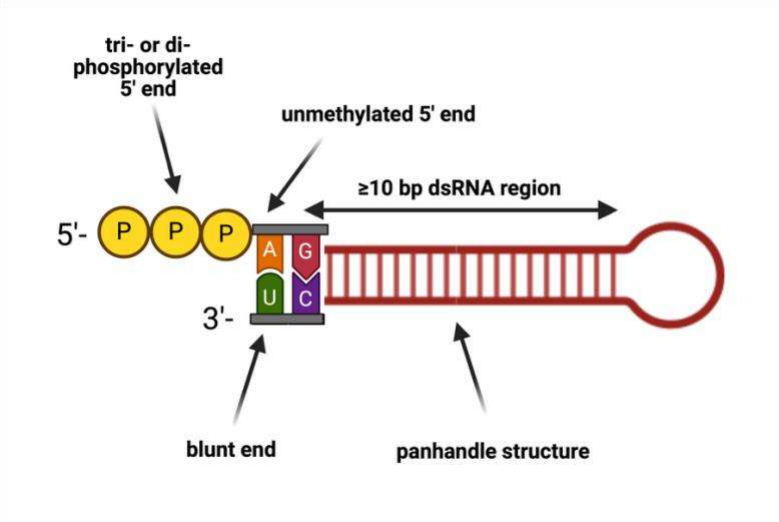

Figure 2. Molecular features of RIG-I ligands

First, dsRNA bearing a 5′-diphosphate group has been found to be as effective as triphosphorylated RNA in activating RIG-I[41]. In contrast, unmodified 5′-hydroxyl (5′-OH) RNA induces only minimal activation, while RNA with a 5′-monophosphate (5′-p) – a modification common in most cellular RNAs – completely prevents RIG-I recognition[42]. Furthermore, methylation of the 5′-terminal nucleotide at the 2′-O position has been shown to drastically reduce RIG-I activation[43].

Beyond the requirement for double-strandness, additional structural features have been evaluated for their influence on RIG-I specificity, including RNA length, dsRNA overhangs, and duplex complementarity. Regarding RNA length, several studies have shown that synthetic dsRNA ligands of approximately 10-15 base pairs are sufficient to activate RIG-I[44–46]. Nevertheless, longer dsRNA molecules are known to be more potent RIG-I agonists. For example, analysis of mini viral RNAs derived from influenza A virus (IAV) infections revealed that the most stimulatory RNA fragments were approximately 80 nucleotides in length[47]. This

enhanced stimulation of the RIG-I pathway by longer dsRNA fragments can be explained by ATP-dependent oligomerization of RIG-I along the duplex, promoting more robust signaling[48].

Notably, RIG-I binding is highly sensitive to the structure of the RNA 5′ end. Optimal binding occurs with a panhandle structure featuring a blunt end; any overhang at this site adversely affects the interaction[49]. However, a single-nucleotide 3′ overhang on the panhandle structure is tolerated with only a slight decrease in binding affinity, while longer overhangs cause a significant reduction in RIG-I binding. At the 5′ terminus, even minimal overhangs eliminate RIG-I recognition[50,51]. Although perfect complementarity is crucial at the first base pair at the 5′ end of the dsRNA, the RIG-I receptor tolerates wobble pairs, mismatches, or small bulges (~3 nucleotides) that begin further away from the 5′ terminus[50].

Altogether, these studies demonstrate that RIG-I activation depends on a combination of structural and chemical features of the RNA ligand, rather than solely on the presence of a 5′-triphosphate. Moreover, there is no strong evidence supporting sequence specificity or the presence of defined motifs recognized by the RIG-I receptor. However, a study by Schlee et al. suggested that the identity of the 5′-terminal nucleotide may influence RIG-I activation[50], the observed difference was marginalised and no longer studied. More recent work found no significant difference in RIG-I activation upon altering the 5′-terminal nucleotide in a short synthetic dsRNA ligand[51]. Nevertheless, the RNA molecules used in that study were suboptimal in terms of length, necessitating the use of extremely high concentrations to elicit activation. In this thesis, a more in-depth analysis of the role of the 5′-terminal nucleotide in modulating RIG-I pathway activity will be presented.

1.3. IVT products – origin of immunogenicity

Currently, IVT by T7 polymerase is the most widely used technique to produce synthetic RNA-based therapeutics. In recent years, mRNA therapeutics produced via IVT have shown great potential, with successful application in COVID-19 vaccines and ongoing exploration in experimental cancer therapies[52]. The main advantages of IVT for RNA production include high yield, scalability, and cost-effectiveness. However, IVT also generates immunogenic dsRNA byproducts, which can negatively affect the safety and efficacy of RNA-based therapeutics.

1.3.1. Various types of dsRNA byproducts

All dsRNA impurities generated during *in vitro* transcription arise from the natural imperfections of T7 RNA polymerase. There are two main stages during T7 transcription where errors leading to byproduct formation are most likely to occur – transcription initiation and termination[53].

Transcription begins with T7 polymerase binding to the promoter sequence on the DNA template and locally unwinding the double-stranded DNA[54]. The enzyme then initiates RNA synthesis by incorporating the first few nucleotides. At this early stage, the DNA-protein

complex is highly unstable. Once the nascent transcript reaches a length of approximately 10 nucleotides, a conformational change occurs, converting the initiation complex into a more stable elongation complex[55,56]. During the unstable initiation phase, short abortive transcripts (typically 2–13 nucleotides in length) may be generated in a process known as abortive cycling[57]. These short RNA fragments can anneal to complementary regions within full-length transcripts. Such structures could act as potent agonists for pattern recognition receptors (PRRs) or serve as primers for RNA-templated, noncanonical transcription, ultimately generating longer dsRNA products.

Transcription termination usually occurs at a specific sequence signal or at the end of a linear DNA template, producing a full-length RNA product[58,59]. However, T7 RNA polymerase can occasionally add extra nucleotides at the 3′ end of the transcript[60,60]. This additional RNA fragment can fold back and base-pair with complementary sequences within the same RNA molecule, forming a loopback structure. The resulting structure can serve as a primer that enables the polymerase's noncanonical RNA-templated activity. As a result, the RNA product may undergo further extension, leading to the synthesis of long double-stranded RNA (dsRNA) regions within the final transcript[61].

In addition to loopback formation, T7 polymerase can exhibit promoter-independent activity using DNA or RNA templates, generating long, fully complementary antisense transcripts. These reverse transcripts can hybridize with sense transcripts, forming long dsRNA molecules[62,63].

All such dsRNA byproducts are potent PRRs' agonists, capable of activating receptors such as RIG-I, MDA5, and toll-like receptors (TLRs), which in turn trigger innate immune responses and undesirable inflammation in host cells. Moreover, activation of the PKR pathway can lead to global translation inhibition, resulting in reduced protein production and possible cytotoxic effects. This compromises the therapeutic efficacy of mRNA-based treatments, whose success depends on efficient translation into the target protein[64].

1.3.2. Avoiding dsRNA byproducts

As described in the previous section, avoiding dsRNA impurities is crucial for the accurate and effective production of RNA therapeutics. Despite the development of several purification strategies to remove immunogenic dsRNA impurities generated during *in vitro* transcription[65], complete elimination of these byproducts remains unachievable. Consequently, additional strategies have been implemented to minimize dsRNA formation during the IVT reaction itself. These approaches primarily focus on optimizing reaction conditions and engineering the RNA polymerase through targeted mutations aimed at reducing its propensity for noncanonical transcription.

Among the reaction components influencing T7 polymerase accuracy, researchers have identified ionic composition, chaotropic agents, and nucleotide modifications as key factors.

First, high concentration of magnesium ions (Mg^{2+}) has been shown to increase levels of dsRNA impurities during IVT[62]. It has been hypothesized that elevated Mg^{2+} concentrations stabilize the elongation complex during promoterless, RNA-dependent transcription[63]. Second, chaotropic agents such as urea and formamide have been demonstrated to reduce dsRNA production by 60–70%. These agents decrease the likelihood of forming undesired back-loop structures, particularly those involving poly(A) tails hybridizing with internal RNA sequences[66]. Interestingly, this backfolding can also be limited by reducing the concentration of UTP in the IVT reaction[67].

Additionally, the use of modified nucleotides – pseudouridine (Ψ), N^1-methylpseudouridine ($m^1\Psi$), and 5-methylcytidine (m^5C) – has been shown to lower production of dsRNA impurities[63]. This strategy has a dual benefit, as these modifications are primarily employed to reduce recognition of RNA therapeutics via PRRs like RIG-I and TLRs by decreasing RNA binding affinity or preventing conformational changes required for receptor activation[68,69].

Beyond reaction composition, substantial efforts have been directed toward engineering T7 polymerase to improve transcription fidelity. Based on the hypothesis that initiation complex conformation is responsible for generation of abortive transcripts, mutations were introduced into the N-terminal domain (NTD) of T7 polymerase to promote a smoother transition to the elongation complex. One such mutation – G47A – was found to significantly reduce dsRNA production while maintaining comparable yields of the main RNA product[70]. Moreover, $FAFA^{883}$ motif, located in carboxy-terminal domain (CTD) of T7 polymerase, was shown to influence both 3′-end homogeneity and overall transcription efficiency[71,70]. Recent work from Dousis et al.[70] reported that 884G mutation perform best results by increasing 3′-end homogeneity from 6–12% to 30–45% and decreased impurities formations by 7–15-fold compared with wild-type enzyme. Finally, increasing the IVT reaction temperature using a commercially available thermostable T7 polymerase variant was shown to reduce dsRNA generated via 3′-end extensions. However, this modification did not affect dsRNA production resulting from strand-switching events[72].

So far, limited data are available on how the RNA product sequence influences dsRNA byproduct formation. In this PhD thesis, I investigate the impact of the initial nucleotide on dsRNA production during IVT using wild-type T7 polymerase.

2. Research objectives

The primary goal of my PhD research was to investigate the impact of the RNA 5′ terminal nucleotide on the innate immune response triggered by the cytoplasmic pattern recognition receptor RIG-I. I was investigating two main questions:

1. How the 5′ terminal nucleotide determines the immunogenicity of *in vitro* transcribed RNA synthesised with T7 polymerase.

2. How the 5′ terminal nucleotide mechanistically modulates RIG-I/IFN signalling in mammalian cells.

3. Results

3.1. 5′ terminal nucleotide determines the immunogenicity of IVT RNAs (Manuscript 1.)

To address the main objective of my PhD thesis, investigating the role of the 5′ terminal nucleotide in the stimulation of RIG-I–mediated innate immunity, I employed IVT using T7 RNA polymerase, a widely used method for RNA synthesis that naturally produces transcripts with 5′-ppp moiety. Two representative single-stranded RNA (ssRNA) fragments, each capable of forming a panhandle-like double-stranded RNA (dsRNA) structure, were generated: IAV-derived short viral RNA and the other derived from endogenous polymerase III transcript Y5 RNA. To evaluate the impact of the 5′ terminal nucleotide, two variants of each RNA were prepared, differing only in the identity of the initial nucleotide – either 5′-pppA or 5′-pppG – while preserving base pairing within the panhandle structure.

Innate immune activation by these RNAs was assessed in human embryonic kidney HEK293 and lung-derived A549 cell lines. Using colorimetric assay, we found that RNAs initiated with 5′-pppA induced up to ~1000-fold higher IFN-α/β production than their 5′-pppG counterparts across a broad range of RNA concentrations (0.1–300 ng/mL), with saturation of the response observed only at the highest concentrations. Furthermore, control experiments involving either enzymatic removal of the 5′-ppp moiety or knockout of RIG-I abolished interferon production, confirming the essential role of RIG-I protein in recognition of those RNAs.

Having established the RIG-I-dependent immunogenicity of 5′-pppA RNAs in human cells, we next investigated whether this phenomenon also occurs in murine systems. We examined immortalized mouse embryonic fibroblasts (MEFs) and primary cell types such as bone marrow-derived macrophages (BMDMs) and fibroblasts. Across all models, RNAs initiated with 5′-pppA consistently triggered stronger RIG-I/IFN responses than those initiated with 5′-pppG. Furthermore, together with a team we expanded our research on *in vivo* model - a reporter knock-in mouse, in which the IFN-β was replaced with the mKate2 fluorescent protein. This model enables us to detect innate immune response activation upon RNAs encapsulated into lipid nanoparticles (RNA-LNP) injection via flow cytometry measurements. We observed higher level of reporter mKate2 in the liver and spleen isolated from 5′-pppA RNA injected mice compared with 5′-pppG RNA treatment. Similar results were obtained in the IFN-β/mKate2 BMDMs. These results indicate that the phenomenon of varying immunogenicity of IVT RNA, depending on the identity of the terminal 5′ nucleotide, is not limited to a single species but occurs across mammals.

To explore the mechanism of increased immunogenicity of 5′-pppA IVT RNAs observed across mammalian systems, we performed in-depth analysis of dsRNA presence in IVT products. At first, we employed anti-dsRNA J2 detection on dot-blot analysis, which showed increased level of dsRNA in 5′-pppA initiated transcripts. Second, RNA pull-down assays coupled with mass

spectrometry (RP-MS) using whole-cell lysates identified a greater enrichment of dsRNA-binding proteins – such as ADAR, PKR (EIF2AK2), and DICER1 – on 5′-pppA RNAs compared to 5′-pppG RNAs. To further investigate origin of dsRNA formation, we performed native polyacrylamide gel electrophoresis (PAGE) analysis as well as J2 antibody based northern blot showed, that additional product enriched in 5′-pppA initiated products corresponds to dsRNA product formed by annealing of main IVT product with its separately synthesized complementary strand. Altogether, the occurrence of additional dsRNA products in 5′-pppA RNA preparations, together with their heightened immunogenicity, suggests that dsRNA impurities may play a direct role in RNA immunogenicity.

To directly assess the contribution of these dsRNA impurities to the immunogenicity, we constructed semisynthetic short viral RNA by splint ligation of initial 55 nucleotides synthesized with IVT and remaining 21 nucleotides – with chemical synthesis. Native PAGE confirmed that this so-called semisynthetic RNA was identical to IVT short viral RNA, except for additional band of dsRNA contamination present in 5′-pppA initiated IVT product. Transfection experiments on human cells showed no immunogenic potential in semisynthetic RNAs. However, supplementing the RNA with just 1–5% of a complementary strand restored RIG-I/IFN activation to the levels like those seen with the 5′-pppA IVT RNA, indicating that the immune stimulation was primarily driven by dsRNA byproducts. These findings demonstrate that otherwise non-stimulatory ssRNAs can become highly immunogenic when antisense strands generated during IVT form dsRNA byproducts.

Given the growing importance of IVT in RNA-based therapeutics, we investigated whether this phenomenon extended to longer transcripts (~1000 nt). Thus, we produced RNAs encoding EPO flanked with UTRs derived from the mRNA sequence of the Moderna SARS-CoV2 vaccine (mRNA-1273) and Segment 8th from the PR8 strain of IAV (Seg. 8th IAV PR8). In both cases, J2 dot-blot analysis showed increased dsRNA contamination for PAGE purified 5′-pppA initiated products. Moreover, HEK239 and A549 cells produced higher levels of IFN-I upon treatment with 5′-pppA initiated transcripts. Altogether, this demonstrates that initiation with 5′-pppA consistently drives the formation of immunogenic dsRNA byproducts, independent of transcript length.

Altogether, we discovered that IVT using T7 polymerase generates substantially higher amount of dsRNA impurities while initiated from 5′-pppA. Moreover, these impurities are not effectively removed by standard size-based purification methods and are primarily responsible for the heightened immunogenicity of 5′-pppA transcripts. Thus, the choice of initiating nucleotide has profound consequences for the safety and reliability of IVT RNAs, underscoring the need for improved strategies to minimize dsRNA impurities in RNA therapeutics and vaccines.

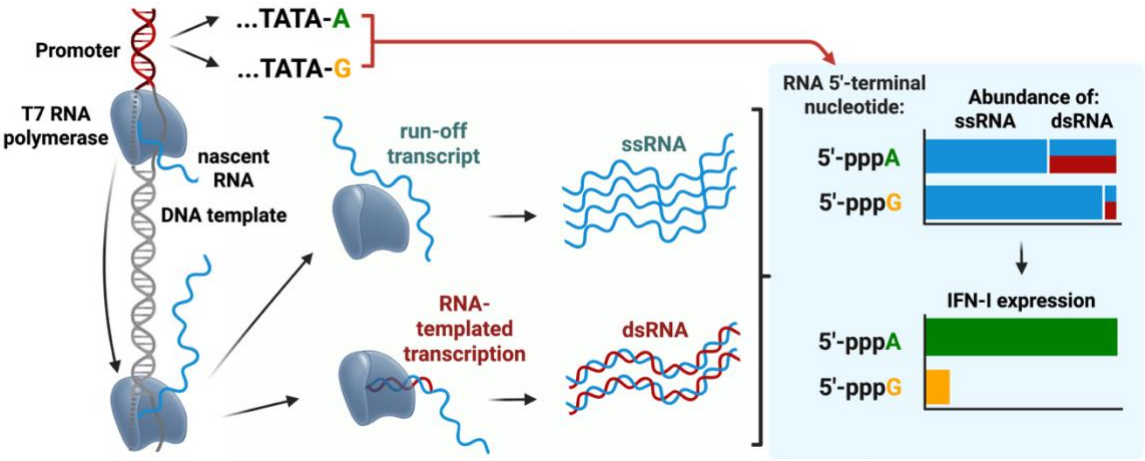

Figure 3. Schematic showing the differences in the immunogenicity of 5'-pppA and 5'-pppG IVT RNAs

Reference – Manuscript 1:

Wolczyk M.*, **Szymanski J.***, Trus I.*, Naz Z., Tame T., Bolembach A., Choudhury N.R., Kasztelan K., Rappsilber J., Dziembowski A., Michlewski G. 5' terminal nucleotide determines the immunogenicity of IVT RNAs. *Nucleic Acids Res.* (2025). DOI: 10.1093/nar/gkae1252.

*Authors contributed equally

3.2. 5′-triphosphate guanosine RNAs recruit GTP-binding proteins to suppress RIG-I/IFN type I signalling (Manuscript 2.)

According to findings reported in the literature, unprocessed RNA polymerase III (Pol III) transcripts naturally possess a 5′-ppp moiety[73]. Although these RNAs are typically hidden from RIG-I detection due to additional post-transcriptional modifications, under certain conditions they can activate the innate immune system via the RIG-I signalling pathway[73,74]. Our sequence analysis revealed that Pol III transcripts in higher eukaryotes predominantly initiate with 5′-ppp guanosine (5′-pppG). In contrast, many RNA viruses capable of triggering RIG-I activation, such as influenza A virus (IAV), begin with a 5′-ppp adenosine (5′-pppA). Notably, some highly pathogenic viruses – including H5N1 IAV, Ebola virus, and hepatitis C virus (HCV) – also initiate with 5′-pppG. This observation led us to investigate whether the 5′ terminal nucleotide influences discrimination via RIG-I between host and viral RNAs.

Since direct manipulation of the 5′ terminal nucleotide in viral genomes is not feasible, we employed synthetic RNAs as a suitable alternative. Although native RIG-I agonists are often single-stranded RNAs (ssRNAs) that fold into panhandle-like secondary structures, their IVT typically leads to the generation of immunogenic dsRNA byproducts – particularly in transcripts initiated with 5′-pppA, as demonstrated in Manuscript 1. To circumvent this, we adopted a strategy using fully complementary dsRNA duplexes, generated either via IVT or chemical synthesis, as defined RIG-I agonists.

Specifically, we synthesized two types of dsRNAs corresponding to the 5′ end of segment 8 of the IAV PR8 strain: a longer 76 bp duplex produced by IVT, and a shorter 24 bp duplex synthesized chemically. Each was generated with either a 5′-pppA or 5′-pppG as an initiator nucleotide. Then we assessed the impact of the 5′ terminal nucleotide on innate immune activation by transfecting these dsRNAs into both human and murine cells. In HEK293 cells, transfection with 5′-pppA dsRNAs led to increased RIG-I expression and elevated levels of phosphorylated IRF3 compared to 5′-pppG dsRNAs. This pattern was also reflected in type I interferon (IFN) activity, particularly following transfection with the 76 bp IVT-derived dsRNA. Enhanced innate immune activation was similarly observed in bone marrow-derived macrophages (BMDMs) isolated from mKate2 reporter mice. Importantly, control dsRNAs lacking the 5′-ppp moiety failed to elicit an immune response, confirming that RIG-I was the primary sensor mediating recognition of these synthetic dsRNAs.

Seeing these differences in cells, we wanted to explore the mechanistic basis underlying the differential activation of RIG-I by dsRNA bearing either 5′-pppA or 5′-pppG. Thus, we analyzed direct interactions between recombinant RIG-I and dsRNAs using biochemical assays. First, electrophoretic mobility shift assay (EMSA) showed significantly higher binding affinity of RIG-I protein to 5′-pppA than 5′-pppG dsRNA. On the other hand, while analysing RIG-I activation by measuring its ATPase activity, no significant difference determined by 5′

terminal nucleotide was observed. Altogether, these results suggest that the presence of a 5′-pppA may enhance RIG-I binding – potentially due to the thermodynamically less stable A–U base pair at the 5′ end, which could provide a more accessible entry point for the helicase domain – yet this increased binding affinity does not necessarily lead to stronger downstream activation of the receptor. Since direct binding between dsRNA and RIG-I does not completely explain the observed differences in pathway activation, additional mechanistic studies were required.

To explore the possibility that cellular factors contribute to the observed differential recognition of RNAs based on their 5′ terminal nucleotide, we performed RP-MS to analyse the interactome of dsRNAs bearing either 5′-pppA or 5′-pppG. While many proteins were found to bind both RNA variants at similar levels, a distinct subset showed preferential binding to one over the other. Among the proteins that preferentially bound 5′-pppG-containing dsRNA, a particularly interesting subset included highly abundant factors involved in translation and RNA transport, exhibiting GTP-binding properties or GTPase activity. Three of those proteins with the highest enrichment – NUDT16, RAN and RANBP1 – were confirmed with RNA pull-down followed by western blotting to bind exclusively to 5′-pppG dsRNA. Notably, binding of those proteins was highly depending on presence of 5′-ppp moiety. Furthermore, preincubation of protein extracts with non-hydrolysable GTP analogues significantly reduced their interaction with 5′-pppG RNA, suggesting that occupancy of the GTP-binding site interferes with RNA binding.

To assess whether GTP-binding proteins influence RIG-I/IFN pathway activation by dsRNA, we aimed to saturate these proteins by increasing intracellular GTP levels. GTP concentrations were elevated by supplementing cells with guanosine, thereby activating the nucleoside salvage pathway. Notably, transfection of dsRNA into HEK293 cells following guanosine treatment led to enhanced innate immune responses compared to DMSO and adenosine controls. Additionally, the typical difference in RIG-I activation between 5′-pppA and 5′-pppG dsRNAs was diminished. These results suggest that elevated GTP levels disrupt the interaction of GTP-binding proteins with 5′-pppG dsRNA, which may act to suppress RIG-I recognition under normal conditions.

In summary, our results show that dsRNAs bearing 5′-pppA more effectively stimulate RIG-I–mediated innate immune responses than those with 5′-pppG. Furthermore, our data support a model in which GTP-binding proteins selectively interact with 5′-pppG dsRNA, thereby limiting its availability for RIG-I activation and modulating the overall immune response.

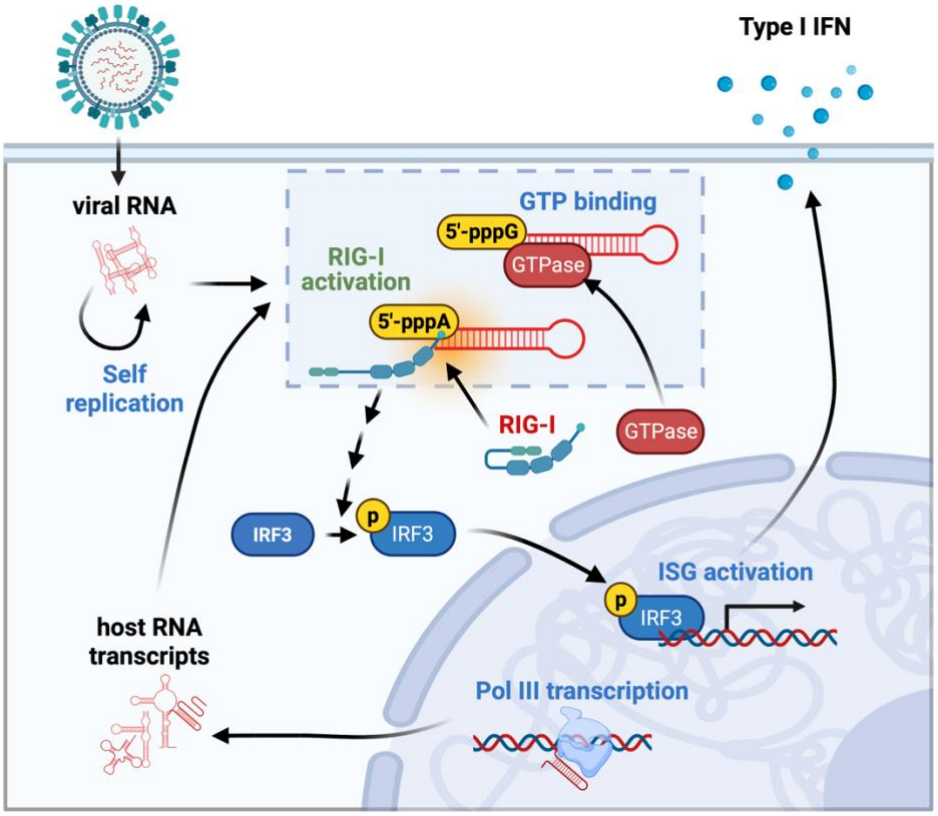

Figure 4. A model presenting a hypothesis of sequence-specific RNA sensing by RIG-I.

Reference – Manuscript 2:

Szymanski J.[*], Wolczyk M.[*], Trus I., Naz Z., Idlin N., Jackiewicz J., Nowak E., Wuebben C., Hartmann G., Rappsilber J., Michlewski G. 5′-triphosphate guanosine RNAs recruit GTP-binding proteins to suppress RIG-I/IFN type I signalling. *bioRxiv* (2025). DOI: https://doi.org/10.1101/2023.12.22.573000

[*]Authors contributed equally

4. Summary and future perspectives

My PhD research primarily focused on investigating the role of the 5′ terminal nucleotide of RNA in the innate immune response mediated by the RIG-I receptor. This topic was inspired by observations in the literature indicating that majority of RNA viruses initiate their genomes with 5′-pppA[75], whereas endogenous transcripts generated by RNA polymerase III typically begin with 5′-pppG[76,77]. Since the initial nucleotide in viral genomes has been shown to be impossible to modify (reference), my research was based on synthetic RNAs imitating native RIG-I agonists.

In the first manuscript, I explored role of 5′ terminal nucleotide on immunogenicity of ssRNA produced by IVT. Although, short RNAs forming not fully complementary panhandle structures were suspected to stimulate RIG-I mediated immune response, our studies showed that their immunogenic potential is mainly affected by the amount of dsRNA impurities produced during IVT reaction. Moreover, we revealed that dsRNA byproducts formation is highly dependent on initial nucleotide, where 5′-pppA increases the level of dsRNA content comparing to 5′-pppG.

Since IVT is the most widely used method for producing RNA therapeutics, our study provides new insights into designing RNA products with reduced immunogenicity. We demonstrated that the increased formation of dsRNA impurities associated with 5′-pppA-initiated transcripts prevailed in longer RNA molecules, such as mRNAs. As shown in our study, currently approved mRNA COVID-19 vaccines differ in their 5′ terminal nucleotide: the Moderna vaccine, which begins with guanosine (G), contains less dsRNA than the BioNTech vaccine, which starts with adenosine (A)[78,79]. This highlights that the knowledge gained from our study may contribute to the optimization and development of future mRNA-based therapeutics. While in the context of antiviral vaccines, dsRNA contamination may be beneficial by acting as an adjuvant and enhancing the immune response to the expressed antigen, in other applications such as mRNA-based cancer therapies or protein replacement therapies, minimizing immunogenicity is critical for therapeutic efficacy.

Notably, our research focused on RNAs containing a 5′-triphosphate moiety, the transcripts used in our experiments did not include a 5′ cap structure, which is essential for mRNA therapeutics. However, enzymatic capping strategy is applied post IVT reaction, another method introducing cap co-transcriptionally with dinucleotide “primer” may affect production of dsRNAs during IVT reaction. Thus, further analysis should be performed, whether 5′ terminal nucleotide of co-transcriptionally introduced cap affects dsRNA formation.

Furthermore, the development of improved RNA therapeutic manufacturing methods includes engineering RNA polymerase variants that generate fewer dsRNA byproducts. Since our study utilized only the wild-type T7 RNA polymerase, future research should explore whether

engineered T7 variants alter the relationship between the 5′ terminal nucleotide and dsRNA production, to better inform strategies for minimizing immunogenicity in mRNA therapeutics.

Since the results presented in the first manuscript demonstrated that ssRNA produced via IVT is largely unsuitable for investigating the impact of the 5′ terminal nucleotide on RIG-I stimulation, we developed a new strategy using chemically synthesized or IVT-generated dsRNA as defined RIG-I agonists. This strategy avoids the issue of dsRNA impurities commonly associated with IVT, and by using this approach, we showed that dsRNA bearing 5′-pppA induces a stronger RIG-I-mediated innate immune response than dsRNA with 5′-pppG. However, observed effect is saturated in higher concentrations of dsRNA, those low concentrations of dsRNA agonists can mimic native condition of early stages of viral infection, when viral RNA is detected with RIG-I receptor.

Moreover, an in-depth investigation of the dsRNA interactome led us to propose a novel hypothetical mechanism for sequence-specific RNA recognition by RIG-I. Interestingly, the discrimination of the 5′ terminal nucleotide does not result from a direct interaction between dsRNA and the RIG-I protein itself but rather appears to be mediated by additional cellular factors. In our model, GTPases and GTP-binding proteins selectively interact with dsRNA containing a 5′-pppG moiety, thereby inhibiting the innate immune response by interfering with RIG-I activation. Notably, recent studies have shown that GTP-binding affinities are typically over 1000-fold higher than those for ATP[80], which may explain why GTP-binding proteins can interfere with RIG-I recognition of 5′-pppG dsRNA, while 5′-pppA-containing dsRNA remains unaffected.

This proposed mechanism not only accounts for the conservation of 5′-pppG in RNA polymerase III transcripts and in some pathogenic RNA viruses as a means of evading RIG-I mediated immune detection but also aligns with broader observations of nucleotide metabolism during viral infection. While previous studies have shown that viral infections can increase the levels of nucleotide precursors through host mRNA degradation and the nucleotide salvage pathway[81], our findings suggest that elevated GTP levels may actually enhance the RIG-I/IFN pathway by saturating GTP-binding proteins, thereby reducing their ability to inhibit RIG-I activation.

Given that our studies on the sequence-specificity of RIG-I–mediated innate immunity were conducted exclusively using synthetic RNAs, further investigations involving more native ligands are necessary. Although viral RNA genomes are inherently difficult to manipulate, future studies could focus on mutating the 5′ terminal nucleotide of endogenous RNA polymerase III transcripts to explore their impact on RIG-I activation.

Furthermore, our findings open a new avenue for therapeutic development, specifically, by targeting the masking interaction between GTP-binding proteins and viral RNAs or endogenous RIG-I agonists. Future experiments could assess whether disruption of these GTP-

binding proteins enhances innate immune responses during viral infection and contributes to viral inhibition.

Summing up, the research presented in this dissertation uncovered a critical role of the 5′ terminal nucleotide in shaping RNA immunogenicity. By focusing on the RIG-I receptor as a key component of innate immunity, my work bridges two important areas of biomedical science – fundamental RNA biology, including the mechanisms by which the immune system differentiates between host and viral RNA, and translational research aimed at improving IVT methods for mRNA therapeutics. Ultimately, this research advances for both – understanding of RIG-I biology and opening new directions for improving RNA therapeutics and antiviral strategies.

5. Bibliography

1. World Health Organization (WHO). https://www.who.int.
2. Tyrrell, C. SB., Allen, J. L. Y. & Gkrania-Klotsas, E. Influenza: epidemiology and hospital management. *Med. Abingdon Engl. UK Ed* **49**, 797–804 (2021).
3. Chung, Y.-S., Lam, C.-Y., Tan, P.-H., Tsang, H.-F. & Wong, S.-C. C. Comprehensive Review of COVID-19: Epidemiology, Pathogenesis, Advancement in Diagnostic and Detection Techniques, and Post-Pandemic Treatment Strategies. *Int. J. Mol. Sci.* **25**, 8155 (2024).
4. Takeuchi, O. & Akira, S. Pattern Recognition Receptors and Inflammation. *Cell* **140**, 805–820 (2010).
5. Kawai, T. & Akira, S. The role of pattern-recognition receptors in innate immunity: update on Toll-like receptors. *Nat. Immunol.* **11**, 373–384 (2010).
6. Fitzgerald, K. A. & Kagan, J. C. Toll-like Receptors and the Control of Immunity. *Cell* **180**, 1044–1066 (2020).
7. Jensen, S. & Thomsen, A. R. Sensing of RNA Viruses: a Review of Innate Immune Receptors Involved in Recognizing RNA Virus Invasion. *J. Virol.* **86**, 2900–2910 (2012).
8. Said, E. A., Tremblay, N., Al-Balushi, M. S., Al-Jabri, A. A. & Lamarre, D. Viruses Seen by Our Cells: The Role of Viral RNA Sensors. *J. Immunol. Res.* **2018**, 9480497 (2018).
9. Alexopoulou, L., Holt, A. C., Medzhitov, R. & Flavell, R. A. Recognition of double-stranded RNA and activation of NF-kappaB by Toll-like receptor 3. *Nature* **413**, 732–738 (2001).
10. Bell, J. K., Askins, J., Hall, P. R., Davies, D. R. & Segal, D. M. The dsRNA binding site of human Toll-like receptor 3. *Proc. Natl. Acad. Sci. U. S. A.* **103**, 8792–8797 (2006).
11. M, T., F, N., T, S. & M, M. Toll-like receptor 3 recognizes incomplete stem structures in single-stranded viral RNA. *Nat. Commun.* **4**, (2013).
12. Diebold, S. S., Kaisho, T., Hemmi, H., Akira, S. & Reis e Sousa, C. Innate antiviral responses by means of TLR7-mediated recognition of single-stranded RNA. *Science* **303**, 1529–1531 (2004).
13. Heil, F. *et al.* Species-specific recognition of single-stranded RNA via toll-like receptor 7 and 8. *Science* **303**, 1526–1529 (2004).
14. Akira, S. & Takeda, K. Toll-like receptor signalling. *Nat. Rev. Immunol.* **4**, 499–511 (2004).
15. Jensen, S. & Thomsen, A. R. Sensing of RNA Viruses: a Review of Innate Immune Receptors Involved in Recognizing RNA Virus Invasion. *J. Virol.* **86**, 2900–2910 (2012).
16. Kang, D. *et al.* mda-5: An interferon-inducible putative RNA helicase with double-stranded RNA-dependent ATPase activity and melanoma growth-suppressive properties. *Proc. Natl. Acad. Sci. U. S. A.* **99**, 637–642 (2002).
17. Yoneyama, M. *et al.* The RNA helicase RIG-I has an essential function in double-stranded RNA-induced innate antiviral responses. *Nat. Immunol.* **5**, 730–737 (2004).

18.Fitzgerald, M. E., Rawling, D. C., Vela, A. & Pyle, A. M. An evolving arsenal: viral RNA detection by RIG-I-like receptors. *Curr. Opin. Microbiol.* **20**, 76–81 (2014).

19.Liu, G. *et al.* Nuclear-resident RIG-I senses viral replication inducing antiviral immunity. *Nat. Commun.* **9**, 3199 (2018).

20.Fuller-Pace, F. V. DExD/H box RNA helicases: multifunctional proteins with important roles in transcriptional regulation. *Nucleic Acids Res.* **34**, 4206–4215 (2006).

21.Takahasi, K. *et al.* Solution Structures of Cytosolic RNA Sensor MDA5 and LGP2 C-terminal Domains: IDENTIFICATION OF THE RNA RECOGNITION LOOP IN RIG-I-LIKE RECEPTORS *. *J. Biol. Chem.* **284**, 17465–17474 (2009).

22.Yoneyama, M. *et al.* The RNA helicase RIG-I has an essential function in double-stranded RNA-induced innate antiviral responses. *Nat. Immunol.* **5**, 730–737 (2004).

23.Andrejeva, J. *et al.* The V proteins of paramyxoviruses bind the IFN-inducible RNA helicase, mda-5, and inhibit its activation of the IFN-β promoter. *Proc. Natl. Acad. Sci. U. S. A.* **101**, 17264–17269 (2004).

24.Hornung, V. *et al.* 5'-Triphosphate RNA is the ligand for RIG-I. *Science* **314**, 994–997 (2006).

25.Schlee, M. *et al.* Recognition of 5′-triphosphate by RIG-I helicase requires short blunt double-stranded RNA as contained in panhandle of negative strand virus. *Immunity* **31**, 25–34 (2009).

26.Schmidt, A. *et al.* 5′-triphosphate RNA requires base-paired structures to activate antiviral signaling via RIG-I. *Proc. Natl. Acad. Sci. U. S. A.* **106**, 12067–12072 (2009).

27.Kato, H. *et al.* Length-dependent recognition of double-stranded ribonucleic acids by retinoic acid–inducible gene-I and melanoma differentiation–associated gene 5. *J. Exp. Med.* **205**, 1601–1610 (2008).

28.Peisley, A. *et al.* Kinetic mechanism for viral dsRNA length discrimination by MDA5 filaments. *Proc. Natl. Acad. Sci.* **109**, E3340–E3349 (2012).

29.Rehwinkel, J. & Gack, M. U. RIG-I-like receptors: their regulation and roles in RNA sensing. *Nat. Rev. Immunol.* **20**, 537–551 (2020).

30.Thoresen, D. *et al.* The molecular mechanism of RIG-I activation and signaling. *Immunol. Rev.* **304**, 154–168 (2021).

31.Pippig, D. A. *et al.* The regulatory domain of the RIG-I family ATPase LGP2 senses double-stranded RNA. *Nucleic Acids Res.* **37**, 2014–2025 (2009).

32.Rothenfusser, S. *et al.* The RNA Helicase Lgp2 Inhibits TLR-Independent Sensing of Viral Replication by Retinoic Acid-Inducible Gene-I1. *J. Immunol.* **175**, 5260–5268 (2005).

33.Venkataraman, T. *et al.* Loss of DExD/H box RNA helicase LGP2 manifests disparate antiviral responses. *J. Immunol. Baltim. Md 1950* **178**, 6444–6455 (2007).

34.Almeida-da-Silva, C. L. C., Savio, L. E. B., Coutinho-Silva, R. & Ojcius, D. M. The role of NOD-like receptors in innate immunity. *Front. Immunol.* **14**, (2023).

35.Girardin, S. E. *et al.* Nod2 Is a General Sensor of Peptidoglycan through Muramyl Dipeptide (MDP) Detection *. *J. Biol. Chem.* **278**, 8869–8872 (2003).

36.Sabbah, A. *et al.* Activation of innate immune antiviral response by NOD2. *Nat. Immunol.* **10**, 1073–1080 (2009).

37.Manche, L., Green, S. R., Schmedt, C. & Mathews, M. B. Interactions between double-stranded RNA regulators and the protein kinase DAI. *Mol. Cell. Biol.* **12**, 5238–5248 (1992).

38.Zhang, F. *et al.* Binding of double-stranded RNA to protein kinase PKR is required for dimerization and promotes critical autophosphorylation events in the activation loop. *J. Biol. Chem.* **276**, 24946–24958 (2001).

39.Lemaire, P. A., Anderson, E., Lary, J. & Cole, J. L. Mechanism of PKR Activation by dsRNA. *J. Mol. Biol.* **381**, 351–360 (2008).

40.Mathews, M. B. Viral evasion of cellular defense mechanisms: regulation of the protein kinase DAI by RNA effectors. *Semin. Virol.* **4**, 247–257 (1993).

41.Goubau, D. *et al.* Antiviral immunity via RIG-I-mediated recognition of RNA bearing 5′-diphosphates. *Nature* **514**, 372–375 (2014).

42.de Regt, A. K. *et al.* A conserved isoleucine in the binding pocket of RIG-I controls immune tolerance to mitochondrial RNA. *Nucleic Acids Res.* **51**, 11893–11910 (2023).

43.Schuberth-Wagner, C. *et al.* A Conserved Histidine in the RNA Sensor RIG-I Controls Immune Tolerance to N1-2'O-Methylated Self RNA. *Immunity* **43**, 41–51 (2015).

44.Luo, D. *et al.* Structural insights into RNA recognition by RIG-I. *Cell* **147**, 409–422 (2011).

45.Kohlway, A., Luo, D., Rawling, D. C., Ding, S. C. & Pyle, A. M. Defining the functional determinants for RNA surveillance by RIG-I. *EMBO Rep.* **14**, 772–779 (2013).

46.Linehan, M. M. *et al.* A minimal RNA ligand for potent RIG-I activation in living mice. *Sci. Adv.* **4**, e1701854 (2018).

47.te Velthuis, A. J. W. *et al.* Mini viral RNAs act as innate immune agonists during influenza virus infection. *Nat. Microbiol.* **3**, 1234–1242 (2018).

48.Patel, J. R. *et al.* ATPase-driven oligomerization of RIG-I on RNA allows optimal activation of type-I interferon. *EMBO Rep.* **14**, 780–787 (2013).

49.Schlee, M. *et al.* Recognition of 5′-triphosphate by RIG-I helicase requires short blunt double-stranded RNA as contained in panhandle of negative strand virus. *Immunity* **31**, 25–34 (2009).

50.Schlee, M. & Hartmann, G. The Chase for the RIG-I Ligand—Recent Advances. *Mol. Ther.* **18**, 1254–1262 (2010).

51.Ren, X., Linehan, M. M., Iwasaki, A. & Pyle, A. M. RIG-I Recognition of RNA Targets: The Influence of Terminal Base Pair Sequence and Overhangs on Affinity and Signaling. *Cell Rep.* **29**, 3807-3815.e3 (2019).

52.Parhiz, H., Atochina-Vasserman, E. N. & Weissman, D. mRNA-based therapeutics: looking beyond COVID-19 vaccines. *The Lancet* **403**, 1192–1204 (2024).

53. Dousis, A., Ravichandran, K., Hobert, E. M., Moore, M. J. & Rabideau, A. E. An engineered T7 RNA polymerase that produces mRNA free of immunostimulatory byproducts. *Nat. Biotechnol.* **41**, 560–568 (2023).

54. Tang, G.-Q. & Patel, S. S. Rapid binding of T7 RNA polymerase is followed by simultaneous bending and opening of the promoter DNA. *Biochemistry* **45**, 4947–4956 (2006).

55. Bandwar, R. P. *et al.* The Transition to an Elongation Complex by T7 RNA Polymerase Is a Multistep Process. *J. Biol. Chem.* **282**, 22879–22886 (2007).

56. Durniak, K. J., Bailey, S. & Stetiz, T. A. The Structure of a Transcribing T7 RNA Polymerase Complex Captured During Its Transition from Initiation to Elongation. *Science* **322**, 553–557 (2008).

57. Martin, C. T., Muller, D. K. & Coleman, J. E. Processivity in early stages of transcription by T7 RNA polymerase. *Biochemistry* **27**, 3966–3974 (1988).

58. Lyakhov, D. L. *et al.* Pausing and termination by bacteriophage T7 RNA polymerase. *J. Mol. Biol.* **280**, 201–213 (1998).

59. Song, H. & Kang, C. Sequence-specific termination by T7 RNA polymerase requires formation of paused conformation prior to the point of RNA release. *Genes Cells Devoted Mol. Cell. Mech.* **6**, 291–301 (2001).

60. Triana-Alonso, F. J., Dabrowski, M., Wadzack, J. & Nierhaus, K. H. Self-coded 3'-extension of run-off transcripts produces aberrant products during in vitro transcription with T7 RNA polymerase. *J. Biol. Chem.* **270**, 6298–6307 (1995).

61. Cazenave, C. & Uhlenbeck, O. C. RNA template-directed RNA synthesis by T7 RNA polymerase. *Proc. Natl. Acad. Sci. U. S. A.* **91**, 6972–6976 (1994).

62. Mu, X., Greenwald, E., Ahmad, S. & Hur, S. An origin of the immunogenicity of in vitro transcribed RNA. *Nucleic Acids Res.* **46**, 5239–5249 (2018).

63. Mu, X. & Hur, S. Immunogenicity of In Vitro-Transcribed RNA. *Acc. Chem. Res.* **54**, 4012–4023 (2021).

64. Lenk, R. *et al.* Understanding the impact of in vitro transcription byproducts and contaminants. *Front. Mol. Biosci.* **11**, 1426129 (2024).

65. Siew, Y. Y. & Zhang, W. Removing immunogenic double-stranded RNA impurities post *in vitro* transcription synthesis for mRNA therapeutics production: A review of chromatography strategies. *J. Chromatogr. A* **1740**, 465576 (2025).

66. Piao, X. *et al.* Double-stranded RNA reduction by chaotropic agents during in vitro transcription of messenger RNA. *Mol. Ther. Nucleic Acids* **29**, 618–624 (2022).

67. Ziegenhals, T. *et al.* Formation of dsRNA by-products during in vitro transcription can be reduced by using low steady-state levels of UTP. *Front. Mol. Biosci.* **10**, 1291045 (2023).

68. Kormann, M. S. D. *et al.* Expression of therapeutic proteins after delivery of chemically modified mRNA in mice. *Nat. Biotechnol.* **29**, 154–157 (2011).

69. Durbin, A. F., Wang, C., Marcotrigiano, J. & Gehrke, L. RNAs Containing Modified Nucleotides Fail To Trigger RIG-I Conformational Changes for Innate Immune Signaling. *mBio* **7**, e00833-16 (2016).

70. Dousis, A., Ravichandran, K., Hobert, E. M., Moore, M. J. & Rabideau, A. E. An engineered T7 RNA polymerase that produces mRNA free of immunostimulatory byproducts. *Nat. Biotechnol.* **41**, 560–568 (2023).

71. Gardner, L. P., Mookhtiar, K. A. & Coleman, J. E. Initiation, Elongation, and Processivity of Carboxyl-Terminal Mutants of T7 RNA Polymerase. *Biochemistry* **36**, 2908–2918 (1997).

72. Wu, M. Z., Asahara, H., Tzertzinis, G. & Roy, B. Synthesis of low immunogenicity RNA with high-temperature in vitro transcription. *RNA* **26**, 345–360 (2020).

73. Naesens, L., Haerynck, F. & Gack, M. U. The RNA polymerase III-RIG-I axis in antiviral immunity and inflammation. *Trends Immunol.* **44**, 435–449 (2023).

74. Vabret, N. *et al.* Y RNAs are conserved endogenous RIG-I ligands across RNA virus infection and are targeted by HIV-1. *iScience* **25**, 104599 (2022).

75. Schlee, M. Master sensors of pathogenic RNA - RIG-I like receptors. *Immunobiology* **218**, 1322–1335 (2013).

76. Ma, H. *et al.* Pol III Promoters to Express Small RNAs: Delineation of Transcription Initiation. *Mol. Ther. Nucleic Acids* **3**, e161 (2014).

77. Gao, Z., Harwig, A., Berkhout, B. & Herrera-Carrillo, E. Mutation of nucleotides around the +1 position of type 3 polymerase III promoters: The effect on transcriptional activity and start site usage. *Transcription* **8**, 275–287 (2017).

78. Vogel, A. B. *et al.* BNT162b vaccines protect rhesus macaques from SARS-CoV-2. *Nature* **592**, 283–289 (2021).

79. Fang, E. *et al.* Advances in COVID-19 mRNA vaccine development. *Signal Transduct. Target. Ther.* **7**, 94 (2022).

80. Bexley, K. *et al.* Metabolic tuning enables immediate adaptation to energy stress in yeast. 2025.06.06.658098 Preprint at https://doi.org/10.1101/2025.06.06.658098 (2025).

81. Nouwen, L. V. *et al.* Modulation of nucleotide metabolism by picornaviruses. *PLoS Pathog.* **20**, e1012036 (2024).

Appendix 1.

Manuscript 1

Wolczyk M.[*], **Szymanski J.**[*], Trus I.[*], Naz Z., Tame T., Bolembach A., Choudhury N.R., Kasztelan K., Rappsilber J., Dziembowski A., Michlewski G. 5' terminal nucleotide determines the immunogenicity of IVT RNAs. *Nucleic Acids Res.* (2025). DOI: 10.1093/nar/gkae1252.

[*]Authors contributed equally

Nucleic Acids Research, 2025, **53**, gkae1252
https://doi.org/10.1093/nar/gkae1252
Advance access publication date: 19 December 2024
RNA and RNA-protein complexes

5′ terminal nucleotide determines the immunogenicity of IVT RNAs

Magdalena Wolczyk[1,†], Jacek Szymanski[1,†], Ivan Trus[1,†], Zara Naz[1], Tola Tame[1], Agnieszka Bolembach[1], Nila Roy Choudhury[1,2], Karolina Kasztelan[1], Juri Rappsilber[3], Andrzej Dziembowski[1] and Gracjan Michlewski[1,*]

[1]International Institute of Molecular and Cell Biology in Warsaw, Ksiecia Trojdena 4, 02-109 Warsaw, Poland
[2]MRC Human Genetics Unit, Institute of Genetics and Cancer, University of Edinburgh, Western General Hospital, Crewe Road South, EH4 1QY Edinburgh, UK
[3] Institute of Biotechnology, Technische Universität Berlin, Gustav-Meyer-Allee 25, 13355 Berlin, Germany

[*]To whom correspondence should be addressed. Tel: +48 22 597 0773; Email: gmichlewski@iimcb.gov.pl
[†]These authors contributed equally to this work.

Abstract

In vitro transcription (IVT) is a technology of vital importance that facilitated the production of mRNA therapeutics and drove numerous breakthroughs in RNA biology. T7 polymerase-produced RNAs can begin with either 5′-triphosphate guanosine (5′-pppG) or 5′-triphosphate adenosine (5′-pppA), generating potential agonists for the RIG-I/type I interferon response. While it is established that IVT can yield highly immunogenic double-stranded RNA (dsRNA) via promoterless transcription, the specific contribution of initiating nucleosides to this process has not been previously reported. Our study shows that IVT-derived RNAs containing 5′-pppA are significantly more immunogenic compared with their 5′-pppG counterparts. We observed heightened levels of dsRNAs triggered by IVT with 5′-pppA RNA, activating the RIG-I signaling pathway in cultured cells, as well as in *ex vivo* and *in vivo* mouse models, where the IFN-β gene was substituted with the mKate2 fluorescent reporter. Elevated levels of dsRNA were found in both short and long 5′-pppA RNAs, including those of COVID-19 vaccines. These findings reveal the unexpected source of IVT RNA immunogenicity, offering valuable insights for both academic research and future medical applications of this technology.

Graphical abstract

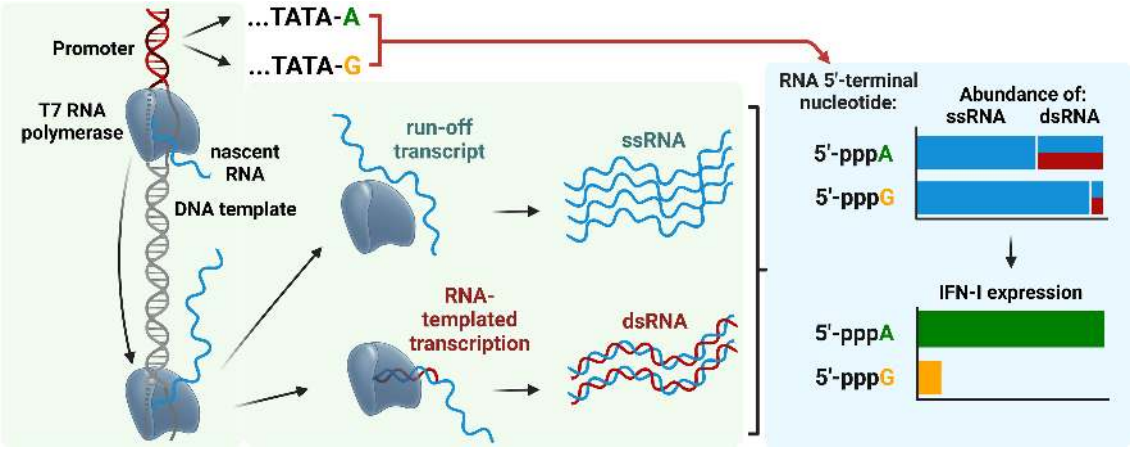

Introduction

The innate immune system of higher eukaryotes is the first line of defense against invading pathogens, including viruses. Pathogen-Associated Molecular Patterns (PAMPs), which are recognized by cellular Pattern Recognition Receptors (PRRs), are shared between viral as well as endogenous RNAs. The 5′-triphosphate (5′-ppp) moiety is an important PAMP, present in many viral RNAs and endogenous polymerase III (Pol III) transcripts (1,2). Highly structured RNAs with 5′-ppp bind to Retinoic Acid Inducible Gene I (RIG-I/DDX58) PRR, provoking its conformational change and K63 ubiquitination by E3 ubiquitin ligase RIPLET (3,4), triggering a signaling cascade that culminates in phosphorylation of IRF3, IRF7 and NF-κB transcription factors (5). Upon activation, transcription factors translocate into the nucleus, initiating the expression of type I interferon (IFN), which in turn triggers an innate

Received: May 31, 2024. **Revised:** December 3, 2024. **Editorial Decision:** December 4, 2024. **Accepted:** December 6, 2024

immune response. This response involves the upregulation of numerous interferon-stimulated genes (ISGs) (6) and is crucial for antiviral activity, but when overstimulated can lead to inflammation and autoimmune diseases (7).

The most potent activators of RIG-I are short, blunt, double-stranded RNAs (dsRNAs) capped with 5′-ppp or 5′-pp moieties (8–11). The 5′-terminal nucleotide must remain unmethylated at its 2′-O position to be recognized by RIG-I (12). dsRNAs with short 3′ overhangs or bulge loops can also serve as potent RIG-I ligands (9). Synthetic dsRNAs, including RNA duplexes and stem loop RNAs, with as few as 10 base pairs, have been also shown to activate RIG-I (13,14). Finally, investigations into immunogenic RNAs during influenza A virus (IAV) infection have identified 5′-ppp single-stranded genomic RNAs (ssRNAs) (15) as well as 80-nucleotide long mini viral RNAs (16) as effective stimulators for the RIG-I/IFN pathway.

In vitro transcription (IVT) employing T7 polymerase serves various purposes, including RNA production for research, mRNA-based drugs and vaccines (17,18). However, it introduces a 5′-ppp moiety that can activate the RIG-I/IFN pathway (19) and IFN-induced proteins with tetratricopeptide repeats 1 and 5 (IFIT1 and IFIT5 proteins) (20–22). Notably, IVT can also generate unintended dsRNA byproducts from random priming of abortive transcripts (23), turnaround transcription of run-off transcripts (24) or via promoterless transcription from sense strand of RNA or antisense strand of template DNA (19,25–27). Cellular response to those dsRNAs can result in undesirable suppression of protein synthesis and cell death, which in turn can drastically reduce the efficacy of mRNA therapies. Such dsRNA byproducts require complex purification processes and strategies to make the IVT less immunogenic, including purification by reversed-phase HPLC (28), cellulose fibers-mediated removal of dsRNAs (29) or incorporation of N1-methylpseudouridine (1mΨ) (30,31).

There are several classes of T7 promoters (32). Class III promoters, the most used, favor the incorporation of guanosine (G), while class II promoters facilitate efficient initiation from adenosine (A) or adenosine-containing coenzymes (33). Crucially, the ability to integrate either 5′-pppG or 5′-pppA by T7 polymerase has been leveraged in the production of SARS-CoV-2 mRNA vaccines. Moderna incorporated Cap1 enzymatically on the 5′-pppG-containing IVT RNAs (33), while BioNTech employed co-transcriptional addition of an AG-trinucleotide Cap1 analog (CleanCap) (34). However, even the most advanced capping protocols leave a fraction of uncapped, immunogenic 5′-ppp RNA (35). Although widely utilized in medicine and research, the impact of different 5′ nucleosides on the immunogenicity and purity of IVT RNAs has not been investigated.

Here, we demonstrate that despite their similar structures, IVT RNAs originating from 5′-pppA exhibit significantly higher immunogenicity compared to those originating from 5′-pppG. This difference was observed across human and mouse cultured cells and was further validated in our novel mouse model, where the IFN-β gene was replaced with the mKate2 fluorescent reporter. The activation of innate immunity by 5′-pppA RNAs relied on both RIG-I and the presence of 5′-ppp. Unexpectedly, our findings revealed that IVT reactions initiated with 5′-pppA generate significantly greater levels of highly immunogenic, blunt-end dsRNAs, compared to their 5′-pppG counterparts. Elevated amounts of dsRNA were detected in short 5′-pppA RNAs and full-length mRNAs, including erythropoietin (EPO) mRNA and COVID-19 vaccine mRNA harbouring the complete sequence of the spike protein, where terminal adenosine was employed during IVT reaction. This has significant implications for understanding the immunogenicity of IVT RNAs, existing mRNA medicines and their future development.

Materials and methods

Production of RNA with IVT reaction

RNA transcripts representing both viral and host origin, were prepared using IVT reaction (Supplementary Table S1). RNA representing miniviral RNA (36) was derived by truncating 76 nucleotides from segment 8th of the IAV genome (GenBank: NC_002020.1). Short non-coding Y5 RNA (84 nucleotides; GenBank: NR_001571.2) was representing the host RNA.

The transcription template was first amplified using the High-Fidelity Phusion DNA Polymerase (Thermo #F530L) and primers (Supplementary Table S2) appending T7 Class III (TAATACGACTCACTATA) or ϕ2.5 Class II (TAATACGACTCACTATT) promoter sequence to produce 5′-pppA RNA or 5′-pppG RNAs, respectively. (37) Subsequent IVT reaction producing 5′-triphosphorylated RNAs was performed with NxGen T7 RNA Polymerase (Biosearch Technologies #30223–1). Then RNA was precipitated with 3 M Sodium Acetate (pH 5.1) and 100% EtOH, washed with 100% EtOH and resuspended in UP water. The RNA in 2 × loading buffer (7 M urea, bromophenol blue, and xylene cyanol) was then run on a denaturing polyacrylamide gel (10% polyacrylamide, 7.5 M urea in 1 × TBE) for 2 h. RNA was stained with Stains-all (Sigma-Aldrich #E9379) and bands of a specific size corresponding to respective RNA were excised with individual scalpel blades. Then RNA was extracted (0.3 M Sodium Acetate pH 5.2; 0.5 mM EDTA; 0.1% SDS) and precipitated again. RNA was washed with 100% EtOH, resuspended in UP water and filtered on Spin-X Centrifuge Tube Filters (Costar #8160) to remove remaining gel residues. RNA concentrations were assessed with NanoDrop and adjusted to 50 ng/μl. RNA was aliquoted and stored at -80°C. Denaturing PAGE/urea gel electrophoresis was repeated to confirm that no extra bands were observed in the final RNA preparation. Dephosphorylated RNA was produced with FastAP enzyme (Thermo #EF0654) and cleaned using column purification (Invitek Invisorb Spin Virus RNA Mini Kit). The 3p-hpRNA at a concentration of 100 ng/ml (InvivoGen #tlrl-hprna) or no RNA were used as positive and negative controls, respectively.

Splint ligation

RNA was produced by ligation of *in vitro* transcribed 5′ acceptor RNA fragment with chemically produced 3′ donor RNA containing 5′ monophosphate essential for ligase activity using T4 Ligase 2 (NEB #M0239S). Additionally, the ssDNA fragment complementary to the 3′ end of the acceptor and the 5′ end of the donor was used as a splint to increase the specificity of ligation. Ligation was performed according to the manufacturer protocol for the T4 Ligase 2 enzyme. Ligated RNA was precipitated and purified from PAGE/urea gel with the procedure described in the IVT reaction section.

Production of dsRNA

Fully complementary RNA strands were produced with IVT or splint ligation reaction described above. The sequences and primers are listed in the Supplementary Tables S1 and S2. Equal quantities of sense and antisense strands were mixed in a refolding buffer (0.1 M Tris-HCl pH 7.5, 0.1 M NaCl, 5 mM $MgCl_2$) and incubated at + 80°C for 10 min and then at room temperature for 30 min. dsRNA was placed in tubes on ice and then used for further experiments.

Native polyacrylamide gel electrophoresis

For native polyacrylamide gel electrophoresis, a native gel loading buffer (1 mM Tris-HCl pH 7.5, 5% glycerol, 0.001% bromophenol blue) was added to the samples and mixed. The mixtures were overlaid on a non-denaturing 12% polyacrylamide gel (prerun step was performed at 8 W for 45 min at + 4°C). After electrophoresis at 8 W for 120 min at + 4°C, the gels were stained with SYBR Gold nucleic acid gel stain (Invitrogen #S11494). Imaging was performed with a Chemidoc MP (Bio-Rad Laboratories).

Cell culture

Murine bone marrow cells and fibroblasts were obtained from C57BL6J/Rj mice as previously described (38,39). Bone marrow cells were cultured with 20 ng/ml of macrophage colony-stimulating factor (BioLegend #576404) for 7 days as previously described (39) to generate BMDMs. Human A549, HEK293, THP-1, Calu1, HEK-Blue IFN-α/β cells, and murine MEF, BMDM, primary fibroblasts, B16-Blue IFN-α/β cells were maintained in Dulbecco's Modified Eagle's Medium (DMEM; Gibco #32430) supplemented with 10% fetal bovine serum (Gibco #10270–106). HEK-Blue IFN-α/β were cultured with 100 μg/ml Zeocine (InvivoGen #ant-zn-1) and 30 μg/ml Blasticidine (InvivoGen #ant-bl-05). B16-Blue IFN-α/β cells were supplemented with 100 μg/ml of Zeocine only. Primary cell cultures (fibroblasts and BMDMs) were established in presence of 1 × Penicillin-Streptomycin (Gibco #15140122) and 0.1 mg/ml Gentamicin (Gibco #15710064). Cells were cultured at + 37°C in a 5% CO_2 humidified incubator. The list of cell lines used is provided in Supplementary Table S3.

Transfection of RNAs in cell culture

Cells were seeded in a 12-well plate at a concentration of 0.3–0.7 × 10^6 cells per well and incubated for 24–48 h. RNA was mixed with Lipofectamine: (100 ng RNA was prediluted in 125 μl of OptiMEM (Gibco #11058), then 2 μl of Lipofectamine 2000 (Invitrogen #11668) prediluted in 125 μl of OptiMEM was added) and after incubation at RT for 30 min 750 μl of cell culture medium was added. Leading to a final concentration of 100 ng RNA per ml of medium. RNA with medium was added to cells and incubated for 8 h (A549) or 24 h (HEK293, THP-1, Calu1, MEF, BMDM, primary fibroblasts). Supernatants and cell lysates in Roeder D Buffer (1.38 M glucose; 100 mM KCl, 2 mM EDTA; 100 mM Tris HCl pH 8; 0.2 mM PMSF and 12.5 mM DTT) were collected and processed either for IFN assay or western blot.

Infection with IAV

Firstly, HEK293 cells were seeded in a 48-well plate at a density of 10^5 cells per well in cell culture medium (DMEM supplemented with 10% heat-inactivated FBS). Secondly, after 24h of incubation (5% CO_2, 37°C), cells were transfected with 100 ng/ml of RNA representing a fragment of the IAV genome (short viral RNA) in 0.4 ml per well. Thirdly, after another 24 h of incubation (5% CO_2, 37°C), cells were washed with DMEM and inoculated with the NS1 mutant of the IAV (A/PR/8/34_NS1(R38A/K41A)) at an MOI of 0.0001 in 0.2 ml of medium (DMEM supplemented with 0.14% BSA). After 0.5 h of incubation (5% CO_2, 37°C), one ml of virus growth medium (DMEM supplemented with 0.14% BSA and 0.2 μg/ml TPCK-treated trypsin) was added, and cells were incubated with the virus (5% CO_2, 37°C). Around 50 μl of supernatant was collected at 0, 24, 48, 72 and 96 h and titrated with the endpoint dilution assay. Fifty percent cell culture infective dose (CCID50) endpoint titers were calculated by the Spearman–Kärber formula and expressed as a decimal logarithm.

HEK-blue type I IFN assay

Supernatants from murine cells (MEF, BMDM, primary fibroblasts) were processed with B16-Blue and from human (A549, HEK293, THP-1, Calu-1) with HEK-Blue cells-based assays in quadruplicates. Twenty μl of supernatants (undiluted or prediluted 1:7) were added to 50 000 of HEK-Blue or 100 000 of B16-Blue cells in a 96-well plate. A standard curve was generated in parallel by serial dilutions of recombinant IFN-β standard in DMEM (R&D Systems #8499-IF-010 and #8234-MB-010). After overnight incubation (24 h), 20 μl of supernatants were mixed with 180 μl of the working solution of the QUANTI-Blue reagent (InvivoGen #rep-qbs) and incubated at 37°C for 0.1–3 h. Absorbance was measured at 654 nm using a Tecan's Sunrise absorbance microplate reader. Blank values were subtracted from all wells and the 4PL standard curves were fitted to provide semiquantitative analyses of the IFN concentrations produced in the RNA-transfected cells (40,41).

For estimating the apparent dissociation constant (K_d), first, the optical density values for the blank wells were subtracted from the experimental data. In the colour reaction controlled by alkaline phosphatase, the optical density increased at higher RNA concentrations, and the data were fitted to a four-parameter (4PL) sigmoid curve model (OpticalDensity = Bottom + (Top - Bottom) / (1 + (K_d / RNAConcentration)^{Slope}) with one constraint applied (Bottom = 0). To identify outliers in the dataset, Robust regression and OUTlier removal algorithm (ROUT) was employed. The false discovery rate was set at a 1% level (Q = 1%) (42). To compare K_d values between different datasets, we applied the entropy maximization principle using Akaike's Information Criterion corrected for small sample size (AICc). The probability of a shared K_d value fitting both models was computed using the relative likelihood (Akaike's Probability = 1 - ($e^{\Delta AICc / 2}$ + 1)$^{-1}$).

Detection of dsRNAs in IVT-derived RNAs using dot blot analysis

RNAs were produced with IVT reaction and fully complementary strands were mixed in equal quantities to produce dsRNAs as described above. Refolded RNA was diluted to contain 2 μg, 200 ng, 20 ng, 2 ng or 0.2 ng in 5 μl for dot blotting. DNase I treated RNA was produced according to the protocol provided (Thermo # EN0521) and cleaned using column purification. RNA solution was spotted on a

positively charged nylon membrane (Invitrogen #AM10100) and each dot had an equal volume of 5 µl. The dots were air-dried and then crosslinked to the membrane using 120 mJ/cm2 UV (254 nm) light for 30 s. Membranes were briefly washed with PBS (Gibco #14 190) containing 0.1% Tween (Sigma-Aldrich #P9416). Membranes were then blocked for 2 h at room temperature with blocking solution that contained 50 µg/ml Sheared Salmon DNA (Thermo #AM9680), 5% non-fat milk wt:vol and 0.1 µl/ml RiboLock (Thermo #EO0381) in PBS-Tween. The blocked membranes were incubated with J2 antibody (Jena bioscience #RNT-SCI-10010200; 1/1000) diluted in PBS-Tween with 2% non-fat milk wt:vol overnight at + 4°C. Then, the membranes were washed three times with PBS-Tween, incubated with secondary antibodies (Polyclonal Goat Anti-Mouse Immunoglobulins/HRP, Agilent Dako #P0447, 1/2000) diluted in PBS-Tween with 2% non-fat milk wt:vol for 1 h at room temperature and washed three times with PBS-Tween. For the chemiluminescence reaction, peroxide ECL reagents (Bio-Rad #170–5061) were applied and then, the membranes were visualized using a Chemidoc MP (Bio-Rad Laboratories).

RNAs from Moderna and BioNTech SARS-CoV-2 vaccines were isolated by TRIzol™LS Reagent extraction (Invitrogen #10296028) according to the manufacturer's instructions and dissolved in nuclease-free water. The RNA utilized to generate the standard curve of the amount of dsRNA in SARS-CoV-2 vaccines RNAs was the dsRNA genome of bacteriophage Φ6 (kind gift from dr Krzysztof Skowronek, IIMCB). Φ6 dsRNA was diluted to contain 500, 250, 125, 63, 31 and 16 pg in 5 µl for dot blotting. SARS-CoV-2 vaccines RNAs were diluted to contain 400, 200, 100, 50, 25 and 13 ng in 5 µl for dot blotting. The RNAs were then processed in the same way as IVT-derived RNAs described above.

Standard curve generated by image analysis densitometry of fully complementary RNA was used to calculate the level of dsRNA contamination in IVT-derived RNAs.

dsRNA immuno-northern blot

Around 2 µg of ssRNAs or dsRNAs were subjected to non-denaturing polyacrylamide gel electrophoresis as described above. Then, RNA transfer to a positively charged nylon membrane was performed using a wet transfer apparatus. Cold 0.5 × TBE buffer was used as a transfer buffer. The RNA transferred to the membranes was then crosslinked to the membrane using 120 mJ/cm2 UV light for 30 s. Membranes were briefly washed with PBS-Tween and then blocked for 2 h at room temperature with blocking solution (50 µg/ml Sheared Salmon DNA, 5% non-fat milk wt:vol and 0.1 µl/ml RiboLock in PBS-Tween). The blocked membranes were incubated with J2 antibody (1/1000) diluted in PBS-Tween with 2% non-fat milk wt:vol overnight at + 4°C. Then, the membranes were washed three times with PBS-Tween, incubated with HRP-conjugated anti-mouse secondary antibody (1/2000) diluted in PBS-Tween with 2% non-fat milk wt:vol for 1 h at room temperature and washed three times with PBS-Tween. For the chemiluminescence reaction, peroxide ECL reagents were applied and then, the membranes were visualized using a Chemidoc MP.

Western blotting

Cell monolayers were washed once with ice-cold 1 × DPBS and resuspended in 50 µl of a Roeder D buffer (100 mM KCl, 20% (p/v) glycerol, 0.2 mM EDTA, 100 mM Tris HCl pH 8.0, 0.5 mM DTT, 0.2 mM PMSF). After vortexing, cells were sonicated with Diagenode's Bioruptor Pico sonication device for 10 min and centrifuged (16 000 × g, 5 min, +4°C). Supernatants were moved to pre-chilled low protein binding tubes and after quantifying protein concentration with NanoDrop stored at -80°C. Twenty to hundred µg of protein extract was mixed with 5 × SB buffer (250 mM Tris-HCl, 10% SDS, 50% glycerol, 250 mM DTT, 0.02% bromophenol blue) and resolved using a 10% gel. Proteins were transferred to nitrocellulose membranes (Amersham #10600007) using a wet transfer apparatus. Membranes were blocked with 1% Western Blocking Reagent (WBR; Roche #11 921681001) or 5% BSA in TBST buffer for 1 h at room temperature. Membranes stained for pIRF3 were blocked with 5% BSA in TBST buffer. The blocked membranes were incubated with primary antibodies diluted in 0.5% WBR in TBST overnight at + 4°C (Supplementary Table S4), washed three times with TBST, incubated with secondary antibodies diluted in 0.5% WBR in TBST for 1 h at room temperature (Polyclonal Goat Anti-Rabbit Immunoglobulins/HRP, Agilent Dako #P0448, 1/2000), washed three times with TBST. For the chemiluminescence reaction, peroxide ECL reagents (Bio-Rad #170–5061) were applied to each band and then, the membranes were visualized using a Chemidoc MP (Bio-Rad Laboratories).

SHAPE analysis

RNA was processed with the EclipseBio SHAPE Single RNA Kit according to manufacturer's instructions. Briefly, re-folded RNA molecules were probed with NAI (2-methylnicotinic acid imidazolide), a structure probing agent, or DMSO control. Then an adapter was ligated to the 3′ end of the RNA and during reverse transcription reaction NAI induced mutations in the produced cDNA. Later, PCR-amplified libraries were subjected to Illumina 100-bp single-ended sequencing. We processed two replicates for Y5 and three replicates for short viral RNAs. For each replicate of NAI and DMSO, the data underwent the following analysis: UMI extraction with *umi_tools*, quality, and adapter trimming with *cutadapt*, repetitive element removal, alignment to hg38 using the *STAR aligner*, and PCR deduplication with *umi_tools* (10 bp UMI sequence). The specific alignment parameters were like those used by ShapeMapper2 (43). To access coverage depth reads from DMSO-treated RNA samples were split into either negative or positive strands with *samtools* and analyzed with *bedtools*.

Next, mutations (mismatches, insertions, deletions) and coverages were counted with custom Python scripts to compute mutation rates per base. Finally, NAI and DMSO mutation rates were subtracted and scaled with the interquartile range, which is the raw reactivity divided by $1.5\times(Q_3\text{-}Q_1)$. With Q_3 and Q_1 being the 75th quartile and the 25th quartile of the raw reactivities per RNA. Reactivities for all bases with > 10 000 × coverage was reported.

Statistical comparison between reactivity profiles of two RNAs was conducted via the empirical Bayes (eBayes) t-test implemented in the Bioconductor package *limma* (44). Reactivity scores per replicate were square-root transformed. Next, a standard linear model was fitted, and a t-test was performed to identify positions where both RNA molecules have significantly different reactivity scores.

The eBayes method shrinks position-wise variances for the computation of t-statistics which effectively increases the degrees of freedom, and consequently, the power to identify significant differences. Finally, mean reactivity per RNA was plotted. $P < 0.001$ was considered statistically significant.

IFN-β/mKate2 mouse

A genetically modified mouse line was created in the Genome Engineering Unit at the International Institute of Molecular and Cell Biology (https://geu.iimcb.gov.pl/).

The mKate2 fluorescent marker nucleotides sequence, optimized for the mouse genome was inserted at the beginning of the IFN-β coding sequence [GenBank: NM_010510.2] using the CRISPR/*Cas9*-based methodology as previously described (45) (Supplementary Figure S5). Briefly, C57BL6J/Rj zygotes were microinjected with *Cas9* mRNA (25 ng/μl), sgRNA (GGUAGCAGCCGACACCAGCC; 12.5 ng/μl), and repair template dsDNA with 60 bp homology arms. To ensure proper transcription termination, two SV40 early mRNA polyadenylation signal sequences were added after the mKate2 sequence. An additional G > C mutation in the 5′ UTR was introduced to destroy the PAM sequence. Zygotes were surgically transferred to surrogate females and pups were screened by the PCR method using primers flanking the inserted sequence (forward primer: TGGGAAATTCCTCTGAGGCAG; reverse primer: AGGCAGTGTAACTCTTCTGCATC) and the presence of the correct insert (Supplementary Figure S5) was confirmed through Sanger sequencing. Founder mice were backcrossed with wild-type mice to get N1 generation animals. For routine genotyping, DNA from ear tips was extracted using the HotShot method (46), and a 3-primer method was used for PCR (forward primer: TGGGAAATTCCTCTGAGGCAG; reverse primer #1: AGGCAGTGTAACTCTTCTGCATC; reverse primer #2: TTACCGGTGGCCGAGCTTAC).

Mice were bred and maintained in the animal facilities of the IIMCB under standard conditions with the approval of the Polish Ministry of the Environment (decision #29/2023). The housing conditions in ventilated cages (Tecniplast #EM500) filled with wood chip bedding, enriched with nesting material, plastic houses, and cardboard tubes were in adherence with the Regulation of the Minister of Agriculture and Rural Development of 29 April 2022.

Mice were provided *ad libitum* with water and rodent feed (Altromin #1324TPF). The environmental conditions included a relative humidity of 45–65% and a room temperature of 20–24°C. The ventilation system ensured 75 air changes per hour for each cage. The lighting schedule followed a 12-h light/12-h dark cycle (lights on from 6:00 to 18:00).

Regular health monitoring was conducted at the IDEXX laboratory, and all animal procedures adhered to the guidelines of the EU Directive #2010/63/EU for animal experiments.

RNA encapsulation into lipid nanoparticles

Lipid mix composition (50:10:38.5:1.5 molar ratio of DLin-MC3-DMA:DSPC:Cholesterol:PEG2000-DMG) was composed as previously described (47). RNA was encapsulated with a vortex mixing method (3:1 vol:vol ratio of RNA to lipid) and the N/P ratio (cationic nitrogen groups from the ionizable lipid over anionic phosphate groups from the mRNA) was ∼3. Buffer was exchanged for 1 × DPBS and LNPs were concentrated by centrifugation on Amicon 50 kDa filter unit (Merck #UFC805024). Size distribution and polydispersity index were determined using dynamic light scattering on Zetasizer Ultra Red (Malvern) in PBS buffer at 25°C in backscatter mode. Encapsulation efficiency and concentration of mRNA entrapped in LNPs were determined using the Quant-iT Ribogreen RNA assay (Invitrogen #R11490) by comparing fluorescence intensities in the presence or absence of 0.1% (w/v) Triton X-100.

IV injection of RNA-LNP complexes in IFN-β/mKate2 reporter mice and preparing cell suspensions

The study protocol (#WAW2/124/2023) was approved by the 2nd Local Ethics Committee for Animal Experimentation in Warsaw. Randomly selected IFN-β/mKate2 heterozygous male animals over 6 weeks of age were intravenously injected with 100 μg/kg of RNA encapsulated into LNP-RNA complexes and resuspended in sterile 0.85% NaCl up to 60 μl. In 24 h, animals were euthanized with CO_2 and exsanguinated. The spleen and liver were extracted, minced with scissors, and pressed through a 70 μm strainer (Corning #431751) in the presence of ice-cold HBSS (Gibco #14025092). Cells were centrifuged at 200 × g for 3 min at 4°C and the pellet was washed. Red blood cell depletion was made with lysis buffer (BioLegend #420301) according to manufacturer's recommendations.

Flow cytometry

Flow cytometry was performed on a Beckman Coulter CytoFLEX flow cytometer. Data acquisition and analysis were done with Beckman Coulter CytExpert 2.3 software. Dead cells were excluded from the analysis using live/dead Fixable Violet Dead Cell Stain Kit (Life Technologies #L34955) according to the manufacturer's protocol. Life/dead stain was excited using a 405 nm laser and the signal was detected using a 450/45 detector. mKate2 was excited using a 561 nm laser and the signal was detected using a 610/20 detector. The compensation matrix for relevant channels was calculated by the software. For the 450/45 detector, the compensated value was 14.57 and for the 610/20 detector the compensated value was 1.4. One million events were collected per sample.

Image acquisition and analysis with Opera Phenix

BMDM plated in 96-well plates (Greiner Bio-One #655090) at a density of 10^4 cells per well were subjected to lipofection with RNAs. Then nine non-overlapping images per well with a resolution of 1080 × 1080 were captured on an hourly base using a 10 × objective and 2 × binning in non-confocal mode on the PerkinElmer Opera Phenix High-Content Screening System. Image acquisition and quantitative analysis were performed using the built-in software, Harmony 4.9. The chamber temperature was maintained at 37°C, with CO_2 levels set at 5%.

Before analysis, flat-field correction was applied and, subsequently, cells were segmented based on the mKate2 signal. The subpopulation of cells with 150–800 μm^2 of area occupied that started to exhibit mKate2+ ('+'-positive) signal with a mean intensity of ≥ 400 was counted.

HEK293 RIG-I CRISPR/*Cas9* knockout and A549 MAVS CRISPR/*Cas9* knockout

HEK293 cells were co-transfected with 200 ng of GeneArt CRISPR Nuclease mRNA (Invitrogen #A29378) in addition to sgRNA prepared by mixing fluorescently labelled Alt-R CRISPR-*Cas9* tracrRNA, ATTO 488, (IDT #10010170) with Alt-R CRISPR-*Cas9* crRNA targeting sequence in intron 1 of DDX58 gene encoding RIG-I protein (IDT #Hs.Cas9.DDX58.1.AA – GGAUUAUAUCCGGAAGACCC) at 4 nM final concentration. After 24 h, fluorescence-positive cells were sorted using BD FACSAria II cell sorter to a 96-well plate at a seeding concentration of one cell per well, and the cells were grown in penicillin/streptomycin (Gibco #15140–122) containing DMEM until single colonies were established. Next, cells were split into two 96-well plates, one of which was used for a dot blot analysis. For the dot blot analysis, cells were washed once in cold PBS before adding 20 µl of Roeder D Buffer per well and sonication for 10 min (30 s ON/30 s OFF). Six microliters of protein from each well were spotted directly onto a nitrocellulose membrane followed by western blot. Selected clones were seeded from the second 96-well plate into 6-well plates and grown. The RIG-I levels were validated by standard western blot. Recombinant human IFN-β (R&D Systems #8499-IF-010) treatment was used to induce RIG-I expression and to correctly select clones with no RIG-I detectable. A549 MAVS knockout cell line was kindly provided by Prof. Tomasz Lipniacki. The cell line was generated using CRISPR-*Cas9* as described in (48).

RNA pulldown mass spectrometry (RP-MS) analysis

RP-MS assay was based on a previously described RNA pulldown SILAC Mass Spectrometry method (49). 500 pmol of *in vitro* transcribed and PAGE purified RNA was treated with 100 mM Sodium Acetate and 5 mM sodium (meta)periodate in 200 µl of water and rotated for 1 h at room temperature in the dark. The RNA was precipitated by adding 600 µl of 100% ethanol and 15 µl of 3 M Sodium Acetate and incubating on dry ice for 30 min, followed by centrifugation at 16 000 × g, +4°C for 20 min. The RNA pellet was washed with 70% ethanol, followed by 5 min centrifugation at 16 000 × g and resuspended in 500 µl of 100 mM Sodium Acetate pH 5.2.

For one reaction 250 µl of adipic acid dihydrazide-agarose beads (Sigma-Aldrich #A0802) were washed 3 × with 100 mM Sodium Acetate followed by centrifugation at 2000 × g, +4°C for 2 min, then mixed with 500 µl of the periodate oxidized RNA and incubated overnight at + 4°C in the dark with rotation. The RNA-beads were washed by mixing with 700 µl of 4 M KCl and rocking for 30 min at room temperature and centrifuged at 2000 × g for 5 min, then washed 2 × with 2 M KCl, 2 × with Buffer G (20 mM Tris-HCl pH 7.5, 137 mM NaCl, 1 mM EDTA, 1% Triton X-100, 10% glycerol, 1.5 mM $MgCl_2$, 1 mM DTT and 200 µM PMSF) and 1 × with Roeder D followed by 2 min centrifugation at 2000 × g. Control beads with no RNA attached were also prepared.

One mg of total protein extract was added to RNA-beads. The mixture was supplemented with 1.5 M $MgCl_2$, 25 mM creatine phosphate, 100 mM ATP, and 2.5 µl of RiboProtect Hu RNase Inhibitor (Blirt #RT35). The mixture volume was adjusted to 650 µl with nuclease-free water. The RNA-beads-cell lysates mixtures were incubated at 37°C for 30 min with shaking. After three washes with Buffer G, the beads were mixed with 60 µl of 5 × Sample Buffer. Proteins captured by RNA were denatured at 95°C for 10 min with shaking. Around 30 µl of the supernatant was loaded onto SDS-PAGE or NuPAGE gel and western blot or mass spectrometry analysis was performed to detect the proteins respectively.

For mass spectrometry analysis proteins were separated on gel (NuPAGE Novex 4–12% Bis-Tris gel, Life Technologies), in NuPAGE buffer (MOPS) for 10 min and visualized using InstantBlue stain (Abcam). The stained gel band was excised and de-stained with 50 mM ammonium bicarbonate (Sigma Aldrich) and 100% (v/v) acetonitrile (Sigma Aldrich) and proteins were digested with trypsin, as previously described (50). In brief, proteins were reduced in 10 mM dithiothreitol (Sigma Aldrich) for 30 min at 37°C and alkylated in 55 mM iodoacetamide (Sigma Aldrich) for 20 min at ambient temperature in the dark. They were then digested overnight at 37°C with 13 ng/µl trypsin (Pierce). Following digestion, samples were diluted with an equal volume of 0.1% TFA.

The equivalent of 50 ng of the digest was loaded on the Evotip™ using the standard producer protocol. We utilized EVOSEP coupled to a TimsTOF ULTRA (Bruker) mass spectrometer equipped with a Captive Spray II source (Bruker). The separation was carried out on a Performance Column OE measuring 8 cm × 150 µm ID, with a particle size of 1.5 µm, maintained at 40°C. We employed the standard 60SPD EVOSEP method, applying a 21-min gradient for a total sample-to-sample time of 24 min using Solvent A: 0.1% formic acid (FA) and Solvent B: acetonitrile (ACN)/0.1% FA (Thermo Fisher Scientific™ Optima LCMS grade).

The dia-PASEF acquisition scheme was optimized for a cycle time estimate of 1.38 s. The window scheme was designed to cover most of the charge 2 precursor ions in the range m/z 391 – 1142 and 1/K0 0.68 – 1.36, using 22 × 31 Th windows, with accumulation and ramp times of 100 ms. The mass spectrometer was operated in the 'high sensitivity detection' ('low sample amount') mode.

The DIA-NN software platform (51) version 1.9.1. was used to process the raw files from label-free DIA and the search was conducted against the *Homo sapiens* reference proteome UP000005640 (Uniprot, released in 2019). Precursor ion generation was based on the chosen protein database (automatically generated spectral library) with deep-learning based spectra, retention time and IMs prediction. Digestion mode was set to specific with trypsin allowing maximum of one missed cleavage. Carbamidomethylation of cysteine was set as fixed modification. Oxidation of methionine, and acetylation of the N-terminus were set as variable modifications. MS1 and MS2 mass accuracies were set to 15 ppm. The parameters for peptide length range, precursor charge range, precursor m/z range and fragment ion m/z range as well as other software parameters were used with their default values. The precursor FDR was set to 1%.

Protein intensities were quantified from peptide intensities with directLFQ Python package (52). Statistical analysis was performed with R [R Core Team (2021). R: A language and environment for statistical computing. R Foundation for Statistical Computing, Vienna, Austria. https://www.R-project.org/]. *Protti* R package (53) was used for quality control, data filtration, imputation of missing values and statistical significance calculation using a moderated t-test based on the *limma* R/Bioconductor package (44). For functional validation, *P*-values were adjusted for multiple testing with the

Benjamini-Hochberg correction. Data visualization was performed using the *ggplot2* R package (54).

IVT stability and 5′-end phosphorylation state analyses

HEK293 cells were transfected with short viral RNA and incubated for 24 h. After incubation total RNA was extracted with Trizol, DNA was removed using DNase I treatment and RNA was purified with GeneJET RNA Cleanup and Concentration Micro Kit (Thermo #K0841). Then, 1 mg of purified total RNA sample was treated in three different conditions – without enzyme, with XRN-1 (NEB #M0338S) alone, or with XRN-1 and RppH (NEB #M0356S) together. Reactions were performed at 37°C for 60 min in dedicated buffer for XRN-1 enzyme provided by the producer. Then, treated samples were processed with RNA clean-up again and prepared for quantification analysis by cDNA synthesis using microScript microRNA cDNA Synthesis Kit (Norgen Biotek #54 410). Quantities of short viral RNA upon treatment were measured with one-step qRT-PCR assay with β-actin mRNA as a reference RNA.

Statistical analysis

All data are reported as mean ± standard deviation. Statistical analyses were performed using GraphPad Prism 10.2.1.

Results

Structures of viral and pol III 5′-pppA and 5′-pppG RNAs

To evaluate the significance of the 5′ terminal nucleotide identity derived from IVT, we initially employed two RNAs: IAV-derived short viral RNA and Pol III-derived Y5 RNA. The short viral RNA is a derivative of 3p-hpRNA (InvivoGen), a commonly used RIG-I ligand representing the first 87 nt of the positive strand of segment 8th of the IAV PR8 strain genome. By truncating 11 nucleotides from the 3′ end, we created a 76 nt RNA that contains a blunt end panhandle structure, which should be an optimal RIG-I agonist and which we named *short viral RNA* (Figure 1A) (1,55). To see how the change of the 5′ terminal nucleotide affects Pol III transcripts, we have chosen Y5 RNA (Figure 1B), as it has been shown before to be endogenous trigger of the RIG-I/IFN pathway (56,57). To investigate the role of the terminal nucleotide, we replaced the initial 5′-pppA with 5′-pppG in both short viral and Y5 RNAs, while maintaining the base pairing between the 5′ and 3′-ends by creating Watson-Crick base pairs (A:U and G:C) for the initial 5′-pppA or 5′-pppG (Figure 1A and B). All RNAs, produced by IVT, were purified by denaturing preparative polyacrylamide/urea gel electrophoresis (PAGE) followed by cutting a specific band and then filtered to remove the remaining gel residues.

The RIG-I/IFN signaling pathway is highly dependent on RNA structure and any alterations in RNA ligand base pairing could have an inhibitory effect on the strength of the RIG-I/IFN response (58,59). To find out if the substitution of nucleosides at the RNA ends could affect the structure of 5′-pppA versus 5′-pppG RNAs, *in vitro* RNA Selective 2′-Hydroxyl Acylation analyzed by Primer Extension (SHAPE) analyses for both, short viral and Y5 RNAs, were performed. Secondary structure predictions using the maximum free energy (MFE) algorithm combined with SHAPE results revealed that all tested, cognate RNA pairs exhibited similar secondary structures (Figure 1A and B). This was supported by comparable SHAPE reactivity values for individual nucleotide positions between the 5′-pppA and 5′-pppG RNAs (Figure 1C and D). The Y5 RNA with 5′-pppA showed marginally more relaxed SHAPE reactivity in the lower portion of the stem when compared with the 5′-pppG RNA (Figure 1C and D). Short viral RNA pairs were confirmed to form blunt end panhandle structures, which contain 8-bp double-stranded fragments and one mismatch between the 4th and 73rd nucleotides (Figure 1A) (60). The Y5 RNA pair was found to form long, double-stranded fragments (containing one hairpin loop, single-base bulge, and asymmetric internal loop) with a 9-nt long 3′ overhang corresponding to polyuridine tail (Figure 1B), largely like what has been previously described (61).

IVT 5′-pppA RNAs hyperstimulate the RIG-I/IFN pathway in human cells

To elucidate the role of the 5′ terminal nucleotide present in IVT-derived RNAs on the strength of RIG-I/IFN pathway activation, we transfected IVT short viral RNAs harboring 5′-pppA or 5′-pppG as a 5′ terminal nucleotide into human embryonic kidney HEK293 and lung adenocarcinoma A549 cells. We used a wide range of RNA concentrations between 0.1 ng/ml and 1000 ng/ml. Using HEK-Blue IFN-α/β colorimetric assay, we assessed the expression of IFN-α/β that was stimulated by tested RNAs. Notably, we observed substantially more efficient activation of the RIG-I/IFN pathway by short viral RNA initiating with 5′-pppA compared to the one starting with 5′-pppG in both HEK293 and A549 cells (Figure 2A and B). The production of IFN-I increased several thousandfold when low concentrations of RNAs were used. Only at the highest RNA concentration (1000 ng/ml), no significant difference was observed between the 5′-pppA and 5′-pppG variants. Confirmatory findings were observed in the case of IRF3 protein phosphorylation, which was assessed with western blot analysis (Supplementary Figure S1A).

We compared the capability of IVT RNA to induce a type I IFN response by estimating the apparent dissociation constant (K_d) for each RNA variant. There was a 92-fold difference in apparent K_d values when comparing 5′-pppA with 5′-pppG short viral RNAs in A549 cells, and a 17-fold difference in HEK293 cells (Supplementary Figure S1B and C). Cells exhibited significant IFN production and difference for 5′-pppA and 5′-pppG short viral RNAs as early as at 4 h into the treatment (Supplementary Figure S1D to G) reaching saturation after 24 h. Both types of RNAs (short viral RNA and Y5 RNA) initiating with 5′-pppA tested at a concentration of 100 ng/ml also proved much more potent in phosphorylating IRF3 and inducing RIG-I expression as confirmed by western blot analysis (Figure 2C and D, Supplementary Figure S1E and G), as well as elevating type I IFN, measured with HEK-Blue assay in HEK293 and A549 cells (Figure 2A, B, E and F, Supplementary Figure S1D and F). Moreover, the original 3p-hpRNA, which does not have a blunt end, also showed similar IRF3 phosphorylation pattern in both HEK293 and A549 cells when 5′-pppA and 5′-pppG variants were compared (Supplementary Figure S1H and I).

Control experiments demonstrated that RIG-I was crucial for the activation of the pathway by these and other tested

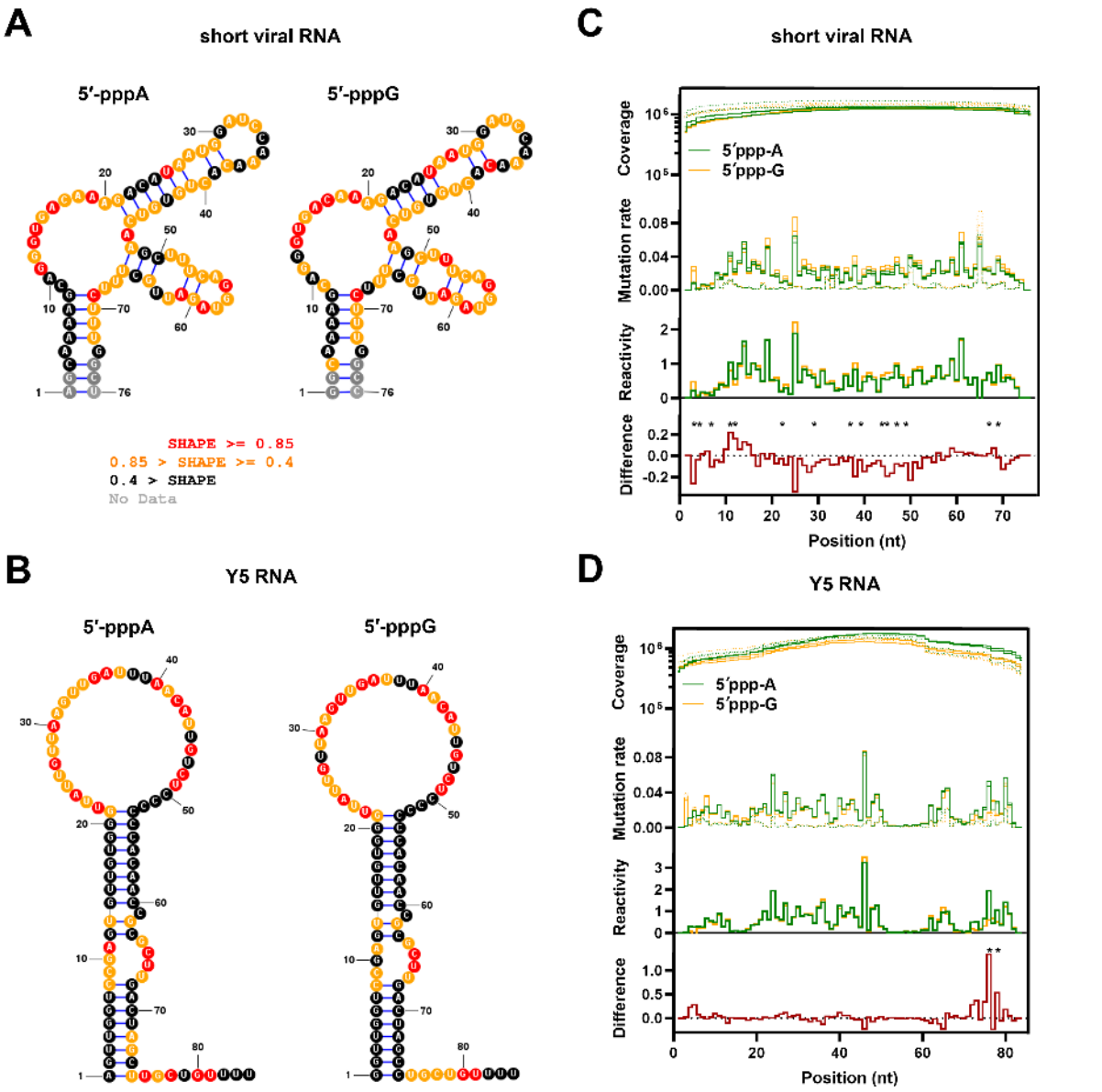

Figure 1. SHAPE analysis suggests no major structure rearrangements for short viral RNA and Y5 5′-pppA or 5′-pppG RNAs. (**A**, **B**) IVT RNAs starting either from 5′-pppA or 5′-pppG were subjected to SHAPE analysis. Secondary structures representing viral RNA and Y5 were predicted using the MFE algorithm with SHAPE constraints specified. (75) (**C**, **D**) Sequencing coverage exceeded the minimal threshold (10 000×) in all replicates of NAI-treated samples (solid lines) and DMSO-treated samples (dotted lines). The mutation rate was higher in NAI-treated samples (solid lines). Corresponding spikes in mutation, found in NAI and DMSO samples, might indicate a single-nucleotide polymorphism in the sample compared to the reference genome. All individual replicates (C: $n = 3$ for short viral RNA; D: $n = 2$ for Y5 RNA) are shown both in coverage and mutation line plots. The following part of the plot shows overlayed average reactivity levels between the set of RNAs. Higher SHAPE reactivity scores across the RNA of interest correlate with a higher likelihood of being unpaired. Negative reactivity values are excluded from the plot. The following part of the plot shows the difference between positive reactivity scores. Positions where reactivities are significantly different ($P < 0.001$) for A variant versus G variant comparison are marked with an asterisk (*).

RNAs (including 3p-hpRNA, EPO mRNA, and Seg 8th PR8 RNA), as no efficient IRF3 phosphorylation was detected in RIG-I KO HEK293, A549 and THP-1 cells (Supplementary Figure S2A to C). Additionally, there were marginal levels of IRF3 phosphorylation and type I IFN production when dephosphorylated short viral and Y5 RNAs were used (Figure 2C–F). Transfection of RIG-I KO cells with poly I:C led to robust IRF3 phosphorylation, confirming the integrity of other innate immune sensing pathways (Supplementary Figure S2A–C). Furthermore, transfection of MAVS KO A549 and THP-1 cells with the tested RNAs resulted in no or marginal IRF3 phosphorylation (Supplementary Figure S2D and E). In contrast, MDA-5 KO A549 and THP-1 cells exhibited increased IRF3 phosphorylation in response to all tested RNAs (Supplementary Figure S2D and E). Differences in the immunogenicity of 5′-pppA and 5′-pppG short

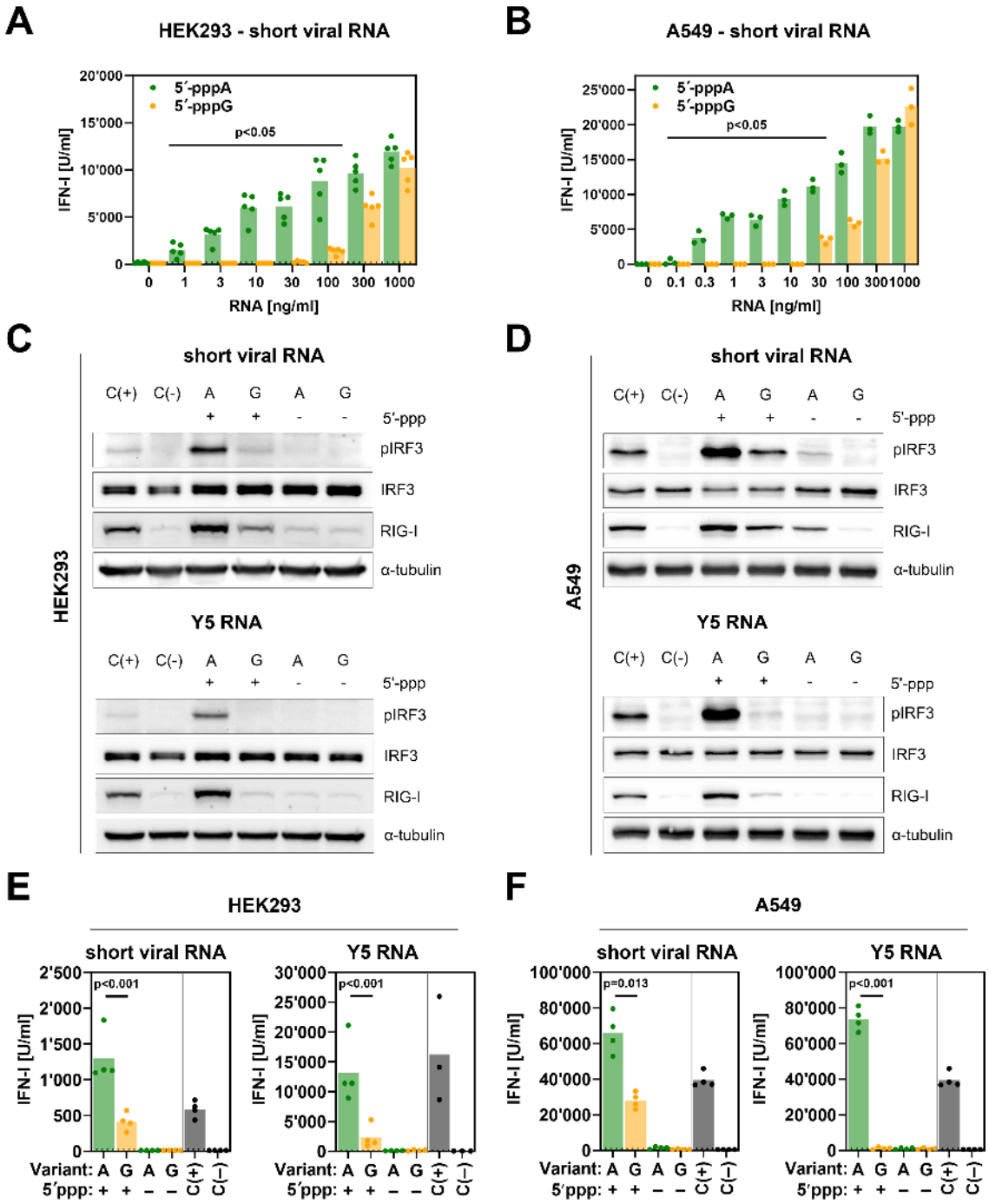

Figure 2. IVT 5′-pppA RNAs stimulate the RIG-I/IFN pathway in human cells more efficiently than 5′-pppG RNAs. (**A**) To compare the RIG-I/IFN responses triggered by RNAs that begin with 5′-pppA and 5′-pppG, IVT RNA, representing a fragment of the IAV genome, was transfected into HEK293 cells at various concentrations. The concentrations of type I IFN in the supernatants were assessed using the HEK-Blue IFN assay after 24 h. A selected concentration of RNA (100 ng/ml) was used to assess RIG-I levels and IRF3 phosphorylation with western blot upon treatment. (**C**) Dephosphorylated viral RNA (100 ng/ml) and Pol III transcript Y5 RNA were subjected to the HEK-Blue IFN assay. (**B**, **D**, **F**) Similar experiments were conducted in A549 cells, with type I IFN concentrations assessed in the supernatants and RIG-I levels and IRF3 phosphorylation in protein lysates in 8 h after treatment. The dotted line represents a lower quantification limit. The positive control (C(+)) involved transfection with 100 ng/ml 3p-hpRNA, while the negative control (C(−)) was mock-transfected with lipofectamine alone. (**A**, **B**, **E**, **F**) Upon log-transformation data were compared using two-way ANOVA with Šídák's multiple comparisons test. Experiments were conducted using either five (**A**), four (**E**, **F**) or three (**B**) biological replicates.

viral and Y5 IVT RNAs were observed in Calu-1 and THP-1 cell lines (Supplementary Figure S2F and G). Notably, pretreatment with 5′-pppA short viral RNA, unlike the 5′-pppG variant or dephosphorylated RNAs, significantly reduced IAV replication *in vitro* (Supplementary Figure S3). These findings suggest that IVT 5′-pppA RNAs activate the innate immune response via the RIG-I signaling pathway.

Next, to broaden our observation, we generated a structurally diverse collection of IVT 5′-pppA and 5′-pppG RNAs, predicted to form blunt ends or 3′ overhangs (the sequences and descriptions can be found in Supplementary Table S1). Irrespective of the predicted RNA structure, all tested 5′-pppA RNAs (excluding serine tRNA) exhibited much stronger RIG-I/IFN pathway stimulation observed as a higher IRF3 protein phosphorylation in HEK293 and A549 cells (Supplementary Figure S4A and B) and increased type I IFN production (Supplementary Figure S4C). These results show that IVT-derived RNAs initiating with 5′-pppA are much more immunogenic in human cells than cognate sequences starting with 5′-pppG and emphasize the significance of RNA structure, concentration and the duration of RIG-I/IFN pathway stimulation in this phenomenon.

IVT-produced 5′-pppA RNAs hyperstimulate the RIG-I/IFN pathway in murine cells

To elucidate the impact of the 5′ terminal nucleotide type on the activation strength of the RIG-I/IFN pathway in murine cells, we repeated transfections with IVT RNAs in cell cultures of murine origin: murine embryonic fibroblasts cell line (MEF), primary cultures of bone marrow-derived macrophages (BMDMs) and skin-derived fibroblasts. Similarly, to human cells, western blot analysis revealed higher levels of phosphorylated IRF3 and increased RIG-I expression for RNAs starting with 5′-pppA compared to RNAs initiating with 5′-pppG (Figure 3A and B). Furthermore, IVT RNAs beginning with 5′-pppA triggered the type I IFN production to a significantly greater extent than those starting with 5′-pppG in all the tested cell cultures (Figure 3C and D). Upon dephosphorylation of the RNAs, we observed significantly reduced RIG-I/IFN pathway activation or type I IFN production (Figure 3A–D). Although some variation in sensitivity was observed across different cell cultures, noteworthy, the highest levels of type I IFN production were observed in immune BMDM cells (Figure 3C and D).

This observation prompted us to create a reporter knock-in mouse line in which the IFN-β gene was replaced with the mKate2 open reading frame (Supplementary Figure S5). By replacing the IFN-β gene with the reporter we aimed to limit the IFN feedback loop and toxicity, focusing mainly on the initial RIG-I/IFN pathway activation. We repeated the transfection experiments using reporter BMDM cells from homozygous mice, enabling us to monitor in real time IFN-β expression represented by mKate2 marker production (Figure 3E). Kinetic data from mKate2+ cells illustrate that the onset of IFN-β response starts as early as at 5 h post transfection with the response peaking at 20 h (Figure 3F). This response was much more potent for RNAs initiating with 5′-pppA and fully triphosphate-dependent. In summary, the elevated induction of the RIG-I/IFN pathway by 5′-pppA RNAs can be detected in human and mouse systems.

IVT 5′-pppA RNAs hyperstimulate the RIG-I/IFN pathway *in vivo*

To test if the phenomenon of 5′-pppA RNAs hyperstimulation of the RIG-I/IFN pathway is observed at the organism level, we have injected the IVT RNAs encapsulated into lipid nanoparticles (RNA-LNP) in IFN-β/mKate2 reporter mice (Figure 4A). RNA-LNP complexes were injected intravenously (IV) into reporter mice within 48 h after production (Figure 4A). Twenty-four hours after administration, IFN-β/mKate2+ cells were observed both in the liver and spleen (Figure 4B to D). The number of gated cells with high level of mKate2+ signal in mice injected with 5′-pppA was 8 and 35 times higher compared to 5′-pppG RNA, as measured by flow cytometry in liver and spleen, respectively (Figure 4C and D). This shows that 5′-pppA RNA-mediated hyperstimulation of the RIG-I/IFN pathway can be also detected in the whole animal.

IVT 5′-pppA RNAs contain a greater amount of dsRNAs compared to 5′-pppG RNAs

To understand the mechanism behind the hyperstimulation of RIG-I/IFN pathway by IVT 5′-pppA RNA, we conducted a comprehensive assessment of the levels of dsRNA generated by IVT (19,25). For measurements of dsRNA impurities, we performed immunodetection using the anti-dsRNA J2 monoclonal antibody, which specifically recognizes dsRNA helices longer than 40 base pairs. We compared the IVT 5′-pppA and 5′-pppG RNA variants, including both short viral RNA and Y5 RNA. Dot blot analysis of RNA sample dilution series revealed approximately a 10-fold higher amounts of dsRNA in the 5′-pppA variants compared to the 5′-pppG variants both for short viral and Y5 RNAs (Figure 5A and B). As a positive control, we prepared dsRNA formed by mixing short viral RNA with its IVT fully complementary antisense strand in a 1:1 ratio. Our results suggest that the main source of enhanced immunogenicity of IVT-derived 5′-pppA RNAs is increased level of dsRNA production.

RNAseq performed while analysing SHAPE experiments revealed low proportion of reads mapping to the full length of the antisense strand (<0.1% for short viral RNA and < 0.4% for Y5 RNA) (Supplementary Figure S6A). Since our RNAs were purified using denaturing PAGE/Urea, we assumed that the differences in sequence coverage were due to sequencing bias. The ratios between sense and antisense strands were batch-dependent but generally higher for the 5′-pppA variants. Although trace amounts of residual contaminants, such as dsDNA from the original plasmid or PCR amplicon, were identified in the final RNA preparation, none of these contaminants triggered a type I IFN response, as determined using the HEK-Blue IFN assay in A549 cells (Supplementary Figure S6B).

Crucially, the denaturing PAGE/Urea analysis detected single, well-defined bands for both short viral and Y5 RNAs (Figure 5C). This, together with the results from RNAseq, led us to a hypothesis that dsRNAs arise from the primary product of IVT, coupled with its perfectly complementary antisense strand of equivalent length, produced through promoterless, RNA-dependent transcription. To validate this hypothesis, we

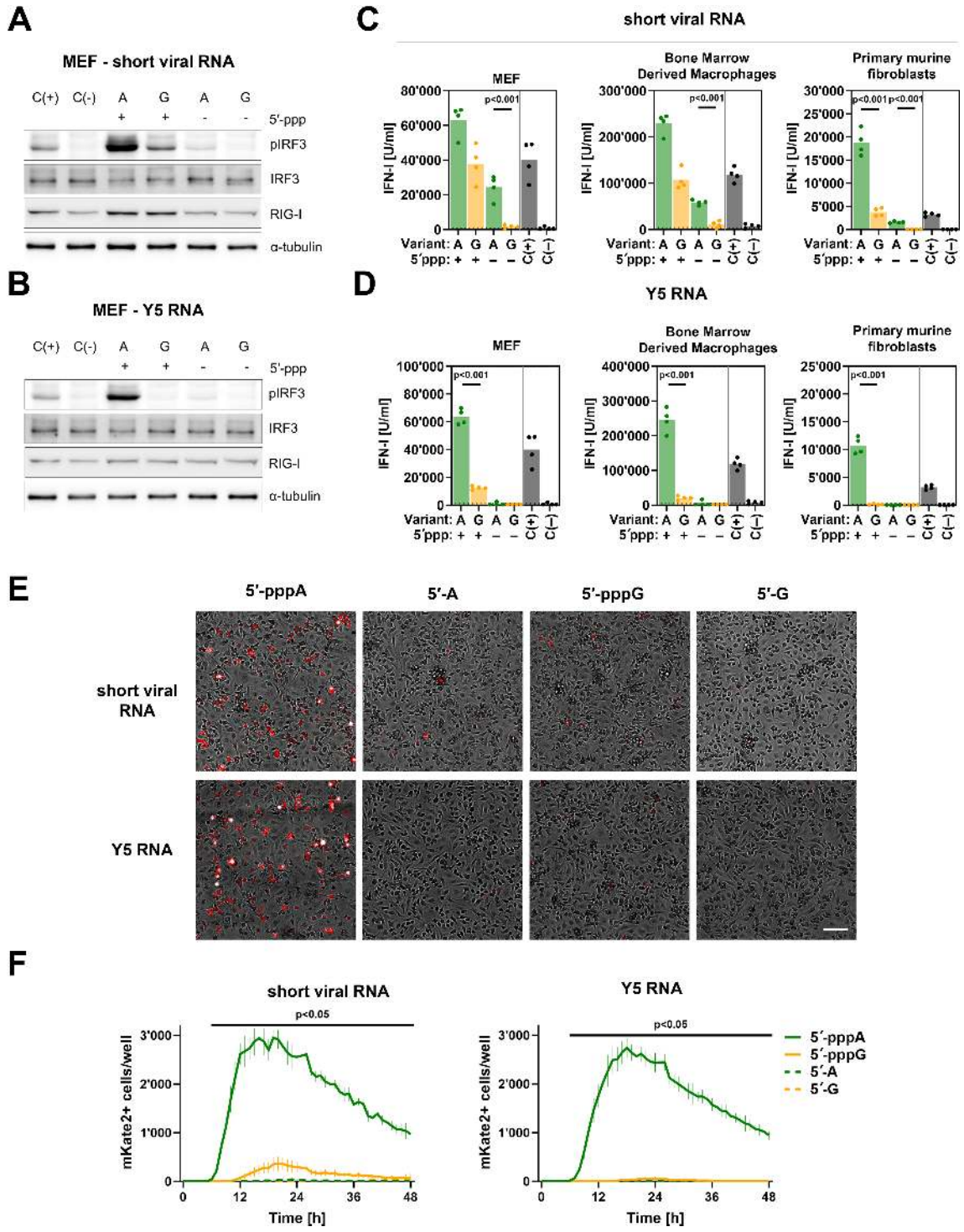

Figure 3. IVT 5′-pppA RNAs stimulate the RIG-I/IFN pathway in murine cells more efficiently than 5′-pppG RNAs. To compare the RIG-I/IFN responses triggered by RNAs that begin with 5′-pppA and 5′-pppG, IVT RNA, representing a fragment of the IAV genome, and Pol III transcript Y5 RNA were transfected into murine cells at a concentration of 100 ng/ml. (**A**, **B**) RIG-I levels and IRF3 phosphorylation in protein lysates were assessed using western blot. The positive control (C(+)) involved transfection with 100 ng/ml 3p-hpRNA, while the negative control (C(−)) was mock-transfected with lipofectamine alone. Upon log-transformation data were compared using two-way ANOVA with Šídák's multiple comparisons test. (**C**, **D**) The concentration of type I IFN in the supernatants was measured using HEK-Blue IFN assay at 24 h after treatment ($n = 4$). The dotted line represents a lower quantification limit. (**E**) Representative images of murine mKate+ BMDMs at 24 h upon RNA transfection. Scale bar is 100 μm. (**F**) Counts of mKate2+ cells at 0–48 h upon RNA transfection. Vertical lines represent standard deviation for $n = 4$. Longitudinal data upon shifted log-transformation ($\log_{10}(x + 1)$) were compared using repeated measures two-way ANOVA (rANOVA) with Geisser-Greenhouse correction and Šídák's multiple comparisons test.

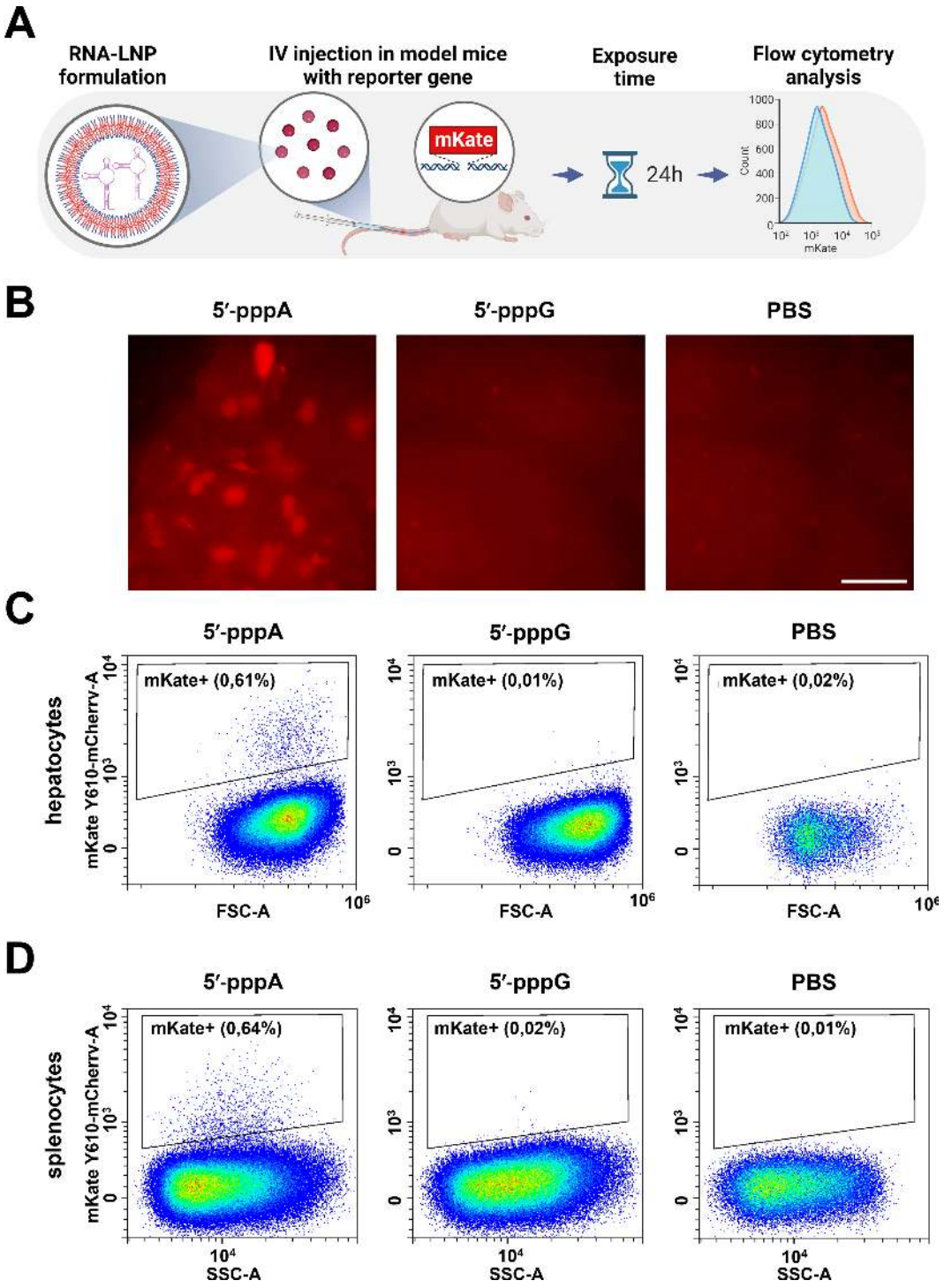

Figure 4. IVT 5′-pppA RNAs stimulate the RIG-I/IFN pathway in mice more efficiently than 5′-pppG RNAs. (**A**) Experimental setup: RNA was encapsulated into LNP and RNA-LNP complexes were IV injected (100 μg of encapsulated RNA per kg of body weight) in mice. Flow cytometry analysis of hepatocytes from reporter mice was conducted 24 h after RNA-LNP inoculation. (**B**) Fluorescent cells in liver. The injection of the 5′-pppA short viral RNA allowed the observation of fluorescent cells in liver before processing the organs into cell suspension. Scale bar is 50 μm. (**C**, **D**) Representative images for flow cytometry analysis of hepatocytes and splenocytes. (**C**) Liver: $P = 0.0005$ using one-way ANOVA with Šídák's multiple comparisons test; 5′pppA: M ± SD = 0.81 ± 0.17%, $n = 3$; 5′pppG: 0.11 ± 0.06%, $n = 2$; PBS control: 0.19 ± 0.12%; $n = 5$. (**D**) Spleen: $P = 0.028$ using one-way ANOVA with Šídák's multiple comparisons test; 5′pppA: M ± SD = 0.40 ± 0.29%, $n = 3$; 5′pppG: 0.01 ± 0.01%, $n = 2$; PBS control: 0.01 ± 0.01%; $n = 5$.

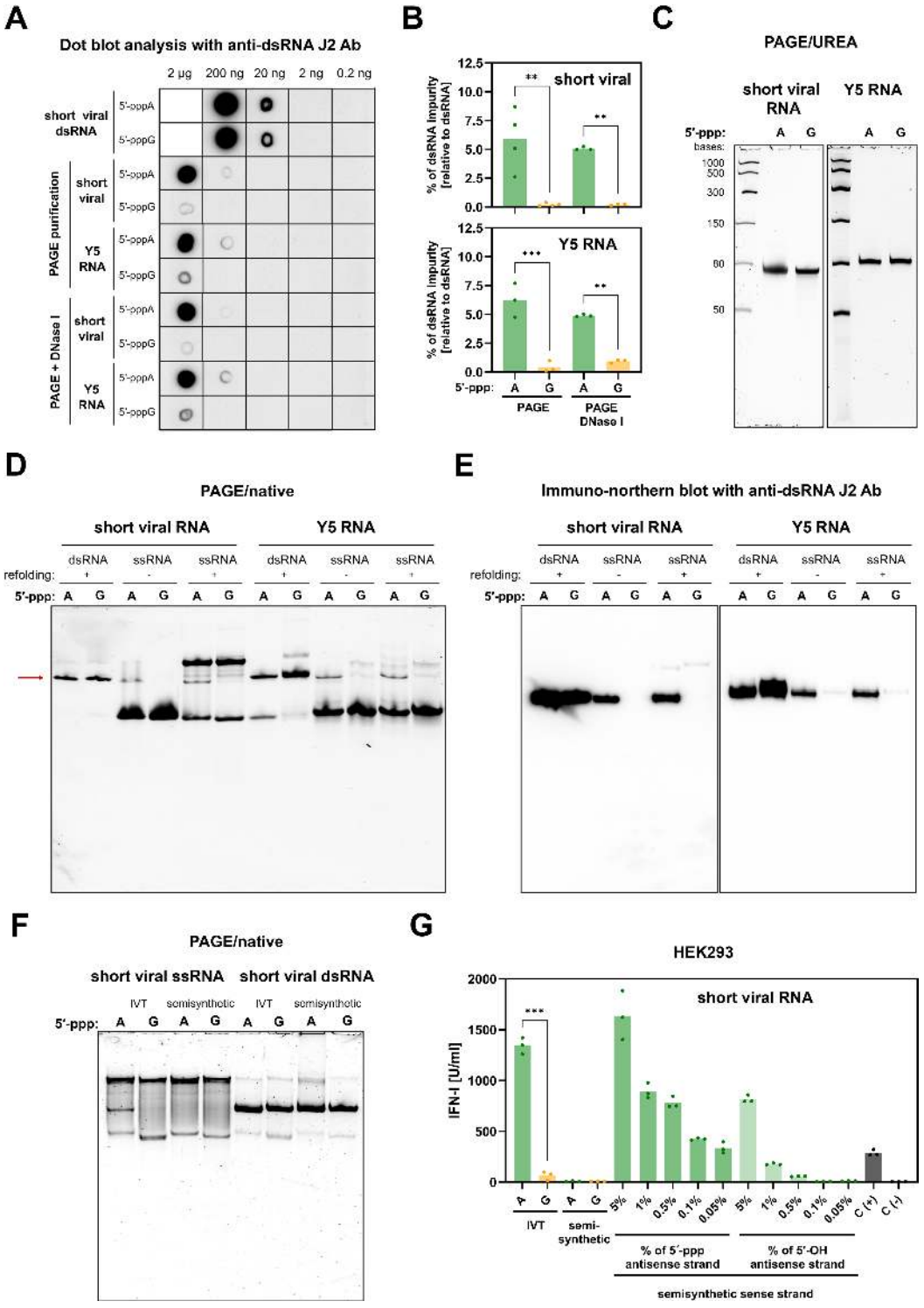

Figure 5. IVT-produced 5′-pppA RNAs contain more dsRNA compared with 5′-pppG RNAs. (**A**) Dot blot analysis of IVT short viral and Y5 RNAs was performed with anti-dsRNA J2 antibody, (**B**) then densitometric analysis ($n = 4$ for short viral RNA, $n = 3$ for Y5 RNA) was conducted to assess the level of dsRNA byproducts in IVT-derived RNAs. (**C**) PAGE/Urea analysis was done on short viral RNA and Y5 RNA. (**D**, **C**) PAGE in native conditions was conducted on IVT control dsRNAs (produced by annealing of sense and antisense RNA strands) and ssRNAs. (**E**) Immuno-northern blot using PAGE native gel followed by transfer to the membrane and detection with anti-dsRNA J2 antibody was used to detect dsRNA. (**F**) PAGE in native conditions of IVT short viral RNAs and semisynthetic short viral RNAs produced by splint ligation revealed the presence of dsRNA in IVT 5′-pppA RNAs but not in semisynthetic counterparts. (**G**) To assess the immunogenic potential of splint-ligated RNAs, an IVT-produced antisense RNA, with or without triphosphate moieties, was added to the sense splint-ligated RNA. The concentration of type I IFN in the supernatants was measured using HEK-Blue IFN assay at 24 h after treatment ($n = 3$). The positive control (C(+)) involved transfection with 100 ng/ml 3p-hpRNA, while the negative control (C(−)) was mock-transfected with lipofectamine alone. (**B**, **G**) Data were compared using two-way ANOVA with Šídák's multiple comparisons test.

compared the migration patterns of IVT short viral and Y5 RNAs with a short viral and Y5 dsRNA control on native PAGE (Figure 5D) and subsequently through native PAGE followed by immuno-northern blot with anti-dsRNA J2 antibody detection (Figure 5E). Both experiments revealed an increased presence of fully dsRNA species in the IVT substrates beginning with 5′-pppA. We also tested the stability of short viral RNAs after transfection in cells by qRT-PCR. The analysis did not reveal significant differences in the abundance of 5′-pppA and 5′-pppG RNAs (Supplementary Figure S7A). Then, to assess the phosphorylation status of their 5′ end, after purification of total RNA from cells transfected either with 5′-pppA or 5′-pppG short viral RNAs, we treated it with XRN1 or RppH combined with XRN1. The XRN1 enzyme degrades dephosphorylated RNAs, while RppH dephosphorylates them. The RNAs were resistant to XRN1 treatment, indicating they still retained 5′-ppp moiety (Supplementary Figure S7A). However, due to higher RppH's affinity for 5′-pppA RNAs (62), only 5′-pppA RNAs were efficiently cleaved after cotreatment with RppH and XRN1. Finally, we verified the activity and specificity of the used enzymes on IVT RNAs, which were not transfected into cells (Supplementary Figure S7B).

To explore whether the immunogenicity was predominantly derived from dsRNAs, we created short viral RNA by combining the initial 55 nt obtained through IVT with the remaining 21 nt chemically synthesized using splint ligation. Native PAGE analysis demonstrated that both IVT and semisynthetic RNAs were indistinguishable, except for the band attributed to fully dsRNA in the 5′-pppA RNA (Figure 5F). The HEK-Blue IFN assay revealed that the semisynthetic ligated RNA showed no immunogenicity at the concentrations tested (Figure 5G). However, the introduction of minimal quantities of a fully complementary antisense RNA strand (1–5%) triphosphorylated or dephosphorylated, mirroring levels found in IVT RNAs, was sufficient to activate the RIG-I/IFN pathway (Figure 5G). Similar results were obtained for IVT and semisynthetic Y5 RNAs (Supplementary Figure S8A and B).

To further validate the increased presence of dsRNAs in IVT RNAs with 5′-pppA, we performed an RNA pull-down Mass Spectrometry (RP-MS) assay. We identified a significant number of dsRNA-binding proteins, such as ADAR, PKR (EIF2AK2), and DICER1, exclusively in the short viral 5′-pppA RP-MS (Supplementary Figure S9A). Validation with western blot analysis confirmed increased binding of RIG-I, PKR and DHX9 to 5′-pppA RNA (Supplementary Figure S9B). These findings collectively demonstrate that IVT RNA starting with 5′-pppA produces significantly higher levels of immunogenic dsRNA.

Enhanced dsRNA production initiated by 5′-pppA is largely independent of RNA sequence and structure

To explore why IVT reactions with 5′-pppA result in increased dsRNA production compared to 5′-pppG, we analyzed a series of Y5 RNA mutants (Supplementary Figure S10, Supplementary Table S1). We hypothesized that the sense RNA's secondary structure and thermodynamic properties might influence dsRNA formation. Mutants were synthesized with either 5′-pppA or 5′-pppG and ended in U-rich tails or no tails, with stem sequences modified to include a six-nucleotide AU or GC clamp (positions from N2:N74 to N7:N69) (Supplementary Figure S10). Dot blot analysis with anti-dsRNA J2 antibody confirmed higher dsRNA levels in RNAs initiated with 5′-pppA than those with 5′-pppG (Figure 5A and B). PAGE/Urea gels showed single RNA bands, consistent with fully sense/antisense source of dsRNA (Figure 6C). Notably, U-rich tail mutants produced more dsRNA than those without (Figure 6A, B, D and E). However, native PAGE and immuno-northern blot (Figure 6D and E) verified increased fully dsRNA species in almost all 5′-pppA mutants. Further assays for RIG-I/IFN pathway activation demonstrated higher IFN production triggered by 5′-pppA RNAs compared to 5′-pppG counterparts (Figure 6F). Notably, Y5 GC clamp RNA lacking a U-rich tail failed to stimulate IFN-I (Figure 6F), implying possible cellular factors limit the immunogenicity of specific 5′-ppp RNAs. These findings indicate that the sense RNA's thermodynamic properties and structure influence global dsRNA contamination levels in IVT. However, consistent increased dsRNA presence in 5′-pppA RNAs suggests an additional mechanism promoting dsRNA formation specific to 5′-pppA. Additional evidence supporting this molecular mechanism came from IVT reactions of short viral and Y5 RNAs performed in the reaction of the same volumes, where we found more dsRNA contamination in 5′-pppA RNAs, despite the total RNA yield being higher for 5′-pppG RNAs (Supplementary Figure S11A-C).

Enhanced dsRNA production in long IVT RNAs

Given the widespread use of IVT reaction for generating mRNA for vaccines and future replacement therapies, we aimed to explore whether the terminal nucleotide could influence the production of dsRNAs in longer substrates (Supplementary Table S1). To evaluate this, we synthesized RNAs encoding EPO flanked with UTRs derived from the mRNA sequence of the Moderna SARS-CoV2 vaccine (mRNA-1273) and Segment 8th from the PR8 strain of IAV (Seg. 8th IAV PR8). Elevated levels of dsRNA were observed with anti-dsRNA J2 dot blot for 5′-pppA EPO and Seg. 8th IAV PR8 RNAs purified via PAGE/Urea (Figure 7A and B), although only for EPO mRNA the differences were statistically significant. Interestingly, the type of T7 promoter did not influence this difference. Higher dsRNA presence was noted in both EPO and Seg. 8th IAV PR8 substrates that were only treated with DNase I and purified on a column (Figure 7A and B). This suggests that there might be additional, different length dsRNA by-products generated during IVT. Functional testing in HEK293 and A549 cells demonstrated that both PAGE-purified EPO and Seg. 8th IAV PR8 RNAs triggered a much higher RIG-I/IFN response when starting with 5′-pppA (Figure 7C-H, and Supplementary Figure S12A-D). Moreover, the nature of the T7 promoter in EPO, Seg. 8th IAV PR8 RNAs and short viral RNA did not have a major influence on the immunogenicity of tested RNAs (Figure 7 and Supplementary Figures S12-S13). However, some dephosphorylated 5′-pppA RNAs retained immunogenicity, either due to incomplete dephosphorylation or activation of alternative innate immune signaling pathways.

Finally, we compared dsRNA levels between RNAs extracted from the Moderna and BioNTech SARS-CoV-2 vaccines. Notably, dsRNAs were clearly detectable in the BioNTech RNA vaccine (Figure 8), which utilized co-transcriptional addition of an AG-trinucleotide

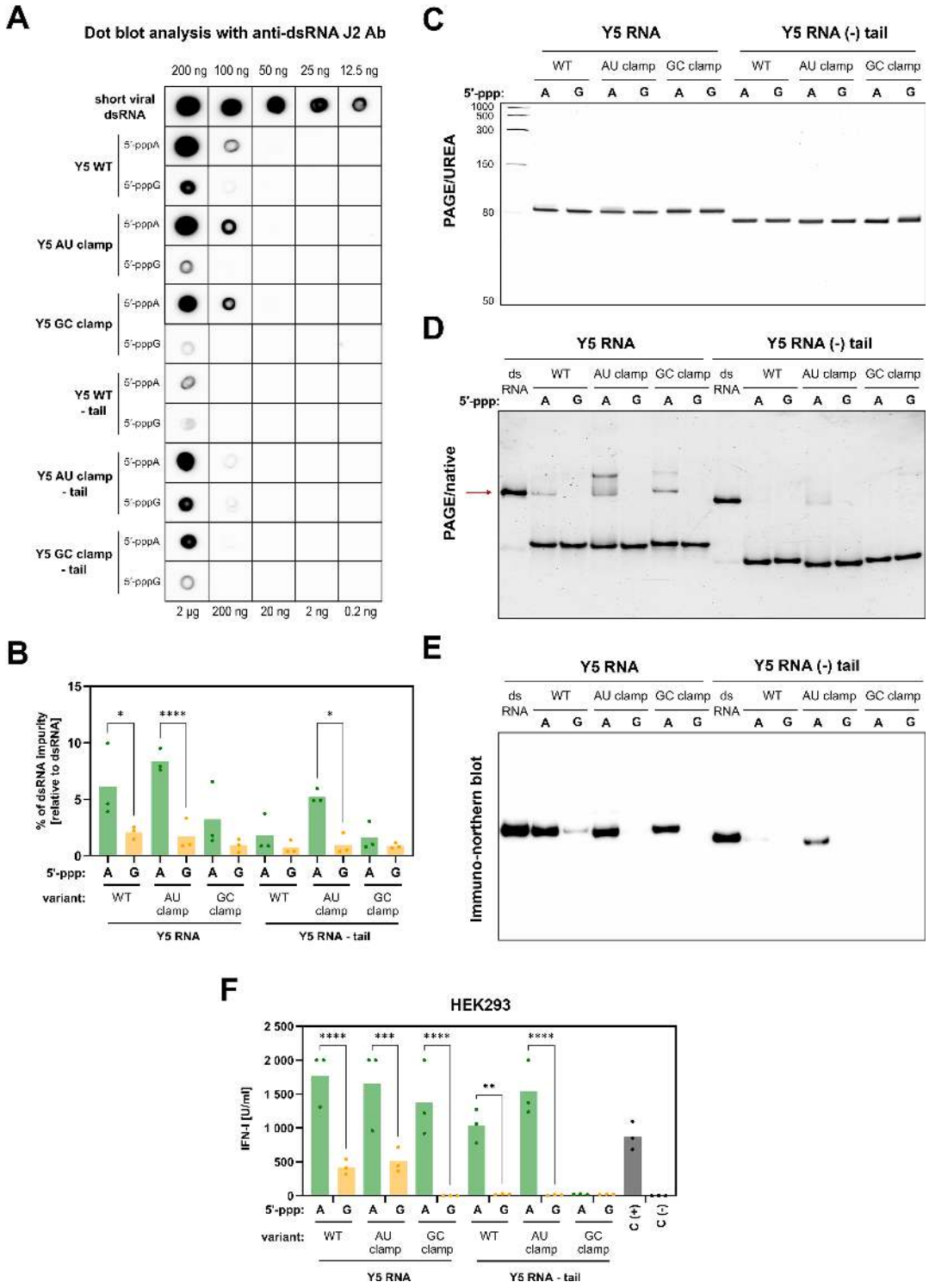

Figure 6. Increased dsRNA production in 5′-pppA is independent of RNA structure and sequence. (**A**) Dot blot analysis of IVT produced variants of Y5 RNA starting from 5′-pppA or 5′-pppG was performed with anti-dsRNA J2 antibody, and (**B**) amount of dsRNA contamination was determined with densitometric analysis ($n = 3$). (**C**) PAGE/Urea analysis of Y5 RNA variants showed single band for each RNA. (**D**) PAGE in native conditions, however, exhibited the presence of additional dsRNA bands. (**E**) Immuno-northern blot using PAGE native gel followed by transfer to the membrane and detection with anti-dsRNA J2 antibody was used to detect the presence of dsRNA formed by annealing with the 78 nt long complementary antisense strand. (**F**) HEK293 cells were transfected with Y5 RNA variants and the concentration of type I IFN in the supernatants was measured using HEK-Blue IFN assay at 24 h $n = 3$). The positive control (C(+)) involved transfection with 100 ng/ml 3p-hpRNA, while the negative control (C(−)) was mock-transfected with lipofectamine alone. (**B**, **F**) Data were compared using two-way ANOVA with Šídák's multiple comparisons test.

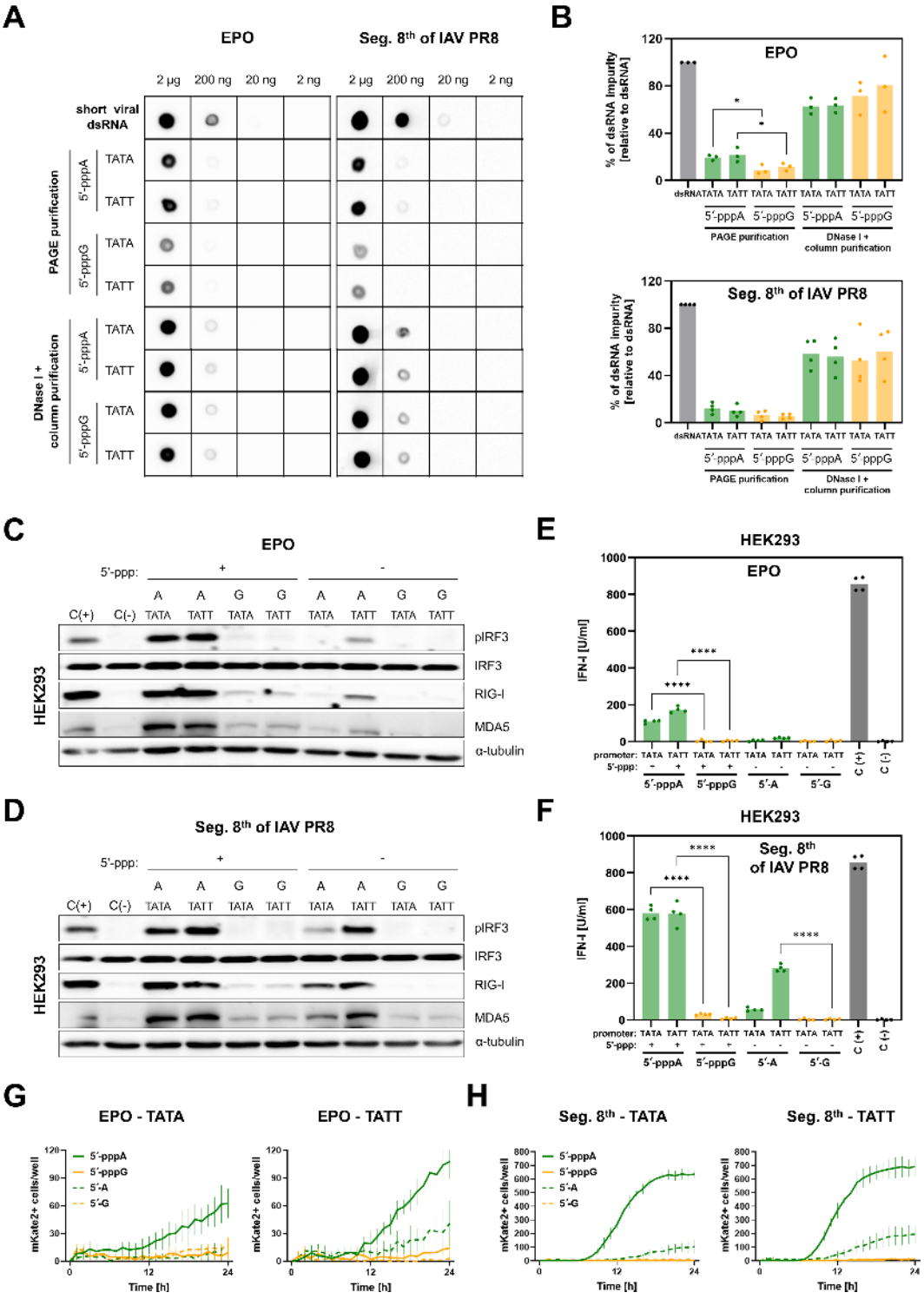

Figure 7. Long IVT-derived 5′-pppA RNAs contain more dsRNA byproducts compared with 5′-pppG RNAs. (**A**) Dot blot analysis of IVT EPO and Seg. 8th of IAV PR8 RNAs starting from 5′-pppA or 5′-pppG and produced either with Class III (TATA) or Class II (TATT) T7 promoter. (**B**) Densitometric analysis ($n = 3$ for EPO RNA, $n = 4$ for Seg. 8th of IAV PR8 RNA) was conducted to assess the level of dsRNA byproducts in IVT-derived RNAs. (**C–F**) RIG-I/IFN pathway responses against EPO and Seg. 8th of IAV PR8 RNAs starting from 5′-pppA or 5′-pppG were assessed with western blot analysis (**C**, **D**) and HEK-Blue IFN assay (**E**, **F**) 24 h after transfection into HEK293 cells ($n = 4$). (**E**, **F**) Data were compared using two-way ANOVA with Šídák's multiple comparisons test. The presence of dsRNA in EPO RNAs (**C**, **E**, **G**) RNAs (**D**, **F**, **H**). dsRNA controls are fully double stranded RNA derived from sense and antisense IVT. The positive control (C(+)) involved transfection with 100 ng/ml 3p-hpRNA, while the negative control (C(−)) was mock-transfected with lipofectamine alone.

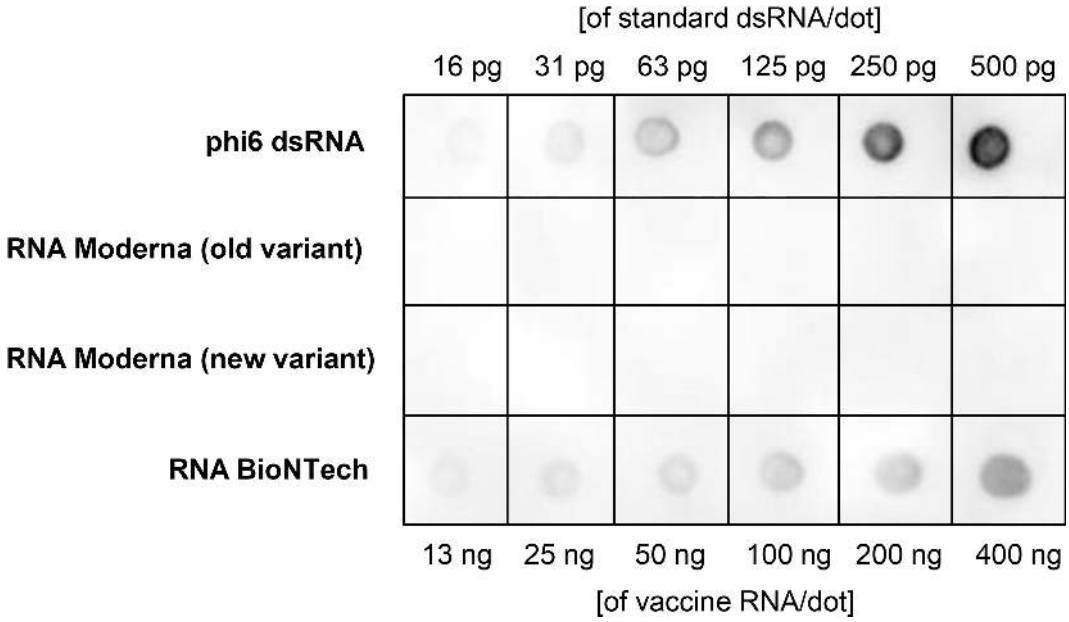

Figure 8. Quantification of dsRNA in mRNAs derived from Moderna and BioNTech SARS-CoV-2 vaccines using the J2 antibody staining. Phi6 dsRNA was used as a positive control standard for J2 antibody detection. The experiment was conducted in triplicate, with a representative image shown. Old variant represents monovalent vaccine, new variant represents bivalent BA.4–5 vaccine.

CleanCap (34). Conversely, the Moderna RNA vaccine, produced by enzymatically incorporating Cap1 on the 5′-pppG-containing IVT RNAs (33), did not exhibit detectable dsRNAs (Figure 8). However, it is important to acknowledge that the disparity in observed dsRNA abundances may be influenced by the utilization of different production and purification protocols by Moderna and BioNTech.

Together, our results reaffirm that IVT generates a considerable amount of dsRNA, and even stringent PAGE purification can lead to increased levels of dsRNA in substrates starting with 5′-pppA.

Discussion

In our study, we demonstrate the hyperactivation of the RIG-I/IFN type I pathway following transfection with IVT-derived 5′-pppA RNAs in human and mouse cells across a broad range of concentrations. While previous research noted increased RIG-I stimulation by short 5′-pppA dsRNA, this aspect remained unexplored (9). Our findings uncover that the primary driver of this phenomenon is the elevated presence of dsRNA in IVT 5′-pppA RNAs compared to their 5′-pppG counterparts. One study found no difference in the induction of IFN-β when using either fully double-stranded or stem-loop synthetic RNAs containing either 5′-pppA or 5′-pppG (63). However, these RNAs were transfected into cells at a high dose of 1 μg. Thus, it aligns with our findings as fully synthetic RNAs would lack dsRNA by-products, and we observed no distinction in immunogenicity between 5′-pppA or 5′-pppG at the highest concentrations.

For decades, T7 polymerase has been employed to produce substrates for investigating a broad spectrum of RNA biology (18). In recent years, it has enabled production of novel classes of SARS-CoV-2 mRNA vaccines, resulting in saving millions of lives (64). It is worth mentioning that the BioNTech vaccine was administered at 30 μg per dose, while the Moderna vaccine was given at 100 μg per dose (65). Our results indicate a greater presence of dsRNA contaminants in the BioNTech vaccine RNA. This could potentially explain the rationale behind using a lower RNA concentration per dose to mitigate unintended innate immune responses. Thus, as we progress towards integrating IVT-based medications into other areas of medicine (66), a comprehensive understanding of this system and its outputs becomes essential.

Prior research has detected specific dsRNA by-products resulting from the IVT synthesis process that trigger cellular immune responses, which has been demonstrated as a primary activator of the immune pathway (19). These dsRNA by-products are proposed to primarily arise through two distinct mechanisms. Firstly, the RNA transcript synthesized by T7 acts as a template for the RNA-dependent RNA runoff polymerase activity (67). If the 3′-end of the transcript possesses adequate complementarity, it may fold back, leading to the extension of the runoff transcript. This extended RNA can be easily differentiated from the main transcript under denaturing gel electrophoresis. The alternative mechanism involves the formation of dsRNA via promoter-independent transcription from the primary RNA product (19). In shorter RNAs, the size of the antisense molecule closely matches that of the main product, yielding highly immunogenic blunt-end dsRNA with 5′-ppp, which remains indistinguishable through denaturing gel electrophoresis. In longer RNAs, the polymerase can generate shorter dsRNA by-products through promoter-independent transcription. While extensive HPLC-based purification has demonstrated efficacy in separating dsRNA by-products from the main IVT RNA products (28), this approach is not conducive to scaling up due to its high cost. Other strategies to mitigate dsRNA production during IVT include reducing magnesium levels (19) or employing cellulose-based chromatography (29). These approaches do not achieve

full elimination of dsRNA. In this study, we illustrate how the selection of the 5′ nucleoside during IVT significantly influences immunogenicity levels by affecting dsRNA generation. Specifically, RNA with a 5′-pppA motif yields elevated quantities of dsRNA and provides abundant perfect RIG-I agonists. We have also shown that both the stability of the sense transcript and the presence of a 3′ overhang affect dsRNA formation, which aligns with previous findings indicating that unintended transcription primarily occurs when the correct product cannot form stable secondary structures at the 3′-end (24). However, in most cases, we consistently observed higher levels of dsRNA contamination in cognate RNAs beginning with 5′-pppA compared to those starting with 5′-pppG. Although the precise molecular mechanism remains unknown, we hypothesize that this could be due to inefficient engagement of T7 polymerase with templates designed to produce 5′-pppA RNA compared to 5′-pppG transcripts. This could allow the T7 to reengage with the 3′ end of the sense RNA and initiate promoterless, RNA-dependent transcription.

Furthermore, we have developed a novel, highly sensitive assay to investigate the immunogenicity of RNAs both *ex vivo* and *in vivo*. Our mouse model, in which the IFN-β gene was substituted with the mKate2 reporter, proved effective in detecting immunogenic RNAs in BMDMs as well as in the cells derived from liver and spleen. While a previous study had utilized a mouse expressing luciferase fused with IFN-β (68), our model allows for the analysis of primary effects of PAMPs, as the most potent type 1 IFN is not produced (69), thus avoiding triggering downstream JAK/STAT pathway. At the same time, alpha IFNs, despite exhibiting 20–30 times lower affinity to IFN type 1 receptors than IFN-β (69), are still expressed, enabling the mice's normal development and physiological function.

IVT reaction is a standard method for producing RNA-based vaccines and therapeutics. These RNAs are typically capped and polyadenylated to ensure proper functionality. However, incomplete capping may result in RNAs with a triphosphate group at the 5′ end, which can trigger an innate immune response (70). Our results demonstrate that IVT RNAs with 5′-pppA, in contrast to 5′-pppG, induce a more robust type I IFN response in *in vitro*, *ex vivo* and *in vivo* settings (Figures 2–7). The primary limitations of the study are the use of only unmodified RNAs, the reliance on a single T7 RNA polymerase, and the testing of a selection of transcripts. Further research is necessary to determine whether this phenomenon applies to capped, polyadenylated, and N1-methylpseudouridine-incorporated mRNAs, and, if so, how it impacts capping, translation, and the effectiveness of the adaptive immune response. Lastly, the differences we identified between 5′-pppA and 5′-pppG RNAs should be considered when designing RIG-I agonists, which can be used to trigger broad antiviral responses (Supplementary Figure S3) (71,72) or promote IFN-I-dependent apoptosis, potentially serving as anti-cancer agents (73).

In summary, our study reveals a significant disparity in immunogenicity between 5′-pppA-containing IVT RNAs and their 5′-pppG counterparts. We have observed that IVT RNAs with 5′-pppA exhibit heightened immunogenicity, characterized by increased levels of dsRNAs and activation of the RIG-I signaling pathway. These findings have important implications for both research and medical applications, shedding light on the mechanisms underlying IVT RNA immunogenicity and offering potential avenues for optimizing therapeutic interventions.

Data availability

The RNAseq data presented in the study have been deposited in the Sequence Read Archive repository (BioProject accession number #PRJNA1054022). The mass spectrometry proteomics data have been deposited to the ProteomeXchange Consortium via the PRIDE (74) partner repository with the dataset identifier PXD057761.

Supplementary data

Supplementary Data are available at NAR Online.

Acknowledgements

Transgenic mice were generated at the IIMCB Genome Engineering Facility and kept at the Rodent Facility (IN-MOL-CELL Infrastructure) funded by the European Union-NextGeneretionEU under National Recovery and Resilience Plan. We thank dr Olga Gewartowska and mgr. Marcin Szpila for their invaluable assistance with GMO mice. Additionally, we extend our thanks to dr Łukasz Majewski, dr Piotr Jan Korzeniowski and Damian Komorowski for their excellent support with animal work. We thank prof. dr hab. Jacek Jemielity and dr Marek Baranowski from ExploRNA for invaluable assistance with encapsulating RNA into lipid nanoparticles. We thank dr Katarzyna Mleczko-Sanecka and Raghunandan Mahadeva for help in establishing cell cultures of BMDMs. We thank dr Lukasz Szyrwiel for his assistance with mass spectrometry experiments. We would also like to thank prof. dr hab. Tomasz Lipniacki and dr Zbigniew Korwek for providing us with A549 MAVS KO cell line.

Author contributions: G.M. conceived this study; G.M., M.W., J.S. and I.T. designed the experiments; M.W., J.S., I.T., A.B., N.R.C., Z.N., T.T. and K.K. performed experiments; G.M, I.T., J.S., M.W., J.R. and A.Dz. analysed data; G.M., M.W., J.S., and I.T. wrote the manuscript with input from other authors. All authors read and approved the final manuscript.

Funding

Project financed under DIOSCURI, a programme initiated by the Max Planck Society, jointly managed with the National Science Centre in Poland, and mutually funded by Polish Ministry of Science and Higher Education and German Federal Ministry of Education and Research [2019/02/H/NZ1/00002 to G.M.]; The project was co-financed by Polish National Agency for Academic Exchange within Polish Returns Programme [PPN/PPO/2020/1/00 006/U/00001 to G.M.] and National Science Centre [2021/01/1/NZ1/00001 to G.M.]; This work was financed by the statutory funding of the International Institute of Molecular and Cell Biology in Warsaw. This research was performed thanks to IIMCB IN-MOL-CELL Infrastructure [PRID:SCR_021630] funded by the European Union – NextGenerationEU under National Recovery and Resilience Plan, RACE Teaming for Excellence funded by European Union under Horizon Europe [Project 101059801 - RACE] and by RACE-PRIME project carried out within

IRAP programme of the Foundation for Polish Science co-financed by the European Union under the European Funds for Smart Economy 2021-2027 (FENG); Deutsche Forschungsgemeinschaft (DFG, German Research Foundation) under Germany's Excellence Strategy – EXC 2008 – 390540038 – UniSysCat and [project 449713269 to J.R.]. Funding for open access charge: DIOSCURI Centre.

Conflict of interest statement

None declared.

References

1. Rehwinkel,J. and Gack,M.U. (2020) RIG-I-like receptors: their regulation and roles in RNA sensing. *Nat. Rev. Immunol.*, **20**, 537–551.
2. Hornung,V., Ellegast,J., Kim,S., Brzozka,K., Jung,A., Kato,H., Poeck,H., Akira,S., Conzelmann,K.K., Schlee,M., *et al.* (2006) 5′-Triphosphate RNA is the ligand for RIG-I. *Science*, **314**, 994–997.
3. Wang,W., Gotte,B., Guo,R. and Pyle,A.M. (2023) The E3 ligase Riplet promotes RIG-I signaling independent of RIG-I oligomerization. *Nat. Commun.*, **14**, 7308.
4. Cadena,C., Ahmad,S., Xavier,A., Willemsen,J., Park,S., Park,J.W., Oh,S.W., Fujita,T., Hou,F., Binder,M., *et al.* (2019) Ubiquitin-dependent and -independent roles of E3 ligase RIPLET in innate immunity. *Cell*, **177**, 1187–1200.
5. Thoresen,D., Wang,W., Galls,D., Guo,R., Xu,L. and Pyle,A.M. (2021) The molecular mechanism of RIG-I activation and signaling. *Immunol. Rev.*, **304**, 154–168.
6. Shaw,A.E., Hughes,J., Gu,Q., Behdenna,A., Singer,J.B., Dennis,T., Orton,R.J., Varela,M., Gifford,R.J., Wilson,S.J., *et al.* (2017) Fundamental properties of the mammalian innate immune system revealed by multispecies comparison of type I interferon responses. *PLoS Biol.*, **15**, e2004086.
7. Barrat,F.J., Elkon,K.B. and Fitzgerald,K.A. (2016) Importance of nucleic acid recognition in inflammation and autoimmunity. *Annu. Rev. Med.*, **67**, 323–336.
8. Goubau,D., Schlee,M., Deddouche,S., Pruijssers,A.J., Zillinger,T., Goldeck,M., Schuberth,C., Van der Veen,A.G., Fujimura,T., Rehwinkel,J., *et al.* (2014) Antiviral immunity via RIG-I-mediated recognition of RNA bearing 5′-diphosphates. *Nature*, **514**, 372–375.
9. Schlee,M., Roth,A., Hornung,V., Hagmann,C.A., Wimmenauer,V., Barchet,W., Coch,C., Janke,M., Mihailovic,A., Wardle,G., *et al.* (2009) Recognition of 5′ triphosphate by RIG-I helicase requires short blunt double-stranded RNA as contained in panhandle of negative-strand virus. *Immunity*, **31**, 25–34.
10. Myong,S., Cui,S., Cornish,P.V., Kirchhofer,A., Gack,M.U., Jung,J.U., Hopfner,K.P. and Ha,T. (2009) Cytosolic viral sensor RIG-I is a 5′-triphosphate-dependent translocase on double-stranded RNA. *Science*, **323**, 1070–1074.
11. Ren,X., Linehan,M.M., Iwasaki,A. and Pyle,A.M. (2019) RIG-I selectively discriminates against 5′-monophosphate RNA. *Cell Rep.*, **26**, 2019–2027.
12. Schuberth-Wagner,C., Ludwig,J., Bruder,A.K., Herzner,A.M., Zillinger,T., Goldeck,M., Schmidt,T., Schmid-Burgk,J.L., Kerber,R., Wolter,S., *et al.* (2015) A conserved histidine in the RNA sensor RIG-I controls immune tolerance to N1-2′O-methylated self RNA. *Immunity*, **43**, 41–51.
13. Tockary,T.A., Abbasi,S., Matsui-Masai,M., Hayashi,A., Yoshinaga,N., Boonstra,E., Wang,Z., Fukushima,S., Kataoka,K. and Uchida,S. (2023) Comb-structured mRNA vaccine tethered with short double-stranded RNA adjuvants maximizes cellular immunity for cancer treatment. *Proc. Natl. Acad. Sci. USA*, **120**, e2214320120.
14. Linehan,M.M., Dickey,T.H., Molinari,E.S., Fitzgerald,M.E., Potapova,O., Iwasaki,A. and Pyle,A.M. (2018) A minimal RNA ligand for potent RIG-I activation in living mice. *Sci. Adv.*, **4**, e1701854.
15. Pichlmair,A., Schulz,O., Tan,C.P., Naslund,T.I., Liljestrom,P., Weber,F. and Reis e Sousa,C. (2006) RIG-I-mediated antiviral responses to single-stranded RNA bearing 5′-phosphates. *Science*, **314**, 997–1001.
16. Te Velthuis,A.J.W., Long,J.C., Bauer,D.L.V., Fan,R.L.Y., Yen,H.L., Sharps,J., Siegers,J.Y., Killip,M.J., French,H., Oliva-Martin,M.J., *et al.* (2018) Mini viral RNAs act as innate immune agonists during influenza virus infection. *Nat. Microbiol.*, **3**, 1234–1242.
17. Kang,D.D., Li,H. and Dong,Y. (2023) Advancements of in vitro transcribed mRNA (IVT mRNA) to enable translation into the clinics. *Adv. Drug. Deliv. Rev.*, **199**, 114961.
18. Borkotoky,S. and Murali,A. (2018) The highly efficient T7 RNA polymerase: a wonder macromolecule in biological realm. *Int. J. Biol. Macromol.*, **118**, 49–56.
19. Mu,X., Greenwald,E., Ahmad,S. and Hur,S. (2018) An origin of the immunogenicity of in vitro transcribed RNA. *Nucleic Acids Res.*, **46**, 5239–5249.
20. Abbas,Y.M., Pichlmair,A., Gorna,M.W., Superti-Furga,G. and Nagar,B. (2013) Structural basis for viral 5′-PPP-RNA recognition by human IFIT proteins. *Nature*, **494**, 60–64.
21. Kumar,P., Sweeney,T.R., Skabkin,M.A., Skabkina,O.V., Hellen,C.U. and Pestova,T.V. (2014) Inhibition of translation by IFIT family members is determined by their ability to interact selectively with the 5′-terminal regions of cap0-, cap1- and 5′ppp-mRNAs. *Nucleic Acids Res.*, **42**, 3228–3245.
22. Johnson,B., VanBlargan,L.A., Xu,W., White,J.P., Shan,C., Shi,P.Y., Zhang,R., Adhikari,J., Gross,M.L., Leung,D.W., *et al.* (2018) Human IFIT3 modulates IFIT1 RNA binding specificity and protein stability. *Immunity*, **48**, 487–499.
23. Milligan,J.F., Groebe,D.R., Witherell,G.W. and Uhlenbeck,O.C. (1987) Oligoribonucleotide synthesis using T7 RNA polymerase and synthetic DNA templates. *Nucleic Acids Res.*, **15**, 8783–8798.
24. Triana-Alonso,F.J., Dabrowski,M., Wadzack,J. and Nierhaus,K.H. (1995) Self-coded 3′-extension of run-off transcripts produces aberrant products during in vitro transcription with T7 RNA polymerase. *J. Biol. Chem.*, **270**, 6298–6307.
25. Konarska,M.M. and Sharp,P.A. (1989) Replication of RNA by the DNA-dependent RNA polymerase of phage T7. *Cell*, **57**, 423–431.
26. Krupp,G. (1989) Unusual promoter-independent transcription reactions with bacteriophage RNA polymerases. *Nucleic Acids Res.*, **17**, 3023–3036.
27. Cazenave,C. and Uhlenbeck,O.C. (1994) RNA template-directed RNA synthesis by T7 RNA polymerase. *Proc. Natl. Acad. Sci. USA*, **91**, 6972–6976.
28. Kariko,K., Muramatsu,H., Ludwig,J. and Weissman,D. (2011) Generating the optimal mRNA for therapy: HPLC purification eliminates immune activation and improves translation of nucleoside-modified, protein-encoding mRNA. *Nucleic Acids Res.*, **39**, e142.
29. Baiersdorfer,M., Boros,G., Muramatsu,H., Mahiny,A., Vlatkovic,I., Sahin,U. and Kariko,K. (2019) A facile method for the removal of dsRNA contaminant from In vitro-transcribed mRNA. *Mol. Ther. Nucleic Acids*, **15**, 26–35.
30. Andries,O., Mc Cafferty,S., De Smedt,S.C., Weiss,R., Sanders,N.N. and Kitada,T. (2015) N(1)-methylpseudouridine-incorporated mRNA outperforms pseudouridine-incorporated mRNA by providing enhanced protein expression and reduced immunogenicity in mammalian cell lines and mice. *J Control Release*, **217**, 337–344.
31. Dousis,A., Ravichandran,K., Hobert,E.M., Moore,M.J. and Rabideau,A.E. (2023) An engineered T7 RNA polymerase that produces mRNA free of immunostimulatory byproducts. *Nat. Biotechnol.*, **41**, 560–568.

32. Dunn,J.J. and Studier,F.W. (1983) Complete nucleotide sequence of bacteriophage T7 DNA and the locations of T7 genetic elements. *J. Mol. Biol.*, **166**, 477–535.
33. Huang,F. (2003) Efficient incorporation of CoA, NAD and FAD into RNA by in vitro transcription. *Nucleic Acids Res.*, **31**, e8.
34. Vogel,A.B., Kanevsky,I., Che,Y., Swanson,K.A., Muik,A., Vormehr,M., Kranz,L.M., Walzer,K.C., Hein,S., Guler,A., *et al.* (2021) BNT162b vaccines protect rhesus macaques from SARS-CoV-2. *Nature*, **592**, 283–289.
35. Warminski,M., Trepkowska,E., Smietanski,M., Sikorski,P.J., Baranowski,M.R., Bednarczyk,M., Kedzierska,H., Majewski,B., Mamot,A., Papiernik,D., *et al.* (2024) Trinucleotide mRNA cap analogue N6-benzylated at the site of posttranscriptional (m6)A(m) mark facilitates mRNA purification and confers superior translational properties In vitro and In vivo. *J. Am. Chem. Soc.*, **146**, 8149–8163.
36. Weis,S. and Te Velthuis,A.J.W. (2021) Influenza virus RNA synthesis and the innate immune response. *Viruses*, **13**, 780.
37. Vasilyev,N. and Serganov,A. (2016) Preparation of short 5′-triphosphorylated oligoribonucleotides for crystallographic and biochemical studies. *Methods Mol. Biol.*, **1320**, 11–20.
38. Bravo,J.I., Kim,M. and Benayoun,B.A. (2021) Protocol for isolation of adult mouse ear pinnae-derived primary fibroblasts. *STAR Protoc.*, **2**, 100406.
39. Slusarczyk,P., Mandal,P.K., Zurawska,G., Niklewicz,M., Chouhan,K., Mahadeva,R., Jonczy,A., Macias,M., Szybinska,A., Cybulska-Lubak,M., *et al.* (2023) Impaired iron recycling from erythrocytes is an early hallmark of aging. *eLife*, **12**, e79196.
40. Rebendenne,A., Valadao,A.L.C., Tauziet,M., Maarifi,G., Bonaventure,B., McKellar,J., Planes,R., Nisole,S., Arnaud-Arnould,M., Moncorge,O., *et al.* (2021) SARS-CoV-2 triggers an MDA-5-dependent interferon response which is unable to control replication in lung epithelial cells. *J. Virol.*, **95**, e02415-20.
41. Mejia-Calvo,I., Munoz-Garcia,L., Jimenez-Uribe,A., Camacho-Sandoval,R., Gonzalez-Gonzalez,E., Mellado-Sanchez,G., Tenorio-Calvo,A.V., Lopez-Morales,C.A., Velasco-Velazquez,M.A., Pavon,L., *et al.* (2019) Validation of a cell-based colorimetric reporter gene assay for the evaluation of type I interferons. *Biotechnol. Rep. (Amst)*, **22**, e00331.
42. Motulsky,H.J. and Brown,R.E. (2006) Detecting outliers when fitting data with nonlinear regression - a new method based on robust nonlinear regression and the false discovery rate. *BMC Bioinf.*, **7**, 123.
43. Busan,S. and Weeks,K.M. (2018) Accurate detection of chemical modifications in RNA by mutational profiling (MaP) with ShapeMapper 2. *RNA*, **24**, 143–148.
44. Ritchie,M.E., Phipson,B., Wu,D., Hu,Y., Law,C.W., Shi,W. and Smyth,G.K. (2015) limma powers differential expression analyses for RNA-sequencing and microarray studies. *Nucleic Acids Res.*, **43**, e47.
45. Kuzniewska,B., Rejmak,K., Nowacka,A., Ziolkowska,M., Milek,J., Magnowska,M., Gruchota,J., Gewartowska,O., Borsuk,E., Salamian,A., *et al.* (2022) Disrupting interaction between miR-132 and Mmp9 3′UTR improves synaptic plasticity and memory in mice. *Front. Mol. Neurosci.*, **15**, 924534.
46. Behringer,R., Gertsenstein,M., Nagy,K.V. and Nagy,A. (2019) Preparation of polymerase chain reaction template DNA from mouse tail tissue. *Cold Spring Harb. Protoc.*, **2019**, 325–326.
47. Wang,X., Liu,S., Sun,Y., Yu,X., Lee,S.M., Cheng,Q., Wei,T., Gong,J., Robinson,J., Zhang,D., *et al.* (2023) Preparation of selective organ-targeting (SORT) lipid nanoparticles (LNPs) using multiple technical methods for tissue-specific mRNA delivery. *Nat. Protoc.*, **18**, 265–291.
48. Korwek,Z., Czerkies,M., Jaruszewicz-Blonska,J., Prus,W., Kosiuk,I., Kochanczyk,M. and Lipniacki,T. (2023) Nonself RNA rewires IFN-beta signaling: a mathematical model of the innate immune response. *Sci. Signal.*, **16**, eabq1173.
49. Choudhury,N.R. and Michlewski,G. (2019) Quantitative identification of proteins that influence miRNA biogenesis by RNA pull-down-SILAC mass spectrometry (RP-SMS). *Methods*, **152**, 12–17.
50. Shevchenko,A., Wilm,M., Vorm,O. and Mann,M. (1996) Mass spectrometric sequencing of proteins silver-stained polyacrylamide gels. *Anal. Chem.*, **68**, 850–858.
51. Demichev,V., Messner,C.B., Vernardis,S.I., Lilley,K.S. and Ralser,M. (2020) DIA-NN: neural networks and interference correction enable deep proteome coverage in high throughput. *Nat. Methods*, **17**, 41–44.
52. Ammar,C., Schessner,J.P., Willems,S., Michaelis,A.C. and Mann,M. (2023) Accurate label-free quantification by directLFQ to compare unlimited numbers of proteomes. *Mol. Cell. Proteomics*, **22**, 100581.
53. Quast,J.P., Schuster,D. and Picotti,P. (2022) protti: an R package for comprehensive data analysis of peptide- and protein-centric bottom-up proteomics data. *Bioinform. Adv.*, **2**, vbab041.
54. Wickham,H. (2016) *Use R*! Springer International Publishing : Imprint : Springer, Cham, pp. 1 online resource (XVI, 260 pages 232 illustrations, 140 illustrations in color.
55. Schlee,M. (2013) Master sensors of pathogenic RNA - RIG-I like receptors. *Immunobiology*, **218**, 1322–1335.
56. Kowalski,M.P. and Krude,T. (2015) Functional roles of non-coding Y RNAs. *Int. J. Biochem. Cell Biol.*, **66**, 20–29.
57. Vabret,N., Najburg,V., Solovyov,A., Gopal,R., McClain,C., Sulc,P., Balan,S., Rahou,Y., Beauclair,G., Chazal,M., *et al.* (2022) Y RNAs are conserved endogenous RIG-I ligands across RNA virus infection and are targeted by HIV-1. *iScience*, **25**, 104599.
58. Marques,J.T., Devosse,T., Wang,D., Zamanian-Daryoush,M., Serbinowski,P., Hartmann,R., Fujita,T., Behlke,M.A. and Williams,B.R. (2006) A structural basis for discriminating between self and nonself double-stranded RNAs in mammalian cells. *Nat. Biotechnol.*, **24**, 559–565.
59. Schmidt,A., Schwerd,T., Hamm,W., Hellmuth,J.C., Cui,S., Wenzel,M., Hoffmann,F.S., Michallet,M.C., Besch,R., Hopfner,K.P., *et al.* (2009) 5′-triphosphate RNA requires base-paired structures to activate antiviral signaling via RIG-I. *Proc. Natl. Acad. Sci. USA*, **106**, 12067–12072.
60. Zuker,M. (2003) Mfold web server for nucleic acid folding and hybridization prediction. *Nucleic Acids Res.*, **31**, 3406–3415.
61. Boccitto,M. and Wolin,S.L. (2019) Ro60 and Y RNAs: structure, functions, and roles in autoimmunity. *Crit. Rev. Biochem. Mol. Biol.*, **54**, 133–152.
62. Foley,P.L., Hsieh,P.K., Luciano,D.J. and Belasco,J.G. (2015) Specificity and evolutionary conservation of the Escherichia coli RNA pyrophosphohydrolase RppH. *J. Biol. Chem.*, **290**, 9478–9486.
63. Ren,X., Linehan,M.M., Iwasaki,A. and Pyle,A.M. (2019) RIG-I recognition of RNA targets: the influence of terminal base pair sequence and overhangs on affinity and signaling. *Cell Rep.*, **29**, 3807–3815.
64. Chaudhary,N., Weissman,D. and Whitehead,K.A. (2021) mRNA vaccines for infectious diseases: principles, delivery and clinical translation. *Nat. Rev. Drug Discov.*, **20**, 817–838.
65. Yau,K., Chan,C.T., Abe,K.T., Jiang,Y., Atiquzzaman,M., Mullin,S.I., Shadowitz,E., Liu,L., Kostadinovic,E., Sukovic,T., *et al.* (2022) Differences in mRNA-1273 (Moderna) and BNT162b2 (Pfizer-BioNTech) SARS-CoV-2 vaccine immunogenicity among patients undergoing dialysis. *CMAJ*, **194**, E297–E305.
66. Huang,X., Kong,N., Zhang,X., Cao,Y., Langer,R. and Tao,W. (2022) The landscape of mRNA nanomedicine. *Nat. Med.*, **28**, 2273–2287.
67. Gholamalipour,Y., Karunanayake Mudiyanselage,A. and Martin,C.T. (2018) 3′ end additions by T7 RNA polymerase are RNA self-templated, distributive and diverse in character-RNA-seq analyses. *Nucleic Acids Res.*, **46**, 9253–9263.
68. Lienenklaus,S., Cornitescu,M., Zietara,N., Lyszkiewicz,M., Gekara,N., Jablonska,J., Edenhofer,F., Rajewsky,K., Bruder,D.,

Hafner,M., *et al.* (2009) Novel reporter mouse reveals constitutive and inflammatory expression of IFN-beta in vivo. *J. Immunol.*, **183**, 3229–3236.
69. Ng,C.T., Mendoza,J.L., Garcia,K.C. and Oldstone,M.B. (2016) Alpha and beta type 1 interferon signaling: passage for diverse biologic outcomes. *Cell*, **164**, 349–352.
70. Mochida,Y. and Uchida,S. (2024) mRNA vaccine designs for optimal adjuvanticity and delivery. *RNA Biol.*, **21**, 1–27.
71. Schwab,L.S.U., Farrukee,R., Eleouet,J.F., Rameix-Welti,M.A., Londrigan,S.L., Brooks,A.G., Hurt,A.C., Coch,C., Zillinger,T., Hartmann,G., *et al.* (2022) Retinoic acid-inducible gene I activation inhibits Human Respiratory syncytial virus replication in mammalian cells and in mouse and ferret models of infection. *J. Infect. Dis.*, **226**, 2079–2088.
72. Ranjan,P., Jayashankar,L., Deyde,V., Zeng,H., Davis,W.G., Pearce,M.B., Bowzard,J.B., Hoelscher,M.A., Jeisy-Scott,V., Wiens,M.E., *et al.* (2010) 5′PPP-RNA induced RIG-I activation inhibits drug-resistant avian H5N1 as well as 1918 and 2009 pandemic influenza virus replication. *Virol. J.*, **7**, 102.
73. Castiello,L., Zevini,A., Vulpis,E., Muscolini,M., Ferrari,M., Palermo,E., Peruzzi,G., Krapp,C., Jakobsen,M., Olagnier,D., *et al.* (2019) An optimized retinoic acid-inducible gene I agonist M8 induces immunogenic cell death markers in human cancer cells and dendritic cell activation. *Cancer Immunol. Immunother.*, **68**, 1479–1492.
74. Perez-Riverol,Y., Bai,J., Bandla,C., Garcia-Seisdedos,D., Hewapathirana,S., Kamatchinathan,S., Kundu,D.J., Prakash,A., Frericks-Zipper,A., Eisenacher,M., *et al.* (2022) The PRIDE database resources in 2022: a hub for mass spectrometry-based proteomics evidences. *Nucleic Acids Res.*, **50**, D543–D552.
75. Reuter,J.S. and Mathews,D.H. (2010) RNAstructure: software for RNA secondary structure prediction and analysis. *BMC Bioinf.*, **11**, 129.

Received: May 31, 2024. **Revised:** December 3, 2024. **Editorial Decision:** December 4, 2024. **Accepted:** December 6, 2024

Supplementary Data

5′ terminal nucleotide determines the immunogenicity of IVT RNAs

Magdalena Wolczyk[1*], Jacek Szymanski[1*], Ivan Trus[1*], Zara Naz[1], Tola Tame[1], Agnieszka Bolembach[1], Nila Roy Choudhury[1,2], Karolina Kasztelan[1], Juri Rappsilber[3], Andrzej Dziembowski[1], Gracjan Michlewski[1]

* These authors contributed equally to this work.

[1] International Institute of Molecular and Cell Biology in Warsaw, Poland

[2] MRC Human Genetics Unit, Institute of Genetics and Cancer, University of Edinburgh, Western General Hospital, Edinburgh, UK

[3] Department of Biotechnology, Technische Universität Berlin, Berlin, Germany

Correspondence should be addressed to G.M. (gmichlewski@iimcb.gov.pl)

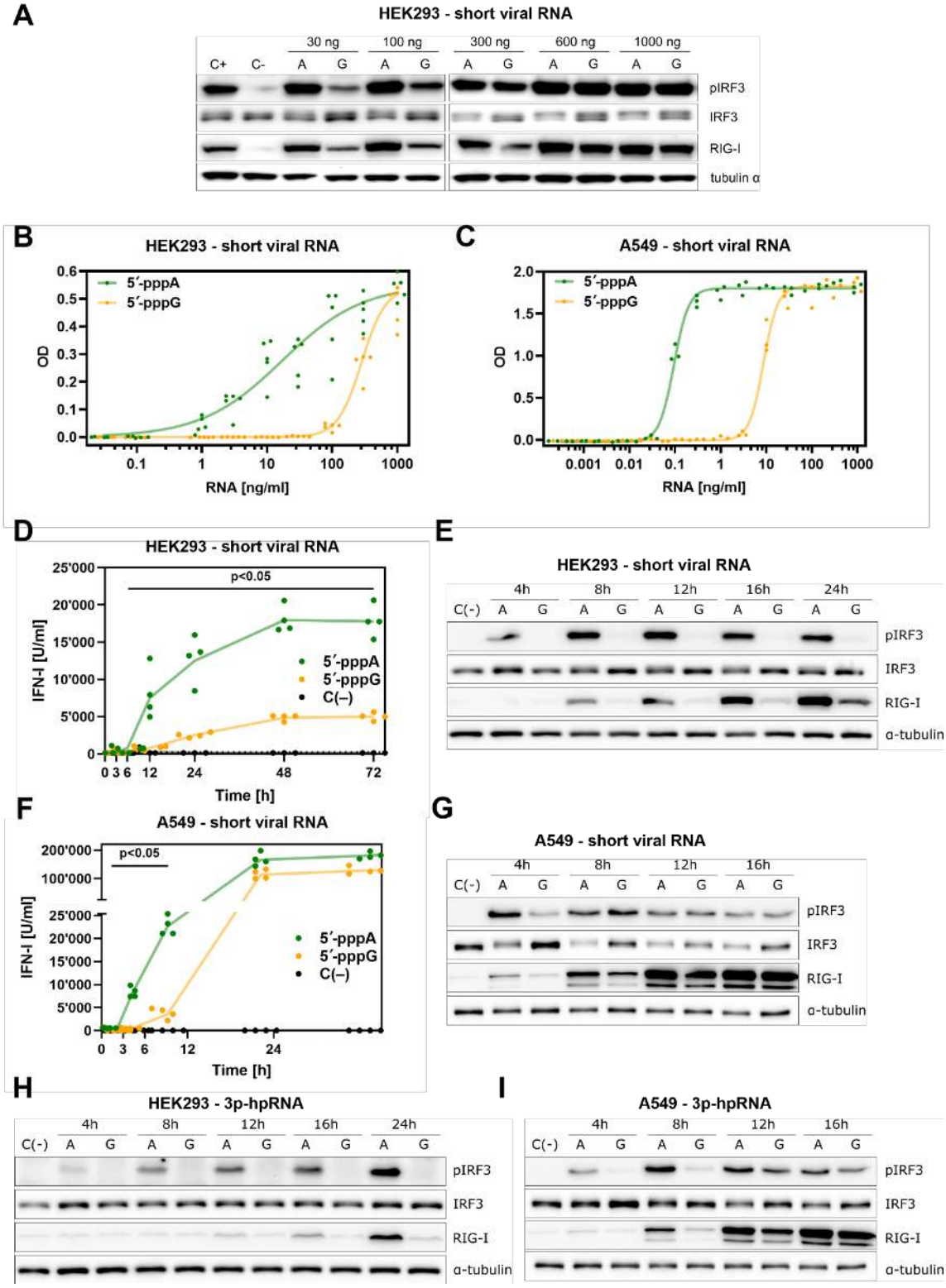

Supplementary figure S1. IVT RNAs starting with 5′-pppA are more immunogenic than those starting with 5′-pppG. (A) Analysis of IRF3 phosphorylation and RIG-I expression assessed by western blot analysis in HEK293 cells after transfection with different concentrations of short viral 5′-pppA *vs.* 5′-pppG RNAs ranging from 30 ng/ml to 1000 ng/ml.

The cells were incubated for 24 h, then cell lysis was performed. (B, C) The apparent dissociation constant (K_d) was estimated for each RNA variant (n = 5). For virus-derived short RNA introduced into A549 cells, K_d was estimated to equal 0.094 ng/ml (3.85 pM) for 5′-pppA RNA (95% confidence limits, 0.089–0.099 ng/ml; R^2_{adj} = 0.9973). For 5′-pppG RNA K_d was estimated to be 8.677 ng/ml (355.8 pM) (95% confidence limits, 8.377–8.975 ng/ml; R^2_{adj} = 0.9987). In the case of HEK293 cells, the estimated K_d values were 17.0 ng/ml for 5′-pppA (95% confidence limits, 9.6–41.8 ng/ml; R^2_{adj} = 0.9175) and 282.8 ng/ml for 5′-pppG RNA variants (95% confidence limits, 280.9–284.8 ng/ml; R^2_{adj} = 0.9999). (D, F) Kinetics of type I IFN production in HEK293 and A549 cells treated with RNA representing fragment of the IAV genome at a concentration of 100 ng/ml (n = 4). The dotted line represents lower quantification limit. The positive control (C(+)) involved transfection with 100 ng/ml 3p-hpRNA, while the negative control (C(−)) was mock-transfected with lipofectamine alone. Upon log-transformation data were compared using two-way ANOVA with Šídák's multiple comparisons test. (E, G) Kinetics of IRF3 phosphorylation and RIG-I expression assessed by Western blot analysis in HEK293 and A549 cells treated with 5′-pppA *vs.* 5′-pppG short viral RNA at a concentration of 100 ng/ml. (H, I) Kinetics of IRF3 phosphorylation and RIG-I expression assessed by Western blot analysis in HEK293 and A549 cells treated with 5′-pppA *vs.* 5′-pppG 3p-hpRNA at a concentration of 100 ng/ml.

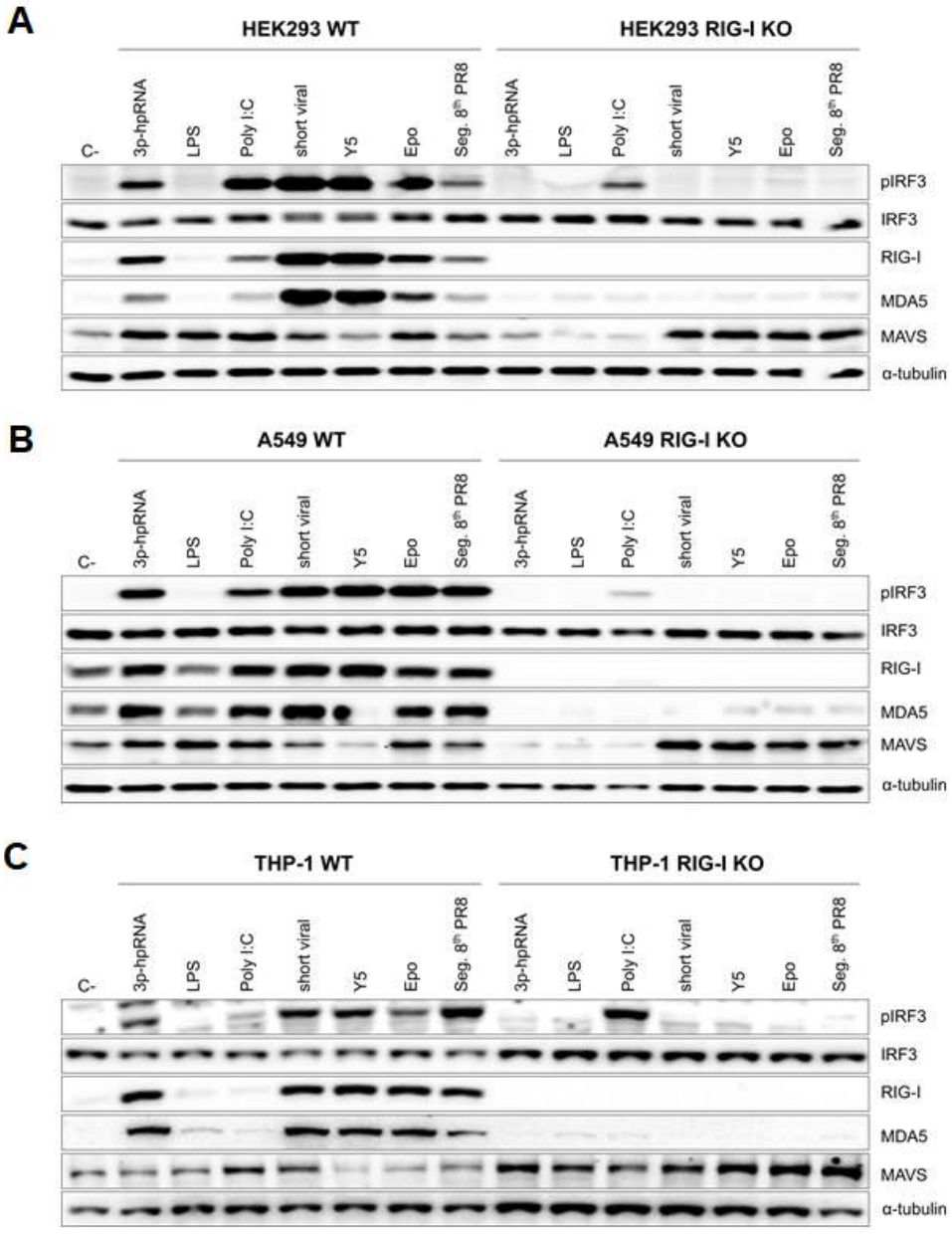
A
HEK293 WT
HEK293 RIG-I KO
C-
3p-hpRNA
LPS
Poly I:C
short viral
Y5
Epo
Seg. 8th PR8
pIRF3
IRF3
RIG-I
MDA5
MAVS
α-tubulin
B
A549 WT
A549 RIG-I KO
C
THP-1 WT
THP-1 RIG-I KO

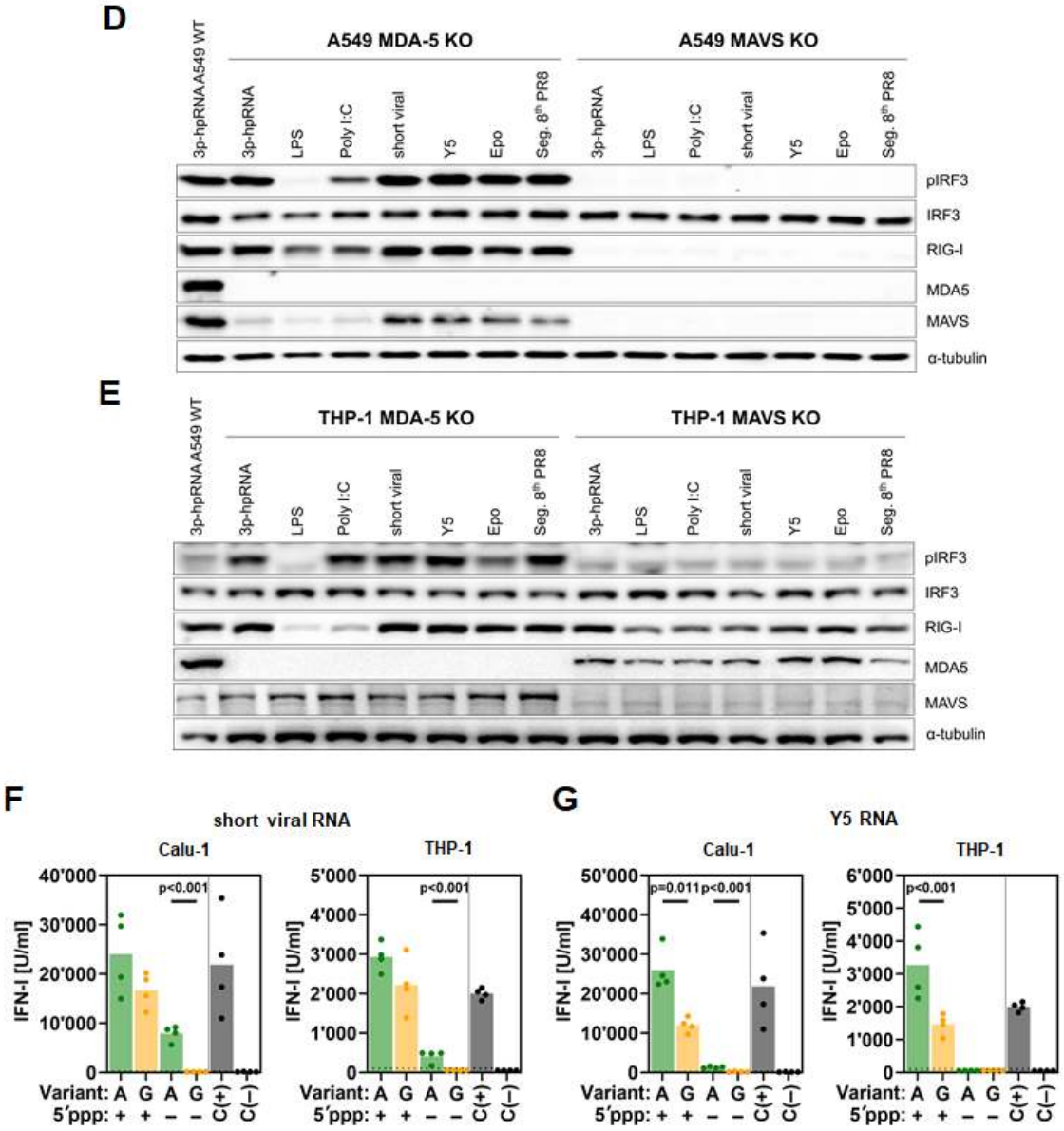

Supplementary Figure S2. RNA used in the study mostly act through RIG-I signalling pathway. (A-E) RIG-I/IFN pathway responses against RNAs starting from 5′-pppA and 5′-pppG in RIG-I KO cells (A-C) and in MDA-5 or MAVS KO cells (D, E). (F, G) Comparison of IFN responses against RNAs starting from 5′-pppA and 5′-pppG in cell cultures of human origin (THP-1 and Calu1). RNAs representing a fragment of the IAV genome (short viral RNA) and Pol III Y5 transcript were transfected into cells at a concentration of 100 ng/ml (n = 4). The positive control (C(+)) involved transfection with 100 ng/ml 3p-hpRNA, while the negative control (C(−)) was mock-transfected with lipofectamine alone. (A-E) The IRF3 phosphorylation pattern/RIG-I expression and (F, G) the concentrations of type I IFN in the supernatants were assessed using Western blot analysis and HEK-Blue assay, respectively, after 24 hours of incubation. (F, G) Upon log-transformation data were compared using two-way ANOVA with Šídák's multiple comparisons test.

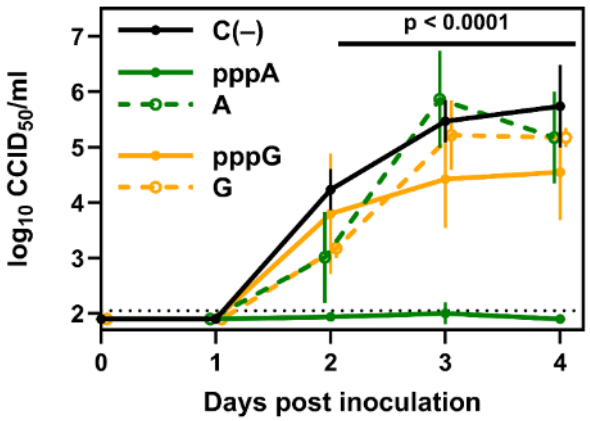

Supplementary Figure S3. 5′-pppA RNA is capable of lowering virus replication *in vitro* compared to 5′-pppG variant and dephosphorylated RNAs. Short viral RNA with either 5′-pppA and 5′-pppG or their dephosphorylated versions were transfected 24 h prior infection with IAV A/PR/8/34_NS1(R38A/K41A) at an MOI of 0.0001. Whiskers represent the standard deviation (SD) from four biological replicates. A significant reduction in virus replication was observed for 5′-pppA RNA with $P < 0.0001$ in two-way ANOVA followed by Dunnett's multiple comparison test to mock-infected cells (C(−)).

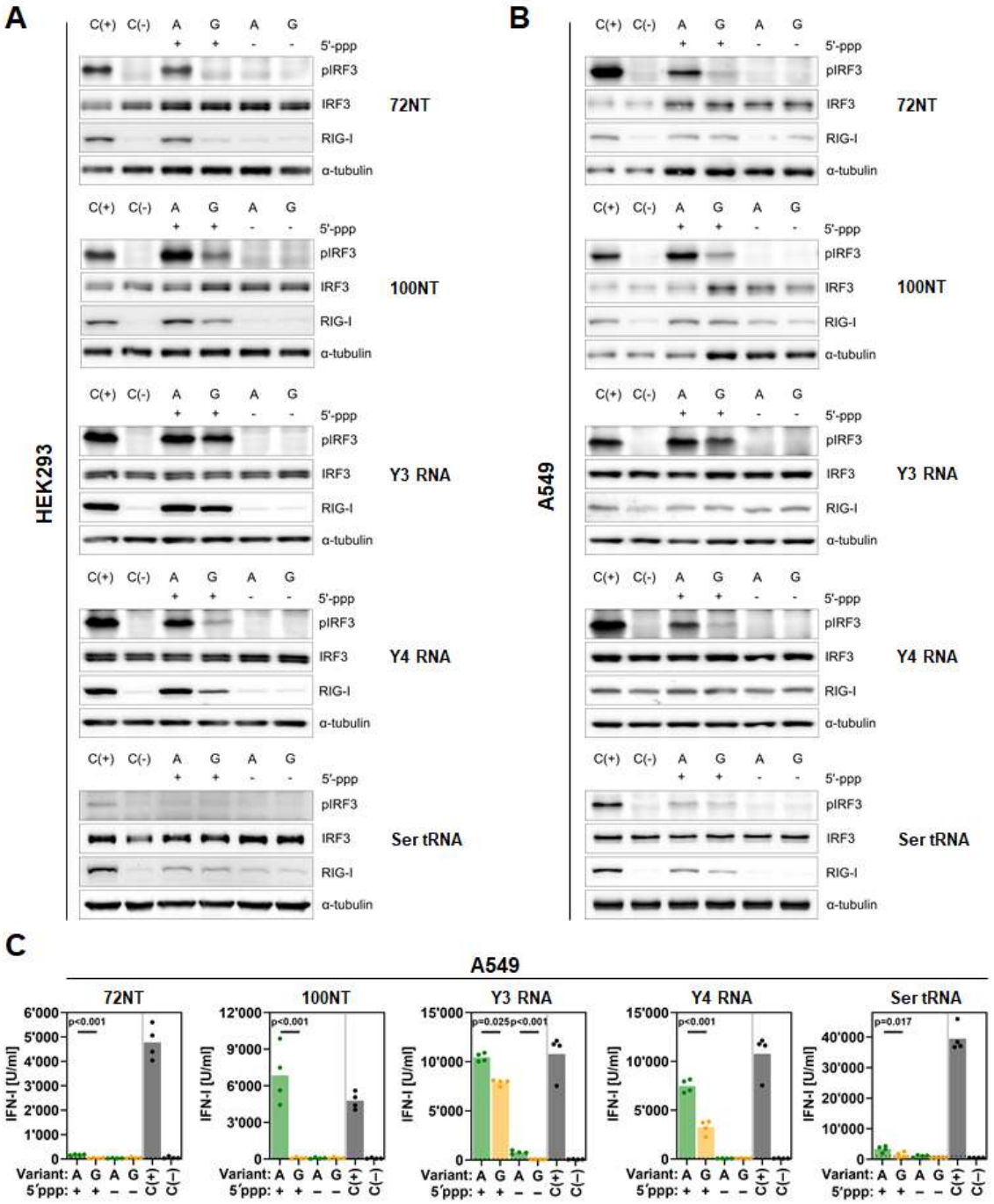

Supplementary Figure S4. Various IVT RNAs starting with 5′-pppA are more immunogenic than those starting with 5′-pppG. (A, B) RIG-I/IFN responses against different RNAs (sequences in Supplementary Table S1) starting from 5′-pppA and 5′-pppG were assessed with Western blot analysis 24 hours after transfection in HEK293 cells (A) and 8 hours in A549 cells (B). (C) The concentrations of type I IFN in the supernatants 8 hours after transfection in A549 cells were assessed with HEK-Blue assay (n = 4). All RNAs were transfected into cells at a concentration of 100 ng/ml. The positive control (C(+)) involved transfection with 100 ng/ml 3p-hpRNA, while the negative control (C(−)) was mock-transfected with lipofectamine alone.

A

ATTCTCACTGCAGCCTTTGACAGCCTTTGCCTCATCTTGCAGGTAGCAGCCGACACCAGCCTGCCT
TCCATCATGGTCAGCGAGTTGATCAAGGAGAACATGCACATGAAGCTGTATATGGAGGGGACCGTC
AACAACCACCACTTCAAATGCACGTCCGAGGGGGAGGGCAAACCGTACGAGGGCACCCAGACGATG
CGGATCAAGGCCGTCGAGGGGGGCCCTCTCCCCTTCGCCTTCGATATCCTCGCGACCAGCTTCATG
TACGGCTCCAAGACGTTCATCAACCACACGCAGGGCATCCCAGACTTCTTCAAGCAGTCGTTCCCG
GAAGGGTTCACGTGGGAGAGGGTGACCACGTACGAAGACGGTGGGGTGTTGACCGCTACGCAAGAC
ACGTCCCTCCAGGACGGCTGCCTGATTTACAACGTCAAGATCCGGGGCGTCAACTTCCCGAGCAAC
GGGCCCGTAATGCAGAAGAAGACTTTGGGGTGGGAGGCCTCGACCGAGACCTTGTACCCCGCCGAC
GGCGGCCTTGAGGGGCGAGCTGACATGGCTCTCAAGCTCGTCGGCGGGGGACACTTGATCTGCAAC
CTAAAAACGACGTACAGGTCCAAGAAGCCGGCGAAGAACCTAAAGATGCCTGGCGTCTACTACGTG
GACCGGAGGCTCGAGAGGATCAAGGAGGCGGACAAAGAGACCTACGTGGAGCAGCACGAGGTGGCA
GTCGCCCGCTACTGCGATCTCCCCAGTAAGCTCGGCCACCGGTAACAGCCATACCACATTTGTAGA
GGTTTTACTTGCTTTAAAAAACCTCCCACACCTCCCCCTGAACCTGAAACATAAAATGAATGCAAT
TGTTGTTGTTAACTTGTTTATTGCAGCTTATAATGGTTACA**AATAAA**GCAATAGCATCACAAATTT
CACA**AATAAA**GCATTTTTTTCACTGCATTCTAGTTGTGGTTTGTCCAAACTCATCAATGTATCTTA
ACGCGTAAATTGTAAGCGTTAATATCCTCTAGTTGGCGCGCC**AACAACAGGTGGATCCTCCACGCT**
GCGTTCCTGCTGTGCTTCTCCACCACAGCCCTCTCC

B

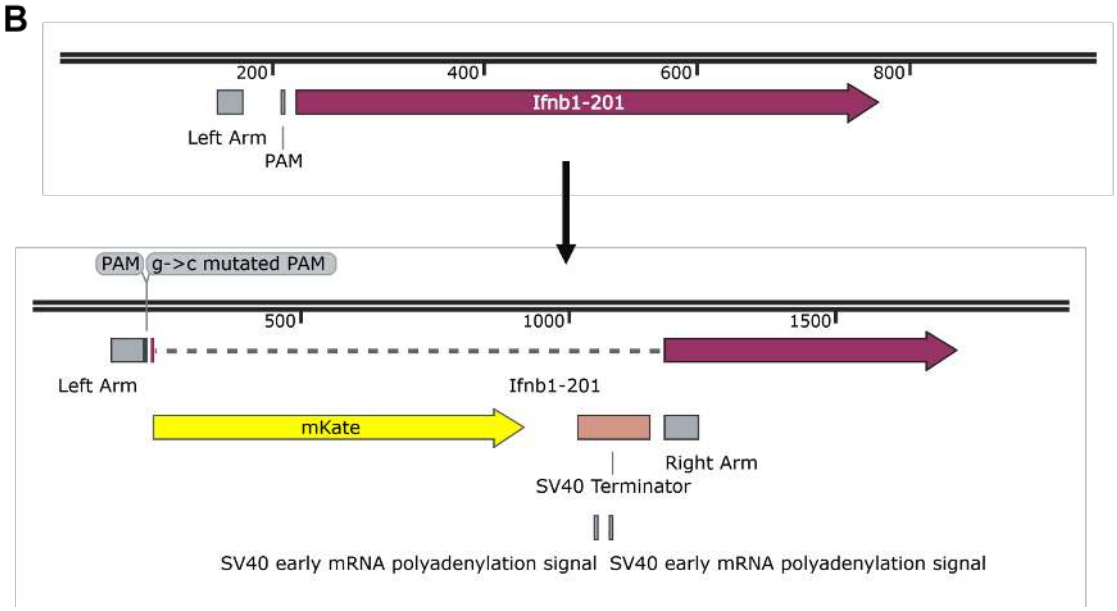

Supplementary Figure S5. Schematics of generating mice line harboring a fluorescent marker mKate2 in the IFN-β gene. (A) The nucleotide sequence of optimized mKate2 marker (highlighted in yellow), mutated protospacer-adjacent motif (highlighted in green), SV40 early mRNA polyadenylation signal (highlighted in red), and flanking regions of the murine genome (highlighted in bold). (B) The genomic context corresponds to *Mus musculus* strain C57BL/6J (the GRCm39 reference genome, chromosome #4, positions NC_000070.7:c88441083-88440949).

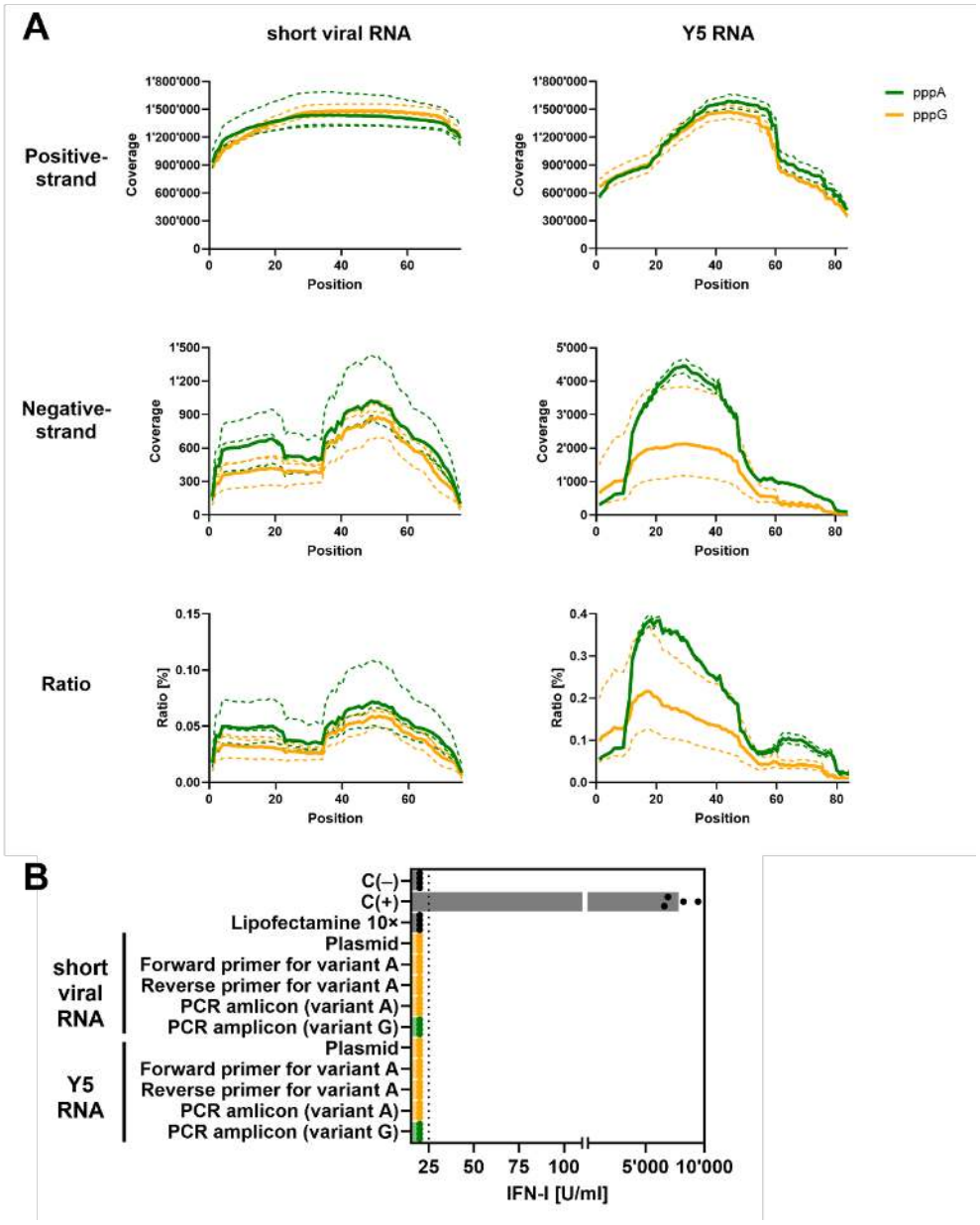

Supplementary Figure S6. Full-length antisense strand of IVT RNAs is detected by NGS. Results of stranded quantification of RNA. (A) Coverage depth for NGS data was separately calculated for reads mapped either to positive or negative, shown as individual dashed lines. Geometric mean values are represented by solid lines. The ratio of negative to positive strand reads was estimated for each replicate (n = 3 for short viral RNA; n = 2 for Y5 RNA). (B) Reagents used for transfection were tested in A549 cells with the HEK-Blue assay for IFN-I induction. Primers, original plasmids, and PCR amplicons were tested at a concentration of 100 ng/ml (n = 4). The positive control (C(+)) involved transfection with 100 ng/ml 3p-hpRNA, while the negative control (C(−)) was mock-transfected with lipofectamine alone. Lipofectamine 2000 was used at transfections at 1× concentration (2 µl/ml), no IFN-I induction was observed at higher (10×) concentrations.

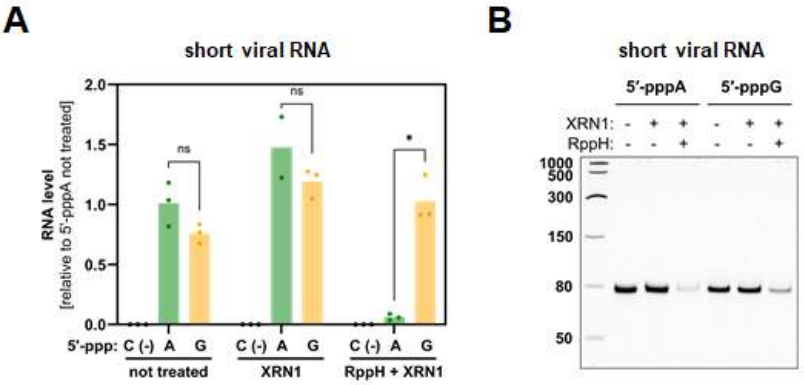

Supplementary Figure S7. 5′-pppA and 5′-pppG short viral RNAs exhibit similar stability and remain triphosphorylated after transfection into HEK293 cells as shown by *ex vivo* (A) and *in vitro* (B) analysis of RNA 5′-end phosphorylation state. (A) HEK293 cells were transfected with tested RNAs, then total RNA isolation followed by XRN1 or RppH combined with XRN1 treatment was performed. RT-qPCR was then used to assess the level of short viral RNA. Mean values of three biological replicates are shown. Data were compared using two-way ANOVA with Šídák's multiple comparisons test. (B) IVT derived short viral RNAs were treated with XRN1 or RppH and XRN1 and then PAGE/Urea was performed.

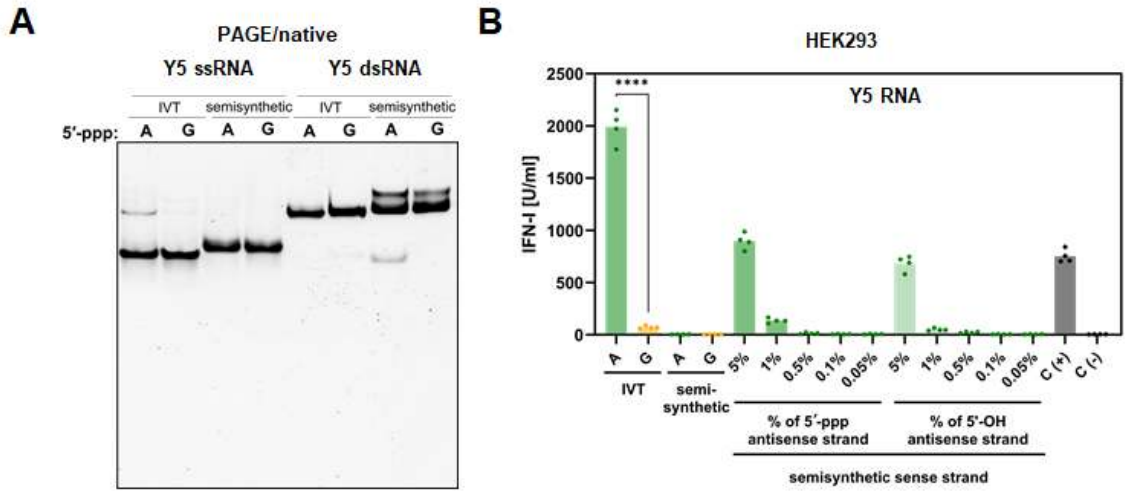

Supplementary Figure S8. Splint-ligated semisynthetic Y5 RNAs exhibit immunogenic potential only after annealing with 78 nt long complementary antisense RNA strand. (A) PAGE in native conditions of IVT Y5 RNAs and semisynthetic Y5 RNAs produced by splint ligation revealed dsRNA presence in IVT 5′-pppA, but not in semisynthetic counterparts. (B) To assess the immunogenic potential of splint-ligated RNAs, an IVT-produced antisense RNA, with or without triphosphate moieties, was added to the sense splint-ligated RNA. The positive control (C(+)) involved transfection with 100 ng/ml 3p-hpRNA, while the negative control (C(−)) was mock-transfected with lipofectamine alone. The concentration of type I IFN in the supernatants was measured using HEK-Blue IFN assay at 24 hours after transfection (n = 4).

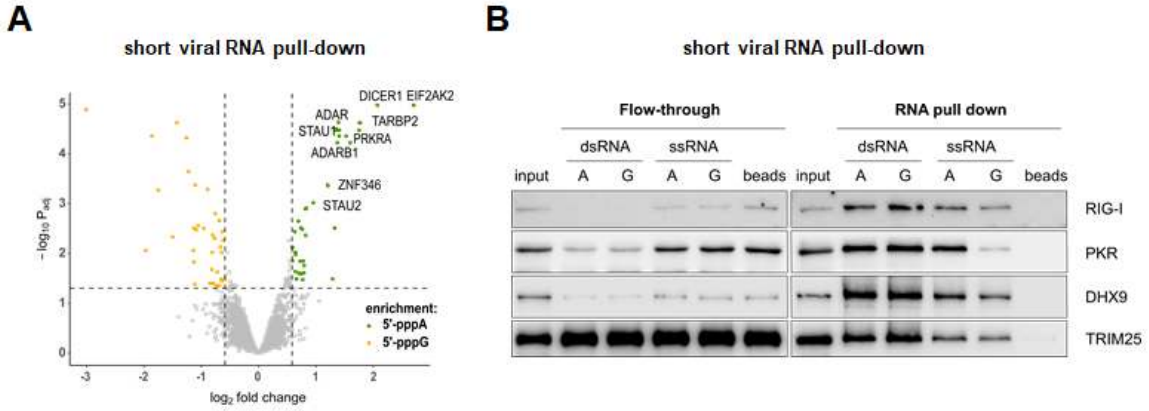

Supplementary Figure S9. dsRNA binding proteins were found to be enriched with 5′-pppA IVT RNA. (A) To assess interactome differences of 5′-pppA and 5′-pppG IVT short viral RNAs, RNA pull-down assay analysed with LC-MS/MS was performed. The volcano plot (A) illustrates protein enrichment based on the 5′ terminal nucleotide. Proteins enriched with 5′-pppA are highlighted in green, while those enriched with 5′-pppG are shown in orange. Double-stranded RNA-binding proteins are indicated on the plot. (B) RNA pull-down assay followed by Western blot analysis was conducted to validate the binding of PKR (EIF2AK2) – double-stranded RNA-binding protein identified through mass spectrometry (MS) analysis.

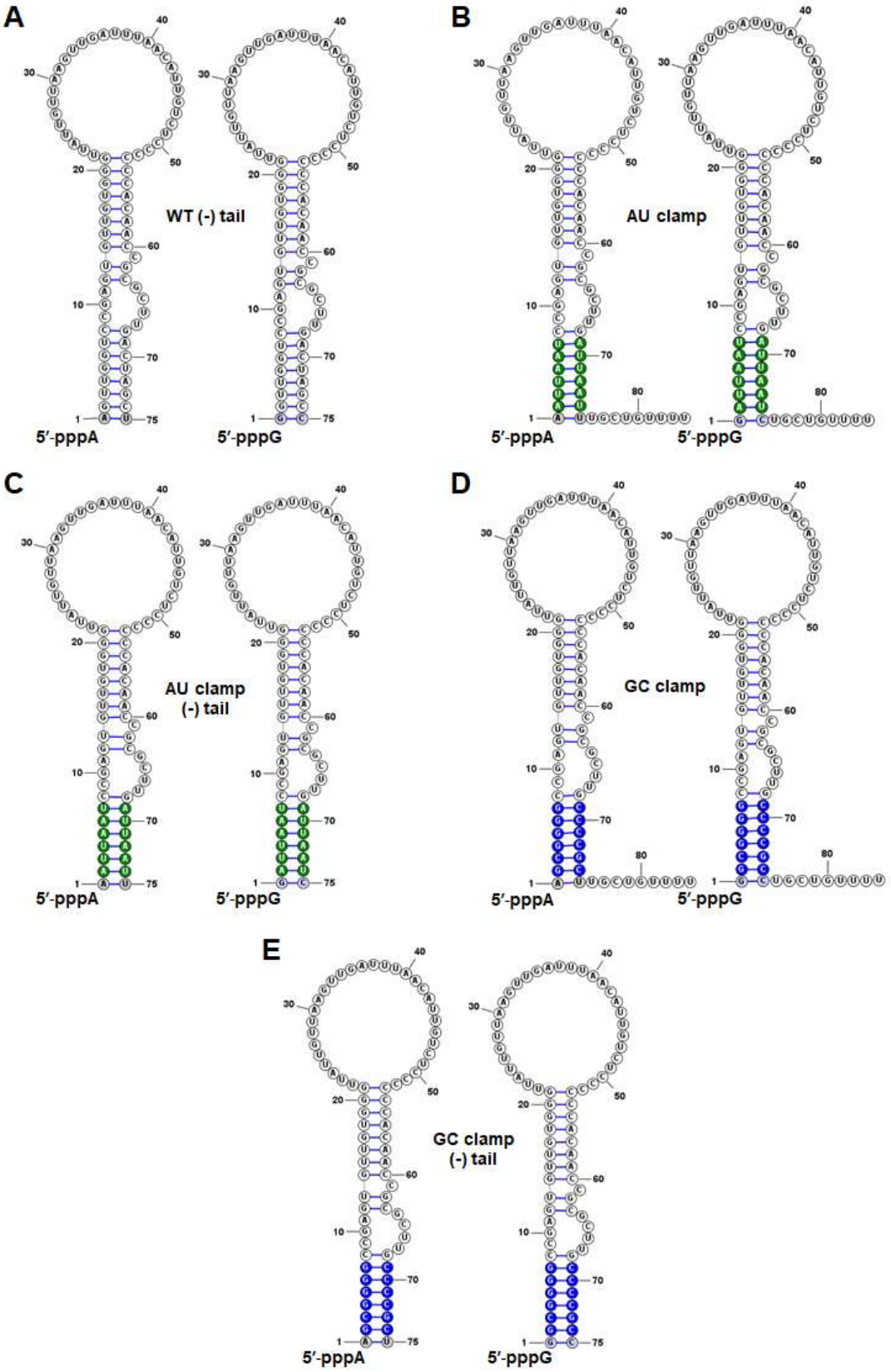

Supplementary Figure S10. Schemetic representation of Y5 RNA structural and sequence mutants. Secondary structures of Y5 RNA mutants were predicted using the MFE algorithm

in RNAstructure 6.4 software. Mutants starting with either 5′-pppA or 5′-pppG: (A) Y5 wild type RNA without a U-rich tail; (B) Y5 RNA with introduction of a six-nucleotide AU clamp (highlighted in green) with a U-rich tail; (C) Y5 RNA with a six-nucleotide AU clamp (highlighted in green) without a U-rich tail; (D) Y5 RNA with introduction of a six-nucleotide GC clamp (highlighted in blue) with U-rich tail; and (E) Y5 RNA with a six-nucleotide GC clamp (highlighted in blue) and without a U-rich tail.

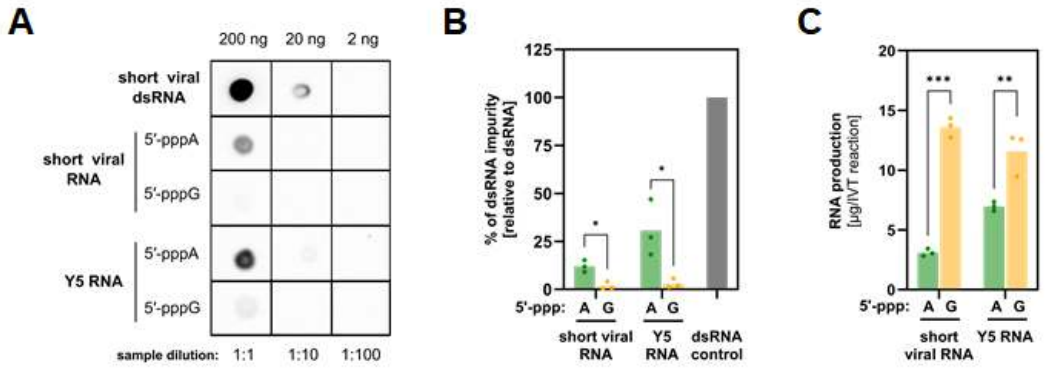

Supplementary Figure S11. *In vitro* transcription of 5′-pppA RNA results in lower production yield and higher dsRNA contamination. (A) Dot-blot analysis of IVT short viral and Y5 RNA starting from 5′-pppA or 5′-pppG was performed with anti-dsRNA J2 antibody. Equal volumes of purified RNA were applied to the membrane directly after IVT production, without normalization for RNA concentration. (B) Densitometric analysis was performed to assess the level of dsRNA contamination in purified RNAs after IVT (n = 3). (C) Yield of short viral and Y5 RNA production initiated with 5′-pppA or 5′-pppG, based on A260 RNA concentration measurements (n = 3). Data were compared using two-way ANOVA with Šídák's multiple comparisons test.

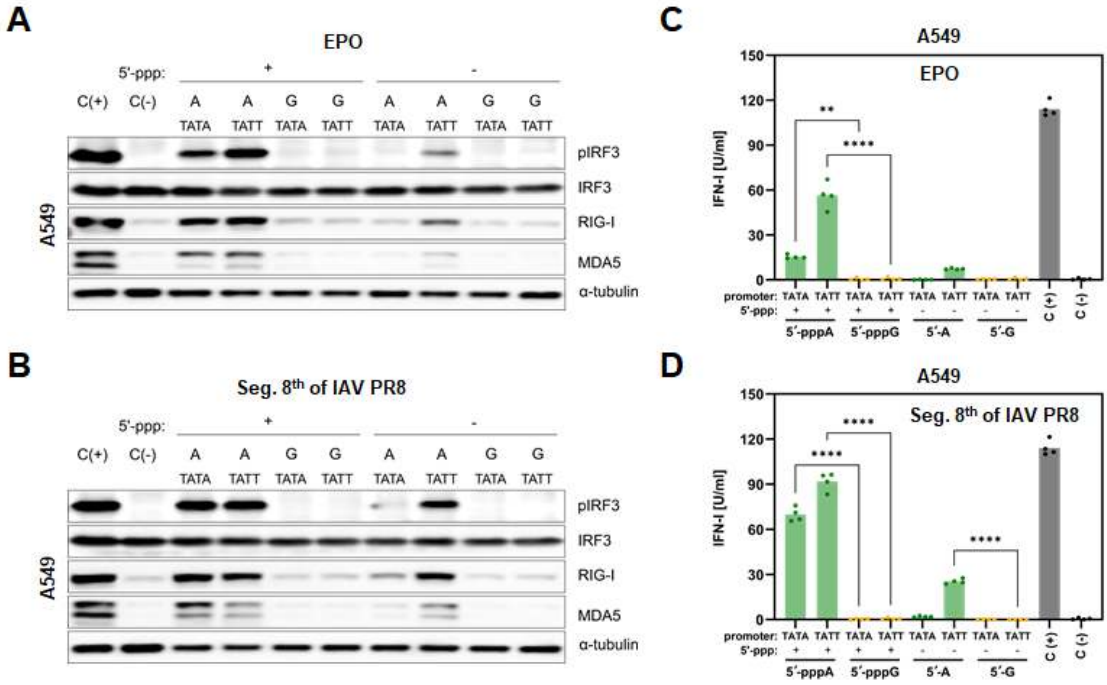

Supplementary Figure S12. Long IVT 5′-pppA RNAs are more immunogenic then 5′-pppG RNAs after transfection into A549 cells. RIG-I/IFN pathway responses against EPO and Seg. 8th of IAV PR8 RNAs starting from 5′-pppA or 5′-pppG were assessed with Western blot analysis (A, B) and HEK Blue IFN assay (C, D) 8 h after transfection into A549 cells (n = 4). The positive control (C(+)) involved transfection with 100 ng/ml 3p-hpRNA, while the negative control (C(−)) was mock-transfected with lipofectamine alone. (C, D) Data were compared using two-way ANOVA with Šídák's multiple comparisons test.

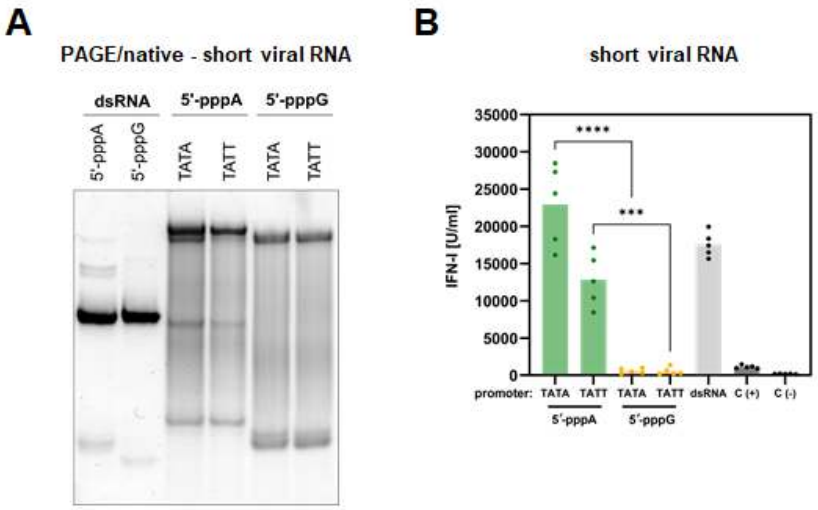

Supplementary Figure S13. Increased production of dsRNA in 5′-pppA IVT RNA is independent of T7 promoter type. (A) Native PAGE analysis of IVT control dsRNAs (produced by annealing of sense and antisense RNA strands) and IVT short viral RNAs starting from either 5′-pppA or 5′-pppG, generated using either Class III (TATA) or Class II (TATT) T7 promoters. (B) The immunogenicity of IVT RNAs was evaluated by measuring type I IFN levels in supernatants from HEK293 cells 24 hours post-transfection using the HEK Blue IFN assay (n = 5). The positive control (C(+)) involved transfection with 100 ng/ml 3p-hpRNA, while the negative control (C(−)) was mock-transfected with lipofectamine alone. Data were compared using two-way ANOVA with Šídák's multiple comparisons test.

Supplementary Table S1. RNA transcripts assessed in the current study.

Transcript	RNA variant	Sequence, 5′-3′
short viral	5′-pppA	AGCAAAAGCAGGGUGACAAAGACAUAAUGGAUCCAAACACUGUGUCAAGCUUUCAGGUAGAUUGCU UUCUUUGGCU
	5′-pppG	GGCAAAAGCAGGGUGACAAAGACAUAAUGGAUCCAAACACUGUGUCAAGCUUUCAGGUAGAUUGCU UUCUUUGGCC
short viral antisense	antisense to 5′-pppA	AGCCAAAGAAAGCAAUCUACCUGAAAGCUUGACACAGUGUUUGGAUCCAUUAUGUCUUUGUCACCC UGCUUUUGCU
	antisense to 5′-pppG	GGCCAAAGAAAGCAAUCUACCUGAAAGCUUGACACAGUGUUUGGAUCCAUUAUGUCUUUGUCACCC UGCUUUUGCC
Y5 WT	5′-pppA	AGUUGGUCCGAGUGUUGUGGGUUAUUGUUAAGUUGAUUUAACAUUGUCUCCCCCCCACAACCGCGCU UGACUAGCUUGCUGUUUU
	5′-pppG	GGUUGGUCCGAGUGUUGUGGGUUAUUGUUAAGUUGAUUUAACAUUGUCUCCCCCCCACAACCGCGCU UGACUAGCCUGCUGUUUU
78 nt Y5 antisense	antisense to 5′-pppA	GCAAGCUAGUCAAGCGCGGUUGUGGGGGGAGACAAUGUUAAAUCAACUUAACAAUAACCCACAACA CUCGGACCAACU
	antisense to 5′-pppG	GCAGGCUAGUCAAGCGCGGUUGUGGGGGGAGACAAUGUUAAAUCAACUUAACAAUAACCCACAACA CUCGGACCAACC
Y5 AU clamp	5′-pppA	AAUUAAUCCGAGUGUUGUGGGUUAUUGUUAAGUUGAUUUAACAUUGUCUCCCCCCCACAACCGCGCU UGAUUAAUUUGCUGUUUU
	5′-pppG	GAUUAAUCCGAGUGUUGUGGGUUAUUGUUAAGUUGAUUUAACAUUGUCUCCCCCCCACAACCGCGCU UGAUUAAUCUGCUGUUUU
Y5 GC clamp	5′-pppA	AGCGGGGCCGAGUGUUGUGGGUUAUUGUUAAGUUGAUUUAACAUUGUCUCCCCCCCACAACCGCGCU UGCCCCGCUUGCUGUUUU
	5′-pppG	GGCGGGGCCGAGUGUUGUGGGUUAUUGUUAAGUUGAUUUAACAUUGUCUCCCCCCCACAACCGCGCU UGCCCCGCCUGCUGUUUU
Y5 WT (-) tail	5′-pppA	AGUUGGUCCGAGUGUUGUGGGUUAUUGUUAAGUUGAUUUAACAUUGUCUCCCCCCCACAACCGCGCU UGACUAGCU
	5′-pppG	GGUUGGUCCGAGUGUUGUGGGUUAUUGUUAAGUUGAUUUAACAUUGUCUCCCCCCCACAACCGCGCU UGACUAGCC
Y5 WT (-) tail antisense	antisense to 5′-pppA	AGCUAGUCAAGCGCGGUUGUGGGGGGAGACAAUGUUAAAUCAACUUAACAAUAACCCACAACACUC GGACCAACU
Y5 AU clamp (-) tail	5′-pppA	AAUUAAUCCGAGUGUUGUGGGUUAUUGUUAAGUUGAUUUAACAUUGUCUCCCCCCCACAACCGCGCU UGAUUAAUU
	5′-pppG	GAUUAAUCCGAGUGUUGUGGGUUAUUGUUAAGUUGAUUUAACAUUGUCUCCCCCCCACAACCGCGCU UGAUUAAUC
Y5 GC clamp (-) tail	5′-pppA	AGCGGGGCCGAGUGUUGUGGGUUAUUGUUAAGUUGAUUUAACAUUGUCUCCCCCCCACAACCGCGCU UGCCCCGCU
	5′-pppG	GGCGGGGCCGAGUGUUGUGGGUUAUUGUUAAGUUGAUUUAACAUUGUCUCCCCCCCACAACCGCGCU UGCCCCGCC
72NT	5′-pppA	AGUAGAAACAAGGGUGUUUUUUAGUAGACACAGUGUUUGGAUCCAUUAUGUUUUUGUCACCCUGCU UUUGCU
	5′-pppG	GGUAGAAACAAGGGUGUUUUUUAGUAGACACAGUGUUUGGAUCCAUUAUGUUUUUGUCACCCUGCU UUUGCC
100NT	5′-pppA	AGUAGAAACAAGGGUGUUUUUUAGUACUAAAUAAGCUGAAACGAGAAAGUGCUUGACACAGUGUUU GGAUCCAUUAUGUUUUUGUCACCCUGCUUUUGCU
	5′-pppG	GGUAGAAACAAGGGUGUUUUUUAGUACUAAAUAAGCUGAAACGAGAAAGUGCUUGACACAGUGUUU GGAUCCAUUAUGUUUUUGUCACCCUGCUUUUGCC
Y3	5′-pppA	GGCUGGUCCGAGUGCAGUGGUGUUUACAACUAAUUGAUCACAACCAGUUACAGAUUUCUUUGUUCC UUCUCCACUCCCACUGCUUCACUUGACUAGCCUUUU
	5′-pppG	GGCUGGUCCGAGUGCAGUGGUGUUUACAACUAAUUGAUCACAACCAGUUACAGAUUUCUUUGUUCC UUCUCCACUCCCACUGCUUCACUUGACUAGCCUUUU
Y4	5′-pppA	GGCUGGUCCGAUGGUAGUGGGUUAUCAGAACUUAUUAACAUUAGUGUCACUAAAGUUGGUAUACAA CCCCCCACUGCUAAAUUUGACUGGCUUUUU
	5′-pppG	GGCUGGUCCGAUGGUAGUGGGUUAUCAGAACUUAUUAACAUUAGUGUCACUAAAGUUGGUAUACAA CCCCCCACUGCUAAAUUUGACUGGCUUUUU
tRNA	5′-pppA	AGAGAGGCCUGGCCGAGUGGUUAAGGCGAUGGACUGCUAAUCCAUUGUGCUCUGCACGCGUGGGUU CGAAUCCCAUCCUCGUUG
	5′-pppG	GGAGAGGCCUGGCCGAGUGGUUAAGGCGAUGGACUGCUAAUCCAUUGUGCUCUGCACGCGUGGGUU CGAAUCCCAUCCUCGUCG
Seg. 8th of IAV	5′-pppA	AGUAGAAACAAGGGUGUUUUUUAGUACUAAAUAAGCUGAAACGAGAAAGUUCUUAUCUCUUGCUCC ACUUCAAGCAAUAGAUGUAAGGCUUGCAUAAAUGUUAUUUGCUCAAAACUAUUCUCUGUUAUCUUC AGUUUGUGUCUCACUUCUUCAAUCAACCAUCUUAUUUCUUCAAACUUCUGACCUAAUUGUUCCCGC CAUUUCUCGUUUCUGUUUUGGAGUGAGUGGAGGUCUCCCAUUCUCAUUACUGCUUCUCCAAGCGAA UCUCUGUAGAGUUUCAGAGACUCGAACUGUGUUAUCAUUCCAUUCAAGUCCUCCGAUGAGGACUCC AACUGCAUUUUUGACAUCCUCAGCAGUAUGUCCUGGAAGAGAAGGCAAUGGUGAAAUUUCGCCAAC AAUUGCUCCCUCUUCGGUGAAAGCCCUUAGCAAUAUUAGAGUCUCCAGCCGGUCAAAAAUCACACU GAAGUUCGCUUUCAGUAUGAUGUUCUUAUCCAUGAUCGCCUGGUCCAUUCUGAUACAAAGAGGGCC UGCCACUUUCUGCUUGGGUAUGAGCAUGGACCAGUCCCUUGACAUUUCCUCAAGAGUCAUGUCAGU UAGGUAACGCGACGCAGGUACAGAGGCCAUGGUCAUUUUAAGUGCCUCAUCGGAUUCUUCUUUCAG AAUCCGCUCCACUAUCUGCUUUCCAGCACGUGUGGCUGUCUUGAUGUCCAGACCGAGAGUACUGCC

		CCUUCCUCUUAGGGAUUUCUGAUCUCGGCGAAGCCGAUCAAGGAAUGGGGCAUCACCUAGUUCUUG GUCUGCAACUCGUUUGCGGACAUGCCAAAGAAAGCAAUCUACCUGAAAGCUUGACACAGUGUUUGG AUCCAUUAUGUUUUUGUCACCCUGCUUUUGCU
	5′-pppG	GGUAGAAACAAGGGUGUUUUUUAGUACUAAAUAAGCUGAAACGAGAAAGUUCUUAUCUCUUGCUCC ACUUCAAGCAAUAGAUGUAAGGCUUGCAUAAAUGUUAUUUGCUCAAAACUAUUCUCUGUUAUCUUC AGUUUGUGUCUCACUUCUUCAAUCAACCAUCUUAUUUCUUCAAACUUCUGACCUAAUUGUUCCCGC CAUUUCUCGUUUCUGUUUUGGAGUGAGUGGAGGUCUCCCAUUCUCAUUACUGCUUCUCCAAGCGAA UCUCUGUAGAGUUUCAGAGACUCGAACUGUGUUAUCAUUCCAUUCAAGUCCUCCGAUGAGGACUCC AACUGCAUUUUUGACAUCCUCAGCAGUAUGUCCUGGAAGAGAAGGCAAUGGUGAAAUUUCGCCAAC AAUUGCUCCCUCUUCGGUGAAAGCCCUUAGCAAUAUUAGAGUCUCCAGCCGGUCAAAAAUCACACU GAAGUUCGCUUUCAGUAUGAUGUUCUUAUCCAUGAUCGCCUGGUCCAUUCUGAUACAAAGAGGGCC UGCCACUUUCUGCUUGGGUAUGAGCAUGGACCAGUCCCUUGACAUUUCCUCAAGAGUCAUGUCAGU UAGGUAACGCGACGCAGGUACAGAGGCCAUGGUCAUUUUAAGUGCCUCAUCGGAUUCUUCUUUCAG AAUCCGCUCCACUAUCUGCUUUCCAGCACGUGUGGCUGUCUUGAUGUCCAGACCGAGAGUACUGCC CCUUCCUCUUAGGGAUUUCUGAUCUCGGCGAAGCCGAUCAAGGAAUGGGGCAUCACCUAGUUCUUG GUCUGCAACUCGUUUGCGGACAUGCCAAAGAAAGCAAUCUACCUGAAAGCUUGACACAGUGUUUGG AUCCAUUAUGUUUUUGUCACCCUGCUUUUGCC
EPO	5′-pppA	AGGAAAUAAGAGAGAAAAGAAGAGUAAGAAGAAAUAUAAGACCCCGGCGCCGCCACCAUGGGGGUC CAUGAGUGCCCAGCUUGGCUCUGGCUGCUUCUGUCUCUGUUGUCCCUGCCAUUGGGCCUGCCUGUA CUGGGCGCACCACCUAGACUCAUAUGCGACAGCCGCGUCUUGGAACGAUAUCUCCUUGAGGCCAAG GAAGCAGAAAACAUCACCACCGGCUGCGCUGAGCAUUGUAGUCUGAAUGAAAACAUAACCGUUCCG GACACAAAGGUUAAUUUCUAUGCGUGGAAACGAAUGGAAGUAGGCCAGCAAGCUGUUGAGGUCUGG CAAGGGUUGGCACUUCUCUCAGAAGCUGUACUUCGCGGCCAGGCGCUCUUGGUCAACUCCAGUCAG CCAUGGGAGCCCCUCCAGCUCCAUGUUGAUAAGGCGGUAUCUGGUCUUCGAUCCCUGACGACUCUG CUUCGAGCGCUGGGGGCACAAAAGGAAGCCAUAUCUCCCCCUGAUGCGGCCUCUGCCGCGCCCCUC AGGACAAUCACAGCAGAUACUUUCAGAAAAUUGUUCAGGGUCUACUCCAAUUUCUUGCGGGGUAAG CUGAAGCUCUACACAGGCGAGGCAUGUCGAACGGGAGAUAGGUGAUAGG
	5′-pppG	GGGAAAUAAGAGAGAAAAGAAGAGUAAGAAGAAAUAUAAGACCCCGGCGCCGCCACCAUGGGGGUC CAUGAGUGCCCAGCUUGGCUCUGGCUGCUUCUGUCUCUGUUGUCCCUGCCAUUGGGCCUGCCUGUA CUGGGCGCACCACCUAGACUCAUAUGCGACAGCCGCGUCUUGGAACGAUAUCUCCUUGAGGCCAAG GAAGCAGAAAACAUCACCACCGGCUGCGCUGAGCAUUGUAGUCUGAAUGAAAACAUAACCGUUCCG GACACAAAGGUUAAUUUCUAUGCGUGGAAACGAAUGGAAGUAGGCCAGCAAGCUGUUGAGGUCUGG CAAGGGUUGGCACUUCUCUCAGAAGCUGUACUUCGCGGCCAGGCGCUCUUGGUCAACUCCAGUCAG CCAUGGGAGCCCCUCCAGCUCCAUGUUGAUAAGGCGGUAUCUGGUCUUCGAUCCCUGACGACUCUG CUUCGAGCGCUGGGGGCACAAAAGGAAGCCAUAUCUCCCCCUGAUGCGGCCUCUGCCGCGCCCCUC AGGACAAUCACAGCAGAUACUUUCAGAAAAUUGUUCAGGGUCUACUCCAAUUUCUUGCGGGGUAAG CUGAAGCUCUACACAGGCGAGGCAUGUCGAACGGGAGAUAGGUGAUAGG

Supplementary Table S2. Primers for IVT of RNAs. Yellow highlights T7 promoter, bold shows modified pair of the nucleotides.

Transcript	RNA variant	Forward primer, 5′-3′	Reverse primer, 5′-3′
short viral	5′-pppA	TAATACGACTCACTATT**A**GCAAAAGCAGGGTGACAA	**A**GCCAAAGAAAGCAATCTACCTG
	5′-pppG	TAATACGACTCACTATA**G**GCAAAAGCAGGGTGACAA	**G**GCCAAAGAAAGCAATCTACCTG
short viral antisense	antisense to 5′-pppA	AAGCTAATACGACTCACTATT**A**GCCAAAGAAAGCAATCTACC	**A**GCAAAAGCAGGGTGACAAAGAC
	antisense to 5′-pppG	AAGCTAATACGACTCACTATA**G**GCCAAAGAAAGCAATCTACC	**G**GCAAAAGCAGGGTGACAAAGAC
Y5 WT	5′-pppA	AAGCTAATACGACTCACTATT**A**GTTGGTCCGAGTGTTGTGGGTTAT	AAAACAGCA**A**GCTAGTCAAGCGCGGTTG
	5′-pppG	AAGCTAATACGACTCACTATA**G**GTTGGTCCGAGTGTTGTGGGTTATTG	AAAACAGCA**G**GCTAGTCAAGCGCGG
78 nt Y5 antisense	antisense to 5′-pppA	AAGCTAATACGACTCACTATTGCA**A**GCTAGTCAAGCGCGG	**A**GTTGGTCCGAGTGTTGTGG
	antisense to 5′-pppG	AAGCTAATACGACTCACTATAGCA**G**GCTAGTCAAGCGCGG	**G**GTTGGTCCGAGTGTTGTGG
Y5 AU clamp	5′-pppA	AAGCTAATACGACTCACTATT**A**ATTAATCCGAGTGTTGTGGGTTATTGTT	AAAACAGCA**A**ATTAATCAAGCGCGGTTGTGGG
	5′-pppG	AAGCTAATACGACTCACTATA**G**ATTAATCCGAGTGTTGTGGGTTATTGTT	AAAACAGCA**G**ATTAATCAAGCGCGGTTG
Y5 GC clamp	5′-pppA	AAGCTAATACGACTCACTATT**A**GCGGGGCCGAGTGTTGTGGGTTATTGTT	AAAACAGCA**A**GCGGGGCAAGCGCGGTTGTGGGGGGA
	5′-pppG	AAGCTAATACGACTCACTATA**G**GCGGGGCCGAGTGTTGTGGGTTATTGTT	AAAACAGCA**G**GCGGGGCAAGCGCGGTTGTGGGGGGA
Y5 WT (-) tail	5′-pppA	AAGCTAATACGACTCACTATT**A**GTTGGTCCGAGTGTTGTGGGTTAT	**A**GCTAGTCAAGCGCGGTTGT
	5′-pppG	AAGCTAATACGACTCACTATA**G**GTTGGTCCGAGTGTTGTGGGTTAT	**G**GCTAGTCAAGCGCGGTTGTG
Y5 WT (-) tail antisense	antisense to 5′-pppA	AAGCTAATACGACTCACTATT**A**GCTAGTCAAGCGCGGTTGTG	**A**GTTGGTCCGAGTGTTGTGG
Y5 AU clamp (-) tail	5′-pppA	AAGCTAATACGACTCACTATT**A**ATTAATCCGAGTGTTGTGGGTTATTGTT	**A**ATTAATCAAGCGCGGTTGTGGGG
	5′-pppG	AAGCTAATACGACTCACTATA**G**ATTAATCCGAGTGTTGTGGGTTATTGTT	**G**ATTAATCAAGCGCGGTTGTGGGG
Y5 GC clamp (-) tail	5′-pppA	AAGCTAATACGACTCACTATT**A**GCGGGGCCGAGTGTTGTGGGTTATTGTT	**A**GCGGGGCAAGCGCGGTTGTGGGGGGA
	5′-pppG	AAGCTAATACGACTCACTATA**G**GCGGGGCCGAGTGTTGTGGGTTATTGTT	**G**GCGGGGCAAGCGCGGTTGTGGGGGGA
72NT	5′-pppA	GCGTAATACGACTCACTATTAGTAGAAACAAGGGTGTTTTTTTAGT	**A**GCAAAAGCAGGGTGACAAAAACATAATG
	5′-pppG	GCGTAATACGACTCACTATAGGTAGAAACAAGGGTGTTTTTTTAGT	**G**GCAAAAGCAGGGTGACAAAAACATAATG
100NT	5′-pppA	GCGTAATACGACTCACTATT**A**GTAGAAACAAGGGTGTTTTTTTAGT	**A**GCAAAAGCAGGGTGACAAAAACATAATG
	5′-pppG	GCGTAATACGACTCACTATA**G**GTAGAAACAAGGGTGTTTTTTTAGT	**G**GCAAAAGCAGGGTGACAAAAACATAATG
Y3	5′-pppA	AAGCTAATACGACTCACTATT**A**GCTGGTCCGAGTGCAGTGGTGTT	AAAA**A**GCTAGTCAAGTGAAGCAG
	5′-pppG	AAGCTAATACGACTCACTATA**G**GCTGGTCCGAGTGCAGTGGTGTT	AAAA**G**GCTAGTCAAGTGAAGCAG
Y4	5′-pppA	AAGCTAATACGACTCACTATT**A**GCTGGTCCGATGGTAGTGGGTTAT	AAAA**A**GCCAGTCAAATTTAGCAG
	5′-pppG	AAGCTAATACGACTCACTATA**G**GCTGGTCCGATGGTAGTGGGTTAT	
tRNA	5′-pppA	AAGCTAATACGACTCACTATT**A**GAGAGGCCTGGCCGAGTG	C**A**ACGAGGATGGGATTCGAACCCAC
	5′-pppG	AAGCTAATACGACTCACTATA**G**GAGAGGCCTGGCCGAGTG	C**G**ACGAGGATGGGATTCGAACCCAC
Seg. 8th IAV	5′-pppA	III class promoter TATA GCGTAATACGACTCACTATA**A**GTAGAAACAAGGGTGTTTTTTAGT II class promoter TATT GCGTAATACGACTCACTATT**A**GTAGAAACAAGGGTGTTTTTTAGT	**A**GCAAAAGCAGGGTGACAAAAACATAATG
	5′-pppG	III class promoter TATA GCGTAATACGACTCACTATA**G**GTAGAAACAAGGGTGTTTTTTAGT II class promoter TATT GCGTAATACGACTCACTATA**G**GTAGAAACAAGGGTGTTTTTTAGT	**G**GCAAAAGCAGGGTGACAAAAACATAATG
EPO	5′-pppA	III class promoter TATA TAATACGACTCACTATA**A**GGAAATAAGAGAGAAAAGAAGAG II class promoter TATT TAATACGACTCACTATT**A**GGAAATAAGAGAGAAAAGAAGAG	TGCCGCCCACTCAGAC
	5′-pppG	III class promoter TATA TAATACGACTCACTATA**G**GGAAATAAGAGAGAAAAGAAGAG II class promoter TATT TAATACGACTCACTATT**G**GGAAATAAGAGAGAAAAGAAGAG	TGCCGCCCACTCAGAC

Supplementary Table S3. Cell lines.

Cell line	Source	Identifier
Human HEK293	ATCC	CRL-1573
Human HEK293 RIG-I KO	CRISPR/Cas9 created	N/A
Human A549	InvivoGen	a549d-nfis
Human A549 Dual RIG-I KO	InvivoGen	a549d-korigi
Human A549 Dual MDA-5 KO	InvivoGen	a549d-komda5
Human A549 MAVS KO	Kindly provided by Prof. Tomasz Lipniacki	N/A
Human THP-1	ATCC	TIB-202
Human THP-1 Dual RIG-I KO	InvivoGen	thpd-korigi
Human THP-1 Dual MDA-5 KO	InvivoGen	thpd-komda5
Human THP-1 Dual MAVS KO	InvivoGen	thpd-komavs
Human HEK-Blue IFN-α/β	InvivoGen	hkb-ifnab
Murine MEF	ATCC	CRL-2991
Murine bone marrow derived macrophages	N/A	N/A
Primary murine fibroblasts	N/A	N/A
Murine B16-Blue IFN-α/β	InvivoGen	bb-ifnt1

Supplementary Table S4. Primary antibodies.

Antigen	Vendor	Code	Dilution ratio
RIG-I	CellSignaling	3743	1/1000
pIRF3	CellSignaling	4947	1/1000
IRF3	Proteintech	11312-1-AP	1/1000
MDA-5	CellSignaling	5321	1/1000
MAVS	CellSignaling	3993	1/1000
α-tubulin	Proteintech	11224-1-AP	1/4000
dsRNA	Jena Bioscience	10010200 (J2)	1/1000

Warsaw, 03-09-2025

Jacek Szymański

Laboratory of RNA-Protein Interactions
– Dioscuri Centre

International Institute of Molecular
and Cell Biology in Warsaw
Ks. Trojdena 4 Street
02-109 Warsaw

Candidate's Contribution Statement

Article's title: 5' terminal nucleotide determines the immunogenicity of IVT RNAs

Authors: Magdalena Wolczyk*, Jacek Szymanski*, Ivan Trus*, Zara Naz, Tola Tame, Agnieszka Bolembach, Nila Roy Choudhury, Karolina Kasztelan, Juri Rappsilber, Andrzej Dziembowski, Gracjan Michlewski
Authors contributed equally

Journal: Nucleic Acid Research

Date of publishing: 19th December 2024

DOI: 10.1093/nar/gkae1252

I hereby declare that I, Jacek Szymański, made a substantive contribution to the development of this publication. My contribution consisted of:

- production and purification of RNAs prepared with *in vitro* transcription;

- optimalisation of splint ligation method and production of semi-synthetic RNAs;

- designing and conducting transfections RNAs in cell culture and analysis of RIG-I pathway activation via Western-blotting and HEK-blue type I IFN assay;

- designing and conducting RNA pulldown mass spectrometry (RP-MS) analysis, including proteomic data analysis;

- designing and conducting IVT stability and 5'-end phosphorylation state analyses;

INTERNATIONAL INSTITUTE OF MOLECULAR AND CELL BIOLOGY IN WARSAW
4 Ks. Trojdena Street, 02-109 Warsaw, Poland; phone: +48 22 597 07 00, fax: +48 22 597 07 15
e-mail: secretariat@iimcb.gov.pl, www.iimcb.gov.pl

- designing and conducting detection of dsRNAs equal volumes IVT production experiment using dot blot analysis;

- co-writing the manuscript and creating figures.

Candidate's Signature

Signature of the Corresponding Author

Appendix 2.

Manuscript 2

Szymanski J.[*], Wolczyk M.[*], Trus I., Naz Z., Idlin N., Jackiewicz J., Nowak E., Wuebben C., Hartmann G., Rappsilber J., Michlewski G. 5′-triphosphate guanosine RNAs recruit GTP-binding proteins to suppress RIG-I/IFN type I signalling. *bioRxiv* (2025). DOI: https://doi.org/10.1101/2023.12.22.573000

[*]Authors contributed equally

5′-triphosphate guanosine RNAs recruit GTP-binding proteins to suppress RIG-I/IFN type I signaling

Jacek Szymanski[1*], Magdalena Wolczyk[1*], Ivan Trus[1], Zara Naz[1], Nathalie Idlin[1], Justyna Jackiewicz[1], Elzbieta Nowak[1], Christine Wuebben[2], Gunther Hartmann[2], Juri Rappsilber[3,4,5] and Gracjan Michlewski[1]

* These authors contributed equally to this work.

[1] International Institute of Molecular and Cell Biology in Warsaw, Poland

[2] Institute of Clinical Chemistry and Clinical Pharmacology - Immunology in Translation, University Hospital Bonn, Germany

[3] The Wellcome Centre for Cell Biology, University of Edinburgh, UK

[4] Department of Biotechnology, Technische Universität Berlin, Germany

[5] Si-M/"Der Simulierte Mensch", a Science Framework of Technische Universität Berlin and Charité - Universitätsmedizin Berlin, Berlin, Germany

Correspondence should be addressed to G.M. (gmichlewski@iimcb.gov.pl)

Running Title: 5′-pppG RNAs recruit GTPases to block RIG-I signaling

Key words: RIG-I, IFN type I, 5′-triphosphate RNA guanosine (5′-pppG), 5′-triphosphate RNA adenosine (5′-pppA)

Abstract

The interferon (IFN) response is crucial for antiviral activity, but its overstimulation can lead to a wide range of autoimmune disorders. The cytoplasmic pattern recognition receptor RIG-I detects viral double-stranded RNAs (dsRNAs) and endogenous polymerase III transcripts carrying a 5′-triphosphate (5′-ppp) or 5′-diphosphate (5′-pp) moiety, triggering phosphorylation of IRF3 and IFN immune response. While many viral RNAs initiate with 5′-ppp-adenosine (5′-pppA) and most endogenous Pol III transcripts in higher eukaryotes start with 5′-ppp-guanosine (5′-pppG), no apparent reason for this bias has been identified so far. Here we demonstrate that dsRNAs initiating with 5′-pppA trigger stronger RIG-I/IFN response than those starting with 5′-pppG. We show that several GTP-binding proteins interact preferentially with 5′-pppG RNAs. Finally, supplementation with guanosine, but not adenosine, which rapidly increases intracellular concentrations of GTP and ATP, respectively, eliminates the difference in immunogenicity between 5′-pppG and 5′-pppA RNAs. Our findings suggest that 5′-pppG RNAs may enable certain RNA viruses and Pol III transcripts to limit detection by innate immune receptors. These results offer new insights into the sequence-dependent activation of the RIG-I/IFN pathway and have important implications for both antiviral immunity and the role of Pol III-derived RNAs in autoimmune diseases.

Introduction

In higher eukaryotes, the innate immune system acts as a rapid and essential defence mechanism against viral infections. This response is initiated when cellular sensors, known as Pattern Recognition Receptors (PRRs), detect molecular signatures commonly associated with pathogens, referred to as Pathogen-Associated Molecular Patterns (PAMPs). [1] One such molecular signature is the 5′-triphosphate (5′-ppp) group, which marks uncapped RNAs typically produced by viruses, but also present in some transcripts generated by RNA polymerase III. [2,3] Among the PRRs, Retinoic Acid-Inducible Gene I (RIG-I) plays a central role in detecting viral RNA that carries 5′-ppp motifs. Binding of such RNA induces a structural rearrangement in RIG-I and promotes its K63-linked ubiquitination by the E3 ligase Riplet. [4,5] This modification initiates a signaling cascade via the mitochondrial antiviral signaling protein (MAVS), leading to the activation of transcription factors IRF3, IRF7, and NF-κB. [6] Once activated, these factors migrate into the nucleus and drive the production of type I interferons, which initiate a broad antiviral program by upregulating interferon-stimulated genes (ISGs). [7] While essential for antiviral defence, uncontrolled activation of this pathway can result in chronic inflammation or autoimmunity. [8]

RIG-I protein displays highly selective ligand recognition, responding to both structural and chemical features of RNA. Its activation is triggered by short double-stranded RNAs (dsRNAs) with blunt ends, as well as by distinct molecular signatures such as 5′-triphosphate (5′-ppp) or 5′-diphosphate (5′-pp) groups. [9-12] Crucially, RIG-I can distinguish these ligands from host RNAs by recognizing the absence of 2′-O-methylation, a modification typically found in the capped ends of eukaryotic mRNAs. [13] Even minimal synthetic RNA constructs, including 10-base-pair duplexes or stem-loop structures, are sufficient to robustly activate RIG-I. [14,15] During Influenza A virus infection, short viral RNA fragments approximately 80 nucleotides in length

have been identified as highly potent RIG-I agonists, underscoring the critical role of RNA structure and composition in the activation of immune response. [16]

It has been noted that a substantial number of RNA viruses' genomes begin with 5′-ppp adenosine (5′-pppA) [17] and Pol III transcripts of higher eukaryotes and the genomes of some highly pathogenic RNA viruses initiate with 5′-ppp guanosine (5′-pppG). [18-22] To revisit this notion, we collated 5′-terminal nucleotides of representative RNA viruses, which are known to have 5′-ppp (Figure 1A and 1B). This collection revealed that some RNA viruses (such as influenza A virus - IAV) start predominantly from 5′-pppA, whereas other pathogenic viruses (including Ebola, Lassa, and HCV) can start from 5′-pppG or other nucleosides. Notably, attempts of mutations of the first nucleotide in viral genomes have already been noted in the literature. Intriguingly, IAV reverts to its wild-type configuration upon mutation or deletion of the first nucleotide, [23] while modifying the 5′ terminal nucleotide to another purine nucleotide in hepatitis C virus (HCV) is not feasible. [21,24] Moreover, HCV genotypes starting with 5′-pppA are largely capped with flavin adenine dinucleotide (FAD), which might prevent them from inducing RIG-I, while genotypes starting with 5′-pppG remain uncapped. [21]

On the other hand, Pol III transcripts are known to be synthesized with 5′-ppp (Figure 1A). Interestingly, most Pol III transcripts in higher eukaryotes, including non-coding tRNA, Y RNA, vault RNA, and 5S RNA, initiate from 5′-pppG. Although those transcripts are suboptimal RIG-I agonists with their 3′ end uridine-rich tails, they have been shown to be endogenous triggers of the RIG-I/IFN pathway. [25,26] Notably, among four human Y RNAs, only Y5 RNA starts from 5′-pppA, while the three others start from 5′-pppG. It has been reported that Y5 RNA shows mainly nuclear localization, [27] and our qRT-PCR (quantitative reverse transcription and polymerase chain reaction assay)-based quantification shows that Y5 RNA levels are the lowest compared to other Y RNAs in HEK293 cells (Supplementary

Figure S1). The reasons for these sequence preferences in both viral RNA genomes and Pol III transcripts remain unknown.

Our goal was to investigate the impact of the first nucleotide on RIG-I pathway activation. Since viral RNA genomes cannot be readily mutated at the 5′ end, the most suitable alternative was to use synthetic RNAs, which can be easily manipulated. Currently, the most widely used method for RNA production in both research and the RNA-based drug industry is T7 polymerase-based *in vitro* transcription (IVT). While this technique offers several advantages, such as relatively low cost and high production efficiency, it is also associated with the generation of various side products. [28] These include transcripts resulting from random priming of abortive products, read-through transcription of run-off transcripts, and promoter-independent transcription from either the sense strand of RNA or the antisense strand of the DNA template. [29-33] Although numerous purification strategies have been proposed to eliminate IVT-derived contaminants (reviewed in [34]), even RNAs purified by urea-PAGE will still contain highly immunogenic impurities formed by perfectly complementary RNA duplexes and the main RNA product. Notably, we have shown that IVT-based production of 5′-pppA generates much more immunogenic dsRNA than 5′-pppG. [35] Altogether, this makes the IVT-based preparation of single-stranded RNAs unsuitable for testing differences in immunogenicity between 5′-pppA and 5′-pppG transcripts.

To address this issue, we developed a strategy that utilizes only perfect dsRNA duplexes, produced using two different methodologies depending on the transcript length. For RNA molecules shorter than 40 nucleotides, we employed chemical solid-phase synthesis in two batches, in which the first strand, called “sense,” was synthetized with a 5′-ppp moiety and the second (“antisense”) lacked any phosphate modification (5′-OH). For transcripts longer than 40 nucleotides, we used IVT reactions to prepare both sense and antisense strands separately with each strand containing a 5′-ppp moiety. Our approach of using perfectly complementary

dsRNA duplexes has two major advantages: first, the dsRNA products are highly potent RIG-I agonists, and second, preparation of IVT-derived dsRNA by mixing sense and antisense strands in 1:1 ratio eliminates the confounding effects caused by a tiny fraction of dsRNA impurities overrepresented in the 5′-pppA RNAs. [35]

Here we provide the evidence that dsRNAs commencing with 5′-pppA elicit a considerably more robust RIG-I/IFN response in comparison to those originating with 5′-pppG. Notably, both dsRNAs exhibit comparable binding affinity and similar RIG-I activation in isolated systems, suggesting that differences in stimulation of the RIG-I/IFN pathway are unlikely to result from variations in their direct interaction with the receptor. Using RNA pull-down combined with mass spectrometry, we demonstrate that several GTPases and GTP-binding proteins exhibit a specific binding affinity for 5′-pppG RNAs. Finally, supplementation with guanosine which promptly elevates intracellular GTP levels through the nucleoside salvage pathway, but not with adenosine which increases ATP levels, abolishes the difference between 5′-pppG and 5′-pppA RNAs immunogenicity. We hypothesize that the highly abundant GTPases and GTP-binding proteins cause steric hindrance, thereby reducing RIG-I-mediated activation of the IFN response induced by 5′-pppG RNAs. Our findings suggest that 5′-pppG RNAs may enable certain RNA viruses and Pol III transcripts to evade detection by cellular immune sensors, uncovering a novel mechanism controlling sequence-dependent RIG-I/IFN pathway activation.

Results

5′-pppA dsRNAs stimulate the RIG-I/IFN pathway stronger than 5′-pppG dsRNAs in human and murine cells

To evaluate the biological significance of the observed 5′ terminal nucleoside identity in RIG-I agonists, we hypothesized that retention of the 5′-pppG RNAs may be an adaptation that

allows some RNA viruses and Pol III transcripts to evade detection by the RIG-I/IFN pathway. As stated in the introduction, direct mutagenesis of viruses or the use of IVT reactions to generate cognate single-stranded Pol III transcripts with similar levels of immunogenic dsRNA was not achievable. Instead, we employed two IAV-derived dsRNAs, which sense strand represents the beginning of the positive strand of segment 8th of the IAV PR8 strain – 76 bp IVT-produced dsRNA (Figure 2A) and its shorter analogue 24 bp dsRNA produced by chemical synthesis (Figure 2B). To investigate the role of the terminal nucleoside, we replaced the initial 5′-pppA with 5′-pppG in both IVT produced and synthetic dsRNAs, while maintaining the base pairing between the 5′-end of the first strand and 3′-end of the second strand by creating Watson-Crick base pairs (A:U and G:C) for the initial 5′-pppA or 5′-pppG (Figures 2A and 2B). The quality of dsRNA production was assessed through a two-step evaluation process. First, the integrity of the individual RNA strands was analyzed using denaturing urea-polyacrylamide gel electrophoresis (urea-PAGE) (Supplementary Figures S2A and S2C). Subsequently, successful duplex formation was verified via native polyacrylamide gel electrophoresis (native PAGE) (Supplementary Figures S2B and S2D). Then, HEK293 human embryonic kidney cells were transfected with either IVT 76 bp and synthetic 24 bp dsRNAs bearing 5′-pppA or 5′-pppG as a 5′ terminal nucleotide. The IVT 76 bp dsRNAs were tested at concentrations ranging from 0.1 ng/ml to 100 ng/ml, while the synthetic 24 bp dsRNAs were tested between 1 ng/ml and 1000 ng/ml. After 24 hours post transfection, IRF3 phosphorylation and RIG-I protein levels were assessed by western blot analysis. In cells treated with IVT 76 bp dsRNAs, higher levels of phosphorylated IRF3 (pIRF3) and RIG-I protein were observed in 5′-pppA dsRNA-transfected cells compared to 5′-pppG dsRNA-transfected cells, particularly at concentrations between 0.1 and 10 ng/mL (Figure 2C). The difference in pIRF3 and RIG-I was observed in all tested time points from 4 up to 24 hours post transfection (Supplementary Figure S3A). Moreover, the effects of varying strength of

RIG-I signaling activation were also observed at the mRNA level of *IFN1β* and *ISG15* (Interferon-Stimulated Gene 15) measured by qRT-PCR (Supplementary Figure S3B). A similar trend in RIG-I and pIRF3 expression was observed in cells transfected with synthetic 24 bp dsRNAs, although the effect was shifted to higher concentrations. Enhanced pIRF3 and RIG-I levels for 5′-pppA over 5′-pppG 24bp dsRNA were detected for 10 and 100 ng/ml concentrations, whereas no signs of RIG-I stimulation were observed at 1 ng/ml (Figure 2D). IVT-derived dsRNAs appeared to be more stimulatory for the RIG-I pathway, which may be attributed to a higher length but also the presence of 5′-ppp moieties on both ends of the RNA duplex in contrast to synthetic dsRNAs, which carry a 5′-triphosphate only on one strand. At higher dsRNA concentrations (10 ng/ml for IVT dsRNA and 100 ng/ml for synthetic dsRNA), a saturation effect was observed, with no observed difference in pIRF3 and RIG-I levels between 5′-pppA and 5′-pppG (Figures 2C and 2D).

Using IFN-α/β reporter HEK293 cells and colorimetric HEK-Blue IFN type I assay, we assessed the activity of IFN-α/β induced by the tested RNAs. Notably, IVT dsRNAs bearing a 5′-pppA induced significantly stronger IFN responses compared to those with 5′-pppG (Figure 2E). However, this difference reached statistical significance only at the lowest concentration tested (0.1 ng/ml). In case of synthetic dsRNAs, a trend of enhanced IFN production by the 5′-pppA variant was observed at 1 ng/ml, but no difference was observed in higher concentrations of dsRNA between the 5′-pppA and 5′-pppG variants (Figure 2F). Importantly, HEK293 cells transfected with either IVT 76 bp or synthetic 24 bp dsRNA lacking the 5′-triphosphate moieties showed no stimulation of IFN-α/β production (Figures 2E and 2F). Removal of 5′-triphosphate groups from the antisense strands of 76 bp dsRNA resulted in reduced phosphorylation of IRF3 and decreased expression of RIG-I for both 5′-pppA and 5′-pppG dsRNA variants (Supplementary Figure S3C). Notably, the differential response between the 5′-pppA and 5′-pppG forms remained evident. Complete dephosphorylation of both RNA

strands in dsRNAs led to full suppression of the RIG-I/IFN signaling pathway (Supplementary Figure S3C).

To minimize potential false positive results due to IVT contaminants, through a semisynthetic approach we generated 76 bp dsRNAs. Specifically, a 55 nt RNA produced by IVT was ligated to a chemically synthesized 21 nt RNA using splint ligation to create a triphosphorylated sense strand, as previously described. [35] When evaluated in the HEK-Blue IFN type I assay, both 76 nt semisynthetic ligated 5′-pppA and 5′-pppG sense strand RNAs exhibited no detectable immunostimulatory activity at the tested concentrations (Supplementary Figure S3D). However, the addition of trace amounts (0.05–1%) of a fully complementary, IVT-produced, dephosphorylated 76 nt antisense RNA strand to form complete dsRNA was sufficient to activate the RIG-I/IFN pathway. Importantly, the distinct responses between 5′-pppA and 5′-pppG RNAs were still observable (Supplementary Figure S3D).

We next conducted transfection experiments using reporter bone marrow-derived macrophages (BMDMs) isolated from homozygous *mKate2* reporter mice, which enable real-time visualization of IFN-β expression via *mKate2* fluorescence. [35] A more robust IFN-β promoter activation was observed for RNAs initiating with 5′-pppA in cells transfected with either IVT-derived 76 bp dsRNA or fully synthetic 24 bp dsRNA (Figures 2G and 2H). In the case of 76 bp IVT dsRNA, a statistically significant difference in fluorescence between the 5′-pppA and 5′-pppG variants emerged at 8 hours post-transfection. For the synthetic 24 bp dsRNAs, this distinction became significant at 13 hours post-transfection. Throughout the time course, 5′-pppA RNAs were up to three times and fourteen times more immunogenic than the corresponding 5′-pppG constructs, for 76 bp and 24 bp dsRNAs respectively (Supplementary Figures S3E and S3F). Notably, no activation of the RIG-I/IFN signaling pathway was detected in BMDMs transfected with dsRNAs lacking 5′-triphosphate moieties, confirming the requirement of this structural feature for immune activation.

The observed effects were not limited to our two representative RNAs. Similar patterns were seen with IVT-derived dsRNAs, whose sense-strand sequences were taken from pre-let-7a and Y5 RNA (Supplementary Figures S4 and S5). Notably, the immunogenicity of Y5 RNA-derived dsRNA was strongly dependent on its concentration. At 0.1 ng/ml, the 5′-pppA Y5 dsRNA was up to forty times more immunogenic than the corresponding 5′-pppG construct, whereas at 10 ng/ml it was only about twice as immunogenic (Supplementary Figures S5F and S5G). Additionally, Y5-derived dsRNAs with 6xGC clamps at both ends exhibited substantially lower immunogenic potential than their wild type counterparts. Furthermore, a short synthetic, partially double-stranded RIG-I agonist with a blunt end (details available in the patent WO/2025/088117A1*)* also demonstrated that 5′-pppA RNA is up to twenty times more potent RIG-I stimulant than 5′-pppG RNA (Supplementary Figure S6). These results show that the increased immunogenicity of 5′-pppA-containing RNAs, compared with 5′-pppG, can be observed across a range of RIG-I agonists.

Taken together, these findings reveal a consistent pattern whereby dsRNAs bearing 5′-pppA ends are more immunogenic in both human and murine cells than equivalent sequences bearing a 5′-pppG terminus, highlighting the importance of RNA concentration in this context. Although this difference is observed in the human continuous cell line, a murine assay using primary cells (BMDMs with an *mKate2* reporter that allows real-time monitoring of IFN-β promoter activity) reveals a more robust difference in immunogenicity based on the identity of the 5′ terminal nucleotide. Furthermore, this effect is associated with the RIG-I/IFN signaling pathway, as stimulation is entirely reliant on the presence of 5′-triphosphate moieties.

5′-pppA and 5′-pppG RNAs show different binding affinity but similar activation in biochemical assays with recombinant RIG-I

To further investigate whether the observed significant difference in RIG-I/IFN pathway activation by 5′-pppA and 5′-pppG RNAs could be due to impaired binding of RIG-I to these RNAs, electrophoretic mobility shift analysis (EMSA) was performed. This assay was used to measure the binding affinities of 5′-pppA and 5′-pppG double-stranded RNAs to purified, recombinant RIG-I protein (Figures 3A and 3B and Supplementary Figure S7). Due to the method requirement of a fluorophore presence in the RNA molecule, 3′ end modification of the sense strand for IVT-produced dsRNA and 5′ end modification of the antisense strand with fluorescein amidite (6-FAM) for synthetic 24 bp dsRNA was introduced. Binding affinity measurements revealed that RIG-I binds to 5′-pppA IVT 76 bp dsRNA with significantly higher affinity (K_d = 1.47 nM) compared to 5′-pppG dsRNA (K_d = 2.32 nM) (Figure 3E and Supplementary Table S1). Notably, dephosphorylation of the 5′-pppA dsRNA resulted in an ~8-fold reduction in RIG-I binding affinity (K_d = 10.84 nM), whereas the corresponding 5′-OH-G dsRNA exhibited only a modest, non-significant decrease in binding affinity (K_d = 2.94 nM) relative to its triphosphorylated counterpart. A similar trend was observed for direct interaction between recombinant RIG-I and synthetic 24 bp dsRNA (Figure 3B). The binding affinity for 5′-pppA (K_d = 0.40 nM) was significantly higher compared to 5′-pppG (K_d = 0.94 nM). Consistent with previous observations, the interaction of RIG-I with 5′-OH-A dsRNA was approximately 8-fold weaker (K_d = 4.50 nM) than with its triphosphorylated form and decrease in binding affinity to 5′-OH-G was reduced by only ~2-fold (K_d = 1.81 nM) relative to 5′-pppG, but in this case the difference was significant (Figure 3E and Supplementary Table S1).

To gain a deeper understanding of the interaction between RIG-I and dsRNA in relation to the 5′ terminal nucleotide under isolated conditions, we performed a RIG-I activation

measurement. Based on previous studies that demonstrate a correlation between RIG-I activation by 5′-ppp RNA and its ability to hydrolyse ATP to ADP, an ATPase assay was applied to assess the activity of recombinant RIG-I upon dsRNA binding. A parameter used to compare RIG-I activity upon binding to different RNAs was the half maximal effective concentration (EC_{50}) of the tested RNAs (Figures 3C and 3D). The result obtained for IVT 76 bp dsRNA by this methodology showed that triphosphorylated dsRNAs were most triggering RIG-I activity and differences between 5′-pppA (EC_{50} = 0.074 nM) and 5′-pppG (EC_{50} = 0.081 nM) were minimal and non-significant. Triphosphate-depleted dsRNAs were less effective ATPase activators, and in line with EMSA results, 5′-OH-A (EC_{50} = 0.308 nM) was much less RIG-I stimulatory than 5′-OH-G (EC_{50} = 0.192 nM). Similarly, synthetic 5′-ppp dsRNAs robustly activated RIG-I, with negligible differences between 5′-pppA (EC_{50} = 0.041 nM) and 5′-pppG (EC_{50} = 0.039 nM), and RNAs lacking triphosphate moiety – 5′-OH-A (EC_{50} = 0.092 nM) and 5′-OH-G (EC_{50} = 0.058 nM) – showed substantially reduced potency (Figure 3E and Supplementary Table S1).

Comparing those results with experiments performed on human and mouse cells, we speculate that immunogenic potential of dsRNA might be only partially explained by the difference in direct binding affinity of RIG-I protein to 5′-pppA and 5′-pppG dsRNA. However, the immunogenic potential of dsRNA does not strictly correlate with ability to activate RIG-I, as we observed no differences in ATPase assays. This suggests that the observed mechanism of differential immunogenic potential of 5′-pppA *vs.* 5′-pppG RNAs cannot be fully recapitulated in isolated conditions with recombinant RIG-I protein. Therefore, the difference in RIG-I pathway activation by 5′-pppA and 5′-pppG RNAs might be due to sequence-specific cellular factors that are not present in biochemical assays.

5′-pppA and 5′-pppG RNAs bind different sets of RBPs

To elucidate the cellular mechanism behind the difference in the immunogenicity of 5′-pppA *vs.* 5′-pppG RNAs, we employed RNA pull-down coupled with label-free quantitative mass spectrometry (RP-MS), [36] identifying proteins in cell extracts that exhibited differential binding affinities to the tested dsRNAs (Figure 4A). While most proteins displayed similar binding between the two RNAs, a subset of proteins emerged as outliers (Figure 4B). The 5′-pppA IVT 76 bp dsRNA pull-down enriched for a substantial group of proteins involved in nucleic acid metabolism, RNA stability, or degradation. Notably, the 5′-pppG IVT 76 bp dsRNA pulled-down proteins associated with translation and RNA transport. A considerable proportion of proteins enriched in the 5′-pppG IVT 76 bp dsRNA pull-down possesses GTP binding, small GTPase binding, or GTPase activity and are involved in translation process (Figure 4C). Conversely, few binders of 5′-pppA IVT 76 bp dsRNA were classified as single stranded RNA binding proteins, which is somewhat unexpected given that a dsRNA molecule was used as the bait in the pull-down assay (Figure 4D).

To further validate these findings, we employed RNA pull-down western blot analysis using HEK293 cell lysates and either IVT 76 bp or synthetic 24 bp dsRNAs (Figure 4E and 4F). These results confirmed the increased binding of NUDT16, RAN, and RANBP1 proteins to the 5′-pppG IVT 76 bp dsRNA and its shorter analogue - synthetic 5′-pppG 24 bp dsRNA. Simultaneously, double-stranded RNA binding proteins PKR and DHX9 were captured by 5′-pppA and 5′-pppG RNAs in a similar way, confirming equal RNA quality and loading (Figures 4E and 4F). Surprisingly, no apparent difference in RIG-I binding between 5′-pppA and 5′-pppG RNAs was observed. This may indicate that RNA pull-down is not sensitive enough to detect subtle differences in protein affinity, or that the factors influencing differential RIG-I stimulation by 5′-pppA and 5′-pppG differ between *in cellulo* and *ex vivo* conditions. Finally, to check the dependence of binding of the identified proteins to the tested RNAs on

the presence of the triphosphate moiety at the 5′ end of RNAs, we also tested dephosphorylated RNAs. Intriguingly, we observed that removing the 5′-ppp group from dsRNAs does not affect binding of RIG-I protein but results in complete inhibition of binding of 5′-pppG enriched proteins to dephosphorylated RNAs initiating with G (Figures 4E and 4F). Next, to investigate the influence of GTP binding proteins on the RIG-I-RNA interaction, we introduced non-hydrolyzable GTP analogs to protein extracts during the RNA pull-down procedure. This approach aimed to occupy the GTP-binding pockets, thereby impeding the interaction of the GTP-binding proteins with 5′-pppG RNAs. Indeed, supplementation with GTP analogs led to a complete blockade of NUDT16, RAN, and RANBP1 binding to RNAs (Figures 4E and 4F). In contrast, the binding of reference proteins DHX9 and PKR to dsRNAs remained unaffected. Taken together, these findings identify for the first time proteins that bind differentially to dsRNA containing 5′-pppG and 5′-pppA and show that GTP-binding proteins use a shared pocket to bind both GTP and 5′-pppG RNAs.

Nucleoside salvage pathway-driven GTP increase equalises immunogenicity of 5′-pppG and 5′-pppA dsRNAs

To assess whether GTP-binding proteins have any effect on the activation of the RIG-I/IFN pathway *in cellulo*, we aimed to saturate them with elevated levels of GTP. To achieve this, we increased intracellular GTP levels by stimulating the nucleoside salvage pathway (Figure 5A) through supplementation of the growth medium with guanosine. [37,38] As a control we used supplementation with adenosine, which results in elevation of ATP levels. HEK293 cells were cultured for 48 hours in medium supplemented with guanosine, adenosine or DMSO serving as a vehicle control. Following this preconditioning, cells were transfected with 76 bp dsRNA bearing either 5′-pppA or 5′-pppG termini to assess the impact of altered purine nucleotide pools on dsRNA sensing and signaling. Following guanosine supplementation, transfection with both 5′-pppA and 5′-pppG 76 bp dsRNAs resulted in elevated IFN production compared

to DMSO or adenosine-treated controls (Figure 5B-D). Importantly, the difference in IFN response, evaluated by measuring IRF3 phosphorylation and RIG-I levels, between 5′-pppA and 5′-pppG dsRNAs was substantially reduced in guanosine-enriched conditions (Figure 5B-D). These findings suggest that *in cellulo* elevated GTP levels enhance the RIG-I/IFN response and saturate GTP-binding proteins that normally bind 5′-pppG dsRNA and block RIG-I recognition through steric interference.

In summary, our study demonstrates that dsRNAs commencing with 5′-pppA trigger a more robust RIG-I/IFN response in comparison to their corresponding counterparts initiating with 5′-pppG. The observed phenomenon holds across various tested RNAs, cell lines as well as in mice and human cells. Our working hypothesis proposes that GTPases and GTP-binding proteins impede the activation of RIG-I by 5′-pppG RNAs within the cellular environment, thereby diminishing their immunogenicity (Figure 6).

Discussion

Viruses possess a range of conserved features, including uncapped 5′-ppp termini, unmethylated CpG-rich motifs, or dsRNAs. Although these features are typically absent or occluded in eukaryotic host RNAs, they function as targets for host innate immune system proteins, including RIG-I. [39,40] Under pathological conditions, host RNAs can trigger the RIG-I pathway. [41,42] To avoid erroneous activation of this pathway, host RNAs have evolved distinct molecular features and some characteristics that prevent recognition by the innate immune system. These include the presence of cap structures and nucleotide modifications on RNA polymerase II-derived mRNAs [42], specific cleavage patterns and chemical modifications on RNA polymerase I-transcribed rRNAs [43], and the clearance of 5′-ppp termini on RNA polymerase III transcripts, achieved through the activity of phosphatases such as triphosphatase dual-specificity phosphatase 11 (DUSP11). [44] Additionally, subcellular compartmentalization,

as seen in the restricted localization of mitochondrial dsRNA, further limits unwanted immune detection. [44] Collectively, these adaptations ensure that host RNAs remain largely undetected by the innate immune system under physiological conditions.

Here we propose a new conceptual model underlying sequence-specific RNA recognition by RIG-I and the ensuing adequate activation of the type I interferon response (Figure 6). In this model, endogenous RNAs, representing most Pol III transcripts in higher eukaryotes, and certain highly pathogenic viruses initiate with 5′-pppG. This would make them relatively weak RIG-I agonists due to interference by GTP-binding proteins and GTPases. Notably, GTPases typically exhibit affinities for GTP in the nanomolar range, whereas known ATPases show affinities in the high micromolar range.[45,46] More recent study indicates that GTP-binding affinities are approximately 3,000-fold higher than those of ATPases.[47] This difference may explain why RNAs with 5′-pppG termini are more affected than those with 5′-pppA ends. This and additional mechanisms, such as dephosphorylation by DUSP11, [44] could contribute to evading detection by the RIG-I signaling pathway. Conversely, RNAs commencing with 5′-pppA, a characteristic of more prevalent viruses like IAV or HCV, exhibit greater potential for RIG-I/IFN pathway activation, which drives them to evolve mechanisms to silence or evade immune response. In the case of IAV, its NS1 protein has multiple functions that interfere with the host immune system [48], while in HCV, subtypes carrying 5′-pppA but not 5′-pppG are capped by FAD.[21] Although some reports suggest that FAD might not be hindering RIG-I activity.[49] Additionally, IAV is known to use a 5′-cap-snatching strategy to hide its transcripts from innate sensors and secure efficient cap-dependant translation. [50] The results presented here demonstrate that IVT-produced or chemically synthesised dsRNAs initiating with 5′-pppA are more immunogenic than those starting with 5′-pppG. Similar differences for short dsRNAs have been observed before but remained unexplored.[10] Substantiating these findings is the observation that the Pol III transcript Y5 RNA, bearing 5′-pppA, is expressed at markedly

lower levels compared to other Y RNAs initiating with 5′-pppG (Supplementary Figure S1) and is retained in the nucleus.[27] Taken together, we speculate that the preservation of more immunogenic 5′-pppA termini in viruses may be influenced by constraints imposed by promoter and polymerase functions. Conversely, elevated IFN signaling could help maintain a balance in viral replication, allowing propagation without killing the host.

The biggest difference in the induction of the I interferon upon transfection with 5′-pppA or 5′-pppG RNAs occurred at very low concentrations. This could represent the early stages of virus infection which are crucial to mount an effective cellular response. [51] Similarly, low levels of immunogenic viral RNAs derived from West Nile virus and generated during the viral replication cycle have been shown to activate the RIG-I response.[52] At the highest RNA concentrations tested (100 ng/ml for IVT 76 bp dsRNA and 1 µg/ml for synthetic 24 bp dsRNA), no significant difference was observed between the 5′-pppA and 5′-pppG variants. This implies an involvement of endogenous factors that may become saturated at very high concentrations of transfected RNAs. Intriguingly, Ren *et al.* reported no difference in IFN-β induction between dsRNAs starting with 5′-pppA or 5′-pppG. [53] The apparent discrepancy with our study may be attributed to different concentrations tested and the distinct dsRNA substrates examined. Ren *et al*. conducted their experiments using fully complementary dsRNAs with two exposed ends at a concentration of 2 µg/ml. Given that their RNAs had a length of 24 nt with 10 bp, the corresponding molar concentration was approximately 259 nM. In contrast, our IVT-produced 76 bp dsRNA, with a length of 76 nt, exhibited optimal results at a concentration of 20 pM (equivalent to 1 ng/ml) and, similarly to the high concentrations tested by Ren *et al*., showed no discernible difference in IFN induction at concentrations of 2 nM (equivalent to 100 ng/ml) and higher. Moreover, the minimal length documented thus far for the RIG-I agonist was 23 bp [17] and 10 bp. [54] We postulate that, beyond base pairing considerations, the overall length of the ligand is pivotal for RIG-I recognition. Supporting a preference for

longer RNAs, Velthuis *et al.* demonstrated that mini viral RNAs ranging from 56 to 125 nucleotides, derived from the IAV, triggered the highest IFN-β promoter activity. [16]

To investigate the mechanisms underlying the differential activation of the RIG-I/IFN type I signaling pathway by 5′-pppA *vs.* 5′-pppG dsRNAs, we employed a combination of biochemical and cellular methods. One of the primary advantages of biochemical assays is their ability to be conducted under defined, isolated conditions, enabling precise characterization of molecular interactions through the quantification of direct binding parameters. [55,56] Using a biochemical approach, we observed that RIG-I exhibits a marginally higher binding affinity for 5′-pppA dsRNA than for 5′-pppG dsRNA. Previous work has shown a correlation between RNA binding affinity to RIG-I and the capacity of RNA agonists to induce the RIG-I/IFN signaling pathway. [57] These findings support the idea that the identity of the 5′ nucleotide can influence the immunogenic potential of dsRNA ligands. In contrast, RIG-I activity, assessed by ATP consumption, showed no significant difference upon binding to 5′-pppA or 5′-pppG dsRNA (Figure 3). However, other studies have demonstrated that the ATPase activity of RIG-I does not fully reflect its functional activation. This is because RIG-I activation primarily depends on ATP binding, which drives essential conformational changes, rather than on ATP hydrolysis itself. [55,56] Thus, biochemical assays did not fully explain the observed difference between 5′-pppA and 5′-pppG dsRNA immunogenicity.

Since biochemical methods did not provide a definitive explanation for the mechanism underlying the differential activation of the RIG-I/IFN pathway by 5′-pppA and 5′-pppG dsRNAs, we investigated whether additional cellular factors might contribute to the observed phenomenon. Here, we employed an RNA pull-down assay combined with mass spectrometry, enabling the identification of proteins that specifically bind to the RNA of interest. We demonstrated that even a single nucleotide difference in the dsRNA sequence can alter the protein-binding profile, leading to the enrichment of distinct protein groups. Interestingly,

when using 5′-pppA dsRNA as bait, we observed the enrichment of proteins typically associated with ssRNA, despite the dsRNA being immobilized on the resin. This finding suggests that A-U base pairs, being less thermodynamically stable, may allow partial or full unwinding of the duplex in the presence of helicases or other RNA-binding proteins in the lysate. Consequently, these transiently exposed ssRNA regions may become accessible to ssRNA-binding proteins. In comparison, Gene Ontology analysis of the 5′-pppG dsRNA pull-down revealed nine proteins classified as GTPases or GTP-binding proteins. Among them, a particularly novel finding is the identification of NUDT16, a known decapping enzyme that catalyzes the cleavage of the 5′ cap structure in snoRNAs and mRNAs. [58] Here, NUDT16 was found to bind to uncapped dsRNA, a previously unreported interaction. Furthermore, our results show that its binding to short dsRNA is strictly dependent on the presence of the 5′-pppG moiety and can be disrupted by blocking the GTP-binding pocket of NUDT16 with a non-hydrolyzable GTP analog. Although our experiment does not establish whether NUDT16 binds directly to dsRNA or as part of a larger protein complex, its interaction with uncapped RNA represents a novel discovery. Importantly, while NUDT16 has not been directly implicated in the activation or inhibition of the RIG-I/IFN innate immune signaling pathway, emerging evidence suggests that it contributes to innate immunity by regulating the turnover of inflammatory mRNAs and maintaining genomic integrity in immune cells. Its expression is upregulated under inflammatory conditions, such as sepsis, indicating a potential modulatory role in controlling the intensity of the innate immune response. [59,60]

Of particular significance is the observed upregulation of the RIG-I/IFN signaling pathway in response to 5′-pppG dsRNA upon stimulation of the GTP salvage pathway. Combined with the finding that GTPase interaction with dsRNA is disrupted when its GTP-binding pocket is occupied, these results demonstrate that elevated GTP levels might relieve the inhibitory interaction between GTPases and 5′-pppG dsRNA. Notably, many viral infections lead to host

mRNA degradation, resulting in increased levels of nucleotide precursors via the salvage pathway, which viruses exploit to support their replication. [61] According to our findings, this increase of nucleotide levels, including GTP, may also benefit the host by enhancing activation of the RIG-I/IFN pathway. Endogenous RNA polymerase III transcripts bearing 5′-pppG ends, such as Y-RNAs, may act as stoichiometric immunostimulatory ligands under these conditions, thereby contributing to the innate immune response during viral infection. In addition to RNA derived from RNA viruses, DNA viruses can also be a source of RNAs recognized by RIG-I. Consequently, many viruses may harbor factors that inhibit RIG-I activity. [17] Notably, RNAs from these DNA viruses (e.g., Epstein-Barr virus (EBV)) also produce RNAs with 5′-pppA termini, which could be highly immunogenic. [62] It is also worth noting that EBV infection is linked to autoimmune diseases such as systemic lupus erythematosus, [63] multiple sclerosis, [64] and rheumatoid arthritis. [65] It is suggested that EBV may contribute to the onset or exacerbation of autoimmune disorders. Despite these insights, the precise role of such RNAs in autoimmune diseases remains unclear, warranting further investigation of the complex interplay between the virus and the host's immune system.

Summary

In summary, our results suggest that accurate recognition of uncapped dsRNA by RIG-I in the cells may rely on the presence of a specific terminal 5′-ppp nucleotide and the surrounding cellular protein environment, with RNAs containing 5′-pppA being more immunogenic than those with 5′-pppG. This novel aspect of sequence-specific signaling in the RIG-I/IFN pathway will be important for advancing knowledge and designing strategies to target pathogenic viruses and host RNAs involved in autoimmunity.

Limitations of the study

While we demonstrated that dsRNAs containing 5′-pppA are more immunogenic than dsRNAs with 5′-pppG, we could not have shown it for pol III transcripts transcribed *in vitro* or for RNA viruses. This is largely due to the IVT bias towards producing more immunogenic dsRNA side products when initiation occurs with 5′-pppA, as well as evolutionary and mechanistic pressures acting on viral promoter sequences. To address this limitation, future studies should focus on endogenously modified pol III transcripts or more extensive viral mutagenesis. However, any viral RNA modifications that enhance robustness through innate immune avoidance should be considered with caution.

Materials and Methods

IVT reaction

RNA transcripts (Supplementary Table S2) were prepared using the IVT reaction. IVT 76 bp dsRNA was derived by truncating 76 nucleotides from the 8th segment of the IAV genome (GenBank: NC_002020.1).

The transcription template was first amplified using the High-Fidelity Phusion DNA Polymerase (Thermo #F530L) and primers (Supplementary Table S3) appending T7 Class III (TAATACGACTCACTATA) or ϕ2.5 Class II (TAATACGACTCACTATT) promoter sequence to produce 5′-pppA RNA or 5′-pppG RNAs, respectively. [66] Subsequent IVT reaction producing 5′-triphosphorylated RNAs was performed with NxGen T7 RNA Polymerase (Biosearch Technologies #30223-1).

Then RNA was precipitated with 3 M sodium acetate pH 5.1 and 100% EtOH, washed with 100% EtOH, and resuspended in UP water. The RNA in 2× loading buffer (7 M urea, bromophenol blue, and xylene cyanol) was then run on a denaturing polyacrylamide gel (10% polyacrylamide, 7.5 M urea in 1× TBE) for 2 h. Bands were stained with Stains-all (Sigma-Aldrich #E9379) and excised with individual scalpel blades. Then RNA was extracted (0.3 M

sodium acetate pH 5.2; 0.5 mM EDTA; 0.1% SDS) and precipitated again. Washed with 100% EtOH and resuspended in UP water. RNA concentrations were assessed with NanoDrop. RNA was aliquoted and stored at −80°C. PAGE/urea gel electrophoresis was repeated to confirm that no extra bands were observed in the final RNA preparation. Dephosphorylated RNA was produced with FastAP enzyme (Thermo #EF0654) and cleaned using column purification (Invitek Invisorb Spin Virus RNA Mini Kit).

Double-stranded RNAs were prepared by mixing a 1:1 molar ratio of sense and antisense strands in 1× RNA refolding buffer (100 mM Tris-HCl pH 7.5, 100 mM NaCl, and 5 mM $MgCl_2$). To obtain proper duplex formation, dsRNA mixture was heated up to +80°C for 10 min and then cooled down at room temperature for 30 min.

The 3p-hpRNA at a concentration of 100 ng/ml (InvivoGen #tlrl-hprna) or no RNA were used as a positive and negative controls, respectively.

Chemical RNA synthesis

Standard solid-phase oligonucleotide synthesis was performed on an Äkta Oligopilot 10 Plus from GE Healthcare in a 4 µmol scale using 2′OTBDMS protected phosphoramidites and the 5′trityl-off modus. Commercially available phosphoramidites, CPG materials and reagents were used, purchased from Sigma Aldrich, Avantor, TCI, and Glen Research.

The triphosphorylation reaction was performed subsequently after solid-phase synthesis with an automated machine adapted version of Goldeck et al. on an Äkta Oligopilot 10 Plus from GE Healthcare. [67] For deprotection, the CPG-bound oligonucleotide was incubated with 1.2 ml 40% methylamine for 45 min at +45°C. The material was diluted in 9 ml DMSO and then 900 µl glycolic acid was added. The 2′ deprotection was carried out using 1 M NH_4F in DMSO for 8 h at room temperature. The reaction was quenched with 1 ml of 100 mM triethylammonium bicarbonate (TEAB) and passed through a Dowex Et_3NH^+ column for ion-exchange prior to

HPLC purification. RP-HPLC purification was performed on a 15RPC Tricorn 10/300 with a linear gradient of 0-80% B in 30 CV at a flow rate of 2 ml/min. Buffer A was 100 mM TEAB and buffer B was 100 mM TEAB in 80% methanol (MeOH). For removal of the 5′decyl-NH-tag, the product fractions were collected, evaporated and desalted by repeated co-evaporation with MeOH. The residue was redissolved in 400 µl deprotection buffer (100 mM acetic acid, TEMED, pH 3.8) and heated to +60°C for 70 min. After cooling the reaction mixtures on ice, 24 µl of 5 M NaCl and 1.2 ml ethanol were added to precipitate the oligonucleotide. The pure product was pelleted by centrifugation, washed with ethanol, dried under vacuum, and dissolved in pure water.

Purity and identity were confirmed by LC-MS analysis which was performed using an ACQUITY-UPLC system (Waters) coupled to an Xevo TQ-S Quadrupole (Waters) equipped with an electrospray source operating in negative ionization mode. All samples were chromatographed on an ACQUITY UPLC BEH C18 column (2.1 × 50 mm; 1.8 µm particle size) at +60°C column temperature. Separation of the analytes was achieved using a gradient of 16.6 mM triethylamine (TEA), 100 mM hexafluoroisopropanol (HFIP) and 10% methanol as eluent A and 16.6 mM TEA, 100 mM HFIP and 95% MeOH as eluent B with a flow rate of 0.3 ml/min. Samples were prepared in 200 mM TEAA and 20 mM EDTA. Segmented gradient for LC-MS analysis is presented in the Supplementary Table S4.

Native polyacrylamide gel electrophoresis

For native polyacrylamide gel electrophoresis, a 10× native gel loading buffer (1 mM Tris-HCl pH 7.5, 5% glycerol, 0.001% bromophenol blue) was added to the samples and mixed. The mixtures were overlaid on a nondenaturing 12% polyacrylamide gel (prerun step was performed at 8 W for 45 min at +4°C). After electrophoresis at 8 W for 120 min at +4°C,

the gels were stained with SYBR Gold nucleic acid gel stain (Invitrogen #S11494). Imaging was performed with a Chemidoc MP (Bio-Rad Laboratories).

Cell cultures

Murine bone marrow cells were obtained from C57BL6J/Rj mice as previously described with modification. [68] Bone marrow cells were cultured with 20% of L929 conditioned medium for 7 days to generate BMDMs.[69] Human HEK293, HEK-Blue IFN-α/β (InvivoGen #hkb-ifnab) cells, and murine BMDM cells were maintained in Dulbecco's Modified Eagle's Medium (DMEM; Gibco #32430) supplemented with 10% fetal bovine serum (Gibco #10270-106). HEK-Blue IFN- α/β cells were cultured with 100 µg/ml Zeocine (InvivoGen #ant-zn-1) and 30 µg/ml Blasticidine (InvivoGen #ant-bl-05). Primary cell cultures (BMDMs) were kept in presence of 1× Penicillin-Streptomycin (Gibco #15140122) and 0.1 mg/ml Gentamicin (Gibco #15710064). Cells were cultured at +37°C in a 5% CO_2 humidified incubator.

Transfection of RNAs in cell cultures

Cells were seeded in a 12-well plate at a concentration of 0.3-0.7×10^6 cells per well and incubated for 24-48 hours. RNA was mixed with Lipofectamine: first, RNA was prediluted in 125 µl of OptiMEM (Gibco #11058), second, 2 µl of Lipofectamine 2000 (InvitroGen #11668) prediluted in 125 µl of OptiMEM was added, third, mix was incubated at RT for 30 min, fourth, 750 µl of cell culture medium was added. The obtained mix of RNA with Lipofectamine in medium was added to cells and incubated for 24 hours. Supernatants and cell lysates in modified Roeder D Buffer[70] (20% (w/v) glycerol, 100 mM KCl, 0.2 mM EDTA; 100 mM Tris-HCl pH 8.0; 0.2 mM PMSF and 0.5 mM DTT) were collected and processed either for type I IFN assay or western blot.

HEK-Blue IFN type I assay

Supernatants from HEK293 cells were processed with the HEK-Blue IFN type I assay in quadruplicates. 20 µl of supernatants (undiluted or prediluted 1:7) were added to 50,000 HEK-Blue IFN-α/β cells per well in a 96-well plate. A standard curve was generated in parallel by serial dilutions of recombinant IFN-β standard in DMEM (R&D Systems #8499-IF-010). After overnight incubation (24 h), 20 µl of supernatant was mixed with 180 µl of the working solution of the QUANTI-Blue reagent (InvivoGen #rep-qbs) and incubated at +37°C for 0.1-3 h. Absorbance was measured at 654 nm using a Tecan Sunrise absorbance microplate reader. Blank values were subtracted from all wells and the four-parameter logistic (4PL) standard curves were fitted to provide semiquantitative analyses of the IFN concentrations produced in the RNA-transfected cells. [71,72]

Western blot analysis

Cell monolayers were washed once with ice-cold 1× DPBS (Gibco #14190) and resuspended in 50 µl of a Roeder D buffer. After vortexing, cells were sonicated with Diagenode's Bioruptor Pico sonication device (10 cycles of 30 s ON/30 s OFF at +4 C) and centrifuged (10000×g, 5 min, +4°C). Supernatants were moved to pre-chilled low protein binding tubes and, after quantifying protein concentration with NanoDrop, stored at −80°C. Twenty to hundred µg of protein extract was resolved using a 10% gel. Proteins were transferred to nitrocellulose membranes (Amersham #10600007) using a wet transfer apparatus. Membranes were blocked with 1% Western Blocking Reagent (WBR; Roche #11921681001) for 1 hour at room temperature. Membranes stained for pIRF3 were blocked with 5% BSA in TBST buffer. The blocked membranes were incubated with primary antibodies diluted in 0.5% WBR in TBST overnight at +4°C (Supplementary Table S5), washed three times with TBST, incubated with secondary antibodies diluted in 0.5% WBR in TBST for 1 hour at room temperature (Polyclonal Goat Anti-Rabbit Immunoglobulins/HRP, Agilent Dako #P0448, 1/2000), washed

three times with TBST. For the chemiluminescence reaction, peroxide ECL reagents (Bio-Rad #170-5061) were applied to each membrane and then, the membranes were visualized and results quantified using an iBright 1500 Imaging System (Thermo).

RNA extraction and qRT-PCR

RNA was extracted with Trizol (Invitrogen #15596018), and one-step qRT-PCR reactions were conducted on the Roche LightCycler 96 System. SYBRgreen-based GoTaq 1-Step qRT-PCR System (Promega #A6020) and LightCycler 96 software were used for RNA quantification. The reaction mixture (20 µl) consisted of 10 µl of 2× MasterMix, 0.4 µl of Reverse Transcription Mix, 0.2 µl of each primer diluted to 20 µM concentration, 7.2 µl of nuclease-free water and 2 µl (100 ng) of RNA template. A reverse transcription step of 15 min at +37°C and an enzyme activation step of 10 min at +95°C were followed by 40 amplification cycles (15 s at +95°C and 60 s at +60°C). The primers used are listed in Supplementary Table S6.

Fluorescence RNA preparation

Fluorescent IVT dsRNA was constituted of sense strand RNA labelled on the 3′-end with fluorescein and unmodified antisense strand, both IVT derived. RNA 3′-end labelling was conducted as described earlier by Qiu *et al*.[73] Briefly, 0.25 nmol of RNA was oxidized with 2.5 nmol of sodium periodate in RNA labelling buffer (0.25 M sodium acetate, pH 5.6), incubating in the dark for 90 min at room temperature. Then, 5 nmol of sodium sulphate was added, followed by 15 min incubation at room temperature. For labelling, 7.5 nmol of fluorescein-5-thiosemicarbazide was added into the mixture and incubated for 3 hours at +37°C. RNA was precipitated by adding 1/10 volume of 8 M LiCl and 2.5 volume of 100% ethanol and incubating on dry ice for 30 min (alternatively, overnight incubation in −20°C), followed by centrifugation at 16000×g at +4°C for 20 min. The RNA pellet was washed twice with 75% ethanol, resuspended in nuclease-free water and stored in −80°C.

Synthetic 24 bp dsRNA was constituted of sense strand unlabelled RNA and antisense strand RNA with 5′-end 6-FAM (6-carboxyfluorescein) modification prepared by IDT.

Electrophoretic mobility shift assay (EMSA)

RNA-protein binding reaction was carried out in a 1× binding buffer containing 50 mM Tris-HCl pH 7.5, 2.5 mM $MgCl_2$, 50 mM NaCl, 0.01% Tween-20 and 5 mM DTT. Serial dilutions of recombinant RIG-I protein were mixed with 0.5 nM fluorescently labelled dsRNA and 20 μM tRNA (Thermo #20159) as a non-specific competitor. Reactions were equilibrated for 30 minutes at room temperature, then mixed with 10× native gel loading buffer (1 mM Tris-HCl pH 7.5, 5% glycerol, 0.001% bromophenol blue) and loaded onto a 5% non-denaturing polyacrylamide gel. A pre-run was performed at 8 W for 45 minutes at +4°C. Free dsRNA and RNA-protein complexes were separated by electrophoresis at 8 W for 90 min at +4°C. Imaging was performed using a Typhoon laser scanner (Cytiva). The fraction of RNA bound to protein was calculated by densitometric analysis of the unbound fluorescent RNA band using the formula:

$$Fraction\ bound = 1 - I_{unbound} / I_0,$$

where: $I_{unbound}$ – the intensity of the unbound RNA band at a given RIG-I concentration; I_0 – the intensity of the unbound RNA band in the absence of RIG-I.

To estimate the apparent dissociation constant (K_d), a 4PL model was fitted to densitometric data.

$$Fraction\ bound = Bottom + C_{RIG\text{-}I}^{HillSlope} \times (Top\text{-}Bottom) / (C_{RIG\text{-}I}^{HillSlope} + K_d^{HillSlope})$$

To compare K_d values across datasets, we used the entropy maximization principle and evaluated model fit using the Akaike Information Criterion corrected for small sample sizes

(AICc). The probability that both datasets share a common Kd was calculated using the relative likelihood: Akaike's Probability = 1 - 1 / (1 + $e^{\Delta AICc / 2}$).

RIG-I ATPase assay

The activity of recombinant RIG-I protein upon dsRNA binding under isolated conditions was assessed by measuring its ability to hydrolyze ATP to ADP. Similarly to the EMSA procedure, the ATP hydrolysis reaction was carried out in a 1× enzymatic reaction buffer. Briefly, a reaction mixture containing 1.3 nM RIG-I protein and 100 µM ATP, with varying concentrations of dsRNA, was prepared and incubated at +37°C for 60 minutes. ATP-to-ADP conversion was detected using Transcreener ADP^2 FP Assay Kit (BellBrook Labs), following the manufacturer's protocol. Fluorescence polarisation (FP) measurements were performed using a Tecan Infinite M1000 microplate reader.

To estimate the relative half-maximal effective concentration (EC_{50}) of each RNA, a 4PL model was fitted to data representing the change in polarization across an RNA concentration gradient:

$$\Delta Polarisation = Bottom + C_{RNA}{}^{HillSlope}) \times (Top\text{-}Bottom)/(C_{RNA}{}^{HillSlope} + EC_{50}{}^{HillSlope})$$

To compare EC_{50} values across datasets, Akaike's methodology was applied as described for K_d estimation in the EMSA section.

RNA pull-down

RNA pull-down assay was carried out to detect proteins binding to RNA immobilized on agarose beads. 250 pmol of *in vitro* transcribed and PAGE-purified sense strand RNA was treated with 100 mM sodium acetate and 5 mM sodium (meta)periodate in 200 µl of water and rotated for 1 h at room temperature in the dark. The RNA was precipitated by adding 600 µl of 100% ethanol and 15 µl of 3 M sodium acetate and incubating on dry ice for 30 min, followed

by centrifugation at 16000×g, +4°C for 20 min. The RNA pellet was washed with 70% ethanol, followed by 5 min centrifugation at 16000×g. Then 250 pmol of antisense strand RNA in 50 µl 1× RNA refolding buffer (100 mM Tris-HCl pH 7.5, 100 mM NaCl, and 5 mM $MgCl_2$) was used to resuspend the sense strand RNA pellet. RNA mixture was incubated for 30 min at room temperature and then 450 µl of 100 mM sodium acetate pH 5.2 was added.

For one reaction, 250 µl of adipic acid dihydrazide-agarose beads (Sigma-Aldrich #A0802) were washed 3× with 100 mM sodium acetate, followed by centrifugation at 2,000×g, +4°C for 2 min, then mixed with 500 µl of the periodate-oxidized RNA and incubated overnight at +4°C in the dark with rotation. The RNA-beads were washed by mixing with 700 µl of 4 M KCl, rocked for 30 min at room temperature, centrifuged at 2,000×g for 5 min, washed 2× with 2 M KCl, washed 2× with Buffer G (20 mM Tris-HCl pH 7.5, 137 mM NaCl, 1 mM EDTA, 1% Triton X-100, 10% glycerol, 1.5 mM $MgCl_2$, 1 mM DTT and 200 µM PMSF) and washed 1× with Roeder D followed by 2 min centrifugation at 2,000×g at room temperature. Control beads with no RNA attached were also prepared. 1 mg of total protein extract was added to RNA-beads. The mixture was supplemented with 1.5 M $MgCl_2$, 25 mM creatine phosphate, 100 mM ATP, and 2.5 µl of RiboProtect Hu RNase Inhibitor (Blirt #RT35). Additionally, for GTP analog treated samples Non-hydrolyzable GTP Test Kit (Jena Bioscience #NK-102) containing 5 analogs – GTPαS, GpCpp, GppCp, GppNHp, GTPγS – was used. Each GTP analog was added at 0.1 mM; combining all five analogs therefore produced a total nucleotide concentration of 0.5 mM, which corresponds to the physiological GTP level in mammalian cells. [74] The mixture volume was adjusted to 650 µl with nuclease-free water. The RNA-beads-cell lysates mixtures were incubated at +37°C for 30 min with shaking. After 3× washes with Buffer G, the beads were mixed with 60 µl of 5× Sample Buffer. Proteins captured by RNA were denatured at +95°C for 10 min with shaking. 30 µl of the supernatant was loaded onto

SDS-PAGE or NuPAGE gel and western blot or mass spectrometry analysis was performed to detect the proteins, respectively.

Mass spectrometry

Proteins were separated on gel (NuPAGE Novex 4-12% Bis-Tris gel, Thermo) in NuPAGE buffer (MES) for 10 min and visualised using InstantBlue stain (Abcam). The stained gel band was excised and de-stained with 50 mM ammonium bicarbonate (Sigma Aldrich) followed by 100% acetonitrile (Sigma Aldrich). Then proteins were digested with trypsin, as previously described. [75] In brief, proteins were reduced in 10 mM DTT (Sigma Aldrich) for 30 min at +37°C and alkylated in 55 mM iodoacetamide (Sigma Aldrich) for 20 min at ambient temperature in the dark. They were then digested overnight at +37°C with 13 ng/µl trypsin (Pierce). Following digestion, samples were diluted with an equal volume of 0.1% TFA and pH was set to ~2 with 10% TFA.

The equivalent of 50 ng of the digest was loaded on the Evotip using the standard producer protocol. We utilized Evosep coupled to a TimsTOF ULTRA (Bruker) mass spectrometer equipped with a Captive Spray II source (Bruker). The separation was carried out on maintained at +40°C column (Evosep EV1115). We employed the standard 60SPD Evosep method, applying a 21-minute gradient for a total sample-to-sample time of 24 minutes using Solvent A (0.1% formic acid) and Solvent B (0.1% formic acid in acetonitrile); Thermo Optima LCMS grade).

The dia-PASEF acquisition scheme was optimized for a cycle time estimate of 1.38 s. The window scheme was designed to cover most of the charge 2 precursor ions in the range m/z 391−1142 and $1/K_0$ 0.68−1.36, using 22 × 31 Th windows, with accumulation and ramp times of 0.1 s. The mass spectrometer was operated in the high-sensitivity mode (“low sample amount”).

The DIA-NN software platform [76] version 1.9.1 was used to process the raw files from label-free DIA and the search was conducted against the *Homo sapiens* reference proteome [UniProt Proeome ID #UP000005640]. Precursor ion generation was based on the chosen protein database (automatically generated spectral library) with deep learning- predictions for spectra, retention times, and ion mobilities. Digestion mode was set to specific with trypsin allowing a maximum of one missed cleavage. Carbamidomethylation of cysteine was set as fixed modification. Oxidation of methionine, and acetylation of the N-terminus were set as variable modifications. MS1 and MS2 mass accuracies were set to 10 ppm. The parameters for peptide length range, precursor charge range, precursor m/z range and fragment ion m/z range as well as other software parameters were used with their default values. The precursor FDR was set to 1%.

Protein intensities were quantified from peptide intensities with directLFQ Python package.[77] Statistical analysis was performed with R.[78] *Protti* R package [79] was used for quality control, data filtration, imputation of missing values, and statistical significance calculation using a moderated t-test based on the *limma* R/Bioconductor package [80]. For functional validation, *p*-values were adjusted for multiple testing with the Benjamini-Hochberg correction. Data visualisation was performed using the *ggplot2* R package.[81] GO enrichment analysis for Biological Processes and Molecular Functions was conducted on the set of enriched proteins using the *clusterProfiler* package in R.[82]

Murine BMDMs-based mKate2/IFN-β activity assay, image acquisition and analysis with Opera Phenix

Murine BMDMs-based mKate2/IFN-β activity assay was performed as described previously.[35] In short, bone marrow-derived macrophages were isolated from a genetically modified mouse expressing the fluorescent protein mKate2 in place of the IFN-β (the mKate2 encoding

sequence was inserted at the start of the IFN-β coding region with added SV40 polyadenylation signals and a mutation disrupting protospacer-adjacent motif-) and plated in 96-well plates (Greiner Bio-One #655090) at a density of 10^5 cells per well. BMDMs were then transfected with different variants of dsRNAs and imaged hourly using the PerkinElmer Opera Phenix High-Content Screening System. Activation of the IFN-β promoter in these cells triggers mKate2 expression instead of IFN-β, allowing single-cell visualisation of IFN pathway induction. To enumerate cells, images were first flat-field–corrected, then segmented on the mKate2 channel with PerkinElmer Harmony software ("*Method C*" from the "*Find Cells"* building block).

Production of the recombinant RIG-I protein

Gene coding RIG-I/DDX58 cDNA [GeneID: 23586] was cloned in pET28-6xHis-SUMO vector (Thermo #K30001). Protein was expressed in *E. coli* BL21-RIL cells (Agilent #230245) cultivated in Lysogeny Broth medium overnight at +18°C after induction with 0.4 mM isopropyl β-D-1-thiogalactopyranoside at OD_{600} of 0.6-0.7. The harvested cells were pelleted by centrifugation at 4,000×g, +4°C for 20 minutes and resuspended in buffer A (50 mM HEPES pH 7.5, 500 mM NaCl, 10% glycerol (w/v), 5 mM β-mercaptoethanol, 20 mM imidazole and 40 mM L-arginine) supplemented with proteinase inhibitors, and sonicated. The lysate was then subjected to ultracentrifugation at 142, 000×g, +4°C for 40 min yielding a clear supernatant. The clarified lysate was applied to a 5 ml His-Trap HP column (Cytiva #17524802) pre-equilibrated with buffer A. The column was washed with buffer A, followed by a wash with the same buffer that included 60 mM imidazole. RIG-I protein was eluted with buffer A that contained 500 mM imidazole. To remove the 6xHis-SUMO tag, the fusion protein was digested with SUMO protease (Ulp1) and dialyzed overnight against buffer A at +4°C. The cleaved-off His-tagged SUMO protein was removed on a His-Trap HP column. For the final purification step, tag-free RIG-I from the flow-through was concentrated

and applied to a size exclusion column Hiload 16/600 Superdex 200 (Cytiva #28989335), pre-equilibrated with buffer A without imidazole. The RIG-I protein fractions were pooled and concentrated using a 30 kDa Amicon Ultra filter (Millipore #UFC903008). Lastly, the concentration of RIG-I was measured with NanoDrop and the purified protein was stored at −80°C.

Induction of nucleotide salvage pathway

To elevate the GTP level in the cells, HEK293 12-well cell cultures were supplemented with 100 µM guanosine (Sigma Aldrich #G6264). DMSO and 100 µM adenosine (Sigma Aldrich #A9251) treatments were utilized as control conditions. The cells were incubated for 48 h in cell culture incubator and then transfected with IVT 76 bp dsRNAs at a final concentration of 0.1 ng/ml. After 24 h incubation the cells were lysed in Roeder D lysis buffer and used for western blot analysis.

Statistical analysis

All data are reported as mean ± standard deviation. Statistical analyses were performed using GraphPad Prism 10.5.0.

Data Availability

The mass spectrometry proteomics data have been deposited in the ProteomeXchange Consortium via the PRIDE [83] partner repository with the dataset identifier PXD065769. Supplementary data available online.

Acknowledgments

Figures 2A, 2B, 4A, 5A, 6, Supplementary Figures S4A and S5A were created with BioRender.com.

Author contributions

G.M. conceived this study; J.S., M.W. and G.M. designed the experiments; J.S., M.W., I.T., Z.N., N.I., E.N., and C.W., performed experiments; J.S., M.W., I.T., Z.N., N.I., G.H., J.R. and G.M. analyzed data; J.S., M.W. and G.M. wrote the manuscript with input from other authors. All authors read and approved the final manuscript.

Funding

Project financed under DIOSCURI, a programme initiated by the Max Planck Society, jointly managed with the National Science Centre in Poland, and mutually funded by Polish Ministry of Science and Higher Education and German Federal Ministry of Education and Research [2019/02/H/NZ1/00002 to G.M.]; Polish National Agency for Academic Exchange within Polish Returns Programme as well as National Science Centre [2021/01/1/NZ1/00001 to G.M.]. This work was financed by the statutory funding of the International Institute of Molecular and Cell Biology in Warsaw. This research was performed thanks to the IIMCB IN-MOL-CELL Infrastructure [RRID: SCR_021630] funded by the European Union – NextGenerationEU under the National Recovery and Resilience Plan. IN-MOL-CELL Infrastructure was also funded by the European Union under Horizon Europe (Project 101059801–RACE) and by the RACE-PRIME project carried out within the IRAP program of the Foundation for Polish Science co-financed by the European Union under the European Funds for Smart Economy 2021–2027 (FENG). J.R. was funded by the Deutsche Forschungsgemeinschaft (DFG, German Research Foundation) under Germany′s Excellence Strategy (EXC 2008–390540038–UniSysCat) and project 449713269. The Wellcome Centre for Cell Biology is supported by core funding from the Wellcome Trust (Grant number 203149). Funding for open access charge: DIOSCURI Centre. This work was supported by the Deutsche Forschungsgemeinschaft (DFG, German Research Foundation) under Germany's Excellence Strategy (EXC 2151–390873048) (G.H.).

Competing interests

The authors declare no competing interests.

Figures

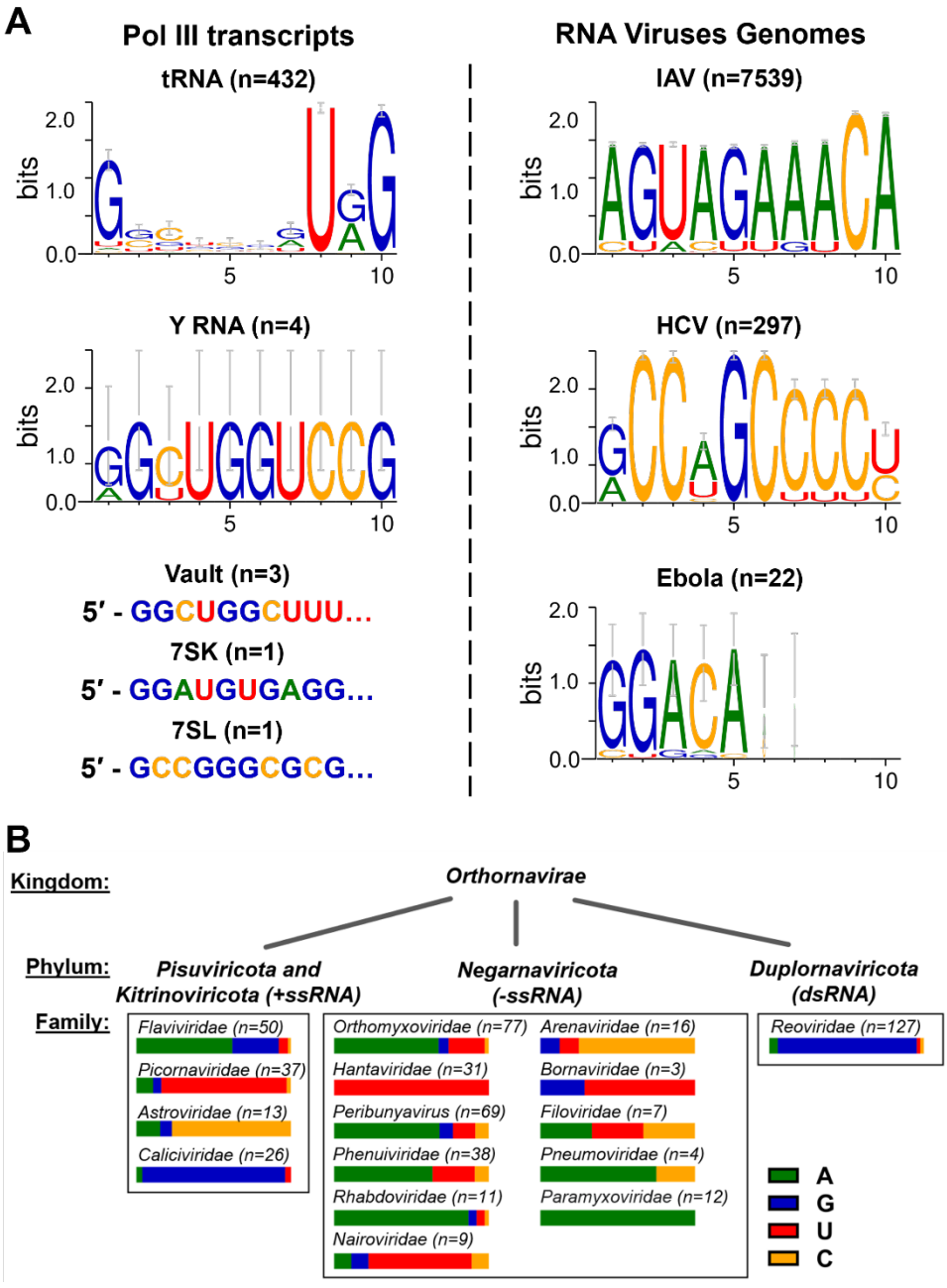

Fig. 1. Terminal 5′-ppp nucleotide conservation in viruses and Pol III transcripts. (**A**) The conservation of the terminal 5′-ppp nucleotide in both Pol III transcripts and selected human viruses with uncapped RNA genomes. Nucleotide sequences representing the 5′ end of specific Pol III transcripts and selected RNA viruses. The sequence probability logos were generated using WebLogo 3. [84] The data sources include GenBank, tRNAscan-SE Genomic tRNA Database (http://gtrnadb.ucsc.edu/), and for Ebola sequences reported by Deflubé *et al.*

[22] (**B**) Variability in the 5′ nucleotide of human viruses in virus families with uncapped RNA genomes. The reference sequences of viral genomes were downloaded from the NCBI Viral Genome Browser (https://www.ncbi.nlm.nih.gov/genome/viruses/). The numbers in parentheses indicate the number of genomes/segments represented per family. The frequencies of initial nucleotides are depicted using horizontal bars.

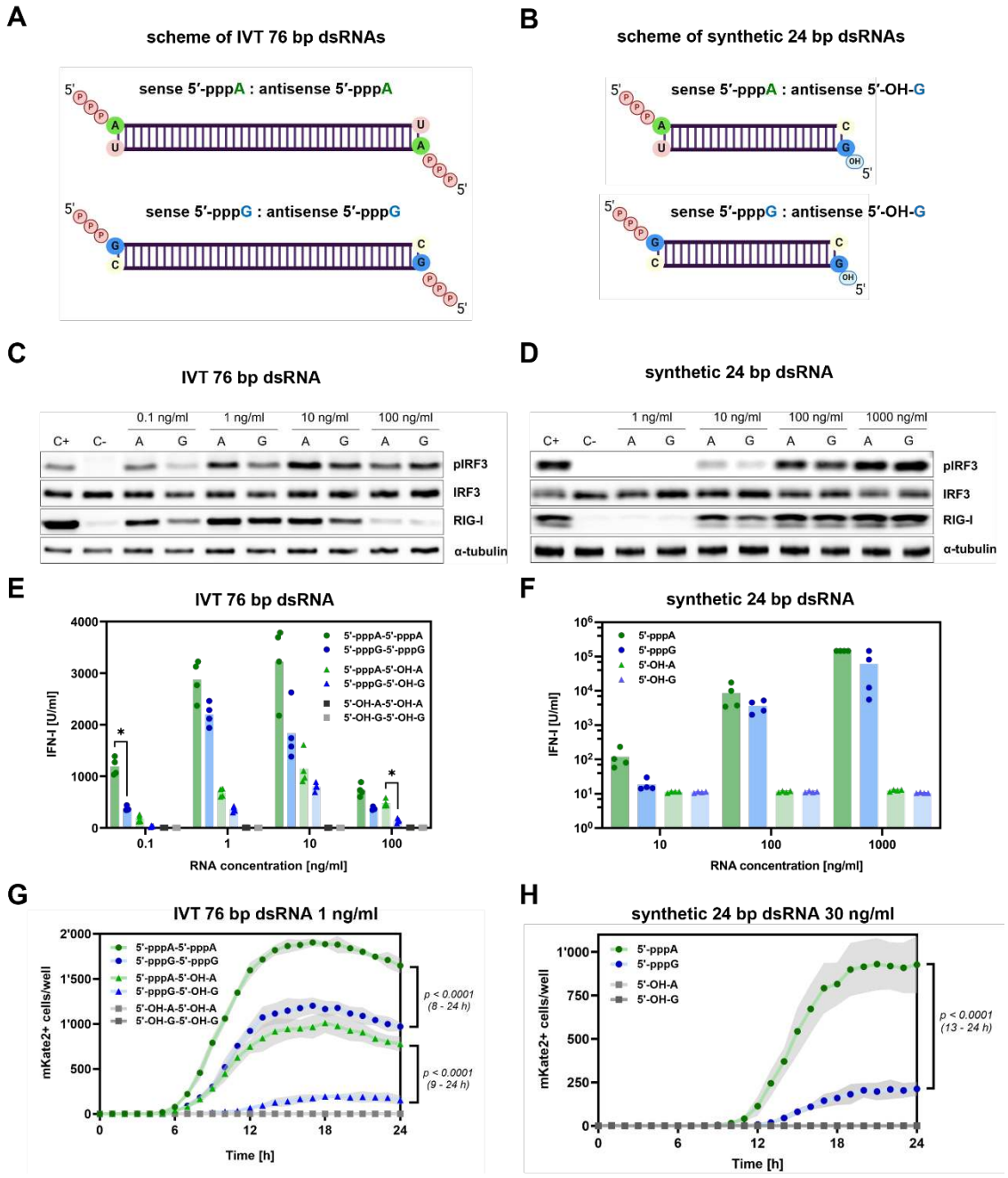

Fig. 2. 5′-pppA dsRNA promotes more robust RIG-I/IFN signaling than 5′-pppG. (**A, B**) Schematic representation of dsRNA variants differing at the 5′ terminal nucleotide (5′-pppA or 5′-pppG) produced via in vitro transcription and chemical synthesis, respectively. (**C, D**) Western blot analysis of IRF3 phosphorylation and RIG-I protein levels in HEK293 cells treated with varying concentrations of 76 bp IVT (**C**) or 24 bp synthetic dsRNAs (**D**). (**E, F**) Type I interferon production in HEK293 cells was assessed with HEK-Blue IFN type I

assay after transfection with dsRNAs. Two-way ANOVA with Šídák's multiple comparisons test was used for statistical analysis. (**G, H**) RIG-I/IFN activation in murine BMDMs upon transfection with tested dsRNAs, shown as mKate2+ cell counts over 0–24 h post-transfection. Grey area represents standard deviation for n=5. Data were analyzed using repeated measures two-way ANOVA on log-transformed values [$\log_{10}(x + 1)$], with Geisser-Greenhouse correction and Šídák's multiple comparisons test.

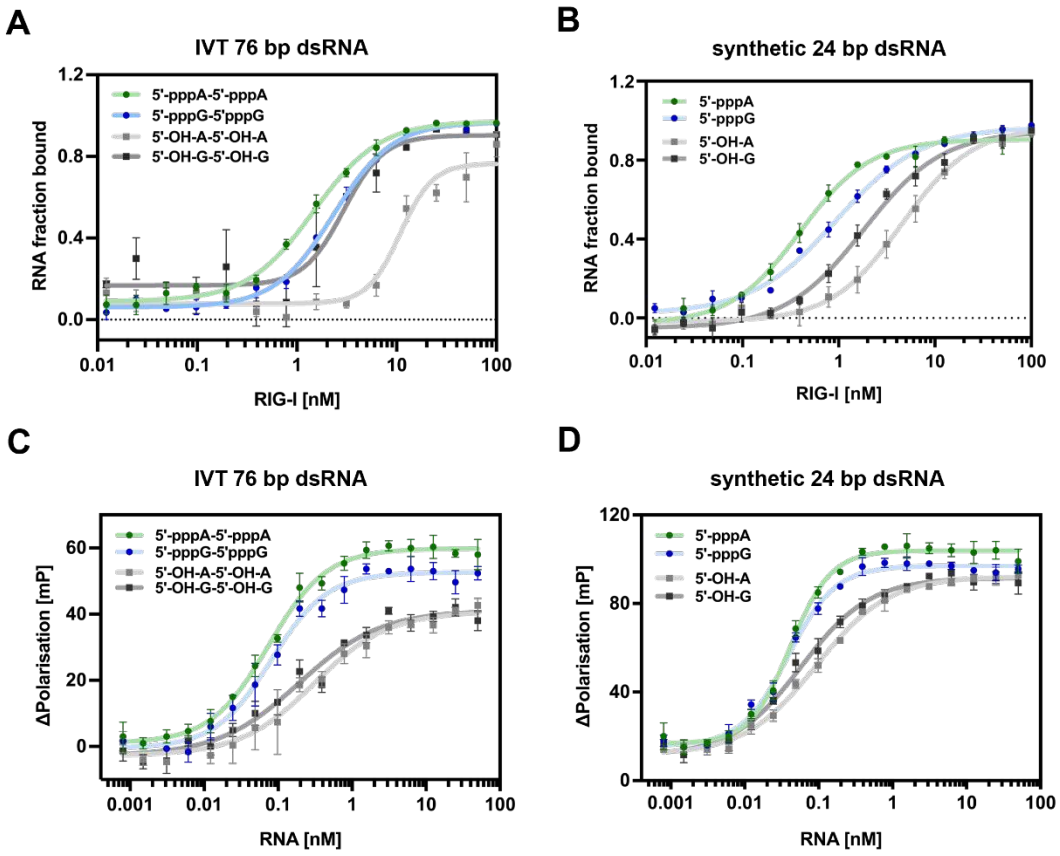

E

RNA variant	Terminal nucleotide	EMSA		RIG-I Activity Assay	
		Kd [nM]	95% CI [nM]	EC_{50} [nM]	95% CI [nM]
IVT 76 bp dsRNA	**5′-pppA**	1.47	1.24 - 1.76	0.074	0.064 - 0.085
	5′-pppG	2.32	2.04 - 2.64	0.081	0.067 - 0.097
	5′-OH-A	10.84	8.35 - 17.34	0.308	0.218 - 0.450
	5′-OH-G	2.94	2.06 - 4.42	0.192	0.138 - 0.269
Synthetic 24 bp dsRNA	**5′-pppA**	0.40	0.33 - 0.49	0.041	0.037 - 0.046
	5′-pppG	0.94	0.79 - 1.11	0.039	0.035 - 0.043
	5′-OH-A	4.50	3.46 - 6.10	0.092	0.081 - 0.105
	5′-OH-G	1.81	1.45 - 2.30	0.058	0.048 - 0.069

Fig. 3. Biochemical analysis of recombinant RIG-I binding affinity and ATPase activity in response to dsRNA. (**A, B**) Binding affinity of recombinant RIG-I to dsRNAs with different 5′-terminal nucleotides (5′-pppA, 5′-pppG, 5′-OH-A, 5′-OH-G) was assessed using an electrophoretic mobility shift assay (EMSA). Plots represent the fraction of RNA bound to RIG-I at increasing protein concentrations. (**C, D**) ATP to ADP conversion was measured in the ATPase to assess recombinant RIG-I protein activation with dsRNAs. The 4PL model was fitted to EMSA and ATPase assay derived data to obtain dissociation constant (K_d) for binding

(**A, B**) and half maximal effective concentration of dsRNA (EC_{50}) for ATPase activity (**C, D**). (**E**) Summary table of biochemical parameters, including K_d and EC_{50} values with corresponding 95% confidence intervals (CI), used to compare RIG-I binding affinity and activation across the different dsRNA variants.

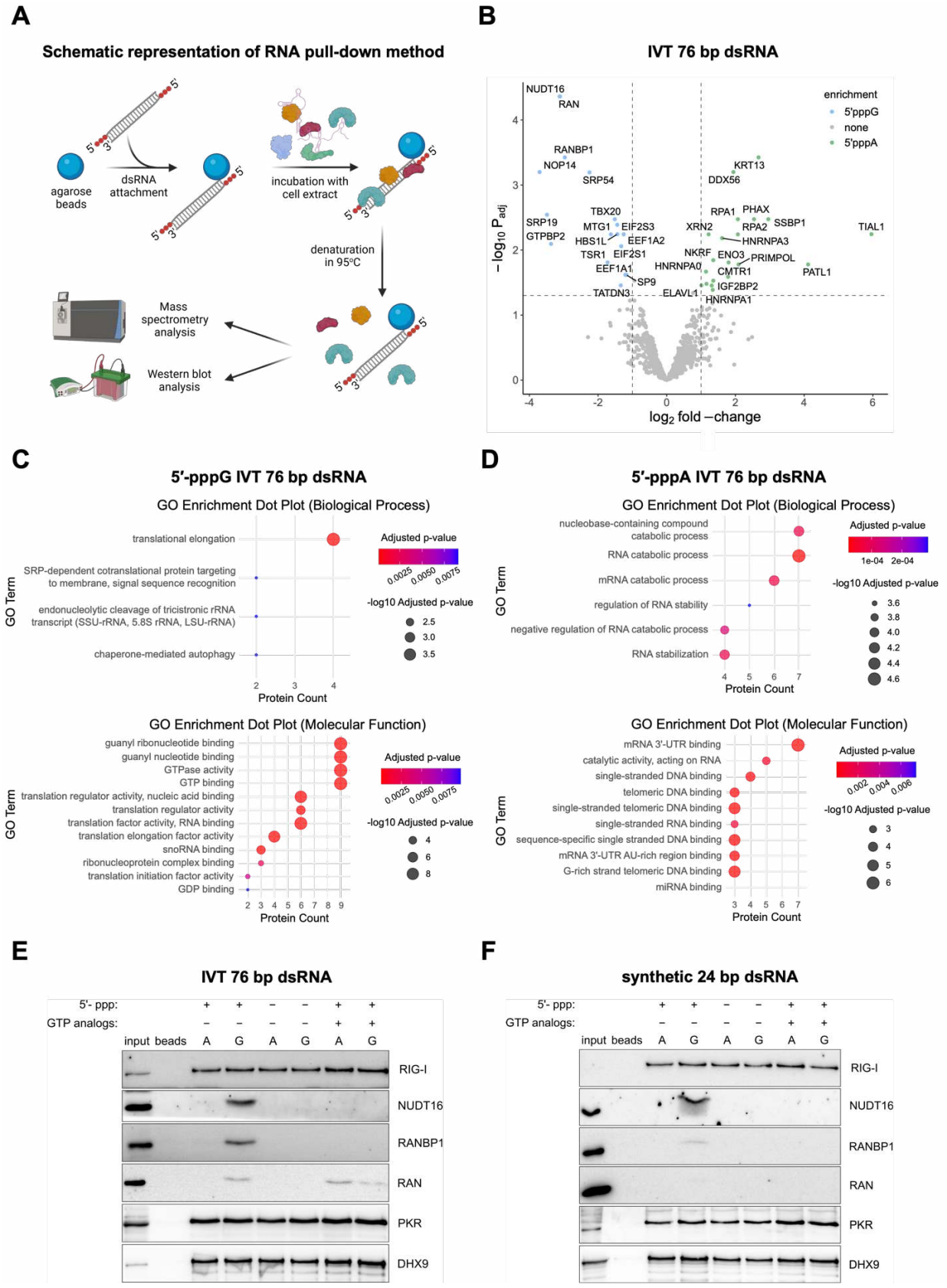

Fig. 4. RNA pull-down analysis reveals RBP binding selectively to 5′-pppA or 5′-pppG dsRNA. (**A**) Schematic representation of RNA pull-down assay. (**B**) RNA pull-down followed

by label-free LC-MS/MS was performed to investigate the interactome of IVT 76 bp dsRNA variants differing at the 5′ terminal nucleotide. Volcano plot represents differential analysis results of proteins enriched with dsRNA bearing 5′-pppA or 5′-pppG. Significance thresholds were set at $|\log_2 FC| > 1$ and $p_{adj} < 0.05$. Proteins enriched with 5′-pppA are highlighted in green, while those enriched with 5′-pppG are shown in blue. (**C, D**) Gene Ontology (GO) analysis was conducted to identify the predominant biological processes and molecular functions associated with the differentially enriched proteins. (**E, F**) Binding of the top three candidate proteins – enriched on 5′-pppG IVT 76 bp dsRNA and associated with GTP-binding activity – was validated by RNA pull-down followed by Western blot analysis. Validation was performed using both IVT 76 bp (**E**) and synthetic 24 bp (**F**) dsRNA. PKR and DHX9 served as positive controls for dsRNA binding. Protein enrichment was further assessed under two conditions: depletion of the 5′-triphosphate moiety, and treatment with GTP nonhydrolyzable analogs, which acts as inhibitors of GTP-binding proteins.

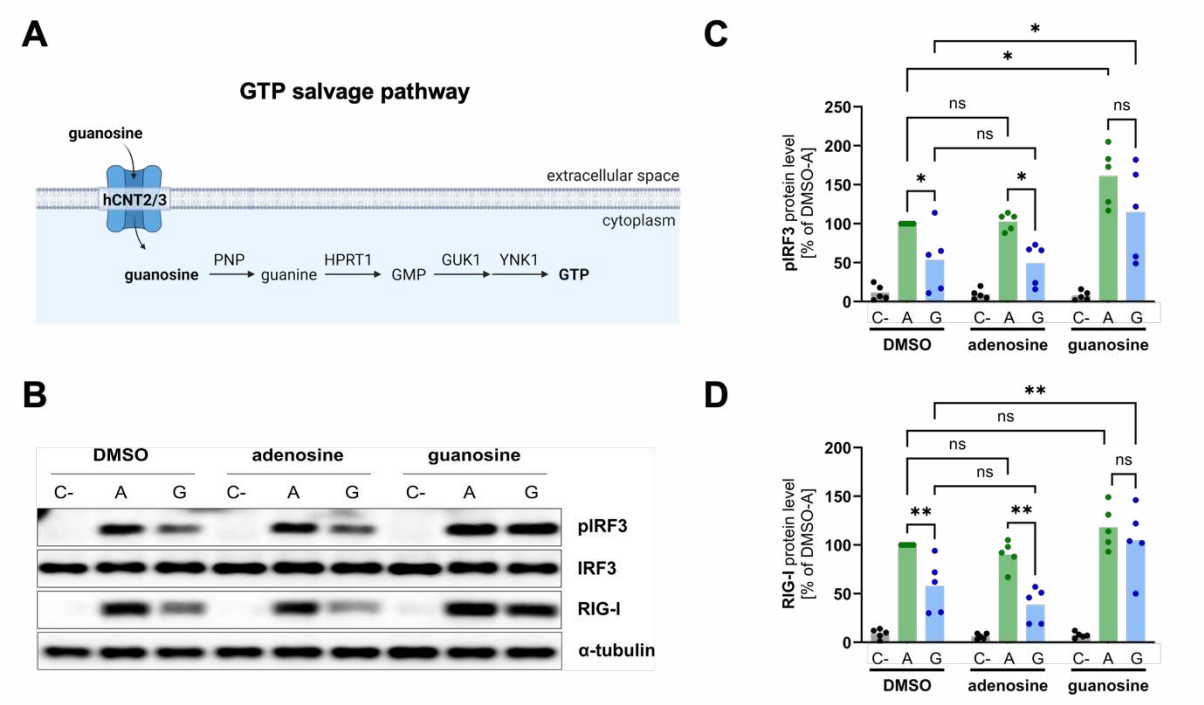

Fig. 5. Increase of cellular GTP level through nucleoside salvage pathway minimizes differences in immune response to 5′-pppA and 5′-pppG dsRNAs. (**A**) Schematic presentation of the GTP salvage pathway. (**B**) Western blot analysis of IRF3 phosphorylation and RIG-I protein levels in HEK293 cells treated with guanosine, adenosine (control), or DMSO (vehicle) and then transfected with lipofectamine alone (C−), 5′-pppA or 5′-pppG IVT 76 bp dsRNAs. (**C, D**) Densitometric analysis of IRF3 phosphorylation (**C**) and RIG-I protein level (**D**) in HEK293 cells treated with guanosine, adenosine (control), or DMSO (vehicle) and then transfected with lipofectamine alone (C−), 5′-pppA or 5′-pppG IVT 76 bp dsRNAs. The results presented are derived from five independent western blot analyses. Two-way ANOVA with Šídák's multiple comparisons test was used for statistical analysis.

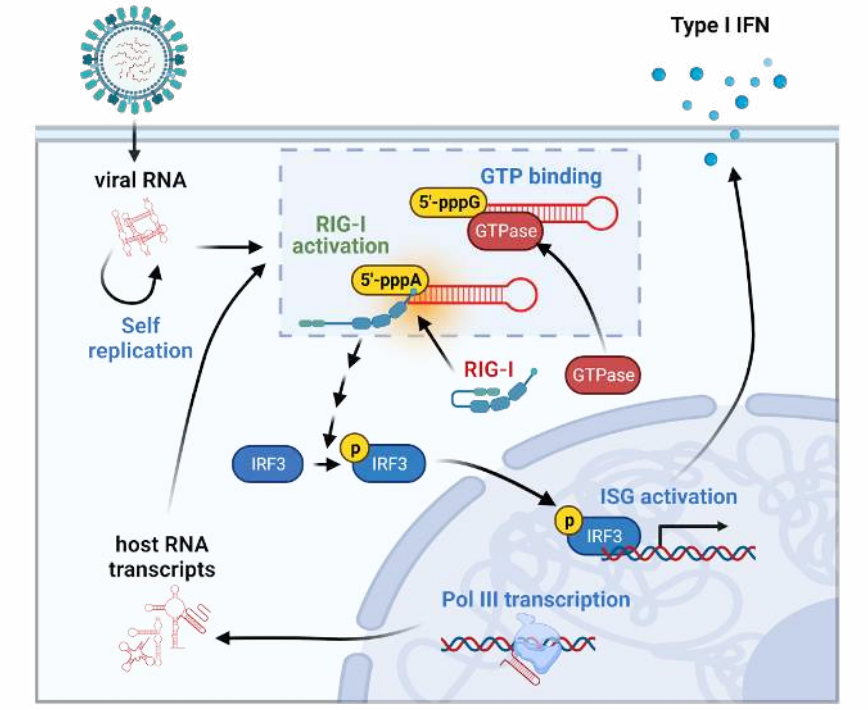

Fig. 6. A model presenting a hypothesis of sequence-specific RNA sensing by RIG-I. Viral RNA, upon entry to the host cells, undergoes self-amplification. RIG-I may sense Pol III transcripts and viral RNAs starting with 5′-pppA. This recognition triggers a cascade of events, including IRF3 phosphorylation, ISG activation, and the subsequent production of type I IFN. RNAs containing a terminal nucleotide of 5′-pppG are identified by GTPases and GTP-binding proteins, which subsequently obstruct their recognition by the RIG-I/IFN pathway.

References

1. Castello, A., Alvarez, L., Kamel, W., Iselin, L., and Hennig, J. (2024). Exploring the expanding universe of host-virus interactions mediated by viral RNA. Mol Cell *84*, 3706-3721. 10.1016/j.molcel.2024.08.027.
2. Rehwinkel, J., and Gack, M.U. (2020). RIG-I-like receptors: their regulation and roles in RNA sensing. Nat Rev Immunol *20*, 537-551. 10.1038/s41577-020-0288-3.
3. Hornung, V., Ellegast, J., Kim, S., Brzozka, K., Jung, A., Kato, H., Poeck, H., Akira, S., Conzelmann, K.K., Schlee, M., et al. (2006). 5'-Triphosphate RNA is the ligand for RIG-I. Science *314*, 994-997. 10.1126/science.1132505.
4. Wang, W., Gotte, B., Guo, R., and Pyle, A.M. (2023). The E3 ligase Riplet promotes RIG-I signaling independent of RIG-I oligomerization. Nat Commun *14*, 7308. 10.1038/s41467-023-42982-0.
5. Cadena, C., Ahmad, S., Xavier, A., Willemsen, J., Park, S., Park, J.W., Oh, S.W., Fujita, T., Hou, F., Binder, M., and Hur, S. (2019). Ubiquitin-Dependent and -Independent Roles of E3 Ligase RIPLET in Innate Immunity. Cell *177*, 1187-1200 e1116. 10.1016/j.cell.2019.03.017.
6. Thoresen, D., Wang, W., Galls, D., Guo, R., Xu, L., and Pyle, A.M. (2021). The molecular mechanism of RIG-I activation and signaling. Immunol Rev *304*, 154-168. 10.1111/imr.13022.
7. Shaw, A.E., Hughes, J., Gu, Q., Behdenna, A., Singer, J.B., Dennis, T., Orton, R.J., Varela, M., Gifford, R.J., Wilson, S.J., and Palmarini, M. (2017). Fundamental properties of the mammalian innate immune system revealed by multispecies comparison of type I interferon responses. PLoS Biol *15*, e2004086. 10.1371/journal.pbio.2004086.
8. Barrat, F.J., Elkon, K.B., and Fitzgerald, K.A. (2016). Importance of Nucleic Acid Recognition in Inflammation and Autoimmunity. Annu Rev Med *67*, 323-336. 10.1146/annurev-med-052814-023338.
9. Goubau, D., Schlee, M., Deddouche, S., Pruijssers, A.J., Zillinger, T., Goldeck, M., Schuberth, C., Van der Veen, A.G., Fujimura, T., Rehwinkel, J., et al. (2014). Antiviral immunity via RIG-I-mediated recognition of RNA bearing 5'-diphosphates. Nature *514*, 372-375. 10.1038/nature13590.
10. Schlee, M., Roth, A., Hornung, V., Hagmann, C.A., Wimmenauer, V., Barchet, W., Coch, C., Janke, M., Mihailovic, A., Wardle, G., et al. (2009). Recognition of 5' triphosphate by RIG-I helicase requires short blunt double-stranded RNA as contained in panhandle of negative-strand virus. Immunity *31*, 25-34. 10.1016/j.immuni.2009.05.008.
11. Myong, S., Cui, S., Cornish, P.V., Kirchhofer, A., Gack, M.U., Jung, J.U., Hopfner, K.P., and Ha, T. (2009). Cytosolic viral sensor RIG-I is a 5'-triphosphate-dependent translocase on double-stranded RNA. Science *323*, 1070-1074. 10.1126/science.1168352.
12. Ren, X., Linehan, M.M., Iwasaki, A., and Pyle, A.M. (2019). RIG-I Selectively Discriminates against 5'-Monophosphate RNA. Cell Rep *26*, 2019-2027 e2014. 10.1016/j.celrep.2019.01.107.
13. Schuberth-Wagner, C., Ludwig, J., Bruder, A.K., Herzner, A.M., Zillinger, T., Goldeck, M., Schmidt, T., Schmid-Burgk, J.L., Kerber, R., Wolter, S., et al. (2015). A Conserved Histidine in the RNA Sensor RIG-I Controls Immune Tolerance to N1-2'O-Methylated Self RNA. Immunity *43*, 41-51. 10.1016/j.immuni.2015.06.015.
14. Tockary, T.A., Abbasi, S., Matsui-Masai, M., Hayashi, A., Yoshinaga, N., Boonstra, E., Wang, Z., Fukushima, S., Kataoka, K., and Uchida, S. (2023). Comb-structured

mRNA vaccine tethered with short double-stranded RNA adjuvants maximizes cellular immunity for cancer treatment. Proc Natl Acad Sci U S A *120*, e2214320120. 10.1073/pnas.2214320120.

15. Linehan, M.M., Dickey, T.H., Molinari, E.S., Fitzgerald, M.E., Potapova, O., Iwasaki, A., and Pyle, A.M. (2018). A minimal RNA ligand for potent RIG-I activation in living mice. Sci Adv *4*, e1701854. 10.1126/sciadv.1701854.
16. Te Velthuis, A.J.W., Long, J.C., Bauer, D.L.V., Fan, R.L.Y., Yen, H.L., Sharps, J., Siegers, J.Y., Killip, M.J., French, H., Oliva-Martin, M.J., et al. (2018). Mini viral RNAs act as innate immune agonists during influenza virus infection. Nat Microbiol *3*, 1234-1242. 10.1038/s41564-018-0240-5.
17. Schlee, M. (2013). Master sensors of pathogenic RNA - RIG-I like receptors. Immunobiology *218*, 1322-1335. 10.1016/j.imbio.2013.06.007.
18. Ma, H., Wu, Y., Dang, Y., Choi, J.G., Zhang, J., and Wu, H. (2014). Pol III Promoters to Express Small RNAs: Delineation of Transcription Initiation. Mol Ther Nucleic Acids *3*, e161. 10.1038/mtna.2014.12.
19. Gao, Z., Harwig, A., Berkhout, B., and Herrera-Carrillo, E. (2017). Mutation of nucleotides around the +1 position of type 3 polymerase III promoters: The effect on transcriptional activity and start site usage. Transcription *8*, 275-287. 10.1080/21541264.2017.1322170.
20. Marq, J.B., Kolakofsky, D., and Garcin, D. (2010). Unpaired 5' ppp-nucleotides, as found in arenavirus double-stranded RNA panhandles, are not recognized by RIG-I. J Biol Chem *285*, 18208-18216. 10.1074/jbc.M109.089425.
21. Sherwood, A.V., Rivera-Rangel, L.R., Ryberg, L.A., Larsen, H.S., Anker, K.M., Costa, R., Vagbo, C.B., Jakljevic, E., Pham, L.V., Fernandez-Antunez, C., et al. (2023). Hepatitis C virus RNA is 5'-capped with flavin adenine dinucleotide. Nature *619*, 811-818. 10.1038/s41586-023-06301-3.
22. Deflube, L.R., Cressey, T.N., Hume, A.J., Olejnik, J., Haddock, E., Feldmann, F., Ebihara, H., Fearns, R., and Muhlberger, E. (2019). Ebolavirus polymerase uses an unconventional genome replication mechanism. Proc Natl Acad Sci U S A *116*, 8535-8543. 10.1073/pnas.1815745116.
23. Deng, T., Vreede, F.T., and Brownlee, G.G. (2006). Different de novo initiation strategies are used by influenza virus RNA polymerase on its cRNA and viral RNA promoters during viral RNA replication. J Virol *80*, 2337-2348. 10.1128/JVI.80.5.2337-2348.2006.
24. Cai, Z., Liang, T.J., and Luo, G. (2004). Effects of mutations of the initiation nucleotides on hepatitis C virus RNA replication in the cell. J Virol *78*, 3633-3643. 10.1128/jvi.78.7.3633-3643.2004.
25. Kowalski, M.P., and Krude, T. (2015). Functional roles of non-coding Y RNAs. Int J Biochem Cell Biol *66*, 20-29. 10.1016/j.biocel.2015.07.003.
26. Vabret, N., Najburg, V., Solovyov, A., Gopal, R., McClain, C., Sulc, P., Balan, S., Rahou, Y., Beauclair, G., Chazal, M., et al. (2022). Y RNAs are conserved endogenous RIG-I ligands across RNA virus infection and are targeted by HIV-1. iScience *25*, 104599. 10.1016/j.isci.2022.104599.
27. Gendron, M., Roberge, D., and Boire, G. (2001). Heterogeneity of human Ro ribonucleoproteins (RNPS): nuclear retention of Ro RNPS containing the human hY5 RNA in human and mouse cells. Clin Exp Immunol *125*, 162-168. 10.1046/j.1365-2249.2001.01566.x.
28. Camperi, J., Lippold, S., Ayalew, L., Roper, B., Shao, S., Freund, E., Nissenbaum, A., Galan, C., Cao, Q., Yang, F., et al. (2024). Comprehensive Impurity Profiling of

mRNA: Evaluating Current Technologies and Advanced Analytical Techniques. Anal Chem *96*, 3886-3897. 10.1021/acs.analchem.3c05539.

29. Martin, C.T., Muller, D.K., and Coleman, J.E. (1988). Processivity in early stages of transcription by T7 RNA polymerase. Biochemistry *27*, 3966-3974. 10.1021/bi00411a012.
30. Triana-Alonso, F.J., Dabrowski, M., Wadzack, J., and Nierhaus, K.H. (1995). Self-coded 3'-extension of run-off transcripts produces aberrant products during in vitro transcription with T7 RNA polymerase. J Biol Chem *270*, 6298-6307. 10.1074/jbc.270.11.6298.
31. Gholamalipour, Y., Karunanayake Mudiyanselage, A., and Martin, C.T. (2018). 3' end additions by T7 RNA polymerase are RNA self-templated, distributive and diverse in character-RNA-Seq analyses. Nucleic Acids Res *46*, 9253-9263. 10.1093/nar/gky796.
32. Mu, X., Greenwald, E., Ahmad, S., and Hur, S. (2018). An origin of the immunogenicity of in vitro transcribed RNA. Nucleic Acids Res *46*, 5239-5249. 10.1093/nar/gky177.
33. Mu, X., and Hur, S. (2021). Immunogenicity of In Vitro-Transcribed RNA. Acc Chem Res *54*, 4012-4023. 10.1021/acs.accounts.1c00521.
34. Siew, Y.Y., and Zhang, W. (2025). Removing immunogenic double-stranded RNA impurities post in vitro transcription synthesis for mRNA therapeutics production: A review of chromatography strategies. J Chromatogr A *1740*, 465576. 10.1016/j.chroma.2024.465576.
35. Wolczyk, M., Szymanski, J., Trus, I., Naz, Z., Tame, T., Bolembach, A., Choudhury, N.R., Kasztelan, K., Rappsilber, J., Dziembowski, A., and Michlewski, G. (2025). 5' terminal nucleotide determines the immunogenicity of IVT RNAs. Nucleic Acids Res *53*. 10.1093/nar/gkae1252.
36. Choudhury, N.R., and Michlewski, G. (2019). Quantitative identification of proteins that influence miRNA biogenesis by RNA pull-down-SILAC mass spectrometry (RP-SMS). Methods *152*, 12-17. 10.1016/j.ymeth.2018.06.006.
37. Chandel, N.S. (2021). Nucleotide Metabolism. Cold Spring Harb Perspect Biol *13*. 10.1101/cshperspect.a040592.
38. Pastor-Anglada, M., and Perez-Torras, S. (2018). Emerging Roles of Nucleoside Transporters. Front Pharmacol *9*, 606. 10.3389/fphar.2018.00606.
39. Hoffmann, H.H., Schneider, W.M., and Rice, C.M. (2015). Interferons and viruses: an evolutionary arms race of molecular interactions. Trends Immunol *36*, 124-138. 10.1016/j.it.2015.01.004.
40. Ficarelli, M., Antzin-Anduetza, I., Hugh-White, R., Firth, A.E., Sertkaya, H., Wilson, H., Neil, S.J.D., Schulz, R., and Swanson, C.M. (2020). CpG Dinucleotides Inhibit HIV-1 Replication through Zinc Finger Antiviral Protein (ZAP)-Dependent and -Independent Mechanisms. J Virol *94*. 10.1128/JVI.01337-19.
41. Streicher, F., and Jouvenet, N. (2019). Stimulation of Innate Immunity by Host and Viral RNAs. Trends Immunol *40*, 1134-1148. 10.1016/j.it.2019.10.009.
42. Devarkar, S.C., Wang, C., Miller, M.T., Ramanathan, A., Jiang, F., Khan, A.G., Patel, S.S., and Marcotrigiano, J. (2016). Structural basis for m7G recognition and 2'-O-methyl discrimination in capped RNAs by the innate immune receptor RIG-I. Proc Natl Acad Sci U S A *113*, 596-601. 10.1073/pnas.1515152113.
43. Eichler, D.C., and Craig, N. (1994). Processing of eukaryotic ribosomal RNA. Prog Nucleic Acid Res Mol Biol *49*, 197-239. 10.1016/s0079-6603(08)60051-3.
44. Choi, J.H., Burke, J.M., Szymanik, K.H., Nepal, U., Battenhouse, A., Lau, J.T., Stark, A., Lam, V., and Sullivan, C.S. (2020). DUSP11-mediated control of 5'-triphosphate RNA regulates RIG-I sensitivity. Genes Dev *34*, 1697-1712. 10.1101/gad.340604.120.

45. Blum, S., Schmid, S.R., Pause, A., Buser, P., Linder, P., Sonenberg, N., and Trachsel, H. (1992). ATP hydrolysis by initiation factor 4A is required for translation initiation in Saccharomyces cerevisiae. Proc Natl Acad Sci U S A *89*, 7664-7668. 10.1073/pnas.89.16.7664.
46. Cavallius, J., and Merrick, W.C. (1998). Site-directed mutagenesis of yeast eEF1A. Viable mutants with altered nucleotide specificity. J Biol Chem *273*, 28752-28758. 10.1074/jbc.273.44.28752.
47. Bexley, K., Ristová, M., Sharma, S., Spanos, C., Chabes, A., and Tollervey, D. (2025). Metabolic tuning enables immediate adaptation to energy stress in yeast. bioRxiv, 2025.2006.2006.658098. 10.1101/2025.06.06.658098.
48. Hale, B.G., Randall, R.E., Ortin, J., and Jackson, D. (2008). The multifunctional NS1 protein of influenza A viruses. J Gen Virol *89*, 2359-2376. 10.1099/vir.0.2008/004606-0.
49. Schweibenz, B.D., Solotchi, M., Hanpude, P., Devarkar, S.C., and Patel, S.S. (2023). RIG-I recognizes metabolite-capped RNAs as signaling ligands. Nucleic Acids Res *51*, 8102-8114. 10.1093/nar/gkad518.
50. Reich, S., Guilligay, D., Pflug, A., Malet, H., Berger, I., Crepin, T., Hart, D., Lunardi, T., Nanao, M., Ruigrok, R.W., and Cusack, S. (2014). Structural insight into cap-snatching and RNA synthesis by influenza polymerase. Nature *516*, 361-366. 10.1038/nature14009.
51. Thoresen, D.T., Galls, D., Gotte, B., Wang, W., and Pyle, A.M. (2023). A rapid RIG-I signaling relay mediates efficient antiviral response. Mol Cell *83*, 90-104 e104. 10.1016/j.molcel.2022.11.018.
52. Genoyer, E., Wilson, J., Ames, J.M., Stokes, C., Moreno, D., Etzyon, N., Oberst, A., and Gale, M., Jr. (2025). Exposure of negative-sense viral RNA in the cytoplasm initiates innate immunity to West Nile virus. Mol Cell *85*, 1147-1161 e1149. 10.1016/j.molcel.2025.01.015.
53. Ren, X., Linehan, M.M., Iwasaki, A., and Pyle, A.M. (2019). RIG-I Recognition of RNA Targets: The Influence of Terminal Base Pair Sequence and Overhangs on Affinity and Signaling. Cell Rep *29*, 3807-3815 e3803. 10.1016/j.celrep.2019.11.052.
54. Schmidt, A., Schwerd, T., Hamm, W., Hellmuth, J.C., Cui, S., Wenzel, M., Hoffmann, F.S., Michallet, M.C., Besch, R., Hopfner, K.P., et al. (2009). 5'-triphosphate RNA requires base-paired structures to activate antiviral signaling via RIG-I. Proc Natl Acad Sci U S A *106*, 12067-12072. 10.1073/pnas.0900971106.
55. Baek, Y.M., Yoon, S., Hwang, Y.E., and Kim, D.E. (2016). Dependence of RIG-I Nucleic Acid-Binding and ATP Hydrolysis on Activation of Type I Interferon Response. Immune Netw *16*, 249-255. 10.4110/in.2016.16.4.249.
56. Guo, R., and Pyle, A.M. (2022). Monitoring functional RNA binding of RNA-dependent ATPase enzymes such as SF2 helicases using RNA dependent ATPase assays: A RIG-I case study. Methods Enzymol *673*, 39-52. 10.1016/bs.mie.2022.03.064.
57. Sikorska, J., Hou, Y., Chiurazzi, P., Siu, T., Baltus, G.A., Sheth, P., McLaren, D.G., Truong, Q., Parish, C.A., and Wyss, D.F. (2023). Characterization of RNA driven structural changes in full length RIG-I leading to its agonism or antagonism. Nucleic Acids Res *51*, 9356-9368. 10.1093/nar/gkad606.
58. Lu, G., Zhang, J., Li, Y., Li, Z., Zhang, N., Xu, X., Wang, T., Guan, Z., Gao, G.F., and Yan, J. (2011). hNUDT16: a universal decapping enzyme for small nucleolar RNA and cytoplasmic mRNA. Protein Cell *2*, 64-73. 10.1007/s13238-011-1009-2.
59. Huang, S.S.Y., Rinchai, D., Toufiq, M., Kabeer, B.S.A., Roelands, J., Hendrickx, W., Boughorbel, S., Bedognetti, D., Van Panhuys, N., Chaussabel, D., and Garand, M.

(2022). Transcriptomic profile investigations highlight a putative role for NUDT16 in sepsis. J Cell Mol Med *26*, 1714-1721. 10.1111/jcmm.17240.

60. Iyama, T., Abolhassani, N., Tsuchimoto, D., Nonaka, M., and Nakabeppu, Y. (2010). NUDT16 is a (deoxy)inosine diphosphatase, and its deficiency induces accumulation of single-strand breaks in nuclear DNA and growth arrest. Nucleic Acids Res *38*, 4834-4843. 10.1093/nar/gkq249.
61. Nouwen, L.V., Breeuwsma, M., Zaal, E.A., van de Lest, C.H.A., Buitendijk, I., Zwaagstra, M., Balic, P., Filippov, D.V., Berkers, C.R., and van Kuppeveld, F.J.M. (2024). Modulation of nucleotide metabolism by picornaviruses. PLoS Pathog *20*, e1012036. 10.1371/journal.ppat.1012036.
62. Rosa, M.D., Gottlieb, E., Lerner, M.R., and Steitz, J.A. (1981). Striking similarities are exhibited by two small Epstein-Barr virus-encoded ribonucleic acids and the adenovirus-associated ribonucleic acids VAI and VAII. Mol Cell Biol *1*, 785-796. 10.1128/mcb.1.9.785-796.1981.
63. Quaglia, M., Merlotti, G., De Andrea, M., Borgogna, C., and Cantaluppi, V. (2021). Viral Infections and Systemic Lupus Erythematosus: New Players in an Old Story. Viruses *13*. 10.3390/v13020277.
64. Gakis, G., Angelopoulos, I., Panagoulias, I., and Mouzaki, A. (2023). Current knowledge on multiple sclerosis pathophysiology, disability progression assessment and treatment options, and the role of autologous hematopoietic stem cell transplantation. Autoimmun Rev, 103480. 10.1016/j.autrev.2023.103480.
65. Takei, M., Kitamura, N., Nagasawa, Y., Tsuzuki, H., Iwata, M., Nagatsuka, Y., Nakamura, H., Imai, K., and Fujiwara, S. (2022). Are Viral Infections Key Inducers of Autoimmune Diseases? Focus on Epstein-Barr Virus. Viruses *14*. 10.3390/v14091900.
66. Vasilyev, N., and Serganov, A. (2016). Preparation of Short 5'-Triphosphorylated Oligoribonucleotides for Crystallographic and Biochemical Studies. Methods Mol Biol *1320*, 11-20. 10.1007/978-1-4939-2763-0_2.
67. Goldeck, M., Tuschl, T., Hartmann, G., and Ludwig, J. (2014). Efficient solid-phase synthesis of pppRNA by using product-specific labeling. Angew Chem Int Ed Engl *53*, 4694-4698. 10.1002/anie.201400672.
68. Slusarczyk, P., Mandal, P.K., Zurawska, G., Niklewicz, M., Chouhan, K., Mahadeva, R., Jonczy, A., Macias, M., Szybinska, A., Cybulska-Lubak, M., et al. (2023). Impaired iron recycling from erythrocytes is an early hallmark of aging. Elife *12*. 10.7554/eLife.79196.
69. Heap, R.E., Marin-Rubio, J.L., Peltier, J., Heunis, T., Dannoura, A., Moore, A., and Trost, M. (2021). Proteomics characterisation of the L929 cell supernatant and its role in BMDM differentiation. Life Sci Alliance *4*. 10.26508/lsa.202000957.
70. Choudhury, N.R., de Lima Alves, F., de Andres-Aguayo, L., Graf, T., Caceres, J.F., Rappsilber, J., and Michlewski, G. (2013). Tissue-specific control of brain-enriched miR-7 biogenesis. Genes Dev *27*, 24-38. 10.1101/gad.199190.112.
71. Rebendenne, A., Valadao, A.L.C., Tauziet, M., Maarifi, G., Bonaventure, B., McKellar, J., Planes, R., Nisole, S., Arnaud-Arnould, M., Moncorge, O., and Goujon, C. (2021). SARS-CoV-2 triggers an MDA-5-dependent interferon response which is unable to control replication in lung epithelial cells. J Virol *95*. 10.1128/JVI.02415-20.
72. Mejia-Calvo, I., Munoz-Garcia, L., Jimenez-Uribe, A., Camacho-Sandoval, R., Gonzalez-Gonzalez, E., Mellado-Sanchez, G., Tenorio-Calvo, A.V., Lopez-Morales, C.A., Velasco-Velazquez, M.A., Pavon, L., et al. (2019). Validation of a cell-based colorimetric reporter gene assay for the evaluation of Type I Interferons. Biotechnol Rep (Amst) *22*, e00331. 10.1016/j.btre.2019.e00331.

73. Qiu, C., Liu, W.Y., and Xu, Y.Z. (2015). Fluorescence labeling of short RNA by oxidation at the 3'-end. Methods Mol Biol *1297*, 113-120. 10.1007/978-1-4939-2562-9_8.
74. Traut, T.W. (1994). Physiological concentrations of purines and pyrimidines. Mol Cell Biochem *140*, 1-22. 10.1007/BF00928361.
75. Shevchenko, A., Wilm, M., Vorm, O., and Mann, M. (1996). Mass spectrometric sequencing of proteins silver-stained polyacrylamide gels. Anal Chem *68*, 850-858. 10.1021/ac950914h.
76. Demichev, V., Messner, C.B., Vernardis, S.I., Lilley, K.S., and Ralser, M. (2020). DIA-NN: neural networks and interference correction enable deep proteome coverage in high throughput. Nat Methods *17*, 41-44. 10.1038/s41592-019-0638-x.
77. Ammar, C., Schessner, J.P., Willems, S., Michaelis, A.C., and Mann, M. (2023). Accurate Label-Free Quantification by directLFQ to Compare Unlimited Numbers of Proteomes. Mol Cell Proteomics *22*, 100581. 10.1016/j.mcpro.2023.100581.
78. Team, R.C. (2021). R: A Language and Environment for Statistical Computing (R Foundation for Statistical Computing).
79. Quast, J.P., Schuster, D., and Picotti, P. (2022). protti: an R package for comprehensive data analysis of peptide- and protein-centric bottom-up proteomics data. Bioinform Adv *2*, vbab041. 10.1093/bioadv/vbab041.
80. Ritchie, M.E., Phipson, B., Wu, D., Hu, Y., Law, C.W., Shi, W., and Smyth, G.K. (2015). limma powers differential expression analyses for RNA-sequencing and microarray studies. Nucleic Acids Res *43*, e47. 10.1093/nar/gkv007.
81. Wickham, H. (2016). ggplot2 : Elegant Graphics for Data Analysis. Use R!,. 2nd ed. Springer International Publishing : Imprint: Springer,.
82. Yu, G., Wang, L.G., Han, Y., and He, Q.Y. (2012). clusterProfiler: an R package for comparing biological themes among gene clusters. OMICS *16*, 284-287. 10.1089/omi.2011.0118.
83. Perez-Riverol, Y., Bai, J., Bandla, C., Garcia-Seisdedos, D., Hewapathirana, S., Kamatchinathan, S., Kundu, D.J., Prakash, A., Frericks-Zipper, A., Eisenacher, M., et al. (2022). The PRIDE database resources in 2022: a hub for mass spectrometry-based proteomics evidences. Nucleic Acids Res *50*, D543-D552. 10.1093/nar/gkab1038.
84. Crooks, G.E., Hon, G., Chandonia, J.M., and Brenner, S.E. (2004). WebLogo: a sequence logo generator. Genome Res *14*, 1188-1190. 10.1101/gr.849004.

Supplementary Data

5′-triphosphate guanosine RNAs recruit GTP-binding proteins to suppress RIG-I/IFN type I signaling

Jacek Szymanski*, Magdalena Wolczyk*, Ivan Trus, Zara Naz, Nathalie Idlin, Justyna Jackiewicz, Elzbieta Nowak, Christine Wuebben, Gunther Hartmann, Juri Rappsilber and Gracjan Michlewski

* These authors contributed equally to this work.

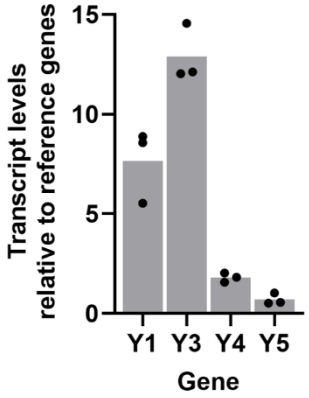

Supplementary Figure S1. The levels of Y RNAs in HEK293 cells. qRT-PCR for Y RNAs (primers listed in Supplementary Table S3) was done for HEK293 cells with three technical and three biological replicates. For normalization, we used the geometric mean of the expression levels for the three reference genes (*IPO8*, *GAPDH*, and *7SL*).

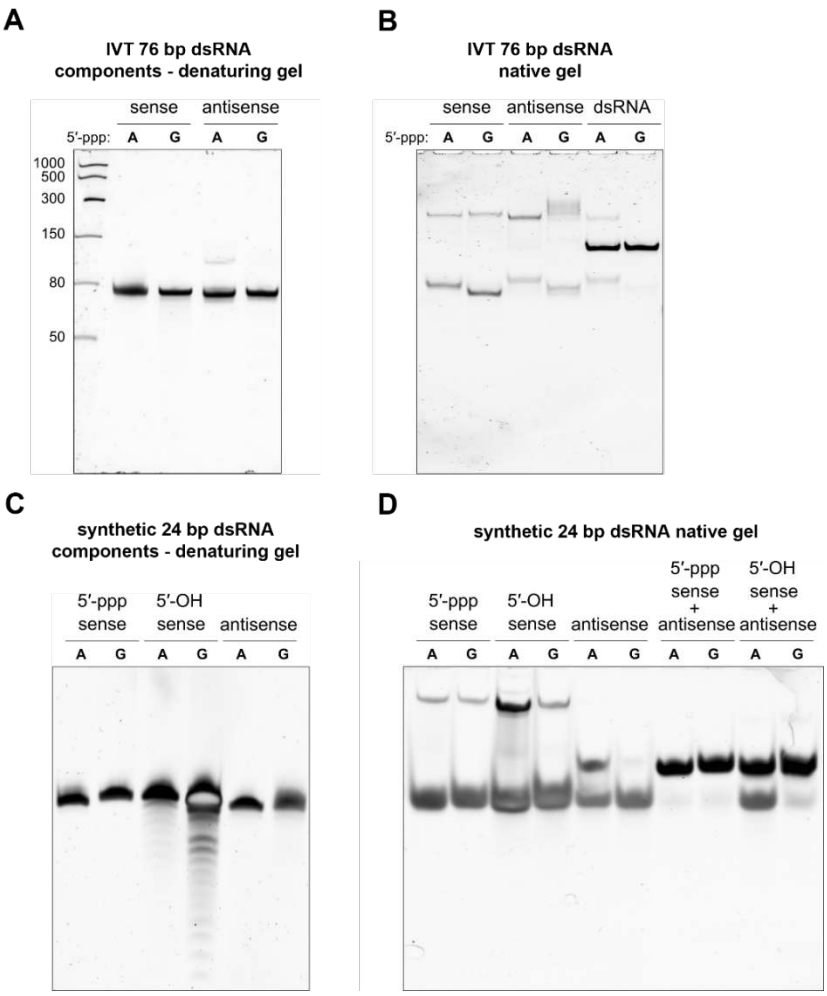

Supplementary Figure S2. Quality control of IVT and chemically synthesised RNA products. (**A, C**) PAGE/Urea analysis of IVT 76 bp (**A**) and synthetic 24 bp (**C**) dsRNA variants. (**B, D**) Native PAGE analysis showing individual single strands used for annealing and the resulting duplexes for the IVT 76 bp (**B**) and synthetic 24 bp (**D**) dsRNAs.

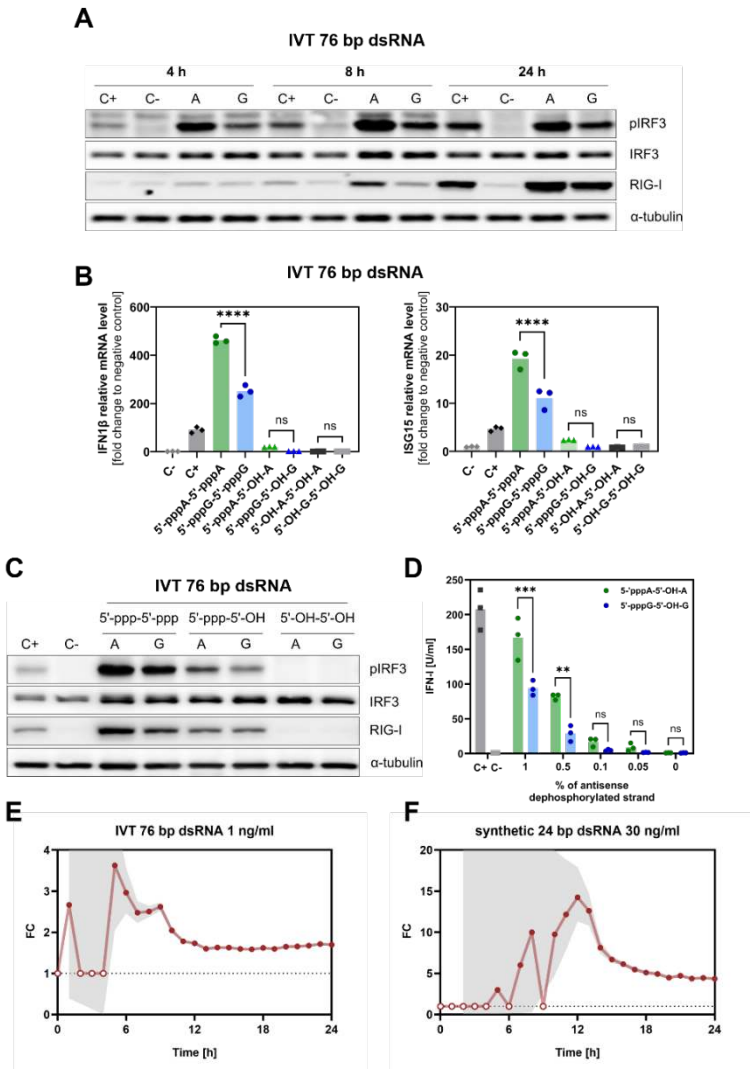

Supplementary figure S3. 5′-pppA 76 bp dsRNA is more immunogenic than 5′-pppG 76 bp dsRNA. (**A**) Analysis of IRF3 phosphorylation and RIG-I expression assessed by Western blot analysis in HEK293 cells after transfection with 1 ng/ml of 5′-pppA *vs.* 5′-pppG IVT 76 bp dsRNAs in 4, 8 and 24 h post transfection. (**B**) Analysis of *IFN1β* and *ISG15* relative mRNA levels in total RNA isolated from HEK293 cells after transfection with 1 ng/ml of 5′-pppA *vs.* 5′-pppG IVT 76 bp dsRNAs. Two-way ANOVA with Šídák's multiple comparisons test was used for statistical analysis (n=3). (**C**) IRF3 phosphorylation and RIG-I expression analysis in HEK293 cells after transfection with 1 ng/ml of 5′-pppA *vs.* 5′-pppG IVT 76 bp dsRNA variants (both strands triphosphorylated, only sense strand triphosphorylated, both strands dephosphorylated) 24 h post transfection. (**D**) Interferon activity measured using HEK Blue IFN type I assay in the supernatants collected from HEK293 cells 24 h after transfection with 3p-hpRNA (C+), lipofectamine (C−) and semisynthetic ligated 5′-pppA *vs.* 5′-pppG 76 nt RNA hybridized with different concentrations of fully complementary antisense dephosphorylated strand. Two-way ANOVA with Šídák's multiple comparisons test was used for statistical analysis (n=3). (**A-D**) The 3p-hpRNA at a concentration of 100 ng/ml (InvivoGen #tlrl-hprna) or lipofectamine were used as positive (C+) and negative (C−) controls, respectively. (**E-F**) Fold-change ratios of mKate2+ cell counts (FC=5′-pppA/5′-pppG) cells treated with either 76 bp IVT (**E**) or 24 bp synthetic dsRNAs (**F**). Grey band is a 95 % confidence interval obtained with the log-delta method. Time-points with either group mean was zero (ratio undefined) are marked by empty circles on the baseline (FC=1).

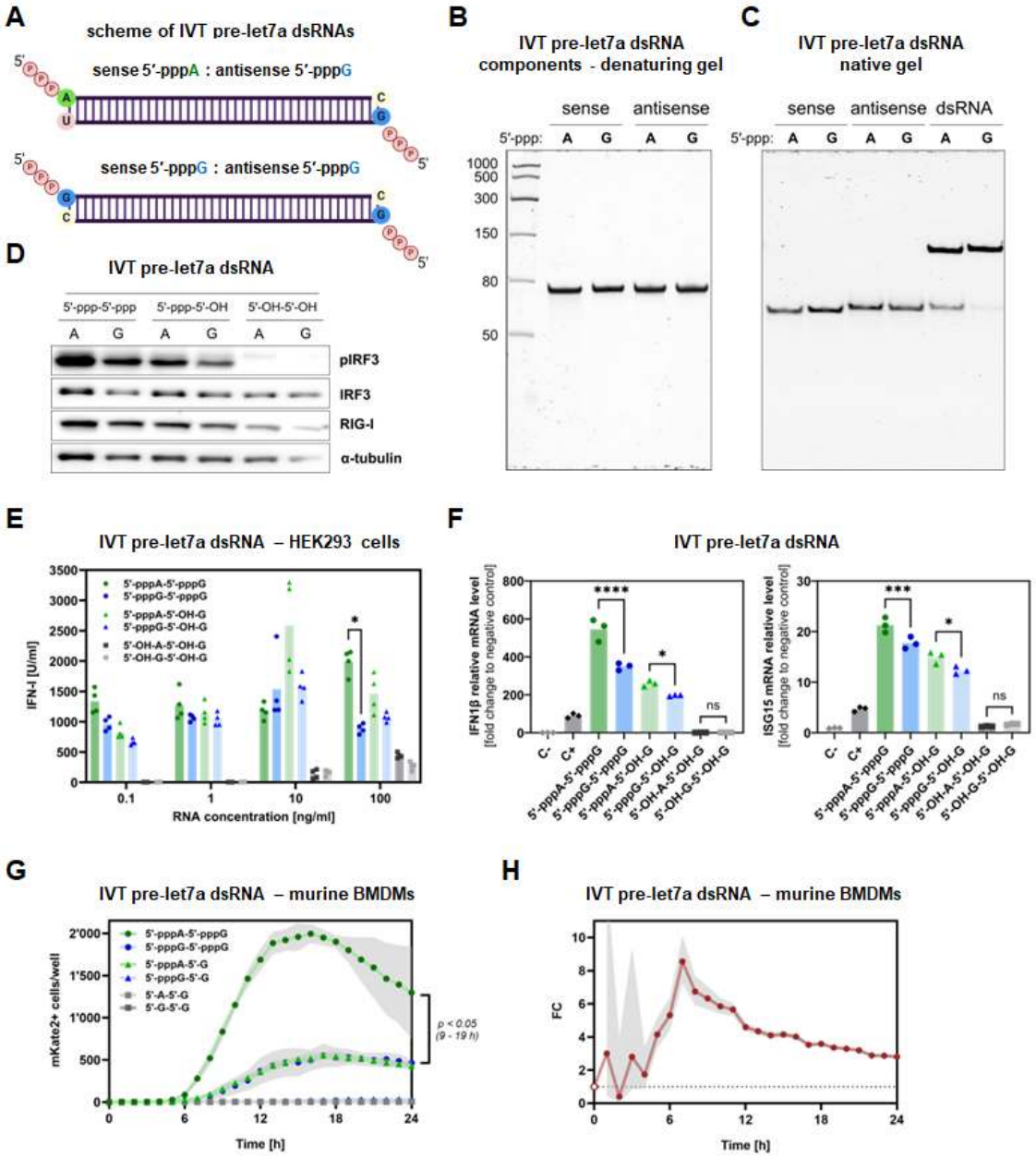

Supplementary Figure S4. 5′-pppA pre-let7a dsRNA is more immunogenic than 5′-pppG pre-let7a dsRNA. (**A**) Schematic representation of IVT-derived pre-let7a dsRNA variants differing at the 5′ terminal nucleotide (5′-pppA or 5′-pppG). (**B**) PAGE/Urea analysis of IVT-derived, single strand components of pre-let7a dsRNA variants. (**C**) Native PAGE analysis showing individual single strands of pre-let7a used for annealing and the resulting duplexes for IVT-derived pre-let7a dsRNA variants. (**D**) Analysis of IRF3 phosphorylation and RIG-I expression assessed by Western blot analysis in HEK293 cells after transfection with 1 ng/ml of IVT-derived pre-let7a dsRNAs with different 5′-terminal nucleotides 24 h post transfection. (**E**) Type I interferon production in HEK293 cells was assessed upon transfection with IVT-derived pre-let7a dsRNA variants with the HEK Blue IFN type I assay. Two-way ANOVA with Šídák's multiple comparisons test was used for statistical analysis (n=4). (**F**) Analysis of *IFN1β* and *ISG15* relative mRNA levels in total RNA isolated from HEK293 cells after transfection with 1 ng/ml of IVT-derived pre-let7a dsRNA variants. Two-way ANOVA with Šídák's multiple comparisons test was used for statistical analysis (n=3). The 3p-hpRNA at a concentration of 100 ng/ml (InvivoGen #tlrl-hprna) or lipofectamine were used as positive

(C+) and negative (C−) controls, respectively. (**G**) RIG-I/IFN activation in murine BMDMs upon transfection with IVT-derived pre-let7a dsRNA variants, shown as mKate2+ cell counts over 0–24 h post-transfection. Grey area represents standard deviation for n=5. Data were analyzed using repeated measures two-way ANOVA on log-transformed values [$\log_{10}(x + 1)$], with Geisser-Greenhouse correction and Šídák's multiple comparisons test. (**H**) Fold-change ratios of mKate2+ cell counts (FC=5′-pppA/5′-pppG) in murine BMDM cells treated with IVT-derived pre-let7a dsRNA variants differing at the 5′ terminal nucleotide (5′-pppA or 5′-pppG). Grey transparent band is a 95 % confidence interval obtained with the log-delta method. Time-points with either group mean was zero (ratio undefined) are marked by empty circles on the baseline (FC=1).

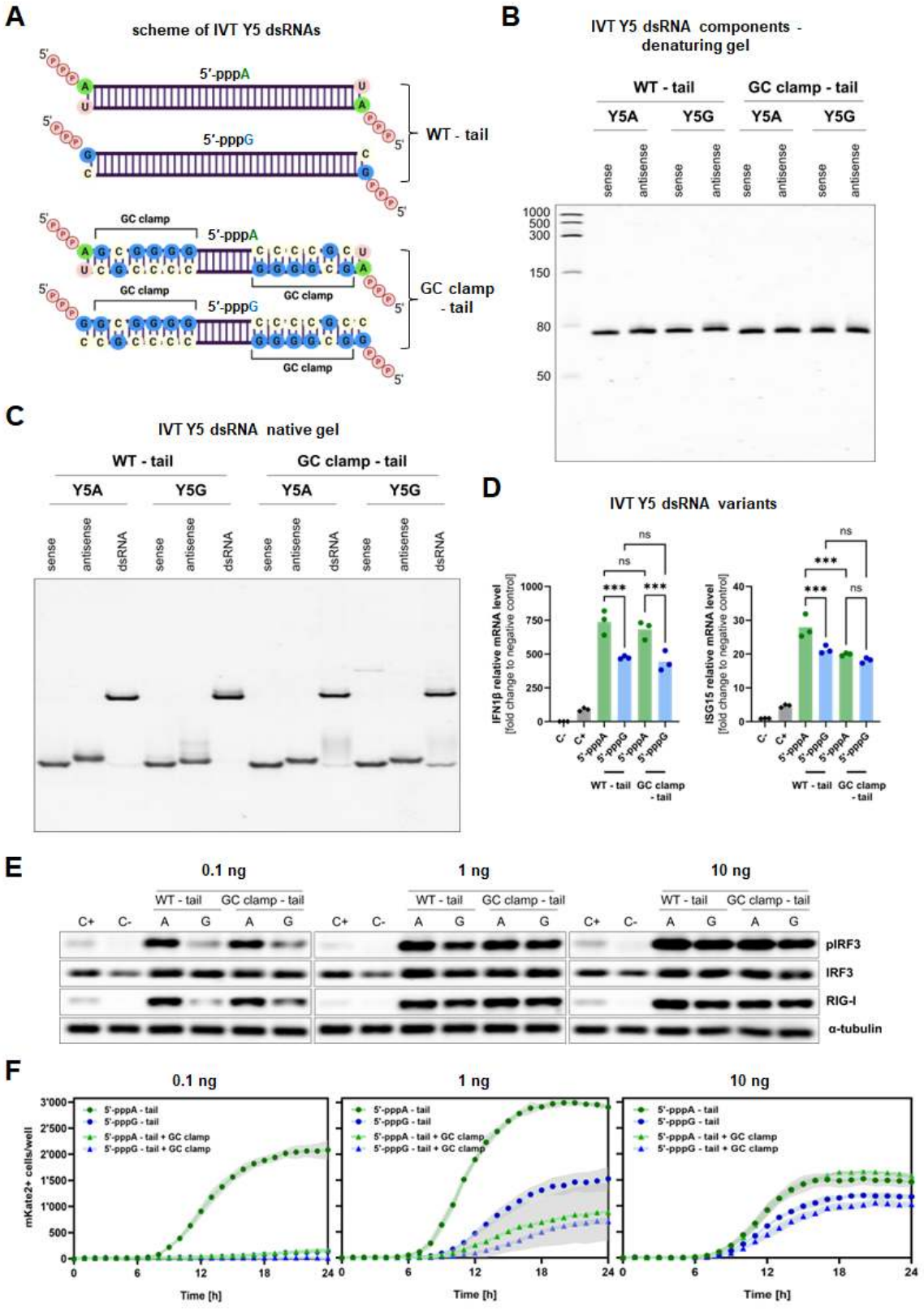
A
scheme of IVT Y5 dsRNAs
5'-pppA
5'-pppG
WT - tail
GC clamp
GC clamp - tail
B
IVT Y5 dsRNA components - denaturing gel
WT - tail
GC clamp - tail
Y5A
Y5G
sense
antisense
1000
500
300
150
80
50
C
IVT Y5 dsRNA native gel
dsRNA
D
IVT Y5 dsRNA variants
IFN1β relative mRNA level [fold change to negative control]
ISG15 relative mRNA level [fold change to negative control]
ns
***
C-
C+
5'-pppA
5'-pppG
E
0.1 ng
1 ng
10 ng
pIRF3
IRF3
RIG-I
α-tubulin
F
mKate2+ cells/well
Time [h]
5'-pppA - tail
5'-pppG - tail
5'-pppA - tail + GC clamp
5'-pppG - tail + GC clamp

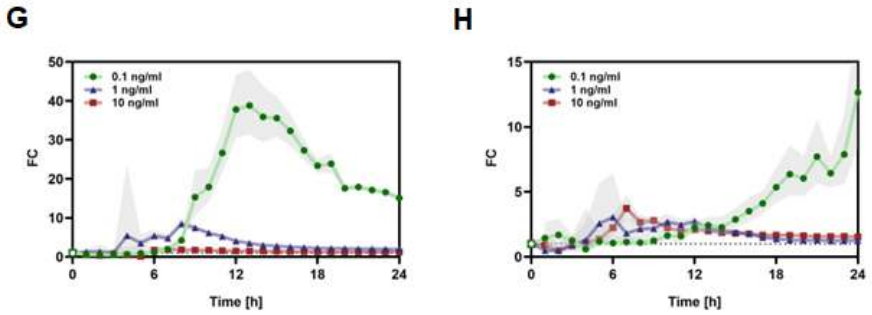

Supplementary Figure S5. 5′-pppA Y5 dsRNA variants are more immunogenic than 5′-pppG Y5 dsRNA variants. (**A**) Schematic representation of Y5 dsRNA variants. (**B**) PAGE/Urea analysis of IVT-derived, single strand components of Y5 dsRNA variants. (**C**) Native PAGE analysis showing individual single strands of Y5 RNAs used for annealing and the resulting duplexes for IVT-derived Y5 dsRNA variants. (**D**) Analysis of *IFN1β* and *ISG15* relative mRNA levels in total RNA isolated from HEK293 cells after transfection with 1 ng/ml of IVT-derived Y5 dsRNA variants. Two-way ANOVA with Šídák's multiple comparisons test was used for statistical analysis (n=3). (**E**) Analysis of IRF3 phosphorylation and RIG-I expression assessed by Western blot analysis in HEK293 cells after transfection with 10, 1 and 0.1 ng/ml of IVT-derived Y5 dsRNA variants 24 h post transfection. (**D** and **E**) The 3p-hpRNA at a concentration of 100 ng/ml (InvivoGen #tlrl-hprna) or lipofectamine were used as positive (C+) and negative (C−) controls, respectively. (**F**) RIG-I/IFN activation in murine BMDMs upon transfection with 10, 1 and 0.1 ng/ml of IVT-derived Y5 dsRNA variants, shown as mKate2+ cell counts over 0–24 h post-transfection. Grey area represents standard deviation for n=5. (**G**-**H**) Fold-change ratios (FC=5′-pppA/5′-pppG) for IVT-derived Y5 dsRNA variants without tail (**G**) and without tail and with GC clamp (**H**). Grey band is a 95 % confidence interval obtained with the log-delta method. Time-points with either group mean was zero (ratio undefined) are marked by empty symbols on the baseline (FC=1).

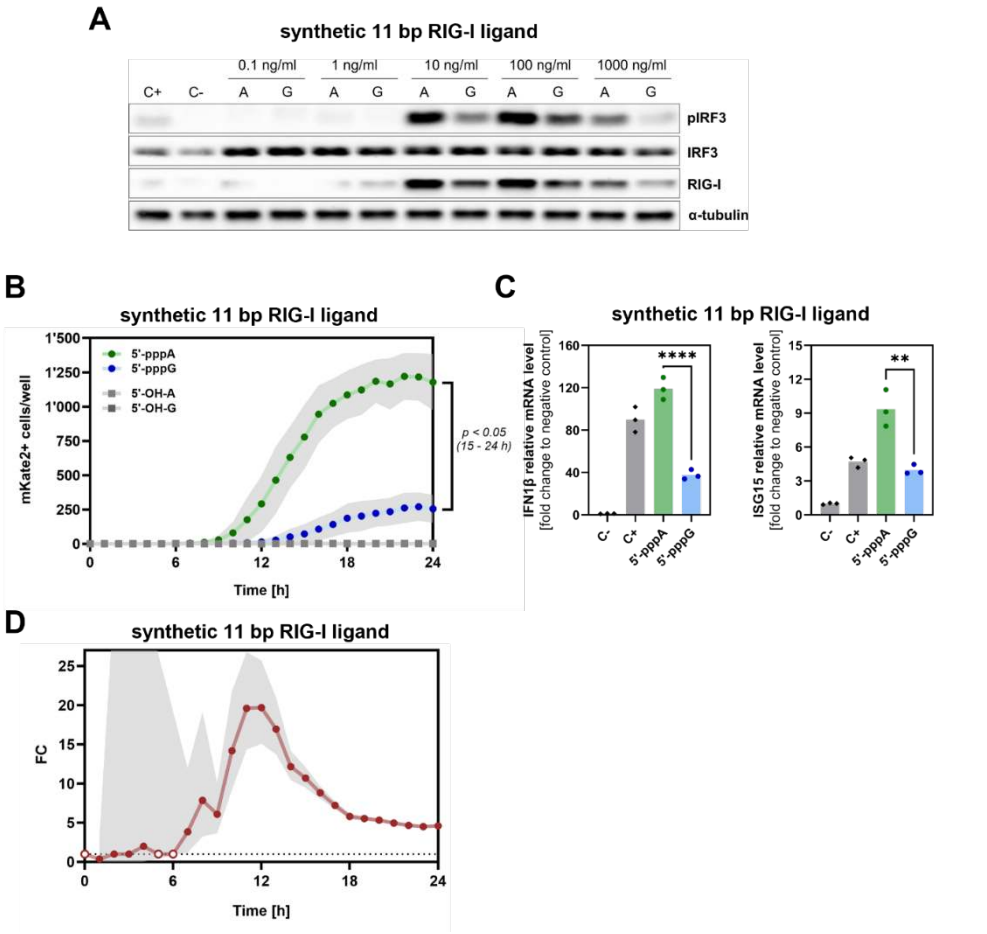

Supplementary Figure S6. Synthetic 5′-pppA 11 bp RIG-I ligand is more immunogenic than synthetic 5′-pppG 11 bp RIG-I ligand. (**A**) Analysis of IRF3 phosphorylation and RIG-I expression assessed by Western blot analysis in HEK293 cells after transfection with various concentrations of 5′-pppA *vs.* 5′-pppG short synthetic, partially double-stranded RIG-I agonist 24 h post transfection. (**B**) RIG-I/IFN activation in murine BMDMs upon transfection with tested synthetic dsRNAs, shown as mKate2^{+} cell counts over 0–24 h post-transfection. Grey area represents standard deviation for n=5. Data were analyzed using repeated measures two-way ANOVA on log-transformed values [$\log_{10}(x+1)$], with Geisser-Greenhouse correction and Šídák's multiple comparisons test. (**D**) Fold-change ratios (FC=5′-pppA/5′-pppG) upon transfection of murine BMDM with synthetic dsRNAs. Grey band is a 95 % confidence interval obtained with the log-delta method. Time-points with either group mean was zero (ratio undefined) are marked by empty circles on the baseline (FC=1). (**C**) Analysis of *IFN1β* and *ISG15* relative mRNA levels in total RNA isolated from HEK293 cells after transfection with 1 ng/ml of IVT-derived Y5 dsRNA variants. Two-way ANOVA with Šídák's multiple comparisons test was used for statistical analysis (n=3). (**A** and **C**) The 3p-hpRNA at a concentration of 100 ng/ml (InvivoGen #tlrl-hprna) or no RNA were used as positive (C+) and negative (C−) controls, respectively.

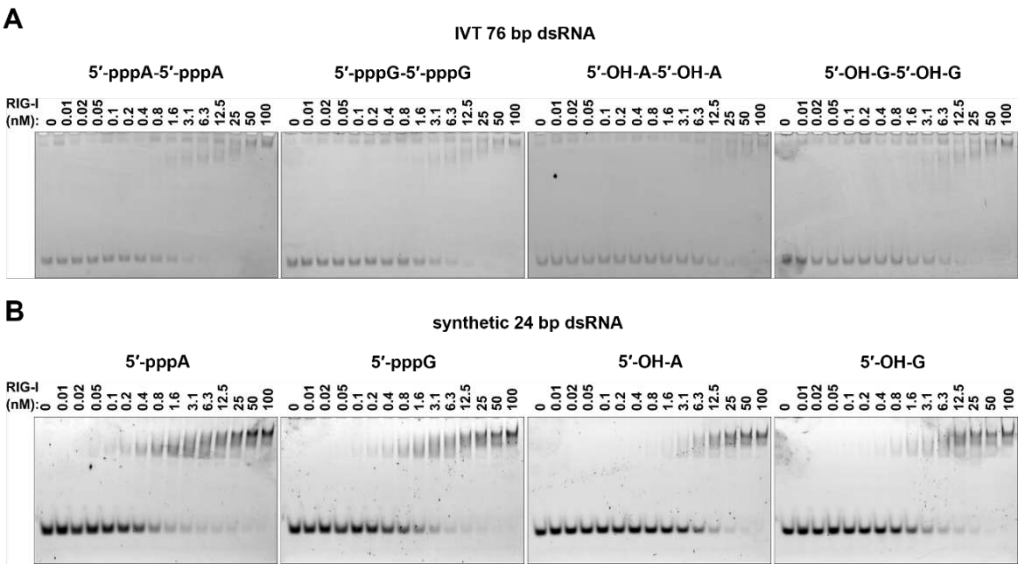

Supplementary Figure S7. Electrophoretic mobility shift assay (EMSA) of recombinant RIG-I protein binding to the IVT 76 bp (A) and synthetic 24 bp (B) dsRNAs with different 5′-terminal nucleotides (5′-pppA, 5′-pppG, 5′-OH-A, 5′-OH-G).

Supplementary Table S1. The dissociation constant (K_d) from EMSA and the half-maximal effective concentration (EC_{50}) for ATPase activity were compared across tested dsRNA variants. The entropy maximization principle was applied, and model fit was evaluated using the Akaike Information Criterion corrected for small sample sizes (AICc). Akaike probability threshold of 0.05 was used to determine statistical significance.

RNA variant	Terminal Nucleotide Comparison	EMSA		RIG-I Activity Assay	
		Akaike's Probability	K_d sigificantly different	Akaike's Probability	EC_{50} sigificantly different
IVT 76 bp dsRNA	**5′-pppA vs 5′-pppG**	< 0.001	Yes	0.71	No
	5′-pppA vs 5′-OH-A	< 0.0001	Yes	< 0.0001	Yes
	5′-pppG vs 5′-OH-G	0.54	No	< 0.0001	Yes
	5′-OH-A vs 5′-OH-G	< 0.0001	Yes	0.30	No
Synthetic 24 bp dsRNA	**5′-pppA vs 5′-pppG**	< 0.0001	Yes	0.70	No
	5′-pppA vs 5′-OH-A	< 0.0001	Yes	< 0.0001	Yes
	5′-pppG vs 5′-OH-G	< 0.001	Yes	< 0.01	Yes
	5′-OH-A vs 5′-OH-G	< 0.0001	Yes	< 0.001	Yes

Supplementary Table S2. RNA transcripts assessed in the current study.

Transcript	RNA variant	Sequence, 5′ – 3′
76 bp dsRNA	5′-pppA	AGCAAAAGCAGGGUGACAAAGACAUAAUGGAUCCAAACACUGUGUCAAGCUUUCAGGUAGAUUGCUUUCUUUGGC
	5′-pppG	GGCAAAAGCAGGGUGACAAAGACAUAAUGGAUCCAAACACUGUGUCAAGCUUUCAGGUAGAUUGCUUUCUUUGGC
76 bp dsRNA antisense	antisense to 5′-pppA	AGCCAAAGAAAGCAAUCUACCUGAAAGCUUGACACAGUGUUUGGAUCCAUUAUGUCUUUGUCACCCUGCUUUUGC
	antisense to 5′-pppG	GGCCAAAGAAAGCAAUCUACCUGAAAGCUUGACACAGUGUUUGGAUCCAUUAUGUCUUUGUCACCCUGCUUUUGC
24 bp dsRNA	5′-pppA	AGCAAAAGCAGGGUGACAAAGACA
	5′-pppG	GGCAAAAGCAGGGUGACAAAGACA
24 bp dsRNA	antisense to 5′-pppA	UGUCUUUGUCACCCUGCUUUUGCU
	antisense to 5′-pppG	UGUCUUUGUCACCCUGCUUUUGCC
pre-let7a	5′-pppA	AGUGAGGUAGUAGGUUGUAUAGUUUUAGGGUCACACCCACCACUGGGAGAUAACUAUACAAUCUACUGUCUUUC
	5′-pppG	GGUGAGGUAGUAGGUUGUAUAGUUUUAGGGUCACACCCACCACUGGGAGAUAACUAUACAAUCUACUGUCUUUC
pre-let7a antisense	antisense to 5′-pppA	GAAAGACAGUAGAUUGUAUAGUUAUCUCCCAGUGGUGGGUGUGACCCUAAAACUAUACAACCUACUACCUCACU
	antisense to 5′-pppG	GAAAGACAGUAGAUUGUAUAGUUAUCUCCCAGUGGUGGGUGUGACCCUAAAACUAUACAACCUACUACCUCACC
Y5 WT – tail	5′-pppA	AGUUGGUCCGAGUGUUGUGGGUUAUUGUUAAGUUGAUUUAACAUUGUCUCCCCCCCACAACCGCGCUUGACUAGCU
	5′-pppG	GGUUGGUCCGAGUGUUGUGGGUUAUUGUUAAGUUGAUUUAACAUUGUCUCCCCCCCACAACCGCGCUUGACUAGCC
Y5 WT – tail antisense	antisense to 5′-pppA	AGCUAGUCAAGCGCGGUUGUGGGGGGAGACAAUGUUAAAUCAACUUAACAAUAACCCACAACACUCGGACCAACU
	antisense to 5′-pppG	GGCUAGUCAAGCGCGGUUGUGGGGGGAGACAAUGUUAAAUCAACUUAACAAUAACCCACAACACUCGGACCAACC
Y5 GC clamp – tail	5′-pppA	AGCGGGGCCGAGUGUUGUGGGUUAUUGUUAAGUUGAUUUAACAUUGUCUCCCCCCCACAACCGCGCUUGCCCCGCU
	5′-pppG	GGCGGGGCCGAGUGUUGUGGGUUAUUGUUAAGUUGAUUUAACAUUGUCUCCCCCCCACAACCGCGCUUGCCCCGCC
Y5 GC clamp – tail antisense	antisense to 5′-pppA	AGCGGGGCAAGCGCGGUUGUGGGGGGAGACAAUGUUAAAUCAACUUAACAAUAACCCACAACACUCGGCCCCGCU
	antisense to 5′-pppG	GGCGGGGCAAGCGCGGUUGUGGGGGGAGACAAUGUUAAAUCAACUUAACAAUAACCCACAACACUCGGCCCCGCC
synthetic 11 bp RIG-I ligand	details provided in the patent WO/2025/088117A1	

Supplementary Table S3. Primers for IVT of RNA. Yellow highlights T7 promoter, bold shows the modified pair of nucleotides.

Transcript	RNA variant	Forward primer, 5′-3′	Reverse primer, 5′-3′
short viral	5′-pppA	TAATACGACTCACTATT**A**GCAAAAGCAGGGTGACAA	**A**GCCAAAGAAAGCAATCTACCTG
	5′-pppG	TAATACGACTCACTATA**G**GCAAAAGCAGGGTGACAA	**G**GCCAAAGAAAGCAATCTACCTG
short viral antisense	antisense to 5′-pppA	AAGCTAATACGACTCACTATT**A**GCCAAAGAAAGCAATCTACC	**A**GCAAAAGCAGGGTGACAAAGAC
	antisense to 5′-pppG	AAGCTAATACGACTCACTATA**G**GCCAAAGAAAGCAATCTACC	**G**GCAAAAGCAGGGTGACAAAGAC
pre-let7a	5′-pppA	TAATACGACTCACTATAAGTGAGGTAGTAGGTTGTATA	GAAAGACAGTAGATTGTATA
	5′-pppG	TAATACGACTCACTATAGGTGAGGTAGTAGGTTGTATA	GAAAGACAGTAGATTGTATA
pre-let7a antisense	antisense to 5′-pppA	AAGCTAATACGACTCACTATAGAAAGACAGTAGATTGTATAGTTATC	AGTGAGGTAGTAGGTTGTATAG
	antisense to 5′-pppG	AAGCTAATACGACTCACTATAGAAAGACAGTAGATTGTATAGTTATC	GGTGAGGTAGTAGGTTGTATAG
Y5 WT – tail	5′-pppA	AAGCTAATACGACTCACTATT**A**GTTGGTCCGAGTGTTGTGGGTTAT	**A**GCTAGTCAAGCGCGGTTGT
	5′-pppG	AAGCTAATACGACTCACTATA**G**GTTGGTCCGAGTGTTGTGGGTTAT	**G**GCTAGTCAAGCGCGGTTGTG
Y5 WT – tail antisense	antisense to 5′-pppA	AAGCTAATACGACTCACTATT**A**GCTAGTCAAGCGCGGTTGTG	**A**GTTGGTCCGAGTGTTGTGG
	antisense to 5′-pppG	AAGCTAATACGACTCACTATA**G**GCTAGTCAAGCGCGGTTGTG	**G**GTTGGTCCGAGTGTTGTGG
Y5 GC clamp – tail	5′-pppA	AAGCTAATACGACTCACTATT**A**GCGGGGCCGAGTGTTGTGGGTTATTGTT	**A**GCGGGGCAAGCGCGGTTGTGGGGGGA
	5′-pppG	AAGCTAATACGACTCACTATA**G**GCGGGGCCGAGTGTTGTGGGTTATTGTT	**G**GCGGGGCAAGCGCGGTTGTGGGGGGA
Y5 GC clamp – tail antisense	antisense to 5′-pppA	AAGCTAATACGACTCACTATT**A**GCGGGGCAAGCGCGGTTGTGGGGGGA	**A**GCGGGGCCGAGTGTTGTGGGTTATTGTT
	antisense to 5′-pppG	AAGCTAATACGACTCACTATA**G**GCGGGGCAAGCGCGGTTGTGGGGGGA	**G**GCGGGGCCGAGTGTTGTGGGTTATTGTT

Supplementary Table S4. Segmented gradient for LC-MS analysis.

Time [min]	% A	% B
0	100	0
1.50	100	0
5	93	7
11.25	85	15
15.75	60	40
16	0	100

Supplementary Table S5. Primary antibodies.

Antigen	Vendor	Code	Dilution ratio
RIG-I	Cell Signaling Technology	3743	1/1000
pIRF3	Cell Signaling Technology	4947	1/1000
IRF3	Proteintech	11312-1-AP	1/1000
NUDT16	Proteintech	12889-1-AP	1/1000
RAN	Cell Signaling Technology	4462	1/1000
RANBP1	Cell Signaling Technology	8780	1/1000
DHX9	Proteintech	17721-1-AP	1/1000
α-tubulin	Proteintech	11224-1-AP	1/4000
PKR	Proteintech	18244-1-AP	1/1000

Supplementary Table S6. Primers for qRT-PCR.

Transcript	Forward primer, 5′-3′	Reverse primer, 5′-3′
Y1	CTGGTCCGAAGGTAGTGA	TAGTCAAGTGCAGTAGTGAGAAGGG
Y3	CTGGTCCGAGTGCAGTGGT	TAGTCAAGTGAAGCAGTGGGAGT
Y4	CCGATGGTAGTGGGTTATCAGAAC	GTCAAATTTAGCAGTGGGGGGTTG
Y5	TCCGAGTGTTGTGGGTTATTG	TAGTCAAGCGCGGTTGTGG
GAPDH [1]	AATCCCATCACCATCTTCCA	TGGACTCCACGACGTACTCA
7SL	GGAGTTCTGGGCTGTAGTGC	TTTGACCTGCTCCGTTTCCG
IPO8 [2]	GGCATACAGTTTAACCTGCCAC	CAGGAGAGGCATCATGTCTGTAA
IFN1β	ACGCCGCATTGACCATCTAT	TGGCCTTCAGGTAATGCAGA
ISG15	CGCAGATCACCCAGAAGAT	GCCCTTGTTATTCCTCACCA

References

1. Nelson, E.A., Walker, S.R., Li, W., Liu, X.S., and Frank, D.A. (2006). Identification of human STAT5-dependent gene regulatory elements based on interspecies homology. J Biol Chem *281*, 26216-26224. 10.1074/jbc.M605001200.
2. Racz, G.A., Nagy, N., Tovari, J., Apati, A., and Vertessy, B.G. (2021). Identification of new reference genes with stable expression patterns for gene expression studies using human cancer and normal cell lines. Sci Rep *11*, 19459. 10.1038/s41598-021-98869-x.

Warsaw, 03-09-2025

Jacek Szymański

Laboratory of RNA-Protein Interactions
– Dioscuri Centre

International Institute of Molecular
and Cell Biology in Warsaw
Ks. Trojdena 4 Street
02-109 Warsaw

Candidate's Contribution Statement

Article's title: 5'-triphosphate guanosine RNAs recruit GTP-binding proteins to suppress RIG-I/IFN type I signalling

Authors: Jacek Szymanski*, Magdalena Wolczyk*, Ivan Trus, Zara Naz, Nathalie Idlin, Justyna Jackiewicz, Elżbieta Nowak, Christine Wuebben, Gunther Hartmann, Juri Rappsilber, Gracjan Michlewski
**Authors contributed equally*

Journal: bioRxiv

Date of publishing: 23rd July 2025

DOI: https://doi.org/10.1101/2023.12.22.573000

I hereby declare that I, Jacek Szymański, made a substantive contribution to the development of this publication. My contribution consisted of:

- production and purification of RNAs prepared with *in vitro* transcription, including fluorescence RNA preparation;

- optimalisation of splint ligation method and production of semi-synthetic RNAs;

- designing and conducting biochemical assays with recombinant RIG-I protein: electrophoretic mobility shift assay (EMSA) and RIG-I ATPase assay;

- designing and conducting all RNA pulldown experiments;

- analyzing all proteomic data;

- designing and optimalisation method for nucleotide salvage pathway induction in HEK293 cells;

- co-writing the manuscript and creating figures.

Candidate's Signature

Signature of the Corresponding Author

INTERNATIONAL INSTITUTE OF MOLECULAR AND CELL BIOLOGY IN WARSAW
4 Ks. Trojdena Street, 02-109 Warsaw, Poland; phone: +48 22 597 07 00, fax: +48 22 597 07 15
e-mail: secretariat@iimcb.gov.pl, www.iimcb.gov.pl